

DOCTORAL THESIS

Enhancing Oil Spill Detection, Response and Modeling in the Baltic Sea

Siim Pärt

TALLINN UNIVERSITY OF TECHNOLOGY
DOCTORAL THESIS
61/2024

Enhancing Oil Spill Detection, Response and Modeling in the Baltic Sea

SIIM PÄRT



TALLINN UNIVERSITY OF TECHNOLOGY
School of Science
Department of Marine Systems

The dissertation was accepted for the defence of the degree of Doctor of Philosophy in Oceanography and Meteorology on 29 September 2024

Supervisor: Prof. Rivo Uiboupin,
Department of Marine Systems, School of Science,
Tallinn University of Technology
Tallinn, Estonia

Co-supervisor: Dr. Jan-Victor Björkqvist,
Norwegian Meteorological Institute,
Bergen, Norway

Opponents: Dr. Kai Myrberg,
Finnish Environment Institute,
Helsinki, Finland

Prof. Inga Dailidiene,
Klaipeda University,
Klaipeda, Lithuania

Defence of the thesis: 5 November 2024, Tallinn

Declaration:

Hereby I declare that this doctoral thesis, my original investigation and achievement, submitted for the doctoral degree at Tallinn University of Technology, has not been submitted for any academic degree elsewhere.

Siim Pärt

signature

Copyright: Siim Pärt, 2024
ISSN 2585-6898 (publication)
ISBN 978-9916-80-214-4 (publication)
ISSN 2585-6901 (PDF)
ISBN 978-9916-80-215-1 (PDF)
DOI <https://doi.org/10.23658/taltech.61/2024>
Printed by Koopia Niini & Rauam

Pärt, S. (2024). *Enhancing Oil Spill Detection, Response and Modeling in the Baltic Sea* [TalTech Press]. <https://doi.org/10.23658/taltech.61/2024>

TALLINNA TEHNIKAÜLIKOOL
DOKTORITÖÖ
61/2024

Õlireostuse tuvastamise, modelleerimise ja sellele reageerimise tõhustamine Läänemeres

SIIM PÄRT



Contents

List of Publications	6
Author's Contributions to the Publications	7
Abbreviations.....	8
1 Introduction and Background	9
1.1 Oil Pollution and the Baltic Sea	9
1.2 Oil Spill Detection	10
1.3 Techniques and Technologies in Oil Spill Response.....	11
1.4 Oil Spill Modeling	12
2 Motivation and Objectives	13
3 Materials and Methods.....	16
3.1 In Situ Operational Oil Spill Detection.....	16
3.1.1 Laboratory Testing.....	16
3.1.2 Field Testing	17
3.2 LainePoiss Buoy Development.....	19
3.2.1 Wind drift factor.....	19
3.3 Utilizing the OpenDrift Framework for Drift Analysis and Oil Spill Simulation	20
4 Results and Discussion	22
4.1 Assessing the Oil-Specific Fluorometers	22
4.2 Assessing In Situ Platforms and Sensor Efficacy for Real-Time Oil Spill De- tection	23
4.3 Enhancing Oil Spill Response with LainePoiss Buoy Technology	25
4.4 Validation of the Opendrift Setup	27
4.5 Hypothetical Oil Spill Scenarios in the Estonian Sea Area	28
5 Conclusions	31
References.....	33
Acknowledgements	45
Abstract.....	46
Kokkuvõte	48
Appendix	51
Paper I.....	51
Paper II	71
Paper III	95
Curriculum Vitae	110
Elulookirjeldus.....	112

List of Publications

The present Ph.D. thesis is based on the following publications that are referred to in the text by Roman numbers.

- I Pärt, S., Kankaanpää, H., Björkqvist, J.-V., & Uiboupin, R. (2021). Oil Spill Detection Using Fluorometric Sensors: Laboratory Validation and Implementation to a FerryBox and a Moored SmartBuoy. *Frontiers in Marine Science*, 8, 1–17. <https://doi.org/10.3389/fmars.2021.778136>
- II Alari, V., Björkqvist, J.-V., Kaldvee, V., Mölder, K., Rikka, S., Kask-Korb, A., Vahter, K., Pärt, S., Vidjajev, N., & Tõnisson, H. (2022). LainePoiss® —A Lightweight and Ice-Resistant Wave Buoy. *Journal of Atmospheric and Oceanic Technology*, 39(5), 573–594. <https://doi.org/10.1175/JTECH-D-21-0091.1>
- III Pärt, S., Björkqvist, J.-V., Alari, V., Maljutenko, I., & Uiboupin, R. (2023). An ocean–wave–trajectory forecasting system for the eastern Baltic Sea: Validation against drifting buoys and implementation for oil spill modeling. *Marine Pollution Bulletin*, 195. <https://doi.org/10.1016/j.marpolbul.2023.115497>

Author's Contributions to the Publications

- I The author significantly contributed to conducting field experiments and was integral in data compilation, analysis, interpretation, and visualization. The manuscript was primarily written by the author with valuable input from co-authors.
- II The author contributed to the design and execution of the field experiments, including deployment tests with UAV, and to the planning and preparation of the manuscript.
- III The author played a pivotal role in conducting field experiments. The author set up and ran the OpenDrift trajectory modeling framework and compiled, analyzed, interpreted, and visualized the data. The manuscript was primarily written by the author, incorporating valuable contributions from co-authors.

Abbreviations

CDOM	Colored dissolved organic matter
ECMWF	European Centre for Medium-Range Weather Forecasts
EMSA	European Maritime Safety Agency
EO/IR	Electromagnetic/infrared
ESA	European Space Agency
FLD	Fluorometric detection
GC-FID	Gas chromatography-flame ionization detection
GC-MS	Gas chromatography-mass spectrometry
HELCOM	Helsinki Commission
IR-UV	Infrared-ultraviolet
LP	LainePoiss
MEMS	Microelectromechanical system
NCLS	Normalized Cumulative Lagrangian Separation
PAH	Polycyclic aromatic hydrocarbons
PSU	Practical salinity unit
PTSA	Pyrenetetrasulfonic acid
SAR	Synthetic Aperture Radar
SLAR	Side-Looking Airborne Radar
SMHI	Swedish Meteorological and Hydrological Institute
SS	Skill score
STW	SeaTrackWeb
UAV	Unmanned aerial vehicle
WAF	Water accommodated fractions
WDF	Wind drift factor
WWF	World Wildlife Fund

1 Introduction and Background

1.1 Oil Pollution and the Baltic Sea

Oil pollution in marine environments is a significant global environmental concern, profoundly affecting ecosystems on both the local and regional scales. This issue is also acute in the Baltic Sea, one of the largest brackish water bodies in the world and a distinctly sensitive area due to its unique characteristics, including slow water exchange, fragmented coastline and particular climatic conditions (HELCOM, 2018). Furthermore, the sea is distinguished by pronounced stratification (e.g. Elken et al., 2015; Liblik and Lips, 2019), elevated nutrient levels (e.g. Savchuk, 2018; Murray et al., 2019), widespread deep-water oxygen deficiency (e.g. Conley et al., 2009; Carstensen et al., 2014; Kõuts et al., 2021), and high horizontal and vertical salinity variability (e.g. Meier and Kauker, 2003a; Lehmann et al., 2022) with an average of 7.4 PSU (Meier and Kauker, 2003b). Limited species diversity makes the sea exceptionally vulnerable, as the disruption or loss of even one critical species can cause significant ecosystem alterations. The Baltic Sea is bordered by nine industrialized nations and has a drainage basin four times larger than its surface area, which supports approximately 85 million people (HELCOM, 2018). It facilitates approximately 15% of global maritime traffic (HELCOM, 2003), with around 20% of the ships classified as tankers (HELCOM, 2010, 2021c). Predictions by the World Wildlife Fund (WWF) suggested that the number of ships in the region would double within 20 years, with oil shipping expected to grow by over 60% (WWF, 2010). For instance, the number of tanker ships operating in the Baltic Sea increased from more than 1800 in 2018 (HELCOM, 2019) to nearly 2000 in 2020 (HELCOM, 2021c). As shipping activities increase, the rising number of vessels heightens the risk of accidents and oil discharges (HELCOM, 2013).

Most of the ships in this region use oil as their main fuel, and intentional or negligent releases of oil and petroleum products into the marine environment are not uncommon. These releases, which are the main source of oil pollution in the Baltic Sea, are called operational oil spills and can be attributed to factors such as oil in the bilge water, the disposal of waste oil, or accidents, especially around ports and major shipping lines (HELCOM, 2021a,c). Vessel groundings are the predominant type of accident in the area, closely followed by collisions and other forms of contact; however, these incidents rarely lead to pollution (HELCOM, 2021c). Fortunately, there has been a decrease in both the frequency and volume of detected illegal oil spills in recent decades and an especially notable reduction in larger spills ($>10 \text{ m}^3$) (HELCOM, 2021a,c). For example, the confirmed mineral oil detections by the countries of the Helsinki Commission (HELCOM) were 390 in 2001 and have decreased to approximately 50-70 in the 2020s (HELCOM, 2023).

Sunken vessels, commonly referred to as "potentially polluting wrecks," have become another growing environmental concern in terms of oil pollution (e.g. Michel et al., 2005; Landquist et al., 2013; NOAA, 2013; Goodsir et al., 2019). Notably, the majority of these wrecks ($>75\%$) are remnants of World War II (Michel et al., 2005). Given that these have been submerged for more than seven decades, they are increasingly susceptible to structural failures due to metal corrosion (Faksness et al., 2015; Landquist et al., 2016; Carter et al., 2021). Michel et al. (2005) have estimated that there are approximately 8600 shipwrecks worldwide that pose a significant risk of oil pollution, potentially containing between 2.5 and 20.4 million tons of oil products. The seabed of the Baltic Sea also contains a relatively large number of potentially polluting wrecks, but unfortunately there is no comprehensive regional data set or registry available (HELCOM, 2018). For example, an exhaustive archive-based survey completed in 2011 identified 2700 shipwrecks with the potential to contaminate Swedish waters (Hassellöv et al., 2014). Of these, around 300

were verified as potential environmental threats, and subsequent research pinpointed 31 shipwrecks chosen for initial oil extraction efforts (Lindgren et al., 2020).

For the Estonian sea area, HELCOM reports that of the 705 identified wrecks, 84 have been identified as having the potential for the risk of oil leakage, of which 14 have been confirmed to have the risk of oil leakage (HELCOM, 2018). Furthermore, in the environmental risk assessment of ships sunk in Estonian waters in the twentieth century, 72 vessels were identified based on historical sources that may pose a medium risk and one wreck that may pose a high risk to the environment in terms of fuel oil (Treffner, 2019). In 2021, the Estonian Ministry of the Environment commissioned an updated environmental risk assessment of shipwrecks, according to which there are 54 environmentally hazardous wrecks in Estonian waters (Kasak et al., 2022).

The increasing trend of the use of marine areas for industrial purposes, with offshore wind farms as a notable example (Musial et al., 2019; Díaz and Guedes Soares, 2020; Soares-Ramos et al., 2020) is similarly observed in the Baltic Sea (Ingmarsson and Hüffmeier, 2019). These developments escalate marine traffic and introduce more complex maritime operations, which in turn increase the likelihood of oil spills. The development and upkeep of these facilities require extensive use of heavy equipment and vehicles, which pose a risk of collisions among themselves or with turbines (Etkin, 2008; Presencia and Shafiee, 2018; Yu et al., 2020).

Oil spills, regardless of their origin and size, pose a substantial threat to marine and coastal ecosystems (e.g. Saadoun, 2015; Bejarano and Michel, 2016; Yim et al., 2017; Huetzel, 2022). Both immediate and long-term toxic effects have been documented (e.g. Lindgren et al., 2012; Langangen et al., 2017; Ruberg et al., 2021b,a). Waterbirds are considered to be most significantly and visibly affected by oil pollution (e.g. Troisi et al., 2016; Piatt and Van Pelt, 1997; Irons et al., 2000; Camphuysen and Heubeck, 2001). Even a small presence of oil on the sea surface can affect the birds by contaminating their plumage, affecting buoyancy and insulation (Jenssen, 1994; O'Hara and Morandin, 2010).

1.2 Oil Spill Detection

Monitoring marine areas for oil pollution is primarily based on remote sensing tools such as satellites, sea vessels, and aircraft. These techniques encompass visible and infrared multispectral, hyperspectral, thermal, microwave, and laser fluorosensors (Fingas and Brown, 2018; Al-Ruzouq et al., 2020). Nowadays, satellite-based Synthetic Aperture Radar (SAR) data are the most preferred for oil spill detection over other sources because they do not have daylight constraints, can penetrate cloud cover, and are available in various weather conditions (Solberg, 2012; Al-Ruzouq et al., 2020).

Detection and registration of oil spills and other harmful materials in the Baltic Sea area is carried out mainly by aerial surveillance (planes, helicopters, drones) (Alcaro et al., 2021; HELCOM, 2021b). These surveillance aircraft typically use standard sensors such as video/photo cameras, side-looking airborne radar (SLAR), infrared-ultraviolet (IR-UV), and electromagnetic/infrared (EO/IR), while supplementary sensors include microwave and laser fluorosensor (HELCOM, 2021b).

Furthermore, the Baltic Sea and other European seas are routinely monitored for illegal oil discharges using SAR satellite images from the European Space Agency (ESA) and the European Maritime Safety Agency (EMSA) CleanSeaNet (Alcaro et al., 2021; HELCOM, 2021a; EMSA, 2021). These images are relayed in near-real time to provide an initial alert of possible oil spills, which are then verified by the aircraft at the location (HELCOM, 2021a). In 2022, for example, out of 295 instances in which satellites detected spills in the waters of HELCOM countries, four were confirmed by direct observations to be mineral oil spills

(HELCOM, 2023).

Although the mentioned remote sensing methods effectively detect surface pollution, they face challenges with crude oil and its derivatives that submerge and disperse deeper into the water column. Factors such as the small size of the spill and evaporation that causes visible slicks to vanish can further contribute to this difficulty. These methods also have issues with data resolution limitations and, in the case of SAR data, the issue of lookalike signatures, that resemble oil pollution (Solberg, 2012; Alpers et al., 2017; Al-Ruzouq et al., 2020). To address these challenges, additional in situ detection systems would be beneficial. Detecting oil below the sea surface is a major challenge, and various fluorometry techniques and sensors are predominantly used for this purpose (Lambert et al., 2003; Lambert, 2003; Chekalyuk and Hafez, 2013; Conmy et al., 2014; Li et al., 2022; Baszanowska and Otremba, 2022; Xie et al., 2022).

1.3 Techniques and Technologies in Oil Spill Response

Oil spill response has become a highly advanced field, utilizing a variety of techniques and technologies. These methods are designed for both immediate action and long-term environmental recovery and protection.

Usually, containment is the first line of defense in response to oil spills. It involves the deployment of floating barriers or booms that surround the oil slick to prevent further spread. These booms are designed to operate under various conditions, including open and protected waters. Some advanced booms are equipped with skirts that hang underwater to capture submerged oil, while others are made with absorbent materials that soak up oil (Pagnucco and Phillips, 2018; Dhaka and Chattopadhyay, 2021).

Once oil spills are contained, the next step is recovery and removal of the oil. Skimmers, available in various forms, serve as the main means of extracting oil from the surface of the water (Dave and Ghaly, 2011; Dhaka and Chattopadhyay, 2021). Chemical dispersants are also used to break down oil into smaller droplets, facilitating microbial degradation. However, the environmental impact of these dispersants is a topic of ongoing concern (Fiocchio and Lewis, 1999; Lessard and Demarco, 2000; Prince, 2015; Kleindienst et al., 2015; Bejarano, 2018). Bioremediation presents a more green alternative, employing microorganisms to break down oil (Hoff, 1993; Baniasadi and Mousavi, 2019; Bhattacharya et al., 2019). Another method, in situ burning, is applied mainly in calm Arctic waters. It quickly reduces the volume of oil but poses risks of ecological damage and air pollution, necessitating careful application (Mullin and Champ, 2003; Fritt-Rasmussen et al., 2015; Wegeberg et al., 2017; Faksness et al., 2022; Fritt-Rasmussen et al., 2023).

In the Baltic Sea, the current guidance is that response to oil spills should be as far as possible done by mechanical means (booms and skimmers), and the use of chemical dispersants is discouraged due to sensitive ecological conditions and low water exchange (Chapman et al., 2007).

Advances in oil spill response technology are constantly evolving and incorporate a variety of innovative solutions, such as more efficient absorbent materials, biodegradable dispersants, advanced skimmers, and improved bioremediation techniques. Current research focuses on refining these technologies for use in challenging environments, such as icy waters or remote, inaccessible areas, ensuring a more effective and timely response to oil spills. These developments are complemented by the development and integration of sophisticated sensors and platforms, crucial for situational awareness and real-time monitoring capabilities.

1.4 Oil Spill Modeling

After an oil spill, the oil undergoes physical and chemical changes known as "weathering", which includes processes such as spreading, advection, diffusion, evaporation, emulsification, and dispersion (e.g. Keramea et al., 2021). The overall movement of oil on the water surface is referred to as "drift." These transformations and movements are mainly influenced by environmental factors, especially wind, currents, and waves.

Operational oil spill modeling uses predictive numerical models, incorporating atmospheric, wave, and hydrodynamical models, to predict the fate and transport of the spill. These models are designed to reflect the current environmental conditions and the chemical composition of the oil, with the purpose of providing predictions that are essential for supporting immediate response actions after an oil spill. In particular, many of these numerical models can perform both hindcasts, useful for tracing pollution sources, and forecasts, which can deliver vital data for swift response actions.

In general, these models serve multiple purposes, from aiding urgent decision making and oil spill response planning to assessing the environmental impact of oil infrastructure and quantifying potential ecological and economic damages post-spill.

There are typically two main methods used for modeling oil drift trajectories: the Lagrangian and Eulerian approaches. Among these, Lagrangian models have been found to be more suitable during oil spill emergencies due to their simplicity, efficiency, and reduced computational demands (Zodiatis et al., 2017).

In recent decades, numerous operational oil spill models with diverse capabilities have been developed and utilized (Spaulding, 2017; Zodiatis et al., 2017; Hole, 2018; Keramea et al., 2021). Some of the most prominent models are ADIOS (Lehr et al., 2002), MEDSLIK-II (De Dominicis et al., 2013a,b), GNOME (Beegle-Krause, 2005), OSCAR (Aamo et al., 2005), and OpenDrift/OpenOil (Dagestad et al., 2018; Röhrs et al., 2018).

The predominant model used in the Baltic Sea area to forecast the behavior of oil spills is SeaTrackWeb (STW) (Ambjörn, 2006; Kostianoy et al., 2008; Ambjörn et al., 2014), an online system developed primarily by the Swedish Meteorological and Hydrological Institute (SMHI). It is also recognized as the official drift model of HELCOM and is accessible to national authorities and designated research organizations.

2 Motivation and Objectives

The main motivation for this thesis is to improve the techniques and tools employed in oil spill management, specifically within the context of the Baltic Sea. Oil spill management is a comprehensive concept that encompasses the techniques, plans, and processes used before, during, and after a pollution event with the purpose of avoiding, recognizing, responding to, and recovering from oil spill occurrences.

The papers on which this thesis is based focus on three critical components of oil spill management, each representing a distinct stage in the addressing of an oil spill incident: detection, response and modeling (Figure 1).

Oil spill detection is one of the first steps in effective spill management, relying on early and accurate identification to guide response strategies. The use and development of advanced detection methods, including remote sensing technologies, in situ monitoring tools, and shoreline surveillance, is essential to identify and quantify marine oil spills quickly and reliably. To enhance these capabilities, the first part of this work is focused on testing and implementing fluorimeters for oil spill detection. Furthermore, these fluorimeters are integrated into in situ systems like FerryBox and SmartBuoy for real-time spill detection. These systems, equipped to detect oil hydrocarbons in water, can offer immediate alerts and continuous monitoring, significantly improving the speed and accuracy of oil spill responses.

Once a significant spill is detected, oil response operations are initiated to mitigate the environmental impact. These oil combatting operations encompass various strategies, including containment and recovery with booms and skimmers, chemical dispersion, in situ burning, bioremediation, and other mechanical or manual methods to extract oil from the environment. Wave and drifter buoys provide accurate wave data, essential for evaluating the sea surface conditions that influence oil dispersion, and real-time information on the oil spill trajectory, which can play a key role in these response efforts (Novelli et al., 2018; Yu et al., 2018). These data are vital for the effective deployment of containment booms, especially in rough sea conditions, and for the coordination of recovery operations to the most affected areas. To further progress in this field, the second part of this work is dedicated to contribution to the development of a compact, durable, and affordable wave buoy. This development aims to improve the ability to collect such crucial information, improving response strategies for oil spills. Additionally, the secondary ability of the wave buoy to function as a drifter enables its use in spill tracking and in predictive modeling for validation purposes.

Oil spill modeling is essential for both planning and responding to potential and actual spill events. These models, utilizing oceanic circulation, meteorological data and the characteristics of oil, predict its movement, behavior, and fate. This approach is crucial to guide response efforts, allocate resources, and inform decision makers about potential impacts and mitigation strategies. In Estonia, the recent implementation of two local high-resolution operational models for hydrodynamics and waves led to the idea of integrating these forecasts into a drift-modeling system. However, the existing drift forecast system did not accommodate this integration. Consequently, an open-source Python-based Lagrangian particle trajectory modeling framework OpenDrift (Dagestad et al., 2018) was chosen. The setup and validation of this framework for the eastern Baltic Sea forms the third part of the work.

These components form a comprehensive approach that helps to ensure readiness and effectiveness in protecting marine environments from the adverse effects of oil spills.

The specific objectives are as follows:

- to evaluate the selectivity and sensitivity of commercially available fluorometric instruments designed for in situ and real-time detection of oil or its compounds (Paper I);
- to assess the possibility of using these fluorometric sensors on platforms like Ferry-Box and SmartBuoy to detect oil spills in real time (Paper I);
- to contribute to the development of an ice-resistant, lightweight wave buoy capable of delivering real-time wave data during oil spill response operations, and could be deployed using an unmanned aerial vehicle (UAV) (Paper II);
- to evaluate the suitability of the developed wave buoy, LainePoiss (LP), for employment as a tracking device in oil spill response operations and as a proxy for oil in spill research (Paper III);
- to setup and validate an open-source Lagrangian particle trajectory modeling framework, coupled with local hydrodynamical and wave models, for modeling oil spills in eastern Baltic Sea (Paper III);
- to simulate potential oil spills under extreme weather scenarios and in high-risk areas such as region with heavy maritime traffic, prospective wind farm site, and near a potentially hazardous wreck (Paper III).

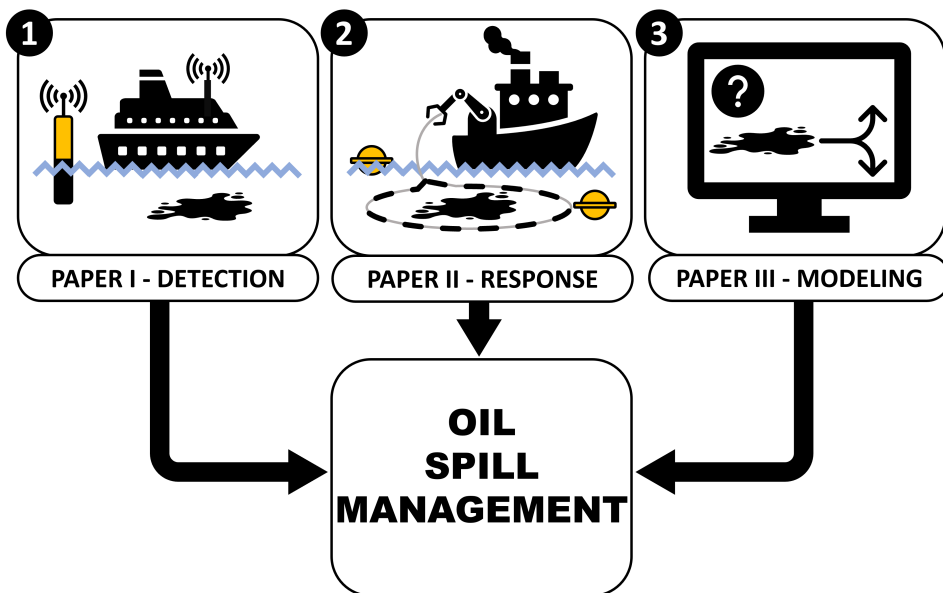


Figure 1: Conceptual overview of the thesis. This figure highlights the three key enhancements to oil spill management explored in this thesis: **1.** Validation of fluorometric sensors for oil detection and their application within flow-through systems on FerryBox and SmartBuoy platforms for real-time spill detection; **2.** Contribution to the development of a compact wave buoy, for providing real-time wave and/or drift data during oil spill response operations; **3.** Setup and validation of a particle trajectory model specifically for the eastern Baltic Sea.

3 Materials and Methods

3.1 In Situ Operational Oil Spill Detection

Fluorometric detection (FLD) is used to measure fluorescence at specific wavelengths but cannot distinguish between different hydrocarbon sources and fluorescent substances, such as crude oil versus refined petroleum products, or emissions from various combustion processes. Despite this limitation, FLD is preferred in field applications for its continuous data, rapid results, and cost efficiency compared to more detailed but complex laboratory methods like gas chromatography-mass spectrometry (GC-MS).

For the experimental study in Paper I, three commercial fluorimeters were selected, capable of measuring oil and its compounds in situ and in real time: the UviLux (Chelsea Technologies Ltd) and EnviroFlu-HC 500 (TriOS Optical Sensors), both integrated into the FerryBox system, and the C3 Submersible Fluorometer (Turner Design), utilized with the SmartBuoy. The first two sensors detect oil on the basis of the presence of polycyclic aromatic hydrocarbons (PAHs), which are present in crude oil and fossil oil-derived products. These sensors are calibrated to carbazole and phenanthrene, respectively. The Turner C3 fluorometer was equipped with three optical sensors: a hydrocarbon sensor specifically optimized for crude oil detection and calibrated with pyrenetetrasulfonic acid (PTSA), a sensor for colored dissolved organic matter (CDOM), and a turbidity sensor.

Before field deployment, all three sensors were tested in controlled laboratory settings.

3.1.1 Laboratory Testing

To assess the specificity and sensitivity of fluorometric sensors for oil detection, two distinct laboratory experiments were carried out as part of Paper I.

The initial experiment aimed to determine the sensors' ability to distinguish oil from other substances in the water of the Baltic Sea. Baltic Sea water (salinity 6.2 PSU) served as a baseline and as a solution for interference substances such as humic substances derived from decomposed plant materials, cyanobacterial algae from dried surface phytoplankton, and clay suspension from the sediment of the Baltic Sea. Additionally, water accommodated fractions (WAF) of diesel oil were prepared by mixing winter-grade diesel with seawater.

These solutions were then systematically introduced into Baltic Sea water, while the fluorescence response of the sensors to each mixture was observed. Data collected over 3- to 5-minute intervals were used to calculate the average and standard deviation of the fluorescence and the response of each fluorometer was normalized against the seawater baseline.

The second laboratory experiment focused on the persistence of diesel oil fractions in seawater and the comparability between different oil detection methods. Readings from fluorometric sensors were compared with those obtained with the HELCOM total oil monitoring protocol, and more detailed analyzes were carried out with two laboratory analytical techniques: gas chromatography with flame ionization detection (GC-FID) for aliphatic hydrocarbons and GC-MS for PAHs.

The experiment lasted three weeks. The three fluorimeters were used in a 25 liter glass aquarium filled with filtered seawater (Paper I, Figure 1) where WAF was added. Additional samples were taken at various points to analyze them according to the total oil HELCOM protocol and with GC-MS and GC-FID. The normalized responses of each method

were calculated by comparing the observed responses with those of the initial sampling point, thus establishing a consistent baseline across different time intervals and methodologies.

3.1.2 Field Testing

Second part of Paper I examined the feasibility of employing the fluorometric sensors on two different platforms for real-time detection of oil spills.

During the first field test, a FerryBox system was utilized, constructed at the Marine Systems Institute at Tallinn University of Technology (Paper I, Figure 2). The system was onboard the M/S Baltic Queen, which navigated the route connecting Tallinn, Mariehamn in Åland, and Stockholm (Figure 2). A FerryBox system is essentially a flow-through setup that draws water from a ship's inlet and circulates it through a series of sensors for real-time analysis (Petersen, 2014).

For this test, UviLux and EnviroFlu-HC sensors were integrated into the FerryBox circuit. These sensors, among others, sampled the water channeled from the vessel's sea chest, located approximately four meters beneath the surface, at a flow rate of nine liters per minute. Measurements were taken at one-minute intervals, resulting in a spatial resolution of approximately half a kilometer along the ship's route, depending on the speed of the ship. Data transmission during this setup was also done every minute, providing real-time information.

Throughout the test period, the FerryBox system, including its sensors, was maintained during four visits to the M/S Baltic Queen to ensure optimal performance and data integrity.

In the second field test, a SmartBuoy from Meritaito Ltd (Paper I, Figure 5) was used. This platform combines a polyethylene spar buoy with satellite and mobile communication capabilities and an array of environmental sensing instruments. Within this buoy, the Turner C3 fluorometer was positioned inside a vertical well that permits continuous exchange with the surrounding sea through an open pipeline, enabling constant water sampling at depths of 2 to 3 meters depending on the water level. The setup tracked hydrocarbon levels to detect oil spills while simultaneously measuring CDOM and water turbidity.

To guarantee the reliability of the collected data, the Turner C3 sensor was equipped with a mechanical wiper designed to clean its trio of optical lenses prior to each measurement, thus eliminating potential inaccuracies caused by residue or fouling.

The SmartBuoy system was programmed to perform measurements and transmit data every hour. It was anchored at a strategic point near the bustling maritime corridors of the Gulf of Finland and remained operational for two months. Toward the end of this period, a maintenance check was performed that included reprogramming the data logger and performing manual maintenance on the sensor suite.

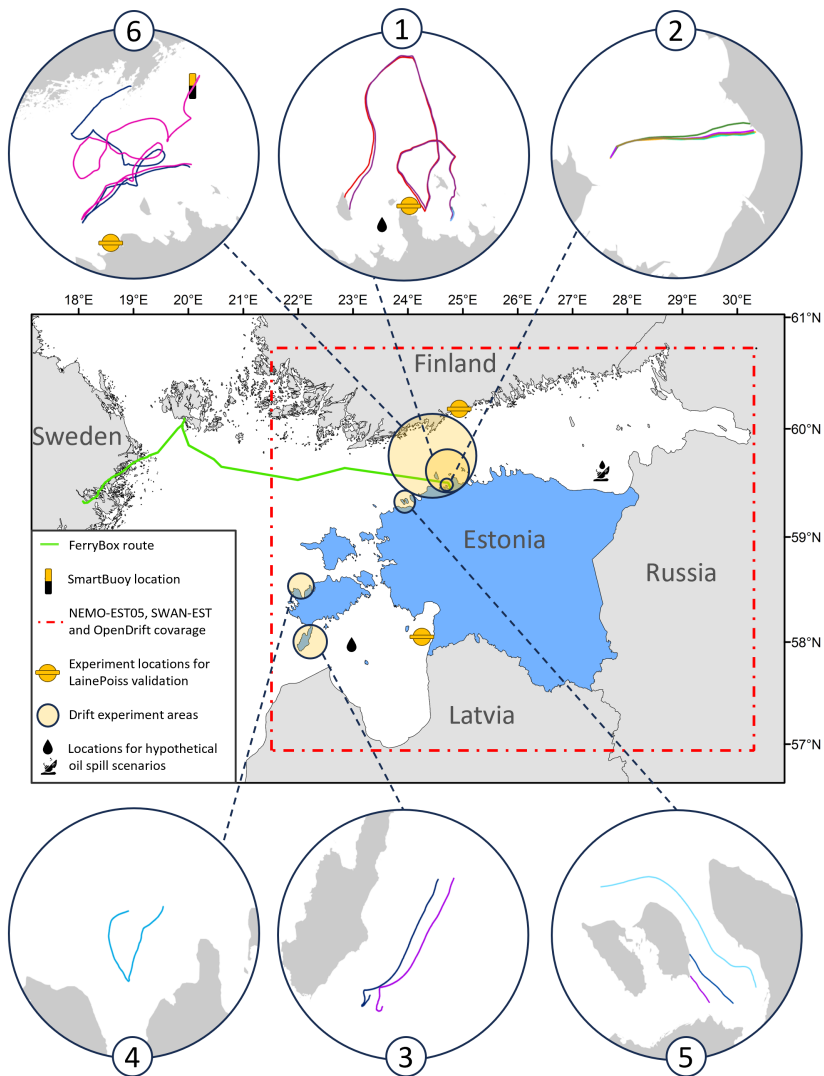


Figure 2: Map illustrating data collection sites. This map details the FerryBox route and SmartBuoy location presented in Paper I. The sites for tests and validation experiments for the LainePoiss, as outlined in Paper II, are also marked. Detailed insets showcase the drift experiment tracks from Paper III in specific areas: 1. Muuga Bay (starting point), 2. Tallinn Bay, 3. Gulf of Riga, 4. Tagalaht Bay, 5. Pakri Bay, 6. Gulf of Finland. Additionally, the map displays the coverage of the NEMO-EST05 hydrodynamic model, the SWAN-EST wave model and the OpenDrift framework, alongside the chosen sites for the hypothetical oil spill scenarios, all of which are detailed in Paper III.

3.2 LainePoiss Buoy Development

LainePoiss[®] (LP) is an accelerometer-based spherical buoy that incorporates a microelectromechanical system (MEMS) inertial measurement unit to monitor surface movements. It functions as a moored or free-floating unit, transmitting its GPS location every 22 minutes (Paper II). LP is developed with a set of key performance attributes in mind; the buoy is designed to be ice resistant, lightweight, functional, compact, and cost effective. Furthermore, the development of LP is an ongoing process, and two iterations have been created and utilized in this work.

The initial model, LP V0.1, is a 32 cm diameter and 22 cm high spherical wave buoy, weighing 3.5 kg. It is constructed from two sturdy halves made of fiberglass (Figure 3A). The more recent LP V1.0 has a slightly different and larger profile, with a diameter of 36 cm, a height of 23 cm, and a weight of 5.5 kg (Figure 3B). This version is crafted from cast plastic and includes a chain at its base.

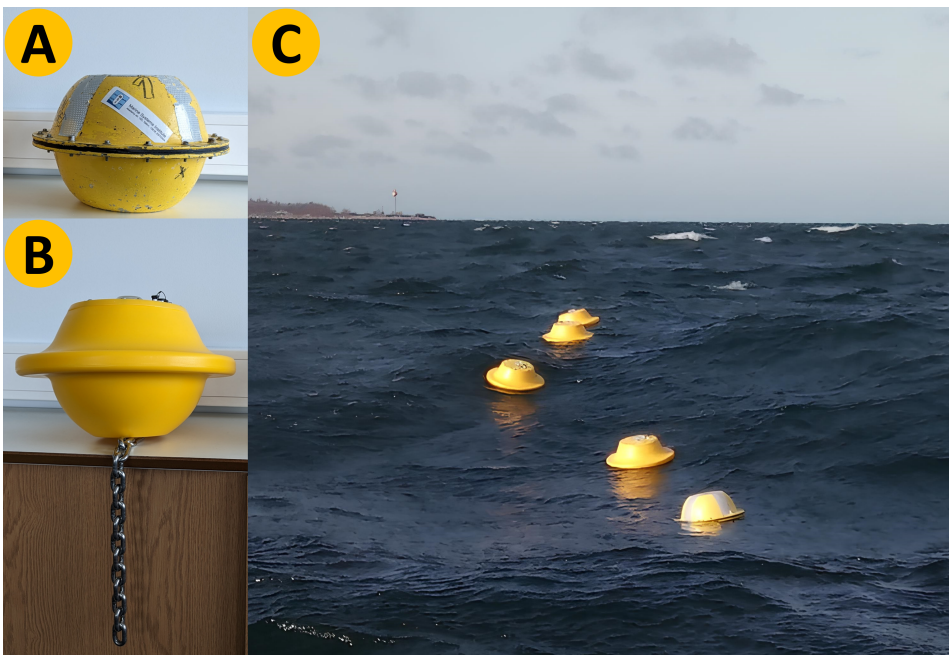


Figure 3: LainePoiss (LP) buoys. (A) is LP V0.1 and (B) LP V1.0. (C) illustrates one of the drift experiments with the buoys (Figure 2, area 2). (Modified from Paper III)

To ensure the buoy's accuracy and reliability for measuring wave parameters in diverse marine environments, LP underwent a comprehensive validation process that included sensor testing, wave tank experiments, field validation against a Directional Waverider (DWR-Mk III), and field measurements conducted in the Baltic Sea's marginal ice zone. Furthermore, experiments with the deployment of the buoy were conducted using an unmanned aerial vehicle (UAV), providing information for the subsequent development of detailed deployment protocols.

3.2.1 Wind drift factor

In trajectory modeling, the "wind drift factor" (WDF) or "wind drag coefficient" quantifies the extent to which objects or substances are influenced by the wind. It describes the

statistical relationship between wind and surface drift vectors and is represented as a fraction of the wind speed. The surface drift vector can be observed or modeled. The WDF value depends on several factors, including the location of the observation, the length of the averaging window, and the statistical procedures applied.

Accurately estimating the WDF for the LP buoys and incorporating it into trajectory models helps improve the interpretation and comparison of a model's accuracy. Furthermore, a comparison of the WDFs of the buoys with those used in oil spill modeling validates their utility as proxies for oil in trajectory studies and confirms their effectiveness in spill track monitoring. Therefore, part of the research in Paper III was the determination of the WDFs for the two versions of the LP buoy. This involved simulating 11 different trajectories for each segment with varying WDFs, ranging from 0% to 5% of the wind speed (Figure 4A). To account for the possibility that not all forcing models may always be available, these trajectories were simulated under different scenarios. First, the simulated drifters were driven by wind alone. Next, a combination of wind and currents was used, followed by wind with Stokes drift. Finally, a comprehensive scenario was used that incorporates all these forcings to model the trajectories. The simulated paths were compared with the actual drift experiment trajectories carried out along the Estonian coast (Figure 2), from which the best-fit trajectories and their corresponding WDFs were determined.

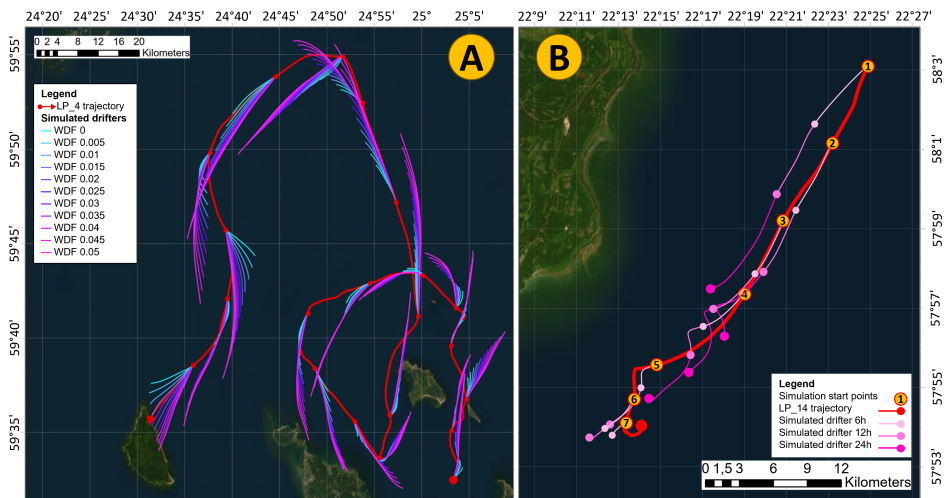


Figure 4: (A) illustrates the estimation of the WDF for the LP. The example is based on the trajectory of LP_4 in Muuga Bay (as shown in Fig. 1, area 1) and displays a series of simulated trajectories over 6-hour intervals with varying WDFs ranging from 0% to 5%. The simulations were forced with wind, currents, and Stokes drift and the model is reset and rerun at 6-hour intervals. (B) demonstrates the evaluation of the accuracy of the setup of the drift model. Here an example of these simulations, specifically the LP_14 track in the Gulf of Riga, along with the corresponding 6-h, 12-h, and 24-h trajectory simulations are presented. (Modified from Paper III)

3.3 Utilizing the OpenDrift Framework for Drift Analysis and Oil Spill Simulation

The OpenDrift framework, created by Dagestad et al. (2018), is a comprehensive open-source platform for simulating the movement and eventual outcomes of drifting substances or objects in marine environments. This tool comprises several specialized mod-

ules, such as OpenOil (Röhrs et al., 2018) for oil drift modeling, each sharing core functionalities; therefore, the validation of one module effectively validates all.

For optimal performance, OpenDrift and its associated modules rely on data from marine and atmospheric models. In this implementation, wind data (speed and direction) was sourced from ECMWF (European Centre for Medium-Range Weather Forecasts) (Owens and Hewson, 2018), complemented by high-resolution (0.5 nmi) local oceanographic models NEMO-EST05 (Maljutenko et al., 2022) for current information (speed and direction) and the SWAN-EST wave model based on SWAN (Booij et al., 1999; Ris et al., 1999) for wave parameters (direction, significant wave height, Stokes drift, wave period).

In 2022, within the framework of Paper III, six drift experiments were carried out, lasting from a few hours to ten days, in regions prone to oil pollution, including areas with heavy maritime traffic and sheltering areas for ships (Figure 2 and Figure 3C). These experiments were aimed at collecting empirical data to validate the drift model.

To estimate the WDF for the LPs and evaluate the trajectory simulation performance of the model, the Normalized Cumulative Lagrangian Separation (NCLS) proposed by Liu and Weisberg (2011) was used. The metric has gained widespread recognition for evaluating trajectory models in different applications, including oil spill and search and rescue models (e.g. Ivichev et al., 2012; De Dominicis et al., 2014; French-McCay et al., 2017; Pereiro et al., 2018; de Aguiar et al., 2022).

This skill score (SS) assesses the divergence of the drifter and model trajectories over their entire paths, normalized by the total length of the path:

$$SS = \begin{cases} 1 - \frac{s}{n} & \text{if } s \leq n \\ 0 & \text{if } s > n, \end{cases}$$

where s is the cumulative Lagrangian separation distance normalized by the associated cumulative observed trajectory length, and n is the tolerance threshold, which was established at 1, following the suggestions of Liu and Weisberg (2011). This implies that the cumulative separation distance should not exceed the total length of the drifter trajectory. A higher SS value indicates a more accurate model performance, with $SS = 1$ denoting an ideal match between observation and simulation, while $SS = 0$ suggests that model simulations lack predictive accuracy.

The cumulative Lagrangian separation distance, s , is calculated as the sum of the Lagrangian separation distances at each time step along the simulated trajectories, normalized by the total length of the observed trajectories:

$$s = \frac{\sum_{t=1}^N d(t)}{L},$$

where N is the total number of time steps, $d(t)$ is the Lagrangian separation distance at time step t , and L is the total length of observed trajectories.

Focusing on oil spill simulation, the OpenOil module within OpenDrift was used to model the drift and evolution of oil spills. To enhance the precision of the results, a range of supplementary variables from the NEMO-EST05 and SWAN-EST models, which affect oil weathering and transport were incorporated. These variables included seawater temperature, salinity, water depth, upward seawater velocity, vertical diffusivity, sea ice fraction, and mean and peak wave periods. To simulate hypothetical oil spills, a scenario was used, involving 10 m^3 of a generic heavy fuel oil type, represented in the model by 1000 particles.

4 Results and Discussion

4.1 Assessing the Oil-Specific Fluorometers

The line plot in Figure 5 illustrates the fluorescence responses of the sensors to each combination of interference solution, normalized to baseline seawater. The different treatment combinations are categorized horizontally. All sensors exhibited a response to the addition of these solutions. The introduction of suspended clay resulted in a slight attenuation of the fluorescence signal in Turner C3 and Enviroflu-HC, but a slight increase in UviLux (Figure 5, series I, S vs. SC). This effect was similar when clay was added to a seawater-WAF solution, with changes in signal intensity that did not exceed 12% (Figure 5, series IV, SW vs. SWC). The sensors were even more sensitive to extracts of humic substances, which increased the signals by 1.05 to 1.8 times across all sensors, with the most significant response observed in Turner C3 (Figure 5). The addition of algae extract had the most pronounced effect, significantly enhancing the fluorescence signal in all scenarios (Figure 5). This suggests that the presence of algae could significantly interfere with the sensors' ability to detect oil compounds in water, with enhancements ranging from 3 to 8 times when added to seawater, and from 2 to 3 times in the seawater-WAF solution (Paper I).

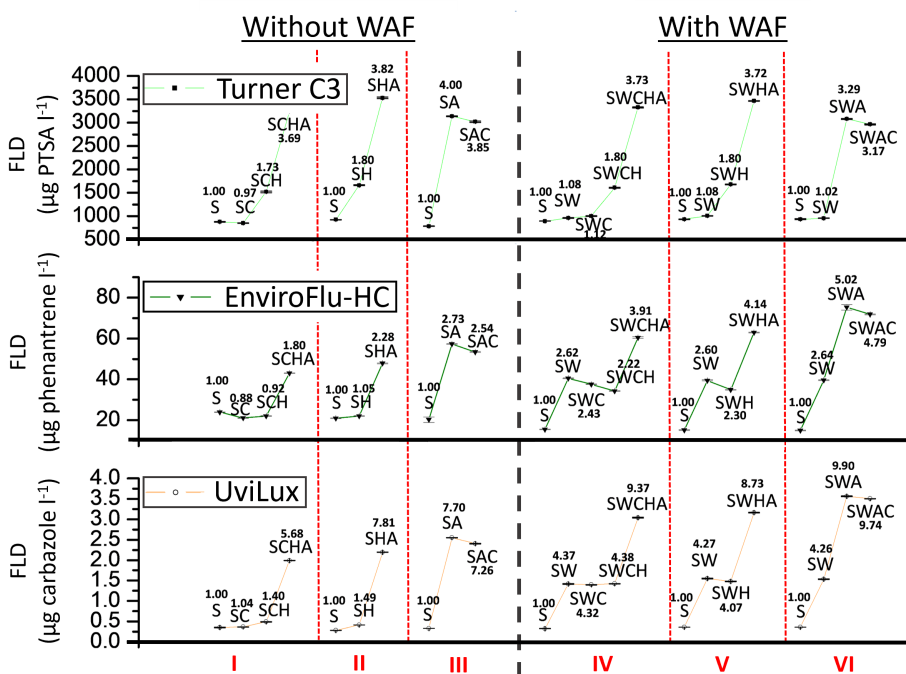


Figure 5: Fluorescence responses from Turner C3 (upper panel), EnviroFlu-HC (middle panel) and UviLux (lower panel) sensors in seawater (S), seawater containing interferences of clay (I), humic substances (II), algae substances (III), and seawater containing diesel WAF (SW) with and without the interferences (IV-VI). S = seawater, C = clay suspension, H = humic substance extract, A = cyanobacterial algae extract, and W = water accommodated fraction (diesel fuel extracted in seawater). The change in FLD response respective to the baseline (S) value in each series (e.g. in series I, S-SC-SCH-SCHA) is indicated adjacent to each treatment. Treatment series are separated with dotted red line and marked with red roman numerals. (Modified from Paper I)

The interference of other compounds in seawater with oil-related fluorescence was also confirmed by the strong correlation between hydrocarbon fluorescence and CDOM fluorescence observed during the field test (Paper I, Figure 9D).

These results of Paper I also align with findings from other studies that highlight how various fluorescent substances in seawater can significantly impact the measurement of petroleum hydrocarbons (Henry et al., 1999; Bugden et al., 2008; Tedetti et al., 2010; Cyr et al., 2019). The Baltic Sea experiences extensive phytoplankton blooms in spring and summer, potentially causing further interference. Although cyanobacterial blooms in summer and the persistent presence of chlorophylls and phycocyanin from phytoplankton could suggest significant interference, this was not observed during the FerryBox experiment. Despite the peak of a spring bloom that coincided with the end of the experiment in 2018 (Almén and Tamelander, 2020), there was no noticeable increase in fluorescence signals that would indicate a magnifying effect of phytoplankton.

Taking these results into account, the Baltic Sea, known for its high concentrations of CDOM and its generally turbid waters, presents particularly challenging conditions for such fluorometers.

The WAF persistence experiment indicates that chemical traces of diesel fuel persist in seawater for at least 20 days, resulting in varying degrees of response from the portable sensors during that period (Paper I, Figure 7). Sensor responses during the experiment were compared with nine samples analyzed using the HELCOM reference method, with the final sample carried out on day 11 of the experiment (Paper I, Figure 7). The temporal changes in the responses observed using the EnviroFlu-HC and UviLux sensors were consistent with the HELCOM method. The Turner C3 sensor showed a gradual increase in fluorescence from the 100th hour, while the signals from the EnviroFlu-HC and UviLux sensors decreased and stabilized.

Several overarching challenges arise when employing fluorometers to detect and estimate the relative concentrations of oil compounds in water. Typically, fluorometers are calibrated with a particular type of oil or specific compounds, which means that the concentration readings they provide are only relative to that specific oil or compound and the calibration method used (Lambert et al., 2003). Furthermore, a fluorometer's reaction to oil varies greatly depending on the oil's composition and its degree of weathering, which adds complexity to accurately quantifying oil concentration (Henry et al., 1999). Additionally, for a meaningful comparison between different sensors, a standardized unit of measurement is required to report FLD-derived results (Paper I).

4.2 Assessing In Situ Platforms and Sensor Efficacy for Real-Time Oil Spill Detection

During a two-month period (February 21 to April 21, 2018) of the FerryBox experiment that involved 58 ship voyages, the system successfully transmitted real-time data, despite occasional GSM network-induced data gaps in the Baltic Proper. The system, which included UviLux and EnviroFlu-HC fluorometers, showed PAH values ranging from 1 to 2.6 µg carbazole/l and 12.4–25.5 µg phenantrene/l, respectively (Figure 6). In particular, lower PAH levels were detected near Åland, with higher values in the Stockholm archipelago, suggesting an influence of organic carbon from river water (Figure 6).

During the SmartBuoy experiment, which also lasted two months (October 25 to December 24, 2018), the integrated Turner C3 sensor recorded values that fluctuated between 790 and 1250 µg PTSA/l (Figure 6), closely mirroring the variation patterns in the levels of CDOM, which ranged from 600 to 890 µg quinine sulfate per liter (Paper I, Figure 9D). Additionally, the correlation between hydrocarbon data and CDOM values was found

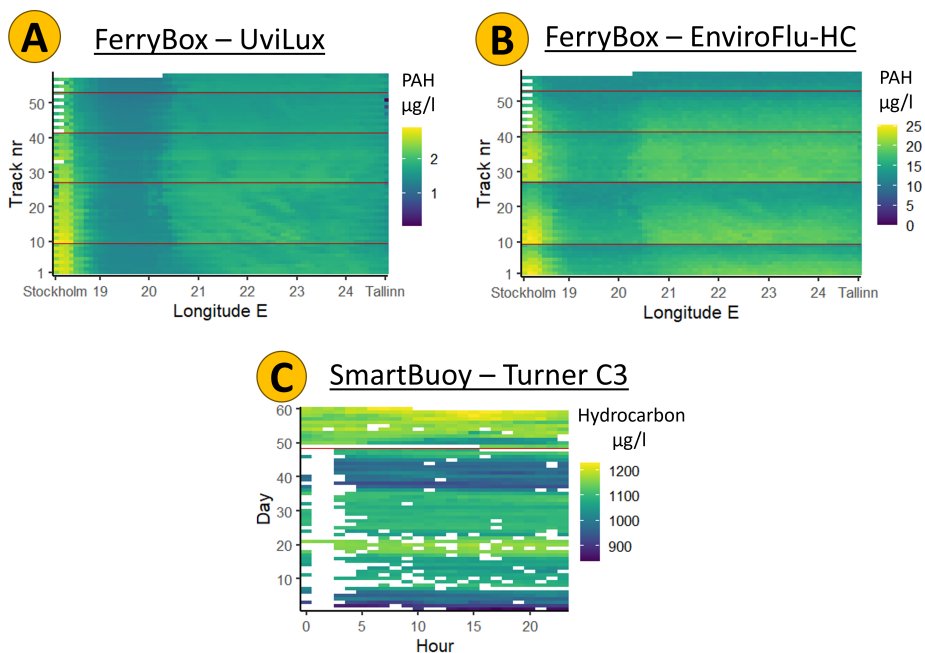


Figure 6: Heatmap plots showing spatiotemporal distributions of PAH signals in seawater along the ship track between Stockholm and Tallinn (February 21 to April 21, 2018) measured with the UviLux (A) and EnviroFlu-HC (B) fluorometric sensors. Accompanied by a separate temporal heatmap depicting hydrocarbon data collected by the Turner C3 sensor (C) on SmartBuoy from October 25 to December 24, 2018. Red lines across the heatmaps denote periods of system maintenance. (Modified from Paper I)

to be significantly high (Paper I, Figure 9D). There were no abnormal spikes in measured hydrocarbon levels suggestive of oil contamination throughout the testing period.

It is inferred that the values detected by the sensors probably do not represent the actual concentrations of PAHs or oil in seawater. This assertion is reinforced by chemical monitoring and analyses of the Baltic Sea, which report that oil hydrocarbon concentrations are typically below 1 µg/l (Pikkarainen and Lemponen, 2005; FIMR, 2007), which is characteristic of seawater without significant oil contamination (Bícego et al., 1996; Zanardi et al., 1999).

Taking into account the natural dispersion of oil as a result of environmental factors, which can distribute oil droplets deeper into the water column, the depth becomes a significant variable in the effective detection of oil spills with such platforms. The use of FerryBox and SmartBuoy oil sensors at depths of approximately 2-4 meters aligns with previous research indicating that these levels are suitable for the detection of dispersed oils (Cormack and Nichols, 1977; Lichtenthaler and Daling, 1983, 1985) (Paper I). Although the study's sensor depths were deemed appropriate for detecting fluorescence anomalies, future designs might benefit from positioning sensors even closer to the surface to enhance detection chances. It should be noted that, in addition, weather conditions, spill size, oil type, and weathering state can have an effect on determining the likelihood of detecting oil spills.

Another notable finding from Paper I was the impact of biofouling on data quality. Biofouling, influenced by various environmental factors, notably affected FerryBox sen-

sors, particularly the EnviroFlu-HC, despite regular cleaning and maintenance (Figure 6). However, the automatic cleaning mechanism of the Turner C3 sensor on SmartBuoy effectively mitigated these effects, maintaining high data integrity. This observation highlights the importance of considering biofouling in long-term aquatic monitoring and the need for effective antifouling strategies.

It is important to acknowledge that these experiments were conducted under the specific conditions of the Baltic Sea, which might limit their direct applicability to other marine environments. However, the innovative FerryBox method introduced in Paper I has been successfully applied to detect the transport of river-induced crude oil seeps into the Strait of Magellan in southern Patagonia (Giesecke et al., 2024), proving the concept and suggesting the potential for broader utility.

Once these systems demonstrate consistent reliability in oil detection, the establishment of an extensive network of SmartBuoys and FerryBoxes across major shipping routes can significantly improve current oil spill monitoring strategies. This network would serve as a valuable supplement to existing methods such as aerial surveillance, ship-based observations, and satellite monitoring. By covering critical transit areas or high-risk locations like potentially polluting shipwrecks, these additional in situ monitoring tools can provide more frequent data, contributing to a more robust and comprehensive approach to oil spill detection. This expanded coverage would aid in the early identification of spills and support ongoing monitoring efforts, ensuring a rapid and informed response to minimize environmental impact. Integrating these technologies would represent a significant step forward in maritime safety and environmental protection, particularly in busy shipping routes and ecologically sensitive areas.

4.3 Enhancing Oil Spill Response with LainePoiss Buoy Technology

In an oil spill response effort, wave data at the site is important as it enhances situational awareness, aids in forecasting oil drift, and assists in executing containment and cleanup strategies.

In field tests, LP's wave measurements closely matched those of a nearby Directional Waverider. Specifically, the wave height (H_{m0}) showed a minimal bias of 0.01 meters, with a high correlation of 0.99 and a scatter index of 8% (Paper II, Table 5). Similarly, the mean wave period (T_{m01}) had a slight bias of 0.08 seconds, a correlation of 0.98, and a scatter index of 3%. The mean absolute deviation of the wave direction was 7 degrees (Paper II, Table 5).

Further experiments described in Paper II showed that LP was highly effective in identifying the high-frequency elements of the wave spectrum (up to 1.28 Hz, around a 1 m wavelength), and matched well with the measurements from a wave gauge in a controlled wave tank environment. In the field, LP's wave spectrum was validated up to the Waverider's cutoff frequency of 0.58 Hz. LP's ability to measure such short waves fills a gap in routine wave measurements, which often do not capture waves shorter than 0.5–0.6 Hz. These shorter waves are crucial to understanding sea-atmosphere processes, contributing significantly to phenomena such as Stokes drift and wave-induced stress, which in turn influence object and oil drift, surface turbulence, and sea-atmosphere fluxes, including CO₂ (Janssen, 1991; Mueller and Veron, 2009; Lenain and Pizzo, 2020).

LPs also showed great ability to measure waves within ice, detecting significant wave heights as low as 1 cm. This was demonstrated in a month-long experiment in the Baltic Sea, where several LP units were deployed amidst ice.

The WDF represents the fraction of wind speed that influences the drifter's movement. Skill scores were calculated and the corresponding WDFs estimated for two versions of the

LP buoys over various track lengths (6, 12, and 24 hours) and under different environmental forcing scenarios. The WDF for each LP version was determined by averaging across all model runs and time intervals.

For LP V0.1, the WDFs were found to be 2% with the inclusion of wind, currents, and Stokes drift, and 3.3% when excluding Stokes drift. The LP V1.0, which features a bottom chain and minor design variations, exhibited a WDF of 1.5% with Stokes drift and 2.1% without it.

The WDFs for LP buoys are broadly consistent with the findings for other similar buoy designs (Röhrs and Christensen, 2015; Pisano et al., 2016; Brekke et al., 2021), considering differences in buoy construction, estimation methods, data variability, model selection, and regional disparities. The streamlined design of LP V1.0, combined with its bottom chain that functions similarly to a drogue, reduces its susceptibility to wind and Stokes drift while increasing its dependence on currents. These design features resulted in lower wind drift factors, matching more closely with the WDFs reported for near-surface drifters (e.g. Sutherland et al., 2020; Delpeche-Ellmann et al., 2021; Pärn et al., 2023). Furthermore, the WDFs for the LPs show a significant similarity to those documented for oil, especially in the case of LP V0.1. ASCE (1996) report drift speeds that vary from 2.5% to 4.4% of the wind speed, with a typical value between 3 and 3.5%. Moreover, Jones et al. (2016) and Brekke et al. (2021) have identified a WDF of 2% when the Stokes drift is considered separately. In scenarios where only wind forcing was used, Reed et al. (1994) and Schwartzberg (1971) found WDFs of 3% and 3.7%, respectively. This relationship increases confidence in using LP data for oil spill modeling and emphasizes their suitability as tracking buoys in oil spill response operations.

Tracking functionality becomes particularly crucial in the context of marine oil spill containment, where preventing spills from reaching the land is a primary mitigation goal. Addressing spills at sea is typically more manageable, cost-effective and efficient compared to onshore cleanup efforts (Etkin, 2000; Ventikos et al., 2004; Etkin and Nedwed, 2021). Therefore, precise monitoring and forecasting of ocean surface movements is vital for effective and proactive response strategies. Although traditional methods such as ships, aircraft, and satellite remote sensing can detect oil slicks, they are not always immediately accessible and their effectiveness is diminished during the night or under cloudy conditions. In such scenarios, drifters like LP play a pivotal role. Deployable either aerially or by means of a vessel into an oil slick, they autonomously transmit their location, offering continuous monitoring and vital real-time information, thus significantly improving response capabilities to an oil spill (e.g. Woodbury et al., 2010; Senga et al., 2014; Yu et al., 2018). The lightweight design of the LP significantly enhances its utility in such applications, as it can be deployed as a drifter up to a distance of at least 2 kilometers using an UAV (Paper II, Figure 1A) as demonstrated by three separate experiments (Paper II).

Effective containment and remediation of relatively small marine oil spills is achieved primarily by using booms and mechanical skimmers (Dave and Ghaly, 2011; Li et al., 2016; National Academies of Sciences, 2022). However, their performance is optimal in calm waters and decreases significantly with increasing wave height and decreasing wave period (Fang and Johnston, 2001; Ventikos et al., 2004; Prendergast and Gschwend, 2014). Currently, the market offers a range of buoy devices, such as Datawell Waveriders, equipped with sensors that remotely transmit wave data (e.g. Raghukumar et al., 2019; Saetre et al., 2023). However, many of these wave buoys require specialized handling due to their size and mooring needs. In response, there is a global trend toward developing compact buoys capable of detailed wave characteristic measurements, such as LP. These buoys are designed to be more versatile and less dependent on specialized equipment (e.g. Raghuku-

mar et al., 2019; Zong et al., 2019; Farber et al., 2019; Carandell et al., 2020; Rabault et al., 2022). The in-depth wave data provided by devices like LP improve situational awareness during oil spill responses and contribute to the efficiency of mechanical skimming operations (Skinner et al., 2018).

4.4 Validation of the Opendrift Setup

To assess the accuracy of the drift model setup, the estimated WDF values for the LP buoys were incorporated and simulations with identical track lengths and environmental forces were rerun (Figure 4B) (Paper III). To evaluate the performance of the model in different forcing scenarios, weighted average skill scores were used.

For the LP V0.1 buoys, which are more influenced by wind drag, significantly higher overall skill scores ranging between 0.63 and 0.66 were observed, indicating better predictability of the wind model (Table 1). This high accuracy was particularly evident when wind, currents, and Stokes drift were combined. In contrast, LP V1.0 buoys demonstrated moderate forecast accuracy, with skill scores ranging from 0.38 to 0.43 (Table 1). Skill scores for LP V1.0 varied significantly across different simulations, with the highest scores recorded in Tallinn Bay (Table 1 and Figure 2, area 2). Low skill scores in the Gulf of Finland simulations (Table 1) can be linked to the complex and dynamic hydrometeorological conditions experienced during and after stormy events, which presents challenges in capturing accurate data even with high-resolution models.

Table 1: Mean skill scores (SS) for 6-hour forecast period, calculated using various combinations of environmental forcings and the wind drift factor (WDF) estimates for each forcing combination. (Modified from Paper II)

	Wind	Wind+Stokes drift	Wind+Currents	Wind+Currents+Stokes drift
LP V0.1				
Muuga Bay LP_3	0.64	0.63	0.65	0.67
Muuga Bay_4	0.64	0.63	0.63	0.65
Number of runs	42	42	41	41
Mean of SSs	0.64	0.63	0.64	0.66
Weighted average SS	0.64	0.63	0.64	0.66
LP V1.0				
Gulf of Riga LP_13	0.39	0.47	0.62	0.66
Gulf of Riga LP_14	0.39	0.44	0.58	0.58
Tagalaht Bay LP_17	0.44	0.44	0.36	0.35
Pakri Bay LP_13	0.61	0.59	0.53	0.55
Pakri Bay LP_14	0.52	0.50	0.57	0.53
Gulf of Finland LP_16	0.35	0.35	0.38	0.37
Gulf of Finland LP_17	0.34	0.34	0.37	0.37
Tallinn Bay LP_7	0.72	0.77	0.73	0.78
Tallinn Bay LP_9	0.74	0.80	0.75	0.81
Tallinn Bay LP_10	0.71	0.77	0.73	0.78
Tallinn Bay LP_11	0.72	0.84	0.74	0.85
Number of runs	96	97	97	96
Mean of SSs	0.54	0.57	0.58	0.60
Weighted average SS	0.38	0.40	0.43	0.43

Throughout the simulations presented in Table 1, the LP V0.1 buoys consistently achieved high skill scores. In particular, using only wind as a forcing factor resulted in a skill score

of 0.64. The introduction of currents as an additional factor did not have any effect on the score. However, when Stokes drift was the sole additional forcing, the skill score decreased slightly to 0.63. Interestingly, the combination of currents and Stokes drift improved the skill score to 0.66. This pattern suggests that the impact of environmental forcing on the buoys' movement is complex and interactive (Paper III).

The results of Paper III also highlighted the importance of using consistent wind data across different models to minimize errors and improve the reliability of the predictions. Using the same ECMWF wind fields to drive the currents in the NEMO-EST05 model, the waves in the SWAN-EST model, and in the OpenDrift simulations, a coherent and synchronized representation of environmental conditions was achieved, enhancing the accuracy of the drift trajectory predictions.

Using an open-source modeling framework that incorporates local high-resolution models for wind and currents specifically for the Estonian sea area presents distinct benefits over more generalized models applied across the entire Baltic Sea. The transparency and adaptability afforded by an open-source framework enable a more customized approach to spill simulations, better reflecting the environmental and hydrodynamic conditions of the area. Local high-resolution models are more capable of capturing the complexities of coastal dynamics, small-scale weather events, and sea surface conditions, crucial for precise oil spill forecasting. This higher level of detail can ensure that response strategies are based on the most accurate and relevant data, facilitating more effective containment, cleanup efforts, and environmental protection.

4.5 Hypothetical Oil Spill Scenarios in the Estonian Sea Area

In the scope of Paper III, three hypothetical oil spill case studies were conducted in three locations with a high probability of oil spills, including two surface spills and one seabed spill from a shipwreck, all initiated during a storm event in December 2022. This period was chosen because it coincided with the sixth drifter experiment. The simulations were started on December 12, 2022, at 00:00 UTC, and the models were run for a duration of 96 hours.

The spill at the first site, Tallinn Bay, which is part of one of the world's busiest maritime routes between Tallinn and Helsinki (Tapaninen and Palu, 2022), experienced rapid oil dispersion. Within an hour, half of the oil was submerged or dispersed, and by 12 hours, most of it had reached the shoreline, although it represented only a small fraction of the total mass (Figure 7). The second site, a future wind energy park in the Gulf of Riga (Estonian Ministry of Finance and Hendrikson & Ko, 2021), saw 75% of the oil submerged or dispersed within an hour due to severe weather conditions (Figure 7). The third scenario was a potentially polluting WWII shipwreck, the German Destroyer T-22, in Narva Bay (Treffner, 2019). Here, most of the oil remained submerged and a small amount surfaced briefly before dispersing (Figure 7).

These scenarios highlight the rapid dispersion and dynamics of oil spills under intricate environmental conditions, emphasizing the importance of immediate response action, as addressing spills at sea is easier and less costly than managing shoreline contamination (Etkin, 2000; Ventikos et al., 2004). The Tallinn Bay spill demonstrated the significant impact of the proximity of the spill to the shore on the likelihood of oil stranding, underlining the vulnerability of the Baltic Sea due to its short distances from potential spill sites to the coastlines.

Although the Narva Bay scenario focused on a solitary spill incident, it is common for polluting shipwrecks to continuously leak oil, leading to persistent contamination and complex response requirements (Gilbert et al., 2003; Daniel et al., 2020). These situations

necessitate prolonged monitoring and the development of adaptable response strategies, especially given the potential for long-term ecological consequences (Hampton et al., 2003).

Severe weather conditions during the simulations demonstrated the importance of considering weather in spill response planning. Adverse conditions can complicate containment and cleanup efforts, making it essential to plan appropriate response measures even in challenging circumstances (Nordvik, 1995; Robertson et al., 2017).

Furthermore, oil-ice interactions are also part of OpenOil, and oil drift can be influenced by ice drift when ice concentrations exceed 30% (de Aguiar et al., 2022). Although the ice concentration at the hypothetical spill sites was below the threshold, this feature enhances the operational applicability of the model and provides new opportunities for further research.

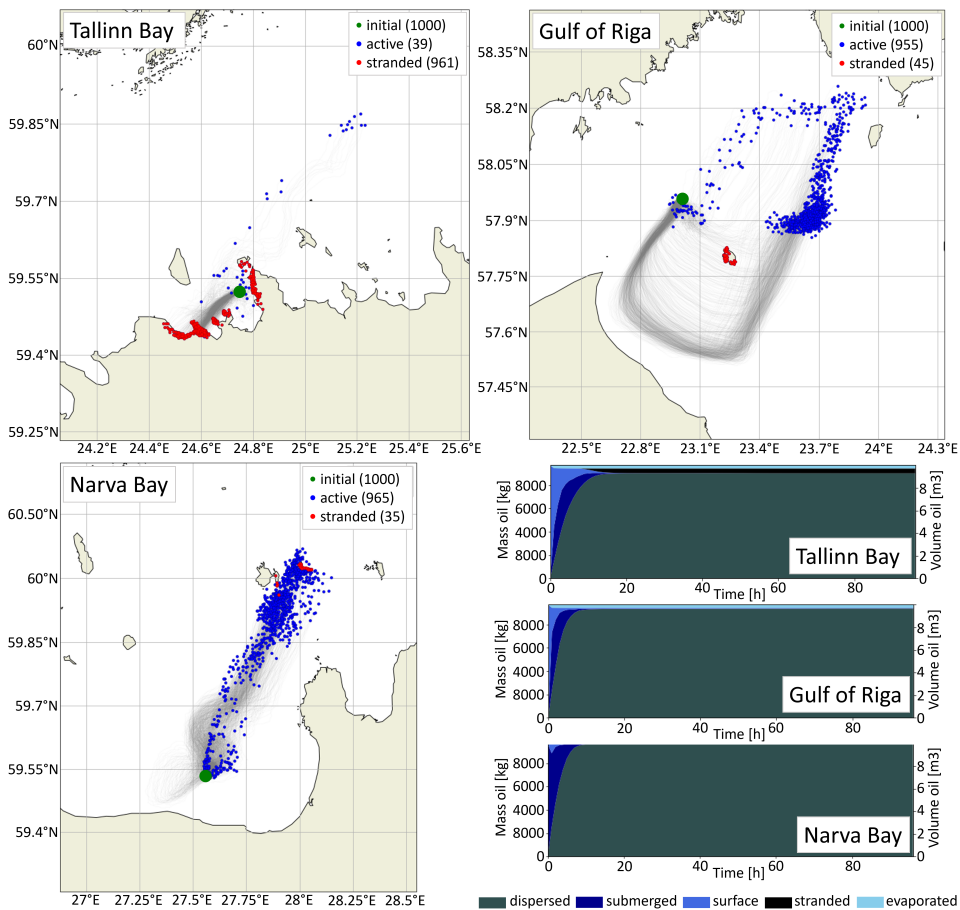


Figure 7: Modeling outcomes for hypothetical oil spill scenarios in three different locations: Tallinn Bay (surface spill), Gulf of Riga (surface spill), and Narva Bay (seafloor spill). The green circle marks the initial location of the spill, the blue particles represent the spread of oil in the water, and the red particles represent oil that has reached the shorelines. The trajectories of the spills are traced with gray lines. Displayed are only the final steps of these simulations. The accompanying graphs in the lower right corner illustrate the change in oil mass and volume throughout the scenarios. (Modified from Paper III)

5 Conclusions

This thesis is dedicated to enhancing the techniques and tools integral to oil spill management within the unique and challenging context of the Baltic Sea. Recognizing the multifaceted nature of oil spill incidents, the research carried out in this work addresses the critical components required for effective management at different stages of an oil spill. From initial detection to the final stages of response and recovery, this work aims to refine existing methodologies and introduce innovative solutions to better prepare, identify, and mitigate the impacts of oil spills in this sensitive marine environment.

Oil spills in the Baltic Sea present distinct challenges due to its ecological significance, busy shipping lanes, and unique hydrodynamic conditions. Consequently, effective management of such incidents requires a comprehensive approach that focuses on immediate response, proactive planning, and general preparedness. Therefore, this study investigates improvements to existing practices and examines new areas in oil spill management, with the goal of enhancing the region's ability to respond promptly and efficiently to these environmental threats.

The research presented in this thesis is structured to reflect key aspects of oil spill management, starting with detection, proceeding to response, and ultimately focusing on predictive modeling. Each part contributes uniquely to the overarching goal of improving oil spill management in the Baltic Sea. In the following sections, the specific contributions and findings of each part of the thesis are detailed.

The first part of this work highlights the importance of real-time and in situ oil spill detection.

- The selectivity and sensitivity of three commercially available fluorometric sensors designed for in situ, real-time oil quantification were evaluated. Laboratory experiments revealed that fluorescent compounds from diesel oil can persist in Baltic Sea water and elicit responses from portable fluorometric sensors for at least 20 days. However, challenges with specificity due to interference from other substances such as humic materials and phytoplankton were noted, indicating a need for further advances in sensor technology or analytical approaches.
- Fluorometric sensors were successfully integrated into the FerryBox and SmartBuoy systems for real-time oil spill detection. The semi-autonomous functioning and real-time data transmission capabilities of these systems demonstrated their potential in early spill detection and ongoing monitoring. Despite the challenge posed by the interference substances in the seawater, this novel approach offers a promising option to improving spill detection accuracy and efficiency in the Baltic Sea and other sea areas.

The second part of the thesis contributed to the development of a compact and durable wave buoy, LainePoiss (LP), which is capable of providing crucial real-time wave data during oil spill response operations.

- Experiments and field tests confirmed that LP's wave measurements were highly accurate. The wave measurements from LP closely matched those from an adjacent Directional Waverider, with the wave height (H_{m0}) showing a negligible bias of 0.01 meters and a correlation coefficient of 0.99, and the mean wave period (T_{m01}) exhibiting a minor bias of 0.08 seconds and a correlation of 0.98.

The accuracy of LP and its capability to detect high-frequency wave spectra (up to 1.28 Hz, roughly 1 m wavelength) are important for comprehending the sea-atmosphere interactions that affect oil drift and surface turbulence.

- The effectiveness of the LP buoy as a tracking device in oil spill response operations and as a proxy for oil in spill research was successfully evaluated. Wind drift factors (WDFs) determined through drift experiments were 2% for the LP V0.1, considering wind, currents, and Stokes drift, and 3.3% when Stokes drift was not included. The LP V1.0, which includes a bottom chain and slight design changes, showed a WDF of 1.5% with Stokes drift and 2.1% without Stokes drift. The approximate alignment of these WDFs with those reported for oil shows the reliability of the LP's in providing essential data for oil spill trajectory modeling and supporting overall response efforts.

The versatility of LP as both a wave measurement instrument and a tracking device makes it a valuable tool in the arsenal of oil spill management technologies. The experiments involving an UAV (Unmanned Aerial Vehicle) showed that LP is sufficiently lightweight and robust to be deployed as a drifter for distances of at least 2 kilometers, adding even more adaptability to its application.

The third part of this work involved the implementation and validation of the OpenDrift framework in the eastern Baltic Sea waters.

- OpenDrift simulations, forced by local high-resolution hydrodynamic and wave models, were validated with data from drift experiments. Weighted average skill scores (SS) for 6-hour forecast ranged between 0.38 and 0.66, influenced by the buoy version and the combinations of forces applied. The findings showed the importance of considering multiple environmental forces, beyond just wind, to improve model accuracy.
- Modeling hypothetical oil spills in areas prone to such incidents, particularly during adverse weather conditions, highlighted the importance of preparedness and rapid response. The scenarios demonstrated how swiftly oil can disperse and the varying impacts based on the location of the spill and the environmental conditions. These findings stress the critical need for efficient and timely response strategies and robust predictive modeling to effectively mitigate the effects of potential spills.

In conclusion, the research conducted in this thesis considerably advances the management of oil spills in the Baltic Sea. It showcases the effectiveness of integrated technologies, ranging from sophisticated detection systems to comprehensive predictive modeling tools, in bolstering preparedness and contributing to improving response strategies. This work underscores the importance of developing and implementing innovative solutions that can effectively serve both research and operational needs in the field of oil spill response and marine environmental protection. These efforts, combined with continuous innovation and collaboration, are vital in protecting marine environments from the adverse effects of oil spills.

To advance this research, the more established concepts of LainePoiss and OpenDrift could be used during an actual oil spill response operation. In addition, OpenDrift could be utilized to assess risk areas for spills originating from potentially polluting wrecks and offshore construction activities.

References

- Aamo, O.M., Reed, M., Downing, K., 2005. Oil spill contingency and response (OSCAR) model system: Sensitivity studies. 2005 International Oil Spill Conference, IOSC 2005 , 5486–5495. doi:10.7901/2169-3358-1997-1-429.
- de Aguiar, V., Dagestad, K.F., Hole, L.R., Barthel, K., 2022. Quantitative assessment of two oil-in-ice surface drift algorithms. *Marine Pollution Bulletin* 175, 113393. doi:10.1016/j.marpolbul.2022.113393.
- Al-Ruzouq, R., Gibril, M.B.A., Shanableh, A., Kais, A., Hamed, O., Al-Mansoori, S., Khalil, M.A., 2020. Sensors, features, and machine learning for oil spill detection and monitoring: A review. *Remote Sensing* 12, 1–42. doi:10.3390/rs12203338.
- Alcaro, L., Brandt, J., Giraud, W., Mannozi, M., Nicolas-Kopec, A., 2021. MARINE HNS RESPONSE MANUAL. Multi-regional Bonn Agreement, HELCOM, REMPEC.
- Almén, A.K., Tamelander, T., 2020. Temperature-related timing of the spring bloom and match between phytoplankton and zooplankton. *Marine Biology Research* 16, 674–682. doi:10.1080/17451000.2020.1846201.
- Alpers, W., Holt, B., Zeng, K., 2017. Oil spill detection by imaging radars: Challenges and pitfalls. *Remote Sensing of Environment* 201, 133–147. doi:10.1016/j.rse.2017.09.002.
- Ambjörn, C., 2006. Seatrack Web, forecast of oil spills, the new version, in: 2006 IEEE US/EU Baltic International Symposium, pp. 1–7. doi:10.1109/BALTIC.2006.7266187.
- Ambjörn, C., Liungman, O., Mattsson, J., Håkansson, B., 2014. Seatrack web: The HELCOM tool for oil spill prediction and identification of illegal polluters. *Handbook of Environmental Chemistry* 27, 155–183. doi:10.1007/698-2011-120.
- ASCE, 1996. State-of-the-Art Review of Modeling Transport and Fate of Oil Spills. *Journal of Hydraulic Engineering* 122, 594–609. doi:10.1061/(asce)0733-9429(1996)122:11(594).
- Baniasadi, M., Mousavi, S.M., 2019. A Comprehensive Review on the Bioremediation of Oil Spills, in: *Microbial Action on Hydrocarbons*. March, pp. 223–254. doi:10.1007/978-981-13-1840-5.
- Baszanowska, E., Otremba, Z., 2022. Fluorometric Detection of Oil Traces in a Sea Water Column. *Sensors* 22. doi:10.3390/s22052039.
- Beegle-Krause, C.J., 2005. General NOAA oil modeling environment (GNOME): A new spill trajectory model. 2005 International Oil Spill Conference, IOSC 2005 , 3277–3283. doi:10.7901/2169-3358-2001-2-865.
- Bejarano, A.C., 2018. Critical review and analysis of aquatic toxicity data on oil spill dispersants. *Environmental Toxicology and Chemistry* 37, 2989–3001. doi:10.1002/etc.4254.
- Bejarano, A.C., Michel, J., 2016. Oil spills and their impacts on sand beach invertebrate communities: A literature review. *Environmental Pollution* 218, 709–722. doi:10.1016/j.envpol.2016.07.065.
- Bhattacharya, M., Guchhait, S., Biswas, D., Singh, R., 2019. Evaluation of a microbial consortium for crude oil spill bioremediation and its potential uses in enhanced oil recovery. *Biocatalysis and Agricultural Biotechnology* 18, 101034. doi:10.1016/j.bcab.2019.101034.

- Bícego, M.C., Weber, R.R., Ito, R.G., 1996. Aromatic hydrocarbons on surface waters of Admiralty Bay, King George Island, Antarctica. *Marine Pollution Bulletin* 32, 549–553. doi:10.1016/0025-326X(96)84574-7.
- Booij, N., Ris, R.C., Holthuijsen, L.H., 1999. A third-generation wave model for coastal regions 1. Model description and validation. *Journal of Geophysical Research: Oceans* 104, 7649–7666. doi:10.1029/98JC02622.
- Brekke, C., Espeseth, M.M., Dagestad, K.F., Röhrs, J., Hole, L.R., Reigber, A., 2021. Integrated Analysis of Multisensor Datasets and Oil Drift Simulations—A Free-Floating Oil Experiment in the Open Ocean. *Journal of Geophysical Research: Oceans* 126, 1–26. doi:10.1029/2020JC016499.
- Bugden, J.B.C., Yeung, C.W., Kepkay, P.E., Lee, K., 2008. Application of ultraviolet fluorometry and excitation – emission matrix spectroscopy (EEMS) to fingerprint oil and chemically dispersed oil in seawater. *Marine Pollution Bulletin* 56, 677–685. doi:10.1016/j.marpolbul.2007.12.022.
- Camphuysen, C.J., Heubeck, M., 2001. Marine oil pollution and beached bird surveys: The development of a sensitive monitoring instrument. *Environmental Pollution* 112, 443–461. doi:10.1016/S0269-7491(00)00138-X.
- Carandell, M., Toma, D.M., Pinto, J.P., Gasulla, M., Del Rio, J., 2020. Impact on the Wave Parameters Estimation of a Kinetic Energy Harvester Embedded into a Drifter, in: *2020 Global Oceans 2020: Singapore - U.S. Gulf Coast*, pp. 1–6. doi:10.1109/IEEECONF38699.2020.9389127.
- Carstensen, J., Conley, D.J., Bonsdorff, E., Gustafsson, B.G., Hietanen, S., Janas, U., Jilbert, T., Maximov, A., Norkko, A., Norkko, J., Reed, D.C., Slomp, C.P., Timmermann, K., Voss, M., 2014. Hypoxia in the Baltic Sea: Biogeochemical cycles, benthic fauna, and management. *Ambio* 43, 26–36. doi:10.1007/s13280-013-0474-7.
- Carter, M., Goodsir, F., Cundall, P., Devlin, M., Fuller, S., Jeffery, B., Hil, G., Talouli, A., 2021. Ticking ecological time bombs: Risk characterisation and management of oil polluting World War II shipwrecks in the Pacific Ocean. *Marine Pollution Bulletin* 164, 112087. doi:10.1016/j.marpolbul.2021.112087.
- Chapman, H., Purnell, K., Law, R.J., Kirby, M.F., 2007. The use of chemical dispersants to combat oil spills at sea: A review of practice and research needs in Europe. *Marine Pollution Bulletin* 54, 827–838. doi:10.1016/j.marpolbul.2007.03.012.
- Chekalyuk, A., Hafez, M., 2013. Next generation Advanced Laser Fluorometry (ALF) for characterization of natural aquatic environments: new instruments. *Optics Express* 21, 14181. doi:10.1364/oe.21.014181.
- Conley, D.J., Björck, S., Bonsdorff, E., Carstensen, J., Destouni, G., Gustafsson, B.G., Hietanen, S., Kortekaas, M., Kuosa, H., Meier, H.E., Müller-Karulis, B., Nordberg, K., Norkko, A., Nürnberg, G., Pitkänen, H., Rabalais, N.N., Rosenberg, R., Savchuk, O.P., Slomp, C.P., Voss, M., Wulff, F., Zillén, L., 2009. Hypoxia-related processes in the Baltic Sea. *Environmental Science and Technology* 43, 3412–3420. doi:10.1021/es802762a.
- Conny, R.N., Coble, P.G., Farr, J., Wood, A.M., Lee, K., Pegau, W.S., Walsh, I.D., Koch, C.R., Abercrombie, M.I., Miles, M.S., Lewis, M.R., Ryan, S.A., Robinson, B.J., King, T.L., Kelble, C.R., Lacoste, J., 2014. Submersible optical sensors exposed to chemically dispersed

- crude oil: Wave tank simulations for improved oil spill monitoring. *Environmental Science and Technology* 48, 1803–1810. doi:10.1021/es404206y.
- Cormack, D., Nichols, J.A., 1977. The concentrations of oil in sea water resulting from natural and chemically induced dispersion of oil slicks. *International Oil Spill Conference Proceedings 1977*, 381–385. doi:10.7901/2169-3358-1977-1-381.
- Cyr, F., Tedetti, M., Besson, F., Bhairy, N., Goutx, M., 2019. A glider-compatible optical sensor for the detection of polycyclic aromatic hydrocarbons in the marine environment. *Frontiers in Marine Science* 6, 1–15. doi:10.3389/fmars.2019.00110.
- Dagestad, K.F., Röhrs, J., Breivik, O., Ådlandsvik, B., 2018. OpenDrift v1.0: A generic framework for trajectory modelling. *Geoscientific Model Development* 11, 1405–1420. doi:10.5194/gmd-11-1405-2018.
- Daniel, P., Paradis, D., Gouriou, V., Roux, A.L., Garreau, P., Le Roux, J.F., Loazel, S., 2020. Forecast of oil slick drift from Ulysse/ CSL Virginia and Grande America accidents Pierre, in: *2020 International Oil Spill Conference*, pp. 1–19.
- Dave, D., Ghaly, A.E., 2011. Remediation technologies for marine oil spills: A critical review and comparative analysis. *American Journal of Environmental Sciences* 7, 424–440. doi:10.3844/ajessp.2011.424.440.
- De Dominicis, M., Falchetti, S., Trotta, F., Pinardi, N., Giacomelli, L., Napolitano, E., Fazioli, L., Sorgente, R., Haley, P.J., Lermusiaux, P.F., Martins, F., Cocco, M., 2014. A relocatable ocean model in support of environmental emergencies. *Ocean Dynamics* 64, 667–688. doi:10.1007/s10236-014-0705-x.
- De Dominicis, M., Pinardi, N., Zodiatis, G., Archetti, R., 2013a. MEDSLIK-II, a Lagrangian marine surface oil spill model for short-term forecasting-Part 2: Numerical simulations and validations. *Geoscientific Model Development* 6, 1871–1888. doi:10.5194/gmd-6-1871-2013.
- De Dominicis, M., Pinardi, N., Zodiatis, G., Lardner, R., 2013b. MEDSLIK-II, a Lagrangian marine surface oil spill model for short-term forecasting-Part 1: Theory. *Geoscientific Model Development* 6, 1851–1869. doi:10.5194/gmd-6-1851-2013.
- Delpeche-Ellmann, N., Giudici, A., Rätsep, M., Soomere, T., 2021. Observations of surface drift and effects induced by wind and surface waves in the Baltic Sea for the period 2011–2018. *Estuarine, Coastal and Shelf Science* 249. doi:10.1016/j.ecss.2020.107071.
- Dhaka, A., Chattopadhyay, P., 2021. A review on physical remediation techniques for treatment of marine oil spills. *Journal of Environmental Management* 288, 112428. doi:10.1016/j.jenvman.2021.112428.
- Díaz, H., Guedes Soares, C., 2020. Review of the current status, technology and future trends of offshore wind farms. *Ocean Engineering* 209, 107381. URL: <https://doi.org/10.1016/j.oceaneng.2020.107381>, doi:10.1016/j.oceaneng.2020.107381.
- Elken, J., Lehmann, A., Myrberg, K., 2015. Second assessment of climate change for the baltic sea basin. Chapter: Recent change—marine circulation and stratification. doi:10.1007/978-3-319-16006-1-7.
- EMSA, 2021. CleanSeaNet service Detections and Feedback data 2020. European Maritime Safety Agency.

- Estonian Ministry of Finance, Hendrikson & Ko, 2021. Estonian maritime spatial plan explanatory memorandum.
- Etkin, D.S., 2000. Worldwide Analysis of Marine Oil Spill Cleanup Cost Factors, in: Arctic and Marine Oilspill Program Technical Seminar, pp. 1-14.
- Etkin, D.S., 2008. Oil spill risk analysis for cape wind energy project. International Oil Spill Conference - IOSC 2008, Proceedings , 571-580doi:10.7901/2169-3358-2008-1-571.
- Etkin, D.S., Nedwed, T.J., 2021. Effectiveness of mechanical recovery for large offshore oil spills. Marine Pollution Bulletin 163, 111848. doi:10.1016/j.marpolbul.2020.111848.
- Faksness, L.G., Daling, P., Altin, D., Dolva, H., Fosbæk, B., Bergstrøm, R., 2015. Relative bioavailability and toxicity of fuel oils leaking from World War II shipwrecks. Marine Pollution Bulletin 94, 123-130. doi:10.1016/j.marpolbul.2015.03.002.
- Faksness, L.G., Leirvik, F., Taban, I.C., Engen, F., Jensen, H.V., Holbu, J.W., Dolva, H., Bråtveit, M., 2022. Offshore field experiments with in-situ burning of oil: Emissions and burn efficiency. Environmental Research 205, 112419. doi:10.1016/j.envres.2021.112419.
- Fang, F., Johnston, A.J., 2001. Oil containment by boom in waves and wind. II: Waves. Journal of Waterway, Port, Coastal and Ocean Engineering 127, 228-233. doi:10.1061/(ASCE)0733-950X(2001)127.
- Farber, S., Allaka, H., Klein, I., Groper, M., 2019. Estimating Sea State Using a Low Cost Buoy, in: 2018 IEEE International Conference on the Science of Electrical Engineering in Israel, ICSEE 2018, IEEE. pp. 1-5. doi:10.1109/ICSEE.2018.8646100.
- FIMR, 2007. FIMR Monitoring of the Baltic Sea Environment - Annual Report 2006. The Finnish Institute of Marine Research. MERI - Report Series of the Finnish Institute of Marine Research No. 59.
- Fingas, M., Brown, C.E., 2018. A review of oil spill remote sensing. Sensors (Switzerland) 18, 1-18. doi:10.3390/s18010091.
- Fiocci, R.J., Lewis, A., 1999. Oil Spill Dispersants. Pure and Applied Chemistry 71, 27-42. doi:10.1201/9781003070160.
- French-McCay, D.P., Tajalli-Bakhsh, T., Jayko, K., Spaulding, M.L., Li, Z., 2017. Validation of Oil Spill Transport and Fate Modeling in Arctic Ice. Arctic Science 97, 71-97. doi:10.1139/as-2017-0027.
- Fritt-Rasmussen, J., Wegeberg, S., Gustavson, K., 2015. Review on Burn Residues from in Situ Burning of Oil Spills in Relation to Arctic Waters. Water, Air, and Soil Pollution 226. doi:10.1007/s11270-015-2593-1.
- Fritt-Rasmussen, J., Wegeberg, S., Lassen, P., Wilms, L.B., Renvald, L., Larsen, M.B., Geertz-Hansen, O., Wiktor, J., Gustavson, K., 2023. Coastline in-situ burning of oil spills, analysis of a Greenland field experiment. Journal of Hazardous Materials 441. doi:10.1016/j.jhazmat.2022.129976.
- Giesecke, R., Galábn-Malagón, C., Salamanca, M., Chandia, C., Ruiz, C., Bahamondes, S., Astorga-Gallano, D., 2024. Automated FerryBox monitoring reveals the first recorded river induced crude oil seep transport to the Strait of Magellan in southern Patagonia. Science of the Total Environment 920. doi:10.1016/j.scitotenv.2024.170706.

- Gilbert, T., Nawadra, S., Tafleichig, A., Yinug, L., 2003. Response to an oil spill from a sunken WWII oil tanker in Yap State, Micronesia, in: 2003 International Oil Spill Conference, pp. 175–182.
- Goodsir, F., Lonsdale, J.A., Mitchell, P.J., Suehring, R., Farcas, A., Whomersley, P., Brant, J.L., Clarke, C., Kirby, M.F., Skelhorn, M., Hill, P.G., 2019. A standardised approach to the environmental risk assessment of potentially polluting wrecks. *Marine Pollution Bulletin* 142, 290–302. doi:10.1016/j.marpolbul.2019.03.038.
- Hampton, S., Ford, R.G., Carter, H.R., Abraham, C., Humple, D., 2003. Chronic oiling and seabird mortality from the sunken vessel S.S. Jacob Luckenbach in Central California. *Marine Ornithology* 31, 35–41.
- Hassellöv, I.M., Olsson, U., Ekberg, G., Östin, A., Simonson, F., Larsson, C., Sender, U., Landquist, H., Lindgren, F., Lindhe, A., Rosén, L., 2014. Environmental Risks Posed by Sunken Wrecks. Research methods and environmental aspects. The Swedish Maritime Administration .
- HELCOM, 2003. The Baltic Marine Environment 1999–2002. *Baltic Sea Environment Proceedings* No. 87. .
- HELCOM, 2010. Maritime Activities in the Baltic Sea – An integrated thematic assessment on maritime activities and response to pollution at sea in the Baltic Sea Region. *Baltic Sea Environment Proceedings* No. 123 , 1–40URL: <https://www.helcom.fi/wp-content/uploads/2019/08/BSEP152-1.pdf>.
- HELCOM, 2013. Risks of Oil and Chemical Pollution.
- HELCOM, 2018. State of the Baltic Sea – Second HELCOM holistic assessment, 2011-2016. *Baltic Sea Environment Proceedings* No.155.
- HELCOM, 2019. Shipping accidents in the Baltic Sea in 2018.
- HELCOM, 2021a. HELCOM Annual report on discharges observed during aerial surveillance in the Baltic Sea 2020.
- HELCOM, 2021b. HELCOM Manual on Co-operation in Response to Marine Pollution.
- HELCOM, 2021c. HELCOM report on Shipping accidents in the Baltic Sea 2020.
- HELCOM, 2023. HELCOM Annual report on observed during aerial surveillance in the Baltic Sea 2022.
- Henry, C.B., Roberts, P.O., Overton, E.B., 1999. A Primer on in Situ Fluorometry to Monitor Dispersed Oil. *International Oil Spill Conference Proceedings* doi:10.7901/2169-3358-1999-1-225.
- Hoff, R.Z., 1993. Bioremediation: an overview of its development and use for oil spill cleanup. *Marine Pollution Bulletin* 26, 476–481.
- Hole, L.R., 2018. APP4SEA - Report on existing oil spill response models.
- Huettel, M., 2022. Oil pollution of beaches. *Current Opinion in Chemical Engineering* 36, 100803. doi:10.1016/j.coche.2022.100803.

- Ingmarsson, P., Hüffmeier, J., 2019. 2030 and 2050 Baltic Sea Energy Scenarios. Swedish Agency for Marine and Water Management URL: <https://vasab.org/wp-content/uploads/2019/05/Baltic-LINes-2030-and-2050-Baltic-Sea-Energy-Scenarios-Ocean-Energy.pdf>.
- Irons, D.B., Kendall, S.J., Erickson, W.P., McDonald, L.L., Lance, B.K., 2000. Nine years after the Exxon Valdez oil spill: Effects on marine bird populations in Prince William Sound, Alaska. *Condor* 102, 723–737. doi:10.2307/1370300.
- Ivichev, I., Hole, L.R., Karlin, L., Wettre, C., Röhrs, J., 2012. Comparison of Operational Oil Spill Trajectory Forecasts with Surface Drifter Trajectories in the Barents Sea. *Geology & Geosciences* 1, 1–8. doi:10.4172/2329-6755.1000105.
- Janssen, P.A.E.M., 1991. Quasi-linear theory of wind-wave generation applied to wave forecasting. *Journal of Physical Oceanography* 21, 1631–1642. doi:10.1175/1520-0485(1991)021<1631:QLTOWW.2.O.CO;2.
- Jenssen, B.M., 1994. Review article: Effects of oil pollution, chemically treated oil, and cleaning on thermal balance of birds. *Environmental Pollution* 86, 207–215. doi:10.1016/0269-7491(94)90192-9.
- Jones, C.E., Dagestad, K.F., Breivik, Ø., Holt, B., Röhrs, J., Christensen, K.H., Espeseth, M., Brekke, C., Skrunes, S., 2016. Measurement and modeling of oil slick transport. *Journal of Geophysical Research: Oceans* , 1–14. doi:10.1002/2016JC012113.
- Kasak, K., Pindus, M., Piirimäe, K., 2022. Veetranspordi reostusjuhtumite analüüs ja reostustõrje võimekuse hindamine aastatel 2012-2021. (In Estonian).
- Keramea, P., Spanoudaki, K., Zodiatis, G., Gikas, G., Sylaios, G., 2021. Oil spill modeling: A critical review on current trends, perspectives, and challenges. *Journal of Marine Science and Engineering* 9, 1–41. doi:10.3390/jmse9020181.
- Kleindienst, S., Paul, J.H., Joye, S.B., 2015. Using dispersants after oil spills: Impacts on the composition and activity of microbial communities. *Nature Reviews Microbiology* 13, 388–396. doi:10.1038/nrmicro3452.
- Kostianoy, A.G., Ambjörn, C., Soloviev, D.M., 2008. Seatrack Web: A numerical tool to protect the baltic sea marine protected areas. *US/EU-Baltic International Symposium: Ocean Observations, Ecosystem-Based Management and Forecasting - Provisional Symposium Proceedings, BALTIC* 1, 3–8. doi:10.1109/BALTIC.2008.4625487.
- Kõuts, M., Maljutenko, I., Elken, J., Liu, Y., Hansson, M., Viktorsson, L., Raudsepp, U., 2021. Recent regime of persistent hypoxia in the baltic sea. *Environmental Research Communications* 3. doi:10.1088/2515-7620/ac0cc4.
- Lambert, P., 2003. A literature review of portable fluorescence-based oil-in-water monitors. *Journal of Hazardous Materials* 102, 39–55. doi:10.1016/S0304-3894(03)00201-2.
- Lambert, P., Goldthorp, M., Fieldhouse, B., Wang, Z., Fingas, M., Pearson, L., Collazzi, E., 2003. Field fluorometers as dispersed oil-in-water monitors. *Journal of Hazardous Materials* 102, 57–79. doi:10.1016/S0304-3894(03)00202-4.
- Landquist, H., Hassellöv, I.M., Rosén, L., Lindgren, J.F., Dahllöf, I., 2013. Evaluating the needs of risk assessment methods of potentially polluting shipwrecks. *Journal of Environmental Management* 119, 85–92. doi:10.1016/j.jenvman.2012.12.036.

- Landquist, H., Rosén, L., Lindhe, A., Hassellöv, I.M., 2016. VRAKA-A probabilistic risk assessment method for potentially polluting shipwrecks. *Frontiers in Environmental Science* 4, 1–14. doi:10.3389/fenvs.2016.00049.
- Langangen, Olsen, E., Stige, L.C., Ohlberger, J., Yaragina, N.A., Vikebø, F.B., Bogstad, B., Stenseth, N.C., Hjermann, D., 2017. The effects of oil spills on marine fish: Implications of spatial variation in natural mortality. *Marine Pollution Bulletin* 119, 102–109. doi:10.1016/j.marpolbul.2017.03.037.
- Lehmann, A., Myrberg, K., Post, P., Chubarenko, I., Dailidienė, I., Hinrichsen, H.H., Hüseyin, K., Liblik, T., Meier, H.E., Lips, U., Bukanova, T., 2022. Salinity dynamics of the Baltic Sea. *Earth System Dynamics* 13, 373–392. doi:10.5194/esd-13-373-2022.
- Lehr, W., Jones, R., Evans, M., Simecek-Beatty, D., Overstreet, R., 2002. Revisions of the ADIOS oil spill model. *Environmental Modelling and Software* 17, 189–197. doi:10.1016/s1364-8152(01)00064-0.
- Lenain, L., Pizzo, N., 2020. The contribution of high-frequency wind-generated surface waves to the Stokes drift. *Journal of Physical Oceanography* 50, 3455–3465. doi:10.1175/JPO-D-20-0116.1.
- Lessard, R.R., Demarco, G., 2000. The Significance of Oil Spill Dispersants. *Spill Science & Technology Bulletin* 6, 59–68. doi:10.1016/S1353-2561(99)00061-4.
- Li, P., Cai, Q., Lin, W., Chen, B., Zhang, B., 2016. Offshore oil spill response practices and emerging challenges. *Marine Pollution Bulletin* 110, 6–27. doi:10.1016/j.marpolbul.2016.06.020.
- Li, Y., Jia, Y., Cai, X., Xie, M., Zhang, Z., 2022. Oil pollutant identification based on excitation-emission matrix of UV-induced fluorescence and deep convolutional neural network. *Environmental Science and Pollution Research* 29, 68152–68160. doi:10.1007/s11356-022-20392-x.
- Liblik, T., Lips, U., 2019. Stratification has strengthened in the Baltic Sea – an analysis of 35 years of observational data. *Frontiers in Earth Science* 7, 1–15. doi:10.3389/feart.2019.00174.
- Lichtenthaler, R.G., Daling, P.S., 1983. Dispersion of chemically treated crude oil in Norwegian offshore waters. *Proceedings of the 1983 Oil Spill Conference*, 7–14.
- Lichtenthaler, R.G., Daling, P.S., 1985. Aerial application of dispersants: comparison of slick behavior of chemically treated versus non-treated slicks, in: *International Oil Spill Conference Proceedings (1985)*, p. 471–478. doi:10.7901/2169-3358-1985-1-471.
- Lindgren, J.F., Åberg, F., Johansson, J.R., 2020. Polluting shipwrecks in Swedish waters: investigations, risk assessment methodology and oil removal operations, in: *2020 International Oil Spill Conference*, p. 1–20. URL: <http://190.119.145.154/handle/20.500.12773/11756>.
- Lindgren, J.F., Hassellöv, I.M., Dahllöf, I., 2012. Meiofaunal and bacterial community response to diesel additions in a microcosm study. *Marine Pollution Bulletin* 64, 595–601. doi:10.1016/j.marpolbul.2011.12.014.

- Liu, Y., Weisberg, R.H., 2011. Evaluation of trajectory modeling in different dynamic regions using normalized cumulative Lagrangian separation. *Journal of Geophysical Research: Oceans* 116, 1–13. doi:10.1029/2010JC006837.
- Maljutenko, I., Lagemaa, P., Verjovkina, S., 2022. Mere operatiivmodelisüsteemi NEMO kasutuselevõtt ja töölerakendamine mereala operatiivprognoside parandamiseks. (In Estonian).
- Meier, H.E., Kauker, F., 2003a. Sensitivity of the Baltic Sea salinity to the freshwater supply. *Climate Research* 24, 231–242. doi:10.3354/cr024231.
- Meier, H.E.M., Kauker, F., 2003b. Modeling decadal variability of the Baltic Sea: 2. Role of freshwater inflow and large-scale atmospheric circulation for salinity. *Journal of Geophysical Research: Oceans* 108. doi:10.1029/2003jc001799.
- Michel, J., Gilbert, T., Etkin, D.S., Urban, R., Waldron, J., Blocksidge, C.T., 2005. Potentially Polluting Wrecks in Marine Waters. *International Oil Spill Conference Proceedings 2005*, 1–84. doi:10.7901/2169-3358-2005-1-1.
- Mueller, J.A., Veron, F., 2009. Nonlinear formulation of the bulk surface stress over breaking waves: Feedback mechanisms from air-flow separation. *Boundary-Layer Meteorology* 130, 117–134. doi:10.1007/s10546-008-9334-6.
- Mullin, J.V., Champ, M.A., 2003. Introduction/overview to in situ burning of oil spills. *Spill Science and Technology Bulletin* 8, 323–330. doi:10.1016/S1353-2561(03)00076-8.
- Murray, C.J., Müller-Karulis, B., Carstensen, J., Conley, D.J., Gustafsson, B.G., Andersen, J.H., 2019. Past, present and future eutrophication status of the Baltic Sea. *Frontiers in Marine Science* 6, 1–12. doi:10.3389/fmars.2019.00002.
- Musial, W., Beiter, P., Schwabe, P., Tian, T., Stehly, T., Spitsen, P., 2019. 2018 Offshore Wind Technologies Market Report. U.S. Department of Energy , 131.
- National Academies of Sciences, 2022. *Oil in the sea: Inputs, fates, and effects*. 1, The National Academies Press, Washington, DC. doi:https://doi.org/10.17226/26410.
- NOAA, 2013. *Risk Assessment for Potentially Polluting Wrecks in U.S. Waters*. National Oceanic and Atmospheric Administration .
- Nordvik, A.B., 1995. The Technology Windows-of-Opportunity for Marine Oil Spill Response as Related to Oil Weathering and Operations. *Spill Science & Technology Bulletin* 2, 17–46. doi:10.1016/1353-2561(95)00013-T.
- Novelli, G., Guigand, C.M., Özgökmen, T.M., 2018. Technological advances in drifters for oil transport studies. *Marine Technology Society Journal* 52, 53–61. doi:10.4031/MTSJ.52.6.9.
- O'Hara, P.D., Morandin, L.A., 2010. Effects of sheens associated with offshore oil and gas development on the feather microstructure of pelagic seabirds. *Marine Pollution Bulletin* 60, 672–678. doi:10.1016/j.marpolbul.2009.12.008.
- Owens, R.G., Hewson, T.D., 2018. *ECMWF Forecast User Guide*. doi:10.21957/m1cs7h.
- Pagnucco, R., Phillips, M.L., 2018. Comparative effectiveness of natural by-products and synthetic sorbents in oil spill booms. *Journal of Environmental Management* 225, 10–16. doi:10.1016/j.jenvman.2018.07.094.

- Pärn, O., Davulien, L., Macias, D., Vahter, K., Stips, A., Torsvik, T., 2023. Effects of Eulerian current, Stokes drift and wind while simulating surface drifter trajectories in the Baltic Sea. *Oceanologia* , 1–13doi:10.1016/j.oceano.2023.02.001.
- Pereiro, D., Souto, C., Gago, J., 2018. Calibration of a marine floating litter transport model. *Journal of Operational Oceanography* 11, 125–133. doi:10.1080/1755876X.2018.1470892.
- Petersen, W., 2014. FerryBox systems: State-of-the-art in Europe and future development. *Journal of Marine Systems* 140, 4–12. doi:10.1016/j.jmarsys.2014.07.003.
- Piatt, J.F., Van Pelt, T.I., 1997. Mass-mortality of guillemots (*Uria aalge*) in the Gulf of Alaska in 1993. *Marine Pollution Bulletin* 34, 656–662. doi:10.1016/S0025-326X(97)00008-8.
- Pikkarainen, A.L., Lemponen, P., 2005. Petroleum hydrocarbon concentrations in Baltic Sea subsurface water. *Boreal Environment Research* 10, 125–134.
- Pisano, A., De Dominicis, M., Biamino, W., Bignami, F., Gherardi, S., Colao, F., Coppini, G., Marullo, S., Sprovieri, M., Trivero, P., Zambianchi, E., Santoleri, R., 2016. An oceanographic survey for oil spill monitoring and model forecasting validation using remote sensing and in situ data in the Mediterranean Sea. *Deep-Sea Research Part II: Topical Studies in Oceanography* 133, 132–145. doi:10.1016/j.dsr2.2016.02.013.
- Prendergast, D.P., Gschwend, P.M., 2014. Assessing the performance and cost of oil spill remediation technologies. *Journal of Cleaner Production* 78, 233–242. doi:10.1016/j.jclepro.2014.04.054.
- Presencia, C.E., Shafiee, M., 2018. Risk analysis of maintenance ship collisions with offshore wind turbines. *International Journal of Sustainable Energy* 37, 576–596. URL: <https://doi.org/10.1080/14786451.2017.1327437>, doi:10.1080/14786451.2017.1327437.
- Prince, R.C., 2015. Oil spill dispersants: Boon or bane? *Environmental Science and Technology* 49, 6376–6384. doi:10.1021/acs.est.5b00961.
- Rabault, J., Nose, T., Hope, G., Müller, M., Breivik, Ø., Voermans, J., Hole, L.R., Bohlinger, P., Waseda, T., Kodaira, T., Katsuno, T., Johnson, M., Sutherland, G., Johanson, M., Christensen, K.H., Garbo, A., Jensen, A., Gundersen, O., Marchenko, A., Babanin, A., 2022. OpenMetBuoy-v2021: An Easy-to-Build, Affordable, Customizable, Open-Source Instrument for Oceanographic Measurements of Drift and Waves in Sea Ice and the Open Ocean. *Geosciences (Switzerland)* 12. doi:10.3390/geosciences12030110.
- Raghukumar, K., Chang, G., Spada, F., Jones, C., Janssen, T., Gans, A., 2019. Performance characteristics of "spotter," a newly developed real-time wave measurement buoy. *Journal of Atmospheric and Oceanic Technology* 36, 1127–1141. doi:10.1175/JTECH-D-18-0151.1.
- Reed, M., Turner, C., Odulo, A., 1994. The role of wind and emulsification in modelling oil spill and surface drifter trajectories. *Spill Science and Technology Bulletin* 1, 143–157. doi:10.1016/1353-2561(94)90022-1.
- Ris, R.C., Holthuijsen, L.H., Booij, N., 1999. A third-generation wave model for coastal regions 2. Verification. *JOURNAL OF GEOPHYSICAL RESEARCH* 104, 7667–7681.
- Robertson, T., Higman, B., Dahlslett, H.P., 2017. Analyzing the Impact of Metocean Conditions on Marine Oil Spill Response, in: *OCEANS 2017 - ANCHORAGE*, pp. 9–14.

- Röhrs, J., Christensen, K.H., 2015. Drift in the uppermost part of the ocean. *Geophysical Research Letters* 42, 10349–10356. doi:10.1002/2015GL066733.
- Röhrs, J., Dagestad, K.F., Asbjørnsen, H., Nordam, T., Skancke, J., Jones, C.E., Brekke, C., 2018. The effect of vertical mixing on the horizontal drift of oil spills. *Ocean Science* 14, 1581–1601. doi:10.5194/os-14-1581-2018.
- Ruberg, E.J., Elliott, J.E., Williams, T.D., 2021a. Review of petroleum toxicity and identifying common endpoints for future research on diluted bitumen toxicity in marine mammals. *Ecotoxicology* 30, 537–551. doi:10.1007/s10646-021-02373-x.
- Ruberg, E.J., Williams, T.D., Elliott, J.E., 2021b. Review of petroleum toxicity in marine reptiles. *Ecotoxicology* 30, 525–536. doi:10.1007/s10646-021-02359-9.
- Saadoun, I.M., 2015. Impact of Oil Spills on Marine Life, in: *Emerging Pollutants in the Environment - Current and Further Implications*, pp. 75–105. doi:10.5772/60455.
- Saetre, C., Tholo, H., Hovdenes, J., Kocbach, J., Hageberg, A.A., Klepsvik, I., Aarnes, O.J., Furevik, B.R., Magnusson, A.K., 2023. Directional wave measurements from navigational buoys. *Ocean Engineering* 268, 113161. doi:10.1016/j.oceaneng.2022.113161.
- Savchuk, O.P., 2018. Large-scale nutrient dynamics in the Baltic Sea, 1970–2016. *Frontiers in Marine Science* 5, 1–20. doi:10.3389/fmars.2018.00095.
- Schwartzberg, H.G., 1971. The movement of oil spills, in: *International Oil Spill Conference Proceedings (1971)*, pp. 489–494. doi:10.7901/2169-3358-1971-1-489.
- Senga, H., Kato, N., Suzuki, H., Akamatsu, T., Yu, L., Yoshie, M., Tanaka, T., 2014. Field experiments and new design of a spilled oil tracking autonomous buoy. *Journal of Marine Science and Technology (Japan)* 19, 90–102. doi:10.1007/s00773-013-0233-2.
- Skinner, E.D., Rooney, M.M., Hinders, M.K., 2018. Low-cost wave characterization modules for oil spill response. *Journal of Ocean Engineering and Science* 3, 96–108. doi:10.1016/j.joes.2018.05.003.
- Soares-Ramos, E.P., de Oliveira-Assis, L., Sarrias-Mena, R., Fernández-Ramírez, L.M., 2020. Current status and future trends of offshore wind power in Europe. *Energy* 202, 117787. URL: <https://doi.org/10.1016/j.energy.2020.117787>, doi:10.1016/j.energy.2020.117787.
- Solberg, A.H., 2012. Remote sensing of ocean oil-spill pollution. *Proceedings of the IEEE* 100, 2931–2945. doi:10.1109/JPROC.2012.2196250.
- Spaulding, M.L., 2017. State of the art review and future directions in oil spill modeling. *Marine Pollution Bulletin* 115, 7–19. doi:10.1016/j.marpolbul.2017.01.001.
- Sutherland, G., Soontiens, N., Davidson, F., Smith, G.C., Bernier, N., Blanken, H., Schillinger, D., Marcotte, G., Röhrs, J., Dagestad, K.F., Christensen, K.H., Breivik, Ø., 2020. Evaluating the leeway coefficient of ocean drifters using operational marine environmental prediction systems. *Journal of Atmospheric and Oceanic Technology* 37, 1943–1954. doi:10.1175/JTECH-D-20-0013.1.
- Tapaninen, U., Palu, R., 2022. Recovery of ro-pax ferry traffic from covid-19 under tightening environmental regulations: case Helsinki-Tallinn. *Journal of Shipping and Trade* 7. doi:10.1186/s41072-022-00112-x.

- Tedetti, M., Guigue, C., Goutx, M., 2010. Utilization of a submersible UV fluorometer for monitoring anthropogenic inputs in the Mediterranean coastal waters. *Marine Pollution Bulletin* 60, 350–362. doi:10.1016/j.marpolbul.2009.10.018.
- Treffner, I., 2019. 20. sajandil uppunud vrakkide keskkonnaohtlikkuse analüüs. Muinsuskaitseamet. (In Estonian).
- Troisi, G., Barton, S., Bexton, S., 2016. Impacts of oil spills on seabirds: Unsustainable impacts of non-renewable energy. *International Journal of Hydrogen Energy* 41, 16549–16555. doi:10.1016/j.ijhydene.2016.04.011.
- Ventikos, N.P., Vergetis, E., Psaraftis, H.N., Triantafyllou, G., 2004. A high-level synthesis of oil spill response equipment and countermeasures. *Journal of Hazardous Materials* 107, 51–58. doi:10.1016/j.jhazmat.2003.11.009.
- Wegeberg, S., Fritt-Rasmussen, J., Boertmann, D., 2017. Oil Spill Response in Greenland: Net Environmental Benefit Analysis, NEBA and Environmental Monitoring. Aarhus University, Scientific Report from DCE – Danish Centre for Environment and Energy No. 221.
- Woodbury, S.K., ACM, FCMOS, 2010. iSPHERE Tracking Oil Spills Around The World. MetOcean Telematics Inc.
- WWF, 2010. Future Trends in the Baltic Sea. Baltic Ecoregion Programme– Future Trends in the Baltic Sea , 1–40.
- Xie, M., Jia, Y., Li, Y., Cai, X., Cao, K., 2022. Experimental Analysis on the Optimal Excitation Wavelength for Fine-Grained Identification of Refined Oil Pollutants on Water Surface Based on Laser-Induced Fluorescence. *Journal of Fluorescence* 32, 257–265. doi:10.1007/s10895-021-02849-3.
- Yim, U.H., Khim, J.S., Kim, M., Jung, J.H., Shim, W.J., 2017. Environmental Impacts and Recovery After the Hebei Spirit Oil Spill in Korea. *Archives of Environmental Contamination and Toxicology* 73, 47–54. doi:10.1007/s00244-017-0375-z.
- Yu, F., Hu, X., Dong, S., Liu, G., Zhao, Y., Chen, G., 2018. Design of a low-cost oil spill tracking buoy. *Journal of Marine Science and Technology (Japan)* 23, 188–200. doi:10.1007/s00773-017-0472-8.
- Yu, Q., Liu, K., Chang, C.H., Yang, Z., 2020. Realising advanced risk assessment of vessel traffic flows near offshore wind farms. *Reliability Engineering and System Safety* 203, 107086. URL: <https://doi.org/10.1016/j.res.2020.107086>, doi:10.1016/j.res.2020.107086.
- Zanardi, E., Bícigo, M.C., Weber, R.R., 1999. Dissolved/dispersed petroleum aromatic hydrocarbons in the Sao Sebastiao Channel, Sao Paulo, Brazil. *Marine Pollution Bulletin* 38, 410–413. doi:10.1016/S0025-326X(97)00194-X.
- Zodiatis, G., Lardner, R., Alves, T.M., Krestenitis, Y., Perivoliotis, L., Sofianos, S., Spanoudaki, K., 2017. Oil spill forecasting (prediction). *Journal of Marine Research* 75, 923–953. doi:10.1357/O02224017823523982.
- Zong, Y., Cheng, H.Y., Chien, H., Koppe, B., 2019. Miniature Wave Buoy-Laboratory and Field Tests for Development of a Robust Low-Cost Measuring Technique. *Coastal Structures*. doi:10.18451/978-3-939230-64-9.

Acknowledgements

First, I would like to express my profound gratitude to my supervisors, Jan-Victor Björkqvist and Rivo Uiboupin, for their invaluable guidance and support throughout my PhD journey.

I am also very grateful to Victor Alari, who involved me in his projects, which were essential for this thesis. In addition, I extend my heartfelt thanks to Kaimo Vahter for his assistance with all the fieldwork; your contributions have been instrumental in this work.

I am thankful to Jüri Elken, Sander Rikka and Victor Alari for reviewing this thesis and providing insightful feedback.

A special thanks goes to my family and friends for their unwavering patience and support.

Lastly, I want to thank my colleagues in the Department of Marine Systems at TalTech for their advice and encouragement along the way.

In different phases, this work was supported by the European Union's Horizon 2020 research and innovation programme (project GRACE, grant no. 679266), by the Estonian Research Council (grant no. PSG22), by the Environmental Investment Center (grant no. KIK21067). The thesis was also co-funded by the European Union and the Estonian Research Council via project TEM-TA38 (Digital Twin of Marine Renewable Energy).

Abstract

Enhancing Oil Spill Detection, Response and Modeling in the Baltic Sea

The Baltic Sea is recognized as a particularly sensitive area, vulnerable due to its unique brackish waters, climate conditions, slow water exchange, fragmented coastline, and limited biodiversity. Oil spills, primarily from operational releases by vessels and potentially polluting wrecks, pose significant threats to this fragile marine and coastal ecosystem.

This thesis aims to enhance oil spill management techniques and tools within the Baltic Sea's context. It encompasses different aspects of managing oil spills that includes detection, response, and operational modeling.

The first phase of this study concentrates on the advancement and evaluation of in situ detection methods. A key focus is on the validation of fluorometric sensors for oil detection and their integration into FerryBox and SmartBuoy systems, with the aim of improving real-time detection capabilities for comprehensive spill monitoring.

Through extensive laboratory experiments, it was found that chemical traces of diesel oil can remain in Baltic Sea water and result in responses from portable fluorometric sensors for at least 20 days. However, challenges in specificity were noted due to interference from substances such as humic materials, phytoplankton, and turbidity. This necessitates further exploration into more sophisticated sensors or advanced mathematical protocols to differentiate oil pollution from other optical interferences. The successful integration of these fluorometers into FerryBox and SmartBuoy systems demonstrated their potential for semiautonomous operation and real-time monitoring, paving the way for improved early detection and continuous monitoring of oil spills.

The second section of the thesis details the development of LainePoiss (LP), a robust and compact wave and drifter buoy that can be used to enhance data collection for more effective oil spill response planning and operations.

Field tests and experiments validated the high accuracy of LP buoy's wave measurements, particularly its capacity to capture high-frequency wave spectra (up to 1.28 Hz, around 1 m wavelength). Relative to close-by Directional Waverider measurements, the wave height (H_{m0}) exhibited a bias of 0.01 meters with a correlation coefficient of 0.99, while the mean wave period (T_{m01}) showed a bias of 0.08 seconds with a correlation of 0.98. Such precision is essential for understanding the sea-atmosphere dynamics that influences surface turbulence and oil movement, and also for improving situational awareness during oil spill responses. The LP's versatility, serving both as a drifter and being UAV-deployable, extends its usefulness in response operations, predictive modeling, and validation efforts. Furthermore, the consistency of the wind drift factors (WDFs) determined for the LP buoys (1.5%–3.3%, depending on the LP version and forcing combination), with those reported for oil underscores its reliability as a tracking instrument, crucial for refining oil spill trajectory models and enhancing response tactics.

The third segment of this study focused on establishing and evaluating the OpenDrift trajectory modeling framework for the eastern Baltic Sea.

By incorporating local high-resolution models for hydrodynamics and waves, OpenDrift simulations were validated using Normalized Cumulative Lagrangian Separation metric and empirical data from drift experiments. For a 6-hour forecast period, the weighted average skill scores for the two LP versions varied from 0.38 to 0.66. The validation highlighted the necessity to account for various environmental dynamics, not just wind, to improve model precision. Simulating oil spill scenarios under extreme weather conditions with this model setup highlighted the urgent need for effective and swift response

strategies to efficiently mitigate oil spill impacts. These simulations illustrated the rapid dispersion of oil and underscored how the location of the spill and the prevailing environmental conditions can influence the outcomes.

Overall, this thesis contributes considerably to the advancement of oil spill management in the Baltic Sea, highlighting the need for innovative solutions that effectively address both research and operational challenges in marine environmental protection and oil spill response.

Kokkuvõte

Õlireostuse tuvastamise, modelleerimise ja sellele reageerimise tõhustamine Läänemeres

Läänemerd võib pidada eriti reostustundlikuks selle riimveelisuse, ainulaadsete kliimatingimuste, aeglase veevahetuse, liigendatud rannajoone ja väikese bioloogilise mitmekesisuse tõttu. Õlireostused, mis tulenevad peamiselt laevade tegevusest, sealhulgas nafta ja naftatoodete tahtlikud või hooletusest tingitud merre laskmised ning keskkonnaohtlikud laevavrakid kujutavad sellele ainulaadsele mere- ja rannikuökosüsteemile märkimisväärset ohtu.

Antud doktoritöö eesmärk on täiustada õlireostusele reageerimise meetodeid ja tööriistu Läänemere kontekstis, hõlmates lähenemist, mis sisaldab reostuse avastamist, sellele reageerimist ja modelleerimist.

Käesoleva uuringu esimene osa keskendub kohapealsete reostuse tuvastamise meetodite edasiarendamisele ja hindamisele. Põhitähelepanu on portatiivsete fluoromeetrite andurite valideerimisel õlireostuse tuvastamiseks. Samuti nende edasisel integreerimisel süsteemidesse nagu nutipoi ja laeval asuv automaatne veeanalüsaator FerryBox, eesmärgiga täiustada reaalsajas reostuse tuvastamist. Laborikatsete käigus leiti, et diiselmootori keemilised jäljed võivad Läänemere vees püsida ja mõjutada andurite näite vähemalt 20 päeva. Samas täheldati andurite probleeme õlireostuste eristamisel muudest merevees sisalduvatest optilistest segajatest, nagu humiinained, fütoplankton ja hägusus. Nende probleemide lahendamine nõuab aga keerukamaid andureid või uusi matemaatilisi lähenemisi. Lisaks kinnitas nende fluoromeetrite andurite edukas integreerimine autonoomsetesse FerryBoxi ja nutipoi süsteemidesse nende potentsiaali reaalsajas, välitingimustes, õlireostuse tuvastamiseks

Töö järgmises osas keskenduti kompakitse, vastupidava ja taskukohase lainepoi, LainePoiss (LP), arendamisele, mille üheks kasutusvõimaluseks on õlireostuse puhul koguda olulisi andmeid lainete ja reostuse liikumistrajektooride kohta. Poi topelfunktsioon triivpoina võimaldab seda lisaks kasutada ka reostuse triivimudelite valideerimisel.

Ekspriimendid kinnitasid LainePoisi mõõtmistäpsust, eriti kõrge sagedusega lainete spektri tabamisel (kuni 1,28 Hz, lainepikkus umbes 1 m). Võrreldes lähedal asuva lainepoi (Directional Waverider) mõõtmistega oli lainekõrguse (H_{m0}) hälve 0,01 meetrit korrelatsioonikoeffitsiendiga 0,99 ning keskmise laineperioodi (T_{m01}) hälve 0,08 sekundit, korrelatsiooniga 0,98. Selline mõõtmistäpsus on oluline mere- ja atmosfäärinähtuste mõistmiseks, mis omakorda mõjutab õli hajumist vees. Poi mitmekülgsus ja drooniga veeskamise võimalus suurendavad oluliselt selle kasulikkust õlireostusele reageerimise operatsioonides. LainePoiste efektiivsust reostuse jälgimisseadmena kinnitavad ka nende arvutatud tuule triivitegurid (1,5%–3,3%, olenevalt LP versioonist ja mõjude kombinatsioonist), mis sarnanevad varasemates uuringutes õlidele saadud triivitegurite väärtustele.

Uuringu kolmanda osa fookus on trajektooride modelleerimise raamistik, OpenDrift, seadistamisel ja valideerimisel Eesti rannikuvetes.

Kasutades OpenDrifti raamistikku koos kohalike kõrglahutusega hüdrodünaamika- ja lainemudelitega ning *Normalized Cumulative Lagrangian Separation* meetodit, võrreldi mudeli simulatsioone triivikatsete empiiriliste andmetega. Kuuetunnise prognoosiperioodi puhul varieerusid kahe LP versiooni kaalutud keskmised oskusskoorid (*skill score*) vahemikus 0,38 kuni 0,66. Nende võrdluste tulemused rõhutavad vajadust arvestada mudeli täpsuse parandamiseks mitte ainult tuule, vaid ka teiste keskkonna mõjuteguritega, nagu hoovused ja lained.

Erinevate õlireostuse stsenaariumide simuleerimine äärmuslikes ilmastikutingimustes

kinnitab vajadust tõhusate ja kiirete reageerimisstrateegiade järele, et reostuse mõju efektiivselt leevendada. Lisaks näitasid need simulatsioonid, et tormise ilmaga hajub raske kütteõli vees kiiresti ning ka seda, kuidas reostuse asukoht ja valitsevad keskkonnatingimused võivad neid tulemusi mõjutada

Uuringud, millest käesolev töö koosneb, edendavad ja tõhustavad õlireostusele reageerimist Läänemeres. Samuti rõhutavad need vajadust arendada ja rakendada uuenduslikke lahendusi, mis aitavad kaasa nii teadusuuringutele, operatiivsele reostustõrjele kui ka üldisele merekeskkonna kaitsele.

Appendix

Paper I

Pärt, S., Kankaanpää, H., Björkqvist, J. V., & Uiboupin, R. (2021). **Oil Spill Detection Using Fluorometric Sensors: Laboratory Validation and Implementation to a FerryBox and a Moored SmartBuoy**. *Frontiers in Marine Science*, 8, 1–17. <https://doi.org/10.3389/fmars.2021.778136>



Oil Spill Detection Using Fluorometric Sensors: Laboratory Validation and Implementation to a FerryBox and a Moored SmartBuoy

Siim Pärt^{1*}, Harri Kankaanpää², Jan-Victor Björkqvist^{1,3,4} and Rivo Uiboupin¹

¹ Department of Marine Systems, Tallinn University of Technology, Tallinn, Estonia, ² Marine Research Centre, Finnish Environment Institute, Helsinki, Finland, ³ Norwegian Meteorological Institute, Bergen, Norway, ⁴ Finnish Meteorological Institute, Helsinki, Finland

OPEN ACCESS

Edited by:

Kenneth Mei Yee Leung,
City University of Hong Kong, Hong
Kong SAR, China

Reviewed by:

Maged Marghany,
Syiah Kuala University, Indonesia
Norimitsu Sakagami,
Tokai University, Japan

*Correspondence:

Siim Pärt
siim.part@taltech.ee

Specialty section:

This article was submitted to
Marine Pollution,
a section of the journal
Frontiers in Marine Science

Received: 16 September 2021

Accepted: 02 November 2021

Published: 30 November 2021

Citation:

Pärt S, Kankaanpää H, Björkqvist J-V
and Uiboupin R (2021) Oil Spill
Detection Using Fluorometric
Sensors: Laboratory Validation and
Implementation to a FerryBox and a
Moored SmartBuoy.
Front. Mar. Sci. 8:778136.
doi: 10.3389/fmars.2021.778136

A large part of oil spills happen near busy marine fairways. Presently, oil spill detection and monitoring are mostly done with satellite remote sensing algorithms, or with remote sensors or visual surveillance from aerial vehicles or ships. These techniques have their drawbacks and limitations. We evaluated the feasibility of using fluorometric sensors in flow-through systems for real-time detection of oil spills. The sensors were capable of detecting diesel oil for at least 20 days in laboratory conditions, but the presence of CDOM, turbidity and algae-derived substances substantially affected the detection capabilities. Algae extract was observed to have the strongest effect on the fluorescence signal, enhancing the signal in all combinations of sensors and solutions. The sensors were then integrated to a FerryBox system and a moored SmartBuoy. The field tests support the results of the laboratory experiments, namely that the primary source of the measured variation was the presence of interference compounds. The 2 month experiments data did not reveal peaks indicative of oil spills. Both autonomous systems worked well, providing real-time data. The main uncertainty is how the sensors' calibration and specificity to oil, and the measurement depth, affects oil detection. We recommend exploring mathematical approaches and more advanced sensors to correct for natural interferences.

Keywords: oil spill, flow-trough system, fluorometric sensors, Baltic Sea, natural interferences, sensor selectivity

1. INTRODUCTION

Oil spills are a major threat to the marine ecosystems, local communities and economy (Samiullah, 1985; Farrington, 2014; Jørgensen et al., 2019; Cãmara et al., 2021; Sandifer et al., 2021). The research into the consequences of oil pollution has been long and extensive. The effects to wildlife are broad, ranging from exposure of birds (Jenssen, 1994; Stephenson, 1997; Fox et al., 2016) and mammals (Engelhardt, 1987; Bodkin et al., 2002; Ridoux et al., 2004) to oil to toxic, mutagenic and/or carcinogenic effects of polycyclic aromatic hydrocarbons (PAHs) present in crude oil and products based on fossil oil (Hylland, 2006; Abdel-Shafy and Mansour, 2016; Hayakawa, 2018; Honda and Suzuki, 2020). Besides harming the natural environment, oil spills can impair the economy in the affected region (Cohen, 1993; Taleghani and Tyagi, 2017; Ribeiro et al., 2021) and have adverse effects on human health and psychology (D'Andrea and Reddy, 2014; Shultz et al., 2015; Sandifer et al., 2021).

The Baltic Sea has always been an important route for maritime trade and transport, accounting for up to 15% of the world's maritime traffic (HELCOM, 2003; WWF, 2010). Oil shipments in the Baltic Sea are projected to grow by 64% by 2030, from about 180 million tons to nearly 300 million tons (HELCOM, 2018a) and the overall volume of ship traffic has been estimated to double during the period 2010–2030 (Rytkönen et al., 2002). The immense volume of shipping in the Baltic Sea is accompanied by a high risk of accidents. According to the Helsinki Commission (HELCOM), 1,520 maritime accidents have occurred in the Baltic Sea area during the period 2011–2015, with a fairly stable rate of 300 accidents per year; 4% of these accidents led to loss of life, serious injuries or environmental damages (HELCOM, 2018a).

A considerable contributor to marine oil pollution is oil pollution by ships, which are concentrated to main shipping lanes and other areas of high maritime activity (Serra-Sogas et al., 2008; Ferraro et al., 2009; Liubartseva et al., 2015; Sankaran, 2019; Polinov et al., 2021). It is estimated that in the Baltic Sea 10% of the total amount of oil hydrocarbons comes from illegal discharges by vessels (HELCOM, 2003). These various smaller spills, referred to as operational oil spills, are not the result of ship accidents, but instead result from discharges of small amounts of oil, or more usually unfiltered oily water. Most of this pollution risk is concentrated along major ship routes (HELCOM, 2013). The number and size of these spills has been decreasing (HELCOM, 2018c). For example, in 2015 the number of observed spills was 80 and the total estimated annual volume of oil spills observed in 2009–2015 was in the order of 20 m³ (HELCOM, 2018a). However, even small amounts of oil can have a negative impact on the marine environment (Brussaard et al., 2016).

Current oil spill remote sensing methods have become more reliable but they still have many drawbacks and limitations (Fingas and Brown, 2018). Nowadays the most dominant and cost-effective means for remote spill detection is the combination of satellite-based synthetic aperture radar (SAR) images and aircraft surveillance flights for verification (Gade et al., 2000; Uiboupin et al., 2008; Solberg, 2012; Fingas and Brown, 2018). SAR sensors give a good coverage and are not limited by cloud cover or weather conditions. Furthermore, there are many studies on algorithms meant for identification of oil spills from SAR data (Marghany, 2016; Krestenitis et al., 2019; Al-Ruzouq et al., 2020; Zeng and Wang, 2020). Besides SAR, optical remote sensing techniques gathering information in different spectral range (ultraviolet, visible, and near-infrared) and can give useful information about oil pollution (Solberg, 2012; Fingas and Brown, 2018; Al-Ruzouq et al., 2020). Ships and aircraft equipped with radar or optical sensor are also widely used for detection and monitoring of oil pollution (Jensen et al., 2008; Xu et al., 2020). Also, sensors like microwave radiometers and laser fluorimeters mounted on aircraft can provide additional information about the oil type and amount (Jha et al., 2008; Solberg, 2012).

Oil spills can be difficult to detect even with modern aerial surveillance equipment for numerous reasons. They can be small, and in rough sea the oil is mixed well below the surface, while a visible slick might also disappear because of evaporation. Optical

methods of satellite sensing are also limited by resolution, cloud cover and the sea state (Brekke and Solberg, 2005; Jha et al., 2008; Fingas and Brown, 2018). Even the most studied and used remote sensing method of detecting oil from SAR images has problems, such as lookalikes—radar signatures similar to oil pollution but which can actually be for example floating algae, ship wakes, cold upwelling water or natural surface films produced by plankton or fish (Sipelgas and Uiboupin, 2007; Alpers et al., 2017; Al-Ruzouq et al., 2020). Even a comprehensive satellite coverage might therefore not be able to detect all oil spills. Nonetheless, PAHs will remain in the water after the spill is no longer visible on the surface but are still detectable by in-water fluorimeters. Thus, the real-time detection of these spills would benefit from additional detection systems. In addition, *in-situ* sensors can be used for validation for remote sensing techniques and vice versa. One possible *in-situ* solution is to use fluorometric sensors installed on a suitable platform.

Ships of Opportunity (SOOPs) fitted with oceanographic instrumentation and automated water sampling systems, so-called FerryBoxes, are commonly used for studies of near surface waters (Petersen et al., 2003, 2011; Hydes et al., 2010; Petersen, 2014). Also, the Baltic Sea is well covered with FerryBox lines (Petersen, 2014; Schneider et al., 2014; Karlson et al., 2016; Kikas and Lips, 2016). FerryBoxes have a great potential for gathering scientific data, especially when installed on ferries and cargo ships cruising the same route on a regular basis. While SOOPs give a good spatial coverage, monitoring buoys give an excellent temporal coverage. Such autonomous monitoring buoy systems are being developed and operated worldwide to measure the physical and biogeochemical properties of coastal surface waters (Mills et al., 2003; Nam et al., 2005). The technological progress has resulted in SmartBuoys with a stable power supply, two-way communication and real-time data acquisition for effective environmental monitoring (Chavez et al., 1997; Mills et al., 2003; Nam et al., 2005; Benson et al., 2008; Papoutsas et al., 2012). Moroni et al. (2016) have developed a sensorized buoy for detecting oil spills from the air-side. Fluorescence-based *in-situ* sensors and systems have been globally used for real-time monitoring of oil spills and determining the levels of the contamination (Lambert et al., 2001, 2003; He et al., 2003; Kim et al., 2010; Malkov and Sievert, 2010; Tedetti et al., 2010). Combining FerryBoxes and SmartBuoys with portable fluorometric sensors could provide an additional method for early notification of oil spills in the sea. Nonetheless, to our knowledge, such an approach has not previously been adopted.

Fluorometric detection (FLD) is essentially about measuring fluorescence at predetermined wavelengths, meaning that FLD can't resolve between different sources of hydrocarbons and fluorescent compounds – for example oil and oil refined products, combustion processes (e.g., power plants, maritime and land-based traffic, forest fires). Compound-specific laboratory methods such as gas chromatography–mass spectrometry can make such distinctions, but field-usability (data continuity), speed and low running costs still make FLD-based field protocols appealing alternatives compared to laboratory-based techniques.

For purposes of the operational detection of oil spills, the accuracy of the sensor is a crucial, but not the sole part. We split

up the operational chain of oil-detection with fluorometers to five steps: 1) the sensors need to accurately and selectively detect oil, 2) the system where the sensors are operating need to function at least semi-autonomously, 3) the system needs to reliably transmit real time data, 4) an automated algorithm detects anomalous events and 5) the data is available to the user in a reliable interface on a short notice. In this study we focus on steps 1–3 and 5. We first present laboratory tests of sensors and then evaluate the real-time oil detection capability of two autonomous *in-situ* remote sensing platforms that are equipped with fluorometers. The two platforms, a FerryBox and a SmartBuoy, covered high-risk areas in the Baltic Sea.

2. MATERIALS AND METHODS

2.1. UviLux, EnviroFlu-HC 500 and Turner Design C3 Fluorometers

Three commercially available fluorometric instruments, designed for *in-situ* and real-time quantification of oil or oil compounds, were chosen for the experiments: UviLux and EnviroFlu-HC 500 for the FerryBox system, and C3 Submersible Fluorometer for the SmartBuoy. All three sensors were also tested in laboratory conditions.

The UviLux UV-fluorometer (Chelsea Technologies Ltd, UK) is an *in-situ* UV fluorometer. Oil detection is based on the measurement of PAH concentrations. The sensitivity of the sensor is 0.005 μg carbazole per liter, the calibrated range is 0.005–2,000 μg carbazole per liter, the excitation wavelength is 255 nm, and the emission wavelength is 360 nm.

The EnviroFlu-HC 500 submersible UV fluorometer (TriOS Optical Sensors, Germany) is an instrument designed for the measurement of PAHs in water. The fluorometer has a minimum detection limit of 0.3 μg phenanthrene per liter, a calibrated range of 0–500 μg phenanthrene per liter, an excitation wavelength 254 nm, and an emission wavelength of 360 nm.

The Turner Design C3 submersible fluorometer (Turner Design, USA) is manufactured according to users' requirements. C3 fluorometers come with a factory-installed temperature probe and can be configured with up to three optical sensors. Each optical sensor is designed with fixed excitation and emission filters. For the SmartBuoy experiment the C3 fluorometer was equipped with three sensors: a hydrocarbon sensor for crude oil with sensitivity of 0.2 μg pyrenetetrasulfonic acid (PTSA) per liter and linear range 0–1500 μg PTSA per liter, excitation light 325/120 nm and emission light 410–600 nm; a sensor for colored dissolved organic matter (CDOM) with minimum detection limit (MDL) 0.1 μg quinine sulfate per liter, linear range 0–1.5 μg quinine sulfate per liter, excitation wavelength 325–120 nm and emission wavelength 470–60 nm; a turbidity sensor with MDL 0.05 Nephelometric Turbidity Units (NTU) and range 0–1,500 NTU, excitation wavelength 850 nm, and emission wavelength 850 nm.

2.2. Laboratory Tests

In order to examine selectivity and sensitivity of fluorometric sensors to oil, two separate laboratory experiments were

performed in 2017. All experiments were performed in a dark climatic room set to a temperature of 16°C.

The first experiment examined the selectivity of the sensors, i.e., interferences to oil detection caused by interfering substances. Baltic Sea water (S; salinity 6.2 PSU) was used as a blank and as a solution for extraction of humic substances (H), cyanobacterial algae (A) and production of clay suspension (C).

Stock solutions (one of each) of clay suspension (from Baltic Sea's clayey sediment), seawater extract of humic substances (originating from decayed plant material) and a seawater extract of cyanobacterial algae (from dried Baltic Sea surface phytoplankton) were produced. Also, two batches of water accommodated fraction (WAF; W) of diesel oil were produced. Each extract was made by combining 100 ml of commercial winter-quality diesel oil with 1,000 ml of seawater under gentle stirring overnight. All solutions were prepared 1 week prior to measurements in the aquarium. Concentrations of PAHs were quantified using gas chromatography—mass spectrometry and aliphatic hydrocarbons (decane-tetracontane) using gas chromatography—flame ionization detection at SYKE laboratory center. No attempt was made to determine chemical composition of each interference solution in detail, instead the solutions mimicked natural constituents in Baltic Sea water.

Altogether six glass beakers (each 2,000 ml) were wrapped with black plastic except for the top section and filled with 1,200 ml of seawater. Aliquots of the clay suspension (50.0 ml), humic extract (50.0 ml), cyanobacteria algae extract (10.0 ml) and diesel WAF (50 ml) were sequentially added so that all combinations of the aforementioned solutions in seawater were achieved. The solutions were kept in slow stirring motion using a magnetic stirrer. In first three sets of measurements no WAF was added. WAF was applied in three last measurement sets. After addition of each solution the responses were measured using one sensor at a time at exactly 50 mm below the upper level of the beakers. The top part of the beakers and the sensor housing were wrapped with black plastic. Fluorescence responses were collected for 3–5 min with each sensor and the average and standard deviation of fluorescence for each period of data collection were calculated.

The logging rates used with fluorometer sensors during the experiment were 1 min (average of values collected at 0.5 Hz), 30 and 1 s for the UviLux, EnviroFlu-HC and Turner C3 sensors, respectively. Data from EnviroFlu-HC were logged into a laptop PC using the TriOS MSDA_XE software and the data from Turner C3 into a PC using Turner C-soft software. Data from UviLux were logged into a portable logger connected to automatic GSM network-based modem and sent via GSM network to Tallinn University of Technology once a minute. Altogether 1.32 million, 79,000 and 30,000 time points of data from Turner C3, Enviroflu-HC and UviLux were generated, respectively. The small dilution effect in WAF solutions, caused by the volume increase by the added interference solutions, was compensated by a corresponding multiplier factor in final calculations thus yielding oil-related fluorescence (ORF) presented. Normalized responses from each fluorometer were calculated by dividing observed responses from different solutions with responses obtained



FIGURE 1 | Above view of the experimental set up. Instruments: TriOS EnviroFlu-HC (with metallic cover, upper part), Turner C3 (with black cover, left) and UviLux (black cover, right). The electric motor of the stirrer is at far right. Photograph: Harri Kankaanpää.

from seawater. No compensation was calculated for CDOM or turbidity values.

The second experiment for diesel WAF persistence and for method comparison lasted for 3 weeks. A 25-liter glass aquarium was used and placed over a black plastic sheet in a steel tank and filled with 21.8 liters of filtered seawater (salinity 6.2 PSU). Thermostatted (11°C) tap water was circulated in the exterior tank. The FLD sensors were fixed into laboratory stands so that the optical window of each sensor was at 10 cm below the surface of liquid (**Figure 1**). Gentle mixing was applied using an electricity-powered laboratory stirrer. The aquarium was covered by a black plastic wrapping except during water sampling and maintenance. The UviLux sensor needed to be moved further away from the two other sensors due to interference that was unfortunately not noticed before 7 days into the experiment. The data transmission, storage and sensors' acquisition rates were as described for the first experiment.

The persistence of diesel oil fractions in seawater and comparability between oil detection methods were measured in the second test. The methods were: the three fluorometric sensors, total oil monitoring method used by Finland, gas chromatography flame ionization detection (GC-FID; for aliphatic hydrocarbons) and gas chromatography—mass spectrometry (GC-MS; for PAHs including 1- and 2-methylnaphthalene). At S1–S9, water samples of 100 ml were collected for total oil HELCOM protocol and another 100 ml for the GC-MS and GC-FID analyses.

The Finnish HELCOM monitoring method for total oil analysis can be described briefly as follows: seawater is extracted with 10 ml of n-hexane under stirring. Fluorescence is measured using 310 and 360 nm excitation and emission wavelengths, respectively. Calibration is performed using solutions of Norwegian crude oil (Ekofisk) dissolved in n-hexane. Limit of quantification is 0.05 μg oil/l and analytical error is $\pm 15\%$.

Aliphatic hydrocarbons (decane-tetracontane) were extracted using n-hexane, cleaned up using adsorbent, concentrated, separated using gas chromatography and quantified by flame ionization detection. The method has a limit of quantification of 100 μg total aliphatics/l and analytical error of 30%. PAHs were extracted using n-hexane under stirring or solid phase extraction. The n-hexane solution was then concentrated and analyzed using GC-MS. The quantification limits of the method were between 0.005 and 0.01 $\mu\text{g}/\text{l}$, while the analytical errors varied between 20 and 40% depending on compound.

Normalized responses for each detection method were calculated by dividing observed responses with period S1 responses at given water sampling time points (S1–S9).

2.3. FerryBox Operation and Oil Detection Capability

A FerryBox system developed by Marine Systems Institute at Tallinn University of Technology is used on board of the M/S Baltic Queen (Tallink Group, Estonia) (**Figure 2**), which commutes between Tallinn (Estonia), Mariehamn (Åland) and

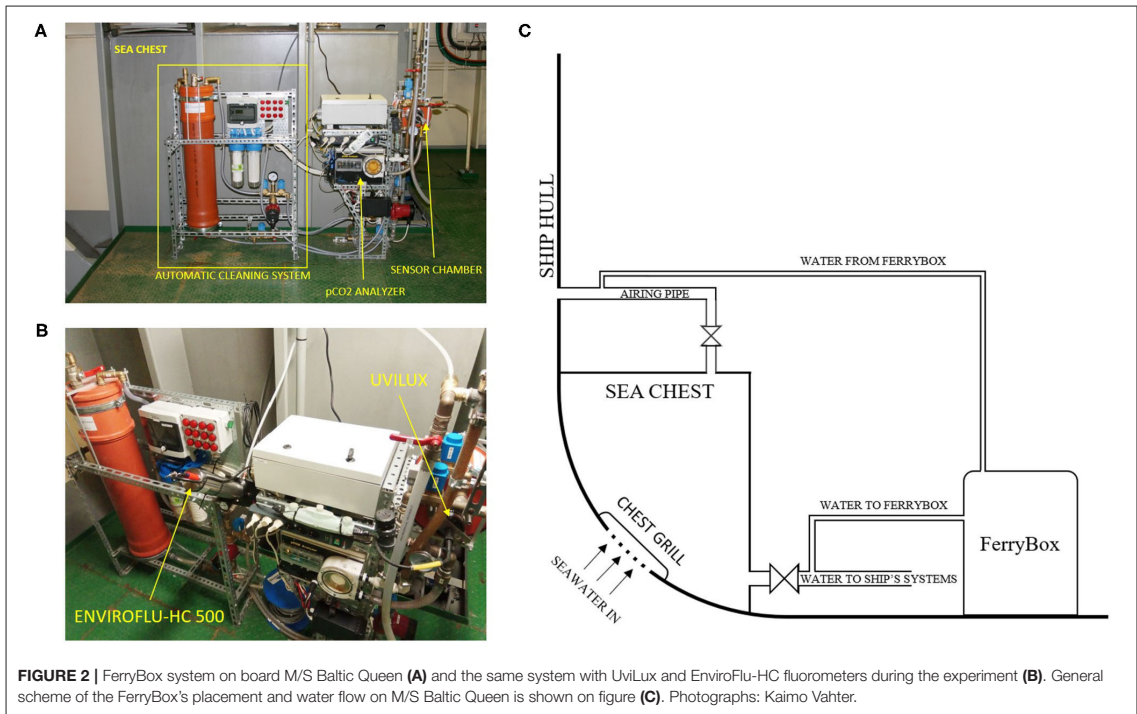


FIGURE 2 | FerryBox system on board M/S Baltic Queen (A) and the same system with UviLux and EnviroFlu-HC fluorometers during the experiment (B). General scheme of the FerryBox's placement and water flow on M/S Baltic Queen is shown on figure (C). Photographs: Kaimo Vahter.

Stockholm (Sweden) (Figure 3). The ship route covers the western Gulf of Finland, Northern Baltic Proper, Southern Archipelago Sea, and Southern Åland Sea (Figure 3). One crossing, including a stop in Mariehamn harbor, is about 425 km long and takes approximately 17 h. The ship then returns after a 7 h stay in the destination harbor.

All FerryBoxes are flow-through systems where the water is taken in from an inlet in a vessel hull and then pumped into a measuring circuit containing sensors (Petersen, 2014). On M/S Baltic Queen the water was taken from the ship's sea chest and pumped continuously through the FerryBox system at a rate of 9 l/min. The opening of the chest is situated about 4 m below the waterline. Parameters were measured with 1-min intervals, giving an approximately 0.5 km spatial resolution along the fairway, depending on the ship's speed. A typical transect contained roughly 1,000 records for each variable.

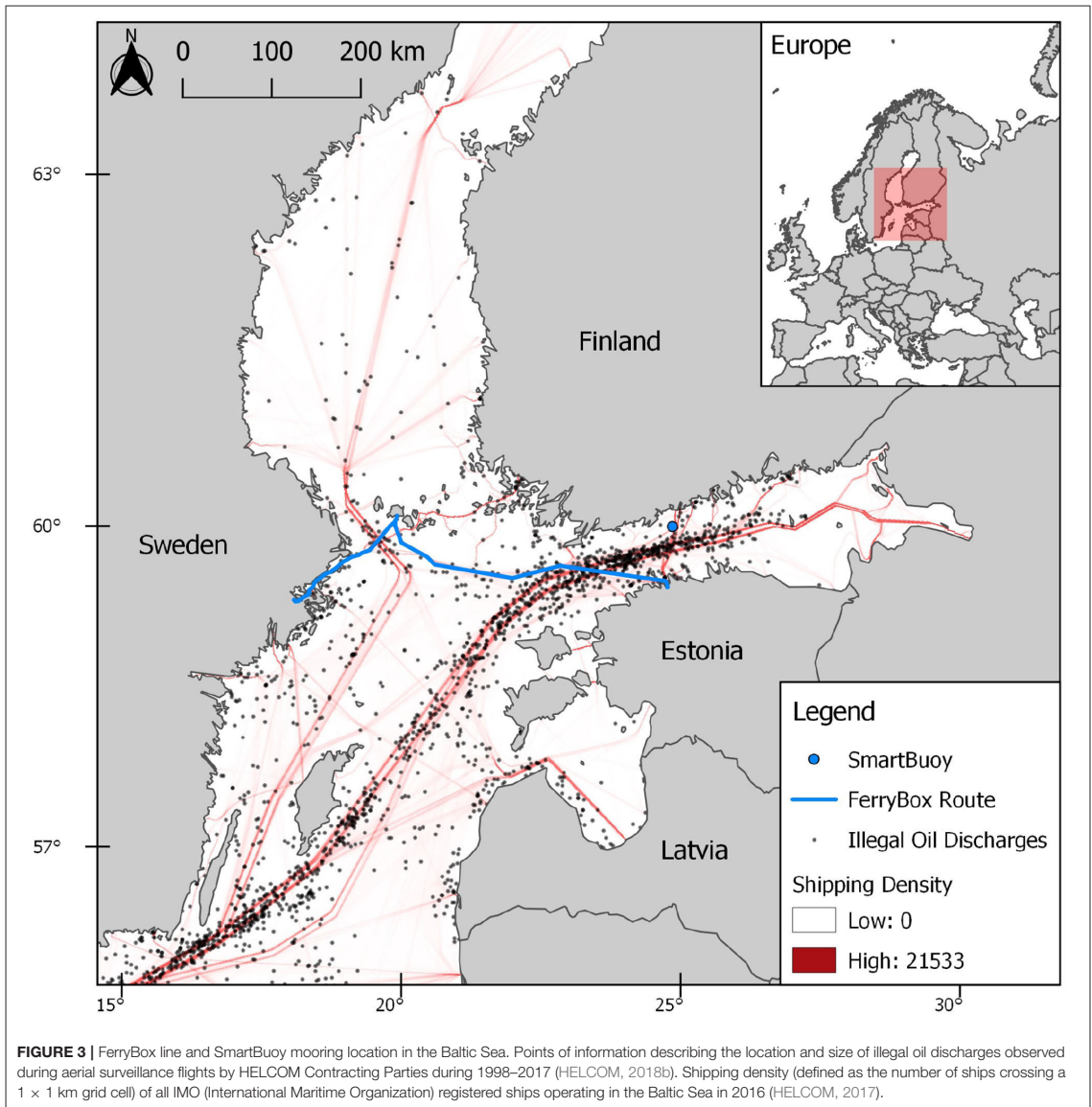
The UviLux and EnviroFlu-HC fluorometers, were installed in parallel to the FerryBox system (Figure 2B), which recorded additional real-time seawater properties. Conductivity (salinity) and temperature was measured with a High-Precision Pressure Level Transmitter Series 36XiW (KELLER AG, Switzerland), turbidity was measured with a Seapoint Turbidity Meter (Seapoint Sensors Inc., USA) and pCO₂ was measured with an OceanPack™ pCO₂ analyzer (SubCtech, Germany).

We made four maintenance visits to M/S Baltic Queen in order to clean the FerryBox system and the sensors. These visits

were made roughly every 2 weeks (March 3, March 20, April 3, April 15) during our 2-month experiment (February 21 to April 21, 2018). The maintenance consisted of washing the system with a solution of oxalic acid and a manual cleaning of the optical sensors. The FerryBox also has an automatic cleaning system, which was not functional during the experiment. Similar automatic acid-washing cleaning method is applied to prevent biofouling on a FerryBox traveling between Tallinn and Helsinki (Lips et al., 2016).

Measurements from the sensors in the FerryBox were collected by a datalogger (RTCU-MX2i pro by Logic IO) on board M/S Baltic Queen. The datalogger includes a modem and a GPS, and adds the position and a time stamp to the measurement before sending the data to an on-shore FTP server of the Marine Systems Institute using the GSM/GPRS protocol. The data were sent in real-time (every minute).

A publicly available, web-based, user interface was built to visualize the data online, where the ship's track, real-time position and gathered FerryBox data was available in real-time (Figure 4) (TalTech, 2017). The web-based user interface is also equipped with different options to view historical data: the user can select parameters or time periods, and construct a map view and 2D graphs of multiple parameters. Data are also available in a tabulated form and parameters can be viewed in color-coded view along the ship's track. The data that were provided in real-time during the experiment is still available on the web-page.



2.4. SmartBuoy Setup and Experiment for Oil Spill Detection

The SmartBuoy, developed by Meritaito Ltd (Finland), is a combination of a polyethylene spar buoy with mobile and/or satellite communication technology and a versatile selection of monitoring sensors (Figure 5). The Turner Design C3 fluorometer was installed inside of the buoy in a vertical monitoring well with an open flow through a pipe, enabling continuous sea water exchange. The monitoring depth was 2–3 m depending on the sea level. Concentration of CDOM

and turbidity values were measured simultaneously with the hydrocarbon measurements. To ensure high data quality, the C3 sensor was equipped with a mechanical wiper cleaning all three optical lenses before taking the measurements. In addition to the water quality monitoring, the SmartBuoy also collected data about current speed and direction at the depth of 7 m to identify spreading direction of potential oil spills. Furthermore, the significant wave height was calculated from roughly 8.5-min time series, measured by a pressure sensor (Aanderaa Wave and Tide Sensor 5218).

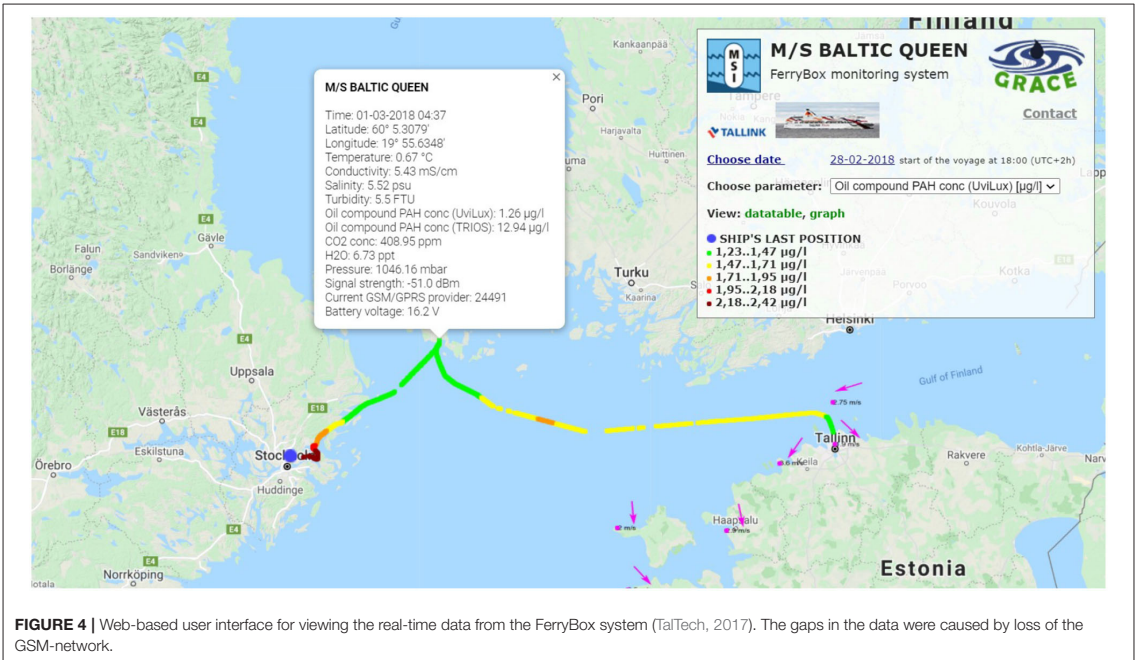


FIGURE 4 | Web-based user interface for viewing the real-time data from the FerryBox system (TalTech, 2017). The gaps in the data were caused by loss of the GSM-network.

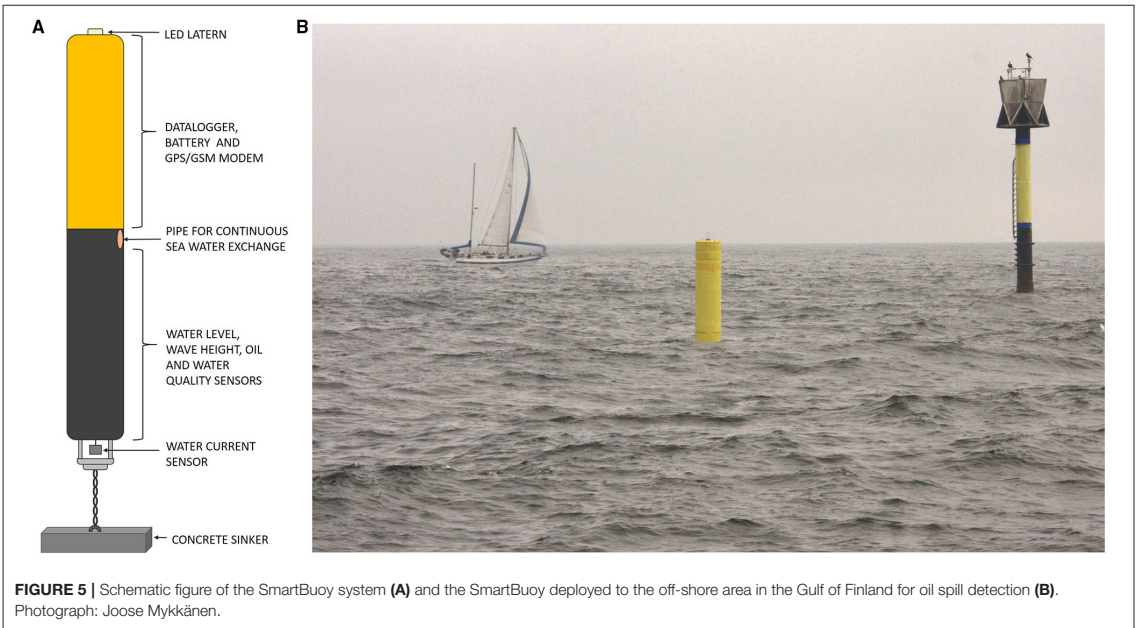


FIGURE 5 | Schematic figure of the SmartBuoy system (A) and the SmartBuoy deployed to the off-shore area in the Gulf of Finland for oil spill detection (B). Photograph: Joose Mykkänen.

TABLE 1 | Relative responses (fold compared to average fluorescence in seawater) of sensors to interference solutions, sensitivity to water accommodated fraction (WAF) of diesel oil.

	UviLux	Turner C3	TriOS Enviroflu-HC
Maximum attenuation without diesel WAF	none	0.95 (clay suspension)	0.97 (clay suspension)
Maximum false positive without diesel WAF	7.61 (algae extract)	3.96 (humic extract + algae extract)	2.64 (algae extract)
Sensitivity to WAF (change from S to SW)	4.48	1.1	2.62
Maximum attenuation during presence of diesel WAF	4.41 (humic extract)	none	2.25 (clay suspension + humic extract)
Maximum false enhancement during presence of diesel WAF	10.6 (algae extract)	3.89 (humic extract + algae extract)	4.95 (algae extract)

Water quality and sea state sensors were connected to a datalogger (Aanderaa SmartGuard 5300) that was programmed to operate the sensors with an 1-h measurement and data transmission interval. Real-time data from the SmartBuoy were transmitted over satellite modem to a server, where it were subjected to an automatic data quality control before being visualized online.

The SmartBuoy buoy was moored on a junction of the main merchant shipping lanes in the Gulf of Finland (Figure 3) for a 2-month measurement period (October 25 to December 24, 2018). Vessels navigating on the north–south direction shipping lane between Helsinki and Tallinn were passing close to the buoy, and vessels on the east–west direction shipping lane passed the buoy further south. The SmartBuoy was visited once during the monitoring period for datalogger reprogramming and manual maintenance of the sensors.

3. RESULTS OF THE LABORATORY EXPERIMENTS

The produced WAF contained the following main PAH constituents (all $\mu\text{g/l}$): naphthalene (65), 1-methylnaphthalene (89), 2-methylnaphthalene (31), anthracene (1.6), acenaphthene (2.7), acenaphthylene (1.2), phenanthrene (1.2), fluoranthene (0.20), fluorene (4.4) and pyrene (0.2). Other PAHs fell below the 0.005 $\mu\text{g/l}$ limit of quantification. The concentration of aliphatic compounds was 1,200 $\mu\text{g/l}$.

3.1. Effect of Interference Solutions

In the first laboratory experiment we investigated how the sensors reacted to the addition of interference solutions. In the absence of interference solutions, Turner C3 showed the largest absolute fluorescence values (primary data), followed by Enviroflu-HC and Uvilux. The data from Turner C3's PAH and CDOM channels had occasional spikes, but overall the data stability from each channel of the detectors were good. When WAF was added to the seawater, the relative change in signal strength (normalized response) was largest for UviLux (4.48-fold), followed by EnviroFlu-HC (2.62-fold) and Turner C3 (1.1-fold) (Table 1).

All sensors reacted when interference solutions were added to seawater. The addition of suspended clay to seawater slightly attenuated the PAH channel's fluorescence signal in Turner C3 and Enviroflu-HC, while slightly enhancing it in UviLux (Figure 6, left half, S vs. SC). When suspended clay was added

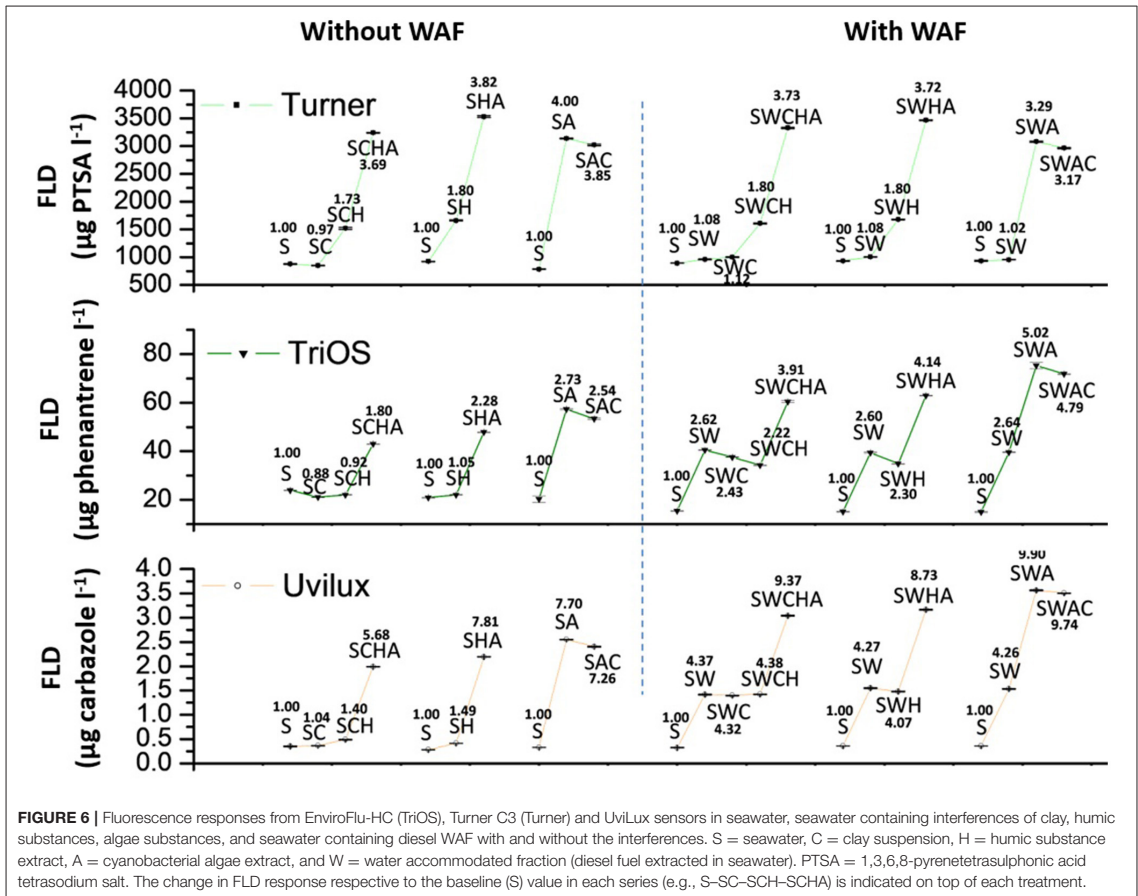
to the seawater-WAF solution, the signal was slightly attenuated in Enviroflu-HC and UviLux, and slightly enhanced in Turner C3 (Figure 6, right half, SW vs. SWC). In all combinations, the changes were at most 12% (0.88–1.04).

The sensors were more sensitive to the presence of humic substance extracts, with the PAH-signals increasing between 1.05- and 1.8-fold in all sensors (compared to seawater). The enhancement was strongest in Turner C3 and weakest in EnviroFlu-HC (Figure 6, left half, S vs. SH). In the seawater-WAF solution the added humic extracts enhanced the PAH signal in Turner C3 (1.67-fold), while slightly attenuating the signal in the other sensors (Figure 6, right half, SW vs. SWH).

Clearly the largest effect on the PAH fluorescence signal was observed after adding algae extract. The signal was enhanced in all combinations of sensors and solutions. Importantly, the enhancement caused by the algae extract was stronger than the PAH signal of the WAF-solution without any interference solutions, which means that the presence of algae can interfere strongly with the sensors ability to detect oil compounds in the water. The enhancements when adding the algae extract to the seawater were roughly between 3- and 8-fold, with UviLux showing the largest change and EnviroFlu-HC showing the smallest change (Figure 6, right half, SW vs. SWA). When the algae extract was added to the seawater-WAF solution, the PAH signal was enhanced roughly 2- to 3-fold in all sensors, with Turner C3 showing the strongest change in signal strength (Figure 6, right half, SW vs. SWA).

3.2. Diesel WAF Persistence and Method Comparison

In the second laboratory experiment we studied how long the sensors can detect oil compounds in seawater, while also comparing detection methods. Lagging software caused several gaps in the Turner C3 data and one gap in the EnviroFlu-HC data. UviLux was relocated after 165 h when we noted that it did not react clearly to the third addition of WAF (WAF3; Figure 7), having large subsequent oscillations in the signal. This behavior was caused by optical interference by the two other sensors. Despite that there was substantial suppression in UviLux responses during the suppressed period, the sensor overall did show slight responses even during this period. These small responses occurred simultaneously when adding WAF 1 and WAF 3 (but not when adding WAF 2), and were also simultaneous with HELCOM and Enviroflu-HC responses (Figure 7). After UviLux was relocated, it provided data with



a considerably higher response and less noise. For response calculations we therefore only used the UviLux data gathered after the relocation.

The responses from all sensors and the standard HELCOM oil monitoring method indicated that fluorescent compounds originating from diesel oil were detectable for at least 20 days since the start of the experiment (Figure 7). The temporal evolution in PAH-related responses measured by the EnviroFlu-HC and UviLux sensors were in line with the HELCOM method, especially after the readjustment of the sensors. In contrast, Turner C3 showed slightly increasing fluorescence between 100 and 505 h while the signal from the other two sensors decayed and leveled off.

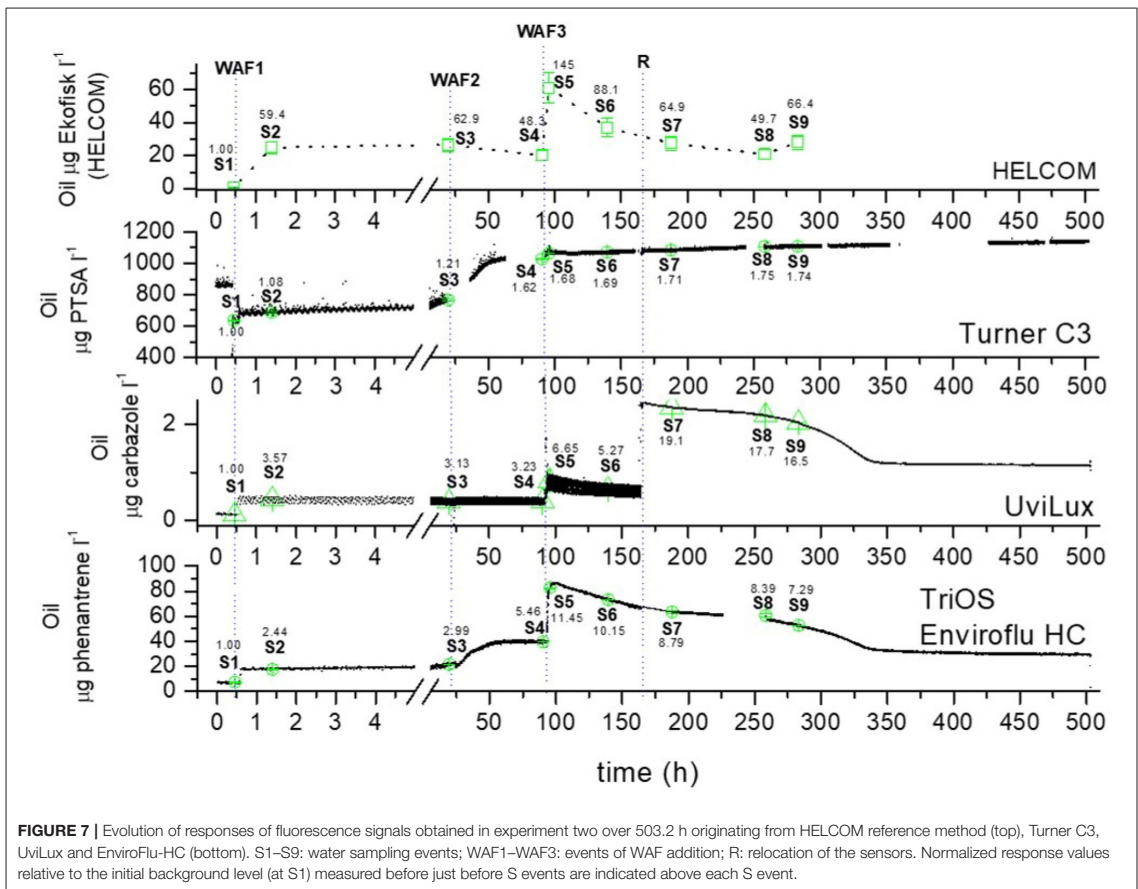
Table 2 summarizes the responses obtained from sensor-based fluorescence right before water samples (GC methods) were collected at events S5 and S7. Event before sample S7 should serve as the primary point for response comparison since it was taken after the readjustment of sensor locations (R). The relative responses compared to initial state S1 of the fluorescence-based

methods, during 165–505 h were (from strongest to weakest): HELCOM, UviLux, EnviroFlu-HC and Turner C3 (Figure 7 including responses at each S event).

Several PAH molecules were good indicators for diesel-originating contamination (Table 2). All naphthalenes provided pronounced responses also at S1 (strongest to weakest): 1-methylnaphthalene (1-MN), naphthalene (NAF) and 2-methylnaphthalene (2-MN) (data not shown). Also, anthracene, acenaphthene and phenanthrene were sensitive and showed a similar temporal evolution as the FLD-based responses and the methylated naphthalenes (1/2-MN).

Concentration of fluoranthene did not change over the experimental period, and Dibenz[a,h]anthracene showed a declining trend compared to the initial seawater (Figure 8). These substances (in addition to acenaphthylene, fluoranthene, dibenzo[a,h]anthracene and pyrene) were poor proxies for WAF contamination in the seawater (Figure 8).

The concentration of aliphatic hydrocarbons followed a similar pattern as those of FLD, methylated naphthalene and



the more sensitive PAHs. The PAH and aliphatic hydrocarbon concentrations also had a similar evolution pattern as the values derived using the HELCOM fluorescence method. Interestingly, the increase in aliphatic hydrocarbon concentrations between S8 and S9 showed a similar increase as the HELCOM method; this change was not visible in any other parameter (Figures 7, 8).

4. RESULTS OF THE FIELD EXPERIMENTS

4.1. FerryBox Experiment

The real-time transmission and online presentation of the FerryBox data worked well, but data gaps occurred systematically in the Baltic Proper due to loss of the GSM network. These gaps typically lasted a maximum of a few hours. An example is presented in Figure 4. The complete data was recovered from the datalogger after the fact. Altogether 58 ship voyages were analyzed. The PAH-transects were visually checked for peaks that would have indicated an oil pollution. No such anomalies were found during the 2-month measurement period

the UviLux and EnviroFlu-HC fluorometers were installed to the FerryBox system.

The detected PAH values stayed between 1 and 2.6 μg carbazole/l for the UviLux and 12.4–25.5 μg phenantrene/l for the EnviroFlu-HC (Figures 9A,B). The detected hydrocarbon values were lowest in the sea areas near Åland and highest in the Stockholm archipelago, where the effect of the natural background of organic carbon from river waters is greater (Figures 9A,B). From 20.5°, longitude eastward, the PAH values were quite homogeneous. Some variation can be seen e.g., between 22°, and 23° longitude (trips 19–23), showing up more clearly in the UviLux data (Figures 9A,B). We surmise that the detected values do not reflect concentration of carbazole, phenantrene or oil in seawater. This interpretation is supported by the chemical monitoring (HELCOM/EU MSFD) and analysis of the Baltic Sea, which has found concentrations below 1 μg oil hydrocarbons/l rather constantly (Pikkarainen and Lemponen, 2005; FIMR and Olsonen, 2007). These low values are considered to be typical for seawater without significant oil pollution (Bicego et al., 1996; Zanardi et al., 1999).

TABLE 2 | Overview on the response levels generated by the fluorescence-based methods and parameters obtained from GC–FID and GC–MS analyses.

Parameter	Background level $\mu\text{g l}^{-1}$	Response at S5 $\mu\text{g l}^{-1}$	Response relative to background level at S5 (-fold)	Response at S7 $\mu\text{g l}^{-1}$	Response relative to background level at S7 (-fold)
Turner C3 fluorescence (PTSA)	634.7 \pm 3.74	1071.7 \pm 2.23	1.68	1084.14 \pm 2.85	1.71
TriOS Enviroflu-HC fluorescence (phenantrene)	7.22 \pm 0.41	82.63 \pm 0.56	11.45	63.4 \pm 1.27	8.79
UviLux fluorescence (carbazole)	0.123 \pm 0.003 ^a	0.819 \pm 0.003 ^a	6.65 ^a	2.351 \pm 0.002	19.10
HELCOM fluorescence	0.42	61 \pm 9.15 ^b (\pm < 0.1) ^c	145.2	27.27 \pm 4.09 (\pm 0.06) ^c	64.92
Aliphatics C10–C21 ^d	98 \pm 29.4	750 \pm 225	7.65	120 \pm 36	1.22
Aliphatics C22–C40 ^d	300 \pm 90	970 \pm 290	3.23	290 \pm 87	0.97
Aliphatics C10–C40 ^d	400 \pm 120	1700 \pm 510	4.25	410 \pm 123	1.025
Total PAHs ^e	0.988 \pm 0.2964 ^e	9.39 \pm 2.82	9.50	1.62 \pm 0.48	1.63
Naphthalene ^f	0.11 \pm 0.02	1.7 \pm 0.34	15.45	0.2 \pm 0.04	1.82
1-methylnaphthalene ^e	0.07 \pm 0.02	2.9 \pm 0.87	41.4	0.25 \pm 0.08	3.57
2-methylnaphthalene ^e	< 0.005	3.5 \pm 1.05	700 ^g	0.17 \pm 0.05	34 ^g
Anthracene ^h	< 0.01	0.10 \pm 0.03	9.7	0.11 \pm 0.04	11
Acenaphthene ^f	0.084 \pm 0.017	0.21 \pm 0.04	2.5	0.098 \pm 0.02	1.17
Acenaphthylene ^d	< 0.005	< 0.005	NA	0.087 \pm 0.026	5.22
Fluoranthene ^d	0.16 \pm 0.05	0.16 \pm 0.05	1	0.16 \pm 0.05	1
Fluorene ^f	0.14 \pm 0.028	0.38 \pm 0.08	2.71	0.18 \pm 0.04	1.29
Dibenz[a,h]anthracene ^d	0.094 \pm 0.028	<0.01	0.11 ^g	< 0.01	0.11 ^g
Phenanthrene ^d	0.22 \pm 0.066	0.32 \pm 0.096	1.45	0.24 \pm 0.072	1.09
Pyrene ^d	0.11 \pm 0.03	0.12 \pm 0.04	1.09	0.12 \pm 0.04	1.09

^aSuppressed signal. ^b \pm 15% error attributed for the method. ^cActual repeatability of parallel samples at S5 and S7. ^dBased on \pm 30% error attributed for the method. ^eBased on \pm 30% error attributed for the method. ^fBased on \pm 20% error attributed for the method. ^gCalculation of relative difference is based on the limit of quantification. ^hBased on \pm 35% error attributed for the method. NA = not available.

The FerryBox and the accompanying sensors were maintained and cleaned frequently. Nevertheless, biofouling still impacted the quality of the measured data as can be seen from the decreasing values between the maintenance visits (Figures 9A,B). The field data suggests that EnviroFlu-HC is affected more strongly by the fouling than UviLux.

4.2. SmartBuoy Experiment

The obtained values ranged between 790 and 1,250 during the monitoring period. The variation pattern was nearly identical with the variation of collected colored organic carbon (CDOM) values, varying between 600 and 890 (Figure 9). The measured data had systematic gaps. On the 12th of December a maintenance visit to the buoy was made to reprogram the datalogger and manually clean the sensors.

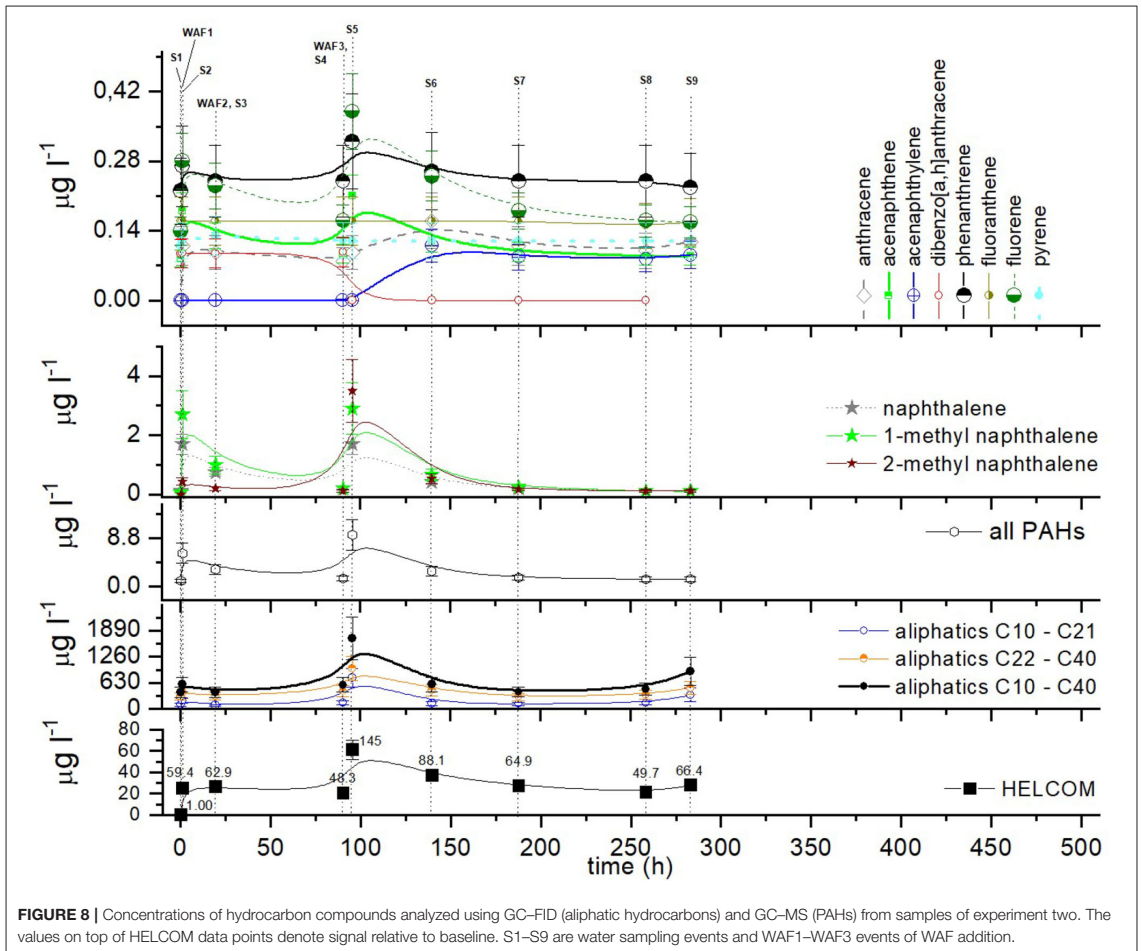
The correlation between the collected hydrocarbon dataset and the CDOM data set collected by the C3 sensor on SmartBuoy was very high (Figure 9D). No anomalous spikes indicative of oil-contamination were present during the test period. The C3 sensor on SmartBuoy was equipped with a mechanical wiper, which cleaned all three optical lenses prior to measuring. No significant reduction in data quality due to biofouling was detected compared to the FerryBox where the detected values gradually decreased after the cleaning (Figure 9). The linear relationship between the two variables changed after the

maintenance on 12 December. This change was probably caused by the readjustment of the mechanical wipers (Joose Mykkänen, Personal communication). Nonetheless, the correlation between the variables remained high (Figure 9D).

During the experimental period, the buoy tolerated several events with significant wave heights over 2 m. The maximum significant wave height reached almost 3 m, which is estimated to be exceeded at this location roughly 1% of the times (Tuomi et al., 2011; Björkqvist et al., 2018). During the monitoring period the current speed reached 39 cm/s, with the mean value being 12 cm/s. The mean yearly current speed (for depth 0–7.5 m) in the area is expected to be under 10 cm/s (Westerlund et al., 2018).

5. DISCUSSION

Laboratory tests showed that optical interferences strongly affected optical PAH detection. The effect of these interferences was corroborated by the strong correlation between oil-related fluorescence and CDOM fluorescence (Figure 9D). CDOM causes interference and false positives whenever it is present sufficiently and not accounted for properly. Similar results arose from the presence of cyanobacteria-derived material. The Baltic Sea contains substantial concentrations of CDOM at any time of year, most prominently close to river outlets. The quenching of



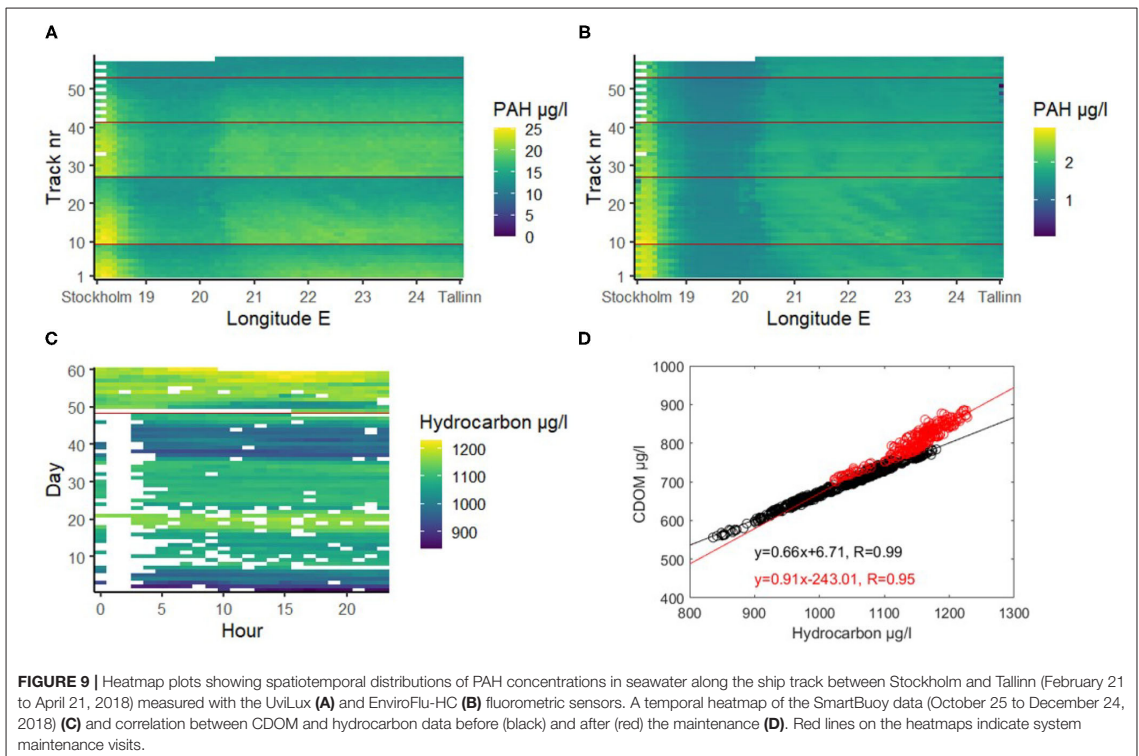
oil-related fluorescence caused by clay-derived turbidity further complicates the interpretation of the signal.

Extensive spring and summer blooms of phytoplankton occur regularly in the Baltic sea (Kahru et al., 2007, 2016; Groetsch et al., 2014). We can also suspect greater interference during summer blooms of cyanobacteria and minor contribution throughout the year as there are always small quantities of chlorophylls and phycocyanin of phytoplankton origin in the surface waters. The spring bloom duration in the Baltic Sea is about one and a half months (Groetsch et al., 2016) and the peak of the bloom in 2018 coincided with the end of the FerryBox experiment (Almén and Tamelander, 2020). Nevertheless, we did not see the signal enhancing effect of the phytoplankton during the FerryBox experiment, as the PAH signals should have increased toward the end of the testing period together with the bloom intensity.

There also exist several overall issues when using fluorometers that are related to the information about the presence and

relative concentration of oil compounds in water. Fluorometers are generally calibrated using a specific oil or specific compounds; thus, the relevant concentration results are relative to the specific oil or compound and the procedure used to calibrate the instrument (Lambert et al., 2003). The response of the fluorometer to oil depends significantly on the oil composition and its weathering state, complicating the quantification of oil concentration further (Henry et al., 1999). Also other studies have noted that the other fluorescent substances in seawater can significantly interfere with direct fluorescence measurements of petroleum hydrocarbons (Henry et al., 1999; Bugden et al., 2008; Tedetti et al., 2010; Cyr et al., 2019). Lastly, a reliable comparison of different sensors would also require a consensus over the units used to report FLD-based results.

Taking account of the aforementioned issues and the knowledge that most of the oil pollution in the Baltic Sea comes from small operational oil spills, and that most cases requiring



criminal prosecution have involved diesel oil, the latter was selected to mimic the oil pollution in our laboratory experiments. Moreover, based on this background and the results of the laboratory tests, the field trials concentrated only on the detection of oil pollution, which should have appeared as a clear peak, deviating from the background fluorescence in the measured response patterns. The question of capabilities to detect different types of oil in the field is not only a question of the detection capabilities of the actual sensors, since also the weathering process for e.g., crude oil and diesel oil differ. In addition, the calibration of the sensors can reflect the a priori expectations of what type of oil might be encountered. It is therefore impossible to give any general recommendations on this subject, and follow-up studies are needed to test the suitability of the sensors used in this study in case they are planned to be used outside the Baltic Sea.

Due to the interfering substances it is difficult to distinguish water quality variations from the responses from oil spills. To combat that problem, suitable mathematical protocols should be explored. Some newer sensors also include built-in correction methods to discriminate oil from the natural interferences. Examples of sensors with such specification are Vlux OilPro (Chelsea Technologies Ltd), SeaOWL UV-A™ (Sea-Bird Scientific) and HM-900 (Pyxis).

Another aspect that needs careful consideration is the measurement or water intake depth of the oil detection systems. After a spill, wind, waves and currents can break the oil spill into droplets and may propel the oil deeper into the water column; this process is called natural dispersion. Dispersion is a complicated physio-chemical process affected by the characteristics of the oil spill (oil type, density, viscosity, thickness) and other seawater properties such as temperature and salinity (Xiankun et al., 1993; Papadimitrakis et al., 2011). Various other physical, chemical, and biological processes begin to alter the oil as well, altogether referred to as weathering process (Mishra and Kumar, 2015; Tarr et al., 2016).

Using sampling and further laboratory analysis the maximum detection depths of naturally dispersed oils has been between 2.5 and 15 m (Cormack and Nichols, 1977; Lichtenthaler and Daling, 1983, 1985). An experiment by Cormack and Nichols (1977), part of which was monitoring naturally dispersed Ekofisk crude oil in the water column, showed comparatively rapid decrease in oil concentration down to 5 m depth, followed by a slower decrease to background levels at 20 m. A similar experiment in Norwegian waters with 10 m³ of topped Statfjord crude oil showed that small concentrations of oil were present to at least a depth of 3 m in the water column under the slick (Lichtenthaler and Daling, 1985). In another experiment done with 2,000 liters of Statfjord

crude oil and of topped Statfjord crude oil the maximum detection depths were 2.5 m (Lichtenthaler and Daling, 1983).

At the Baffin Island Oil Spill experimental site in the Canadian Arctic, flow-through fluorometry was successfully used to monitor a subsurface release of chemically dispersed crude oil cloud over several days, providing real-time and continuous data on oil concentrations in the water column (Green et al., 1983). Nonetheless, during a surface release experiment performed in the same study, petroleum hydrocarbons from the untreated oil were not detected in the water column deeper than 1 m (Humphrey et al., 1987). In a contained oil spill experiment, part of which was 3 liters of crude oil spilled in moored 66 m³ containers in the ocean, a continuous flow-through fluorescence system was capable of detecting oil concentrations down to 8 m, over a period of 7 days (Green et al., 1982). Lunel (1995), using continuous-flow fluorometry (calibrated using discrete samples) found traces of oil down to 5 m after 20 metric ton of a mixture of medium fuel oil and gas oil (in a 50–50 ratio) were experimentally released in United Kingdom waters. Nevertheless, these experiments made in U.K., the Canadian Arctic and inside the British Colombian archipelago might not be directly transferable to the Baltic Sea because of differences in hydrography, and wind and wave conditions.

The probability of detecting oil pollution clearly depends on the weather conditions, and the size, oil type, source and weathering state of the spill. Most of the FerryBox systems are limited to a fixed depth set by the ship's design, as is the case in this study. For the FerryBox system on M/S Baltic Queen, the water is taken in at a depth of approximately 4 m and the SmartBuoy sensors situate 2–3 m below the surface, depending on the sea level. In light of the results of the aforementioned studies, these depths should be suitable for detecting anomalies in fluorescence. Also, for the FerryBox the water will also be mixed by the moving ship itself. Nonetheless, when devising such systems in the future, measurement depths as close to the surface as possible are recommended to ensure higher chance of spill detection.

Biofouling (marine growth) is likewise a major factor limiting the reliability of optical sensors in aquatic studies, especially during long term measurements. Biofouling is the net result of various physical, chemical and biological factors such as water temperature, conductivity, season, and location—to name a few (Delauney et al., 2010). Several antifoulant approaches for optical systems on autonomous platform have been suggested (Manov et al., 2004; Delauney et al., 2010). In our experiments the automatic mechanical cleaning of the sensor on the SmartBoy was satisfactory but the fouling of the FerryBox sensors after the maintenance visits is clearly there. It is not evident how much biofouling affects the oil detection capabilities of the sensors, but in our experiment is seemed to be of secondary importance compared to the presence of the other interfering substances.

6. CONCLUSIONS

Laboratory experiments indicated that the sensitivity of the sensors to diesel oil is good and they provide useful data on oil

in seawater. Fluorescent compounds from the oil were detectable by the fluorometric sensors for at least 20 days. Our laboratory tests were conducted with diesel oil, Baltic Sea water, and local interfering substances and therefore may not be representative of different types of oils or marine areas. The main issue with the sensors we used was their specificity, since the presence of humic substances (CDOM), phytoplankton (phycocyanin and chlorophylls) or high turbidity (suspended/colloidal clay) can cause false positives or signal quenching when detecting oil. In our tests the impact of algal material was clearly the most significant. We suggest exploring mathematical protocols or use of more sophisticated sensors for distinguishing actual oil pollution from co-occurring optical interference.

The three tested portable fluorimeters were successfully integrated to the FerryBox and SmartBuoy systems. The systems functioned semi-autonomously well during the 2-month testing periods, as did the real-time data transmissions and user interfaces/data visualization. The signal quenching effect of the biofouling could be seen on the FerryBox fluorimeters, but it was a secondary problem compared to the interfering substances in the seawater. Nonetheless, automatic cleaning methods of the systems and sensors are recommended.

In this paper we did not touch upon the automatic detection of the anomalous events in the detected values that would indicate an oil spill, but this kind of an algorithm should be developed if the detection system is to be used operationally. When these systems can reliably detect oil, a comprehensive network of SmartBuoys and FerryBoxes covering the major fairways can greatly complement the aerial surveillance, ship-based and satellite monitoring that are presently used to, among other things, detect oil in seawater.

DATA AVAILABILITY STATEMENT

The raw data supporting the conclusions of this article will be made available by the authors, without undue reservation. The data received from the real-time transmission of the FerryBox system can be viewed on a public web-site (TalTech, 2017).

AUTHOR CONTRIBUTIONS

SP: investigation, validation, formal analysis, writing—original draft, and visualization. HK: methodology, investigation, formal analysis, writing—original draft, and visualization. J-VB: validation, writing—review and editing, and supervision. RU: writing—review and editing and supervision. All authors contributed to the article and approved the submitted version.

FUNDING

This manuscript has been produced within project GRACE, which received funding from the European Union's Horizon 2020 research and innovation programme under Grant agreement no. 679266 and supported by the Estonian Research Council (Grant no. PSG22).

ACKNOWLEDGMENTS

We gratefully acknowledge the contributions of Tarmo Kõuts, who was the head of work package 1 (Oil spill detection, monitoring, fate and distribution) in the GRACE project and did the original conceptualization of the FerryBox experiment. We want to thank AS Tallink Grupp for allowing us to use the FerryBox installation of their vessel for the purposes of this study. Furthermore, we would like to thank Kaimo Vahter for his contribution to the installation and upkeep of the FerryBox system, and for transfer and technical advice on the

UviLux. We also appreciate the work done by the employees of Arctia Meritaito Oy and Luode Consulting Oy in carrying out the SmartBuoy experiment, and thank them for providing the consequent data and for lending instrumentation (TriOS HC-500 and Turner C3), especially Jooe Mykkänen from Luode Consulting is thanked for providing technical assistance during the campaign. Jari Nuutinen and Helena Kutramainen are thanked for the GC-MS and GC-FID analyses. Furthermore, we also wish to acknowledge help by Jere Riikonen (SYKE MRC) in laboratory experiments and Kirsten Jørgensen (SYKE MRC) acting as coordinator of GRACE.

REFERENCES

- Abdel-Shafy, H. I., and Mansour, M. S. (2016). A review on polycyclic aromatic hydrocarbons: source, environmental impact, effect on human health and remediation. *Egypt. J. Petroleum* 25, 107–123. doi: 10.1016/j.ejpe.2015.03.011
- Almén, A. K., and Tamelander, T. (2020). Temperature-related timing of the spring bloom and match between phytoplankton and zooplankton. *Mar. Biol. Res.* 16, 674–682. doi: 10.1080/17451000.2020.1846201
- Alpers, W., Holt, B., and Zeng, K. (2017). Oil spill detection by imaging radars: challenges and pitfalls. *Remote Sens. Environ.* 201, 133–147. doi: 10.1016/j.rse.2017.09.002
- Al-Ruzouq, R., Gibril, M. B. A., Shanableh, A., Kais, A., Hamed, O., Al-Mansoori, S., et al. (2020). Sensors, features, and machine learning for oil spill detection and monitoring: a review. *Remote Sens.* 12, 1–42. doi: 10.3390/rs12203338
- Benson, B., Chang, G., Spada, F., Manov, D., and Kastner, R. (2008). “Real-time telemetry options for ocean observing systems,” in *European Telemetry Conference* (Munich), 5.
- Bicego, M. C., Weber, R. R., and Ito, R. G. (1996). Aromatic hydrocarbons on surface waters of Admiralty Bay, King George Island, Antarctica. *Mar. Pollut. Bull.* 32, 549–553. doi: 10.1016/0025-326X(96)84574-7
- Björkqvist, J.-V., Lukas, I., Alari, V., van Vledder, G. P., Hulst, S., Pettersson, H., et al. (2018). Comparing a 41-year model hindcast with decades of wave measurements from the Baltic Sea. *Ocean Eng.* 152, 57–71. doi: 10.1016/j.oceaneng.2018.01.048
- Bodkin, J. L., Ballache, B. E., Dean, T. A., Fukuyama, A. K., Jewett, S. C., McDonald, L., et al. (2002). Sea otter population status and the process of recovery from the 1989 ‘Exxon Valdez’ oil spill. *Mar. Ecol. Prog. Ser.* 241, 237–253. doi: 10.3354/meps241237
- Brekke, C., and Solberg, A. H. (2005). Oil spill detection by satellite remote sensing. *Remote Sens. Environ.* 95, 1–13. doi: 10.1016/j.rse.2004.11.015
- Brussaard, C. P., Peperzak, L., Beggha, S., Wick, L. Y., Wuerz, B., Weber, J., et al. (2016). Immediate ecotoxicological effects of short-lived oil spills on marine biota. *Nat. Commun.* 7:11206. doi: 10.1038/ncomms11206
- Bugden, J. B. C., Yeung, C. W., Kepkay, P. E., and Lee, K. (2008). Application of ultraviolet fluorometry and excitation-emission matrix spectroscopy (EEMS) to fingerprint oil and chemically dispersed oil in seawater. *Mar. Pollut. Bull.* 56, 677–685. doi: 10.1016/j.marpolbul.2007.12.022
- Câmara, S. F., Pinto, F. R., da Silva, F. R., Soares, M. D. O., and De Paula, T. M. (2021). Socioeconomic vulnerability of communities on the Brazilian coast to the largest oil spill (2019–2020) in tropical oceans. *Ocean Coastal Manag.* 202:105506. doi: 10.1016/j.ocecoaman.2020.105506
- Chavez, F. P., Pennington, J. T., Herlien, R., Jannasch, H., Thurmond, G., and Friederich, G. E. (1997). Moorings and drifters for real-time interdisciplinary oceanography. *J. Atmos. Ocean. Technol.* 14, 1199–1211. doi: 10.1175/1520-0426(1997)014<1199:MADFRTan>2.0.CO;2
- Cohen, M. J. (1993). Economic impact of an environmental accident: a time-series analysis of the Exxon Valdez oil spill in southcentral Alaska. *Sociol. Spectrum* 13, 35–63. doi: 10.1080/02732173.1993.9982016
- Cormack, D., and Nichols, J. A. (1977). The concentrations of oil in sea water resulting from natural and chemically induced dispersion of oil slicks. *Int. Oil Spill Conf. Proc.* 1977, 381–385. doi: 10.7901/2169-3358-1977-1-381
- Cyr, F., Tedetti, M., Besson, F., Bhairy, N., and Goux, M. (2019). A glider-compatible optical sensor for the detection of polycyclic aromatic hydrocarbons in the marine environment. *Front. Mar. Sci.* 6:1110. doi: 10.3389/fmars.2019.00110
- D’Andrea, M. A., and Reddy, G. K. (2014). Crude oil spill exposure and human health risks. *J. Occup. Environ. Med.* 56, 1029–1041. doi: 10.1097/JOM.0000000000000217
- Delauney, L., Compare, C., and Lehaitre, M. (2010). Biofouling protection for marine environmental sensors. *Ocean Sci.* 6, 503–511. doi: 10.5194/os-6-503-2010
- Engelhardt, F. (1987). “Assessment of the vulnerability of marine mammals to oil pollution,” in *Fate and Effects of Oil in Marine Ecosystems*, eds J. Kuiper and W. Van den Brink (Dordrecht: Martinus Nijhoff Publishers), 101–115.
- Farrington, J. W. (2014). Oil pollution in the marine environment II: Fates and effects of oil spills. *Environment* 56, 16–31. doi: 10.1080/00139157.2014.922382
- Ferraro, G., Meyer-Roux, S., Muellenhoff, O., Pavliha, M., Svetak, J., Tarchi, D., et al. (2009). Long term monitoring of oil spills in European seas. *Int. J. Remote Sens.* 30, 627–645. doi: 10.1080/01431160802339464
- F. I. M. R., and Olsson, R. (2007). *FIMR Monitoring of the Baltic Sea Environment—Annual Report 2006*. Technical Report 59, The Finnish Institute of Marine Research.
- Fingas, M., and Brown, C. E. (2018). A review of oil spill remote sensing. *Sensors* 18, 1–18. doi: 10.1007/978-1-4939-2493-6_732-4
- Fox, C. H., O’Hara, P. D., Bertazzon, S., Morgan, K., Underwood, F. E., and Paquet, P. C. (2016). A preliminary spatial assessment of risk: Marine birds and chronic oil pollution on Canada’s Pacific coast. *Sci. Total Environ.* 573, 799–809. doi: 10.1016/j.scitotenv.2016.08.145
- Gade, M., Scholz, J., and von Viebahn, C. (2000). On the detectability of marine oil pollution in European marginal waters by means of ERS SAR imagery. *Int. Geosci. Remote Sens. Sympos.* 6, 2510–2512. doi: 10.1109/IGARSS.2000.859623
- Green, D., Humphrey, B., and Fowler, B. (1983). The use of flow-through fluorometry for tracking dispersed oil. *Int. Oil Spill Conf.* 1983, 473–475. doi: 10.7901/2169-3358-1983-1-473
- Green, D. R., Buckley, J., and Humphrey, B. (1982). *Fate of Chemically Dispersed Oil in the Sea, A Report on Two Field Experiments*. Environment Protection Service Report EPS 4-EC-82-5. Environmental Impact Control Directorate, Canada.
- Groetsch, P. M. M., Simis, S. G. H., Eleveld, M. A., and Peters, S. W. M. (2014). Cyanobacterial bloom detection based on coherence between ferrybox observations. *J. Mar. Syst.* 140, 50–58. doi: 10.1016/j.jmarsys.2014.05.015
- Groetsch, P. M. M., Simis, S. G. H., Eleveld, M. A., and Peters, S. W. M. (2016). Spring Blooms in the Baltic Sea have weakened but lengthened from 2000 to 2014. *Biogeosciences* 13, 4959–4973. doi: 10.5194/bg-13-4959-2016
- Hayakawa, K. (2018). “Oil Spills and Polycyclic Aromatic Hydrocarbons,” in *Polycyclic Aromatic Hydrocarbons*, ed K. Hayakawa (Singapore: Springer), 213–223. doi: 10.1007/978-981-10-6775-4_16
- He, L. M., Kear-padilla, L. L., Lieberman, S. H., and Andrews, J. M. (2003). Rapid *in situ* determination of total oil concentration in water using ultraviolet fluorescence and light scattering coupled with artificial neural networks. *Anal. Chim. Acta* 478, 245–258. doi: 10.1016/S0003-2670(02)01471-X
- HELCOM (2003). *The Baltic Marine Environment 1999–2002*. Technical Report 87, The Helsinki Commission. Available online at: <https://www.helcom.fi/wp-content/uploads/2019/10/BSEP87.pdf> (accessed September 2, 2021).

- HELCOM (2013). *Risks of Oil and Chemical Pollution*. Technical report, HELCOM. Available online at: https://helcom.fi/media/publications/BRISK-BRISK-RU_SummaryPublication_spill_of_oil.pdf (accessed September 2, 2021).
- HELCOM (2017). *Helcom Metadata Catalogue-2016 All Ship Types Ais Shipping Density*. Available online at: <http://metadata.helcom.fi/geonetwork/srv/eng/catalog.search#/metadata/95c5098e-3a38-48ee-ab16-b80a99f50fef> (accessed September 2, 2021).
- HELCOM (2018a). *HELCOM Maritime Assessment 2018 - Maritime Activities in the Baltic Sea*. Technical report, The Helsinki Commission. Available online at: <https://www.helcom.fi/wp-content/uploads/2019/08/BSEP152-1.pdf> (accessed September 2, 2021).
- HELCOM (2018b). *Helcom Metadata Catalogue-Illegal Oil Discharges*. Available online at: <http://metadata.helcom.fi/geonetwork/srv/eng/catalog.search#/metadata/345c9b95-6e9c-44a4-b02a-ee4304cccffc> (accessed September 2, 2021).
- HELCOM (2018c). *Operational oil spills from ships - HELCOM core indicator report*. Technical report, HELCOM. Available online at: <https://helcom.fi/media/core%20indicators/Operational-oil-spills-from-ships-HELCOM-core-indicator-2018.pdf> (accessed September 2, 2021).
- Henry, C. B., Roberts, P. O., and Overton, E. B. (1999). "A primer on *in situ* fluorometry to monitor dispersed oil," in *International Oil Spill Conference Proceedings* (Seattle, WA).
- Honda, M., and Suzuki, N. (2020). Toxicities of polycyclic aromatic hydrocarbons for aquatic animals. *Int. J. Environ. Res. Public Health* 17, 1363. doi: 10.3390/ijerph17041363
- Humphrey, B., Green, D. R., Fowler, B. R., Hope, D., and Boehm, P. D. (1987). The fate of oil in the water column following experimental oil spills in the arctic marine nearshore. *Arctic* 40, 124–132. doi: 10.14430/arctic1808
- Hydes, D. J., Kelly-Gerreyn, B. A., Colijn, F., Petersen, W., Schroeder, F., Mills, D., et al. (2010). "The way forward in developing and integrating FerryBox technologies," in *Proceedings of OceanObs'09: Sustained Ocean Observations and Information for Society* (Venice), 503–510.
- Hylland, K. (2006). Polycyclic aromatic hydrocarbon (PAH) ecotoxicology in marine ecosystems. *J. Toxicol. Environ. Health A* 69, 109–123. doi: 10.1080/15287390500259327
- Jensen, H. V., Andersen, J. H., Daling, P. S., and Nost, E. (2008). "Recent experience from multiple remote sensing and monitoring to improve oil spill response operations," in *International Oil Spill Conference-IOSC 2008, Proceedings* (Savannah, GA), 407–412.
- Jenssen, B. M. (1994). Review article: Effects of oil pollution, chemically treated oil, and cleaning on thermal balance of birds. *Environ. Pollut.* 86, 207–215. doi: 10.1016/0269-7491(94)90192-9
- Jha, M. N., Levy, J., and Gao, Y. (2008). Advances in remote sensing for oil spill disaster management: state-of-the-art sensors technology for oil spill surveillance. *Sensors* 8, 236–255. doi: 10.3390/s8010236
- Jørgensen, K. S., Kreutzer, A., Lehtonen, K. K., Kankaanpää, H., Rytönen, J., Wegeberg, S., et al. (2019). The EU Horizon 2020 project GRACE: integrated oil spill response actions and environmental effects. *Environ. Sci. Eur.* 31:44. doi: 10.1186/s12302-019-0227-8
- Kahru, M., Elmgren, R., and Savchuk, O. P. (2016). Changing seasonality of the Baltic Sea. *Biogeosciences* 13, 1009–1018. doi: 10.5194/bg-13-1009-2016
- Kahru, M., Savchuk, O. P., and Elmgren, R. (2007). Satellite measurements of cyanobacterial bloom frequency in the Baltic Sea: interannual and spatial variability. *Mar. Ecol. Prog. Ser.* 343, 15–23. doi: 10.3354/meps06943
- Karlson, B., Andersson, L. S., Kaitala, S., Kronsell, J., Mohlin, M., Seppälä, J., et al. (2016). A comparison of FerryBox data vs. monitoring data from research vessels for near surface waters of the Baltic Sea and the Kattegat. *J. Mar. Syst.* 162, 98–111. doi: 10.1016/j.jmarsys.2016.05.002
- Kikas, V., and Lips, U. (2016). Upwelling characteristics in the Gulf of Finland (Baltic Sea) as revealed by Ferrybox measurements in 2007–2013. *Ocean Sci.* 12, 843–859. doi: 10.5194/os-12-843-2016
- Kim, M., Hyuk, U., Hee, S., Jung, J.-H., Choi, H.-W., An, J., et al. (2010). Hebei Spirit oil spill monitored on site by fluorometric detection of residual oil in coastal waters off Taean, Korea. *Mar. Pollut. Bull.* 60, 383–389. doi: 10.1016/j.marpolbul.2009.10.015
- Krestenitis, M., Orfanidis, G., Ioannidis, K., Avgerinakis, K., Vrochidis, S., and Kompatsiaris, I. (2019). Oil spill identification from satellite images using deep neural networks. *Remote Sens.* 11, 1–22. doi: 10.3390/rs1151762
- Lambert, P., Fingas, M., and Goldthorp, M. (2001). An evaluation of field total petroleum hydrocarbon (TPH) systems. *J. Hazard Mater.* 83, 65–81. doi: 10.1016/S0304-3894(00)00328-9
- Lambert, P., Goldthorp, M., Fieldhouse, B., Wang, Z., Fingas, M., Pearson, L., et al. (2003). Field fluorimeters as dispersed oil-in-water monitors. *J. Hazard Mater.* 102, 57–79. doi: 10.1016/S0304-3894(03)00202-4
- Lichtenthaler, R. G., and Daling, P. S. (1983). "Dispersion of chemically treated crude oil in Norwegian offshore waters," in *Proceedings of the 1983 Oil Spill Conference* (San Antonio, TX), 7–14.
- Lichtenthaler, R. G., and Daling, P. S. (1985). "Aerial application of dispersants comparison of slick behavior of chemically treated versus non-treated slicks," in *International Oil Spill Conference Proceedings (1985)* (Los Angeles, CA), 471–478.
- Lips, U., Kikas, V., Liblik, T., and Lips, I. (2016). Multi-sensor *in situ* observations to resolve the sub-mesoscale features in the stratified Gulf of Finland. *Baltic Sea. Ocean Sci.* 12, 715–732. doi: 10.5194/os-12-715-2016
- Liubartseva, S., De Dominicis, M., Oddo, P., Coppini, G., Pinardi, N., and Greggio, N. (2015). Oil spill hazard from dispersal of oil along shipping lanes in the Southern Adriatic and Northern Ionian Seas. *Mar. Pollut. Bull.* 90, 259–272. doi: 10.1016/j.marpolbul.2014.10.039
- Lunel, T. (1995). Dispersant effectiveness at sea. *Int. Oil Spill Conf. Proc.* 1995, 147–155. doi: 10.7901/2169-3358-1995-1-147
- Malkov, V., and Sievert, D. (2010). Oil-in-water fluorescence sensor in wastewater and other industrial applications. *Power Plant Chem.* 12, 144–154.
- Manov, D. V., Chang, G. C., and Dickey, T. D. (2004). Methods for reducing biofouling of moored optical sensors. *J. Atmos. Ocean. Technol.* 21, 958–968. doi: 10.1175/1520-0426(2004)021andlt;0958:MFRBOMandgt;2.0.CO;2
- Marghany, M. (2016). Automatic mexico gulf oil spill detection from radarsat-2 SAR satellite data using genetic algorithm. *Acta Geophys.* 64, 1916–1941. doi: 10.1515/acgeo-2016-0047
- Mills, D. K., Laane, R., Rees, J. M., Rutgers van der Loeff, M., Suylen, J. M., Pearce, D. J., et al. (2003). Smartbuoy: a marine environmental monitoring buoy with a difference. *Elsevier Oceanogr. Ser.* 69, 311–316. doi: 10.1016/S0422-9894(03)80050-8
- Mishra, A. K., and Kumar, G. S. (2015). Weathering of oil spill: modeling and analysis. *Aquatic Procedia* 4, 435–442. doi: 10.1016/j.aqpro.2015.02.058
- Moroni, D., Pieri, G., Salvetti, O., Tampucci, M., Domenici, C., and Tonacchi, A. (2016). Sensorized buoy for oil spill early detection. *Methods Oceanogr.* 17:221–231. doi: 10.1016/j.mio.2016.10.002
- Nam, S., Kim, G., Kim, K.-r., Kim, K., Cheng, L. O., Kim, K.-W., et al. (2005). Application of real-time monitoring buoy systems for physical and biogeochemical parameters in the coastal ocean around the Korean peninsula. *Mar. Technol. Soc. J.* 39, 70–80. doi: 10.4031/002533205787444024
- Papadimitrakis, I., Psaltaki, M., and Markatos, N. (2011). 3-D oil spill modelling. Natural dispersion and the spreading of oil-water emulsions in the water column. *Global Nest J.* 13, 325–338. doi: 10.30955/gnj.000726
- Papoutsas, C., Kounoudes, A., Milis, M., Toullos, L., Retalis, A., Kyrou, K., et al. (2012). Monitoring turbidity in asprokremmos dam in cyprus using earth observation and smart buoy platform. *Eur. Water* 38, 25–32.
- Petersen, W. (2014). FerryBox systems: State-of-the-art in Europe and future development. *J. Mar. Syst.* 140, 4–12. doi: 10.1016/j.jmarsys.2014.07.003
- Petersen, W., Petschatnikov, M., and Schroeder, F. (2003). FerryBox systems for monitoring coastal waters. Building the European capacity in operational oceanography. *Proc. Third Int. Conf. EuroGOOS* 69, 325–333. doi: 10.1016/S0422-9894(03)80052-1
- Petersen, W., Schroeder, F., and Bockelmann, F. D. (2011). FerryBox - Application of continuous water quality observations along transects in the North Sea. *Ocean Dyn.* 61, 1541–1554. doi: 10.1007/s10236-011-0445-0
- Pikkarainen, A. L., and Lemponen, P. (2005). Petroleum hydrocarbon concentrations in Baltic Sea subsurface water. *Boreal Environ. Res.* 10, 125–134.
- Polinov, S., Bookman, R., and Levin, N. (2021). Spatial and temporal assessment of oil spills in the Mediterranean Sea. *Mar. Pollut. Bull.* 167:112338. doi: 10.1016/j.marpolbul.2021.112338
- Ribeiro, L. C. D. S., Souza, K. B. D., Domingues, E. P., and Magalhães, A. S. (2021). Blue water turns black: economic impact of oil spill on

- tourism and fishing in Brazilian Northeast. *Curr. Issues Tour.* 24, 1042–1047. doi: 10.1080/13683500.2020.1760222
- Ridoux, V., Lafontaine, L., Bustamante, P., Caurant, F., Dabin, W., Delcroix, C., et al. (2004). The impact of the “Erika” oil spill on pelagic and coastal marine mammals: combining demographic, ecological, trace metals and biomarker evidences. *Aquat. Living Resour.* 17, 379–387. doi: 10.1051/alr:2004031
- Rytönen, J., Siitonen, L., Riipi, T., Sassi, J., and Sukselainen, J. (2002). *Statistical Analyses of the Baltic Maritime Traffic*. Technical Report VAL34-012344, VTT Technical research centre of Finland. Available online at: <https://cris.vtt.fi/en/publications/statistical-analyses-of-the-baltic-maritime-traffic> (accessed September 2, 2021).
- Samiullah, Y. (1985). Biological effects of marine oil pollution. *Oil Petrochem. Pollut.* 2, 235–264. doi: 10.1016/S0143-7127(85)90233-9
- Sandifer, P. A., Ferguson, A., Finucane, M. L., Partyka, M., Solo-Gabriele, H. M., Walker, A. H., et al. (2021). Human health and socioeconomic effects of the deepwater horizon oil spill in the gulf of Mexico. *Oceanography* 34, 174–191. doi: 10.5670/oceanog.2021.125
- Sankaran, K. (2019). Protecting oceans from illicit oil spills: environment control and remote sensing using spaceborne imaging radars. *J. Electromag. Waves Appl.* 33, 2373–2403. doi: 10.1080/09205071.2019.1685409
- Schneider, B., Gülzow, W., Sadkowiak, B., and Rehder, G. (2014). Detecting sinks and sources of CO₂ and CH₄ by ferrybox-based measurements in the Baltic Sea: three case studies. *J. Mar. Syst.* 140, 13–25. doi: 10.1016/j.jmarsys.2014.03.014
- Serra-Sogas, N., O'Hara, P. D., Canessa, R., Keller, P., and Pelot, R. (2008). Visualization of spatial patterns and temporal trends for aerial surveillance of illegal oil discharges in western Canadian marine waters. *Mar. Pollut. Bull.* 56, 825–833. doi: 10.1016/j.marpolbul.2008.02.005
- Shultz, J. M., Walsh, L., Garfin, D. R., Wilson, F. E., and Neria, Y. (2015). The 2010 deepwater horizon oil spill: the trauma signature of an ecological disaster. *J. Behav. Health Serv. Res.* 42, 58–76. doi: 10.1007/s11414-014-9398-7
- Sipelgas, L., and Uiboupin, R. (2007). “Elimination of oil spill like structures from radar image using MODIS data,” in *International Geoscience and Remote Sensing Symposium (IGARSS)* (Barcelona), 429–431.
- Solberg, A. H. (2012). Remote sensing of ocean oil-spill pollution. *Proc. IEEE* 100, 2931–2945. doi: 10.1109/JPROC.2012.2196250
- Stephenson, R. (1997). Effects of oil and other surface-active organic pollutants on aquatic birds. *Environ. Conserv.* 24, 121–129. doi: 10.1017/S0376892997000180
- Taleghani, N. D., and Tyagi, M. (2017). Impacts of major offshore oil spill incidents on petroleum industry and regional economy. *J. Energy Resour. Technol. Trans. ASME* 139, 1–7. doi: 10.1115/1.4035426
- TalTech (2017). *M/S BALTIC QUEEN FerryBox Monitoring System*. Available online at: <http://on-line.msi.ttu.ee/GRACEferry/> (accessed September 2, 2021).
- Tarr, M. A., Zito, P., Overton, E. B., Olson, G. M., Adhikari, P. L., and Reddy, C. M. (2016). Weathering of oil spilled in the marine environment. *Oceanography* 29, 126–135. doi: 10.5670/oceanog.2016.77
- Tedetti, M., Guigue, C., and Goutx, M. (2010). Utilization of a submersible UV fluorometer for monitoring anthropogenic inputs in the Mediterranean coastal waters. *Mar. Pollut. Bull.* 60, 350–362. doi: 10.1016/j.marpolbul.2009.10.018
- Tuomi, L., Kahma, K. K., and Pettersson, H. (2011). Wave hindcast statistics in the seasonally ice-covered Baltic Sea. *Boreal Environ. Res.* 16, 451–472.
- Uiboupin, R., Raudsepp, U., and Sipelgas, L. (2008). “Detection of oil spills on SAR images, identification of polluters and forecast of the slicks trajectory,” in *US/EU-Baltic International Symposium: Ocean Observations, Ecosystem-Based Management and Forecasting - Provisional Symposium Proceedings, BALTIC* (Tallinn), 6–10.
- Westerlund, A., Tuomi, L., Alenius, P., Miettunen, E., and Vankevich, R. E. (2018). Attributing mean circulation patterns to physical phenomena in the Gulf of Finland. *Oceanologia* 60, 16–31. doi: 10.1016/j.oceano.2017.05.003
- WWF (2010). *Future Trends in the Baltic Sea. Baltic Ecoregion Programme - Future Trends in the Baltic Sea*, 1–40. Available online at: https://www.wwfse.cdn.triggerfish.cloud/uploads/2019/01/wwf_future_trends_in_the_baltic_sea_2010_1.pdf (accessed September 2, 2021).
- Xiankun, L., Jing, L., and Shuzhu, C. (1993). Dynamic model for oil slick dispersion into a water column—a wind-driven wave tank experiment. *Chin. J. Oceanol. Limnol.* 11, 161–170. doi: 10.1007/BF02850823
- Xu, J., Wang, H., Cui, C., Zhao, B., and Li, B. (2020). Oil spill monitoring of shipborne radar image features using SVM and local adaptive threshold. *Algorithms* 13:69. doi: 10.3390/a13030069
- Zanardi, E., Bicego, M. C., and Weber, R. R. (1999). Dissolved/dispersed petroleum aromatic hydrocarbons in the Sao Sebastiao Channel, São Paulo, Brazil. *Mar. Pollut. Bull.* 38, 410–413. doi: 10.1016/S0025-326X(97)00194-X
- Zeng, K., and Wang, Y. (2020). A deep convolutional neural network for oil spill detection from spaceborne SAR images. *Remote Sens.* 12, 1015. doi: 10.3390/rs12061015

Conflict of Interest: The authors declare that the research was conducted in the absence of any commercial or financial relationships that could be construed as a potential conflict of interest.

Publisher's Note: All claims expressed in this article are solely those of the authors and do not necessarily represent those of their affiliated organizations, or those of the publisher, the editors and the reviewers. Any product that may be evaluated in this article, or claim that may be made by its manufacturer, is not guaranteed or endorsed by the publisher.

Copyright © 2021 Pärt, Kankaanpää, Björkqvist and Uiboupin. This is an open-access article distributed under the terms of the Creative Commons Attribution License (CC BY). The use, distribution or reproduction in other forums is permitted, provided the original author(s) and the copyright owner(s) are credited and that the original publication in this journal is cited, in accordance with accepted academic practice. No use, distribution or reproduction is permitted which does not comply with these terms.

Paper II

Alari, V., Björkqvist, J. V., Kaldvee, V., Mölder, K., Rikka, S., Kask-Korb, A., Vahter, K., Pärt, S., Vidjajev, N., & Tõnisson, H. (2022). **LainePoiss® — A Lightweight and Ice-Resistant Wave Buoy**. *Journal of Atmospheric and Oceanic Technology*, 39(5), 573–594. <https://doi.org/10.1175/JTECH-D-21-0091.1>

LainePoiss[®]—A Lightweight and Ice-Resistant Wave Buoy

VICTOR ALARI,^a JAN-VICTOR BJÖRQVIST,^{b,a,c} VALDUR KALDVEE,^d KRISTJAN MÖLDER,^d SANDER RIKKA,^a
ANNE KASK-KORB,^c KAIMO VAHTER,^a SIIM PÄRT,^a NIKON VIDJAJEV,^a AND HANNES TÖNISSON^f

^a Department of Marine Systems, Tallinn University of Technology, Tallinn, Estonia

^b Norwegian Meteorological Institute, Bergen, Norway

^c Marine Research, Finnish Meteorological Institute, Helsinki, Finland

^d WiseParker OÜ, Tallinn, Estonia

^e Estonian Maritime Academy, Tallinn University of Technology, Tallinn, Estonia

^f Institute of Ecology, Tallinn University, Tallinn, Estonia

(Manuscript received 1 July 2021, in final form 4 December 2021)

ABSTRACT: Wave buoys are a popular choice for measuring sea surface waves, and there is also an increasing interest for wave information from ice-covered water bodies. Such measurements require cost-effective, easily deployable, and robust devices. We have developed LainePoiss (LP)—an ice-resistant and lightweight wave buoy. It calculates the surface elevation by double integrating the data from the inertial sensors of the microelectromechanical system (MEMS), and transmits wave parameters and spectra in real time over cellular or satellite networks. LP was validated through 1) sensor tests, 2) wave tank experiments, 3) a field validation against a Directional Waverider, 4) an intercomparison of several buoys in the field, and 5) field measurements in the Baltic Sea marginal ice zone. These extensive field and laboratory tests confirmed that LP performed well (e.g., the bias of H_{m0} in the field was 0.01 m, with a correlation of 0.99 and a scatter index of 8%; the mean absolute deviation of mean wave direction was 7°). LP was also deployed with an unmanned aerial vehicle and we present our experience of such operations. One issue that requires further development is the presence of low-frequency artifacts caused by the dynamic noise of the gyroscope. For now, a correction method is presented to deal with the noise.

SIGNIFICANCE STATEMENT: Operational wave buoys are large and therefore expensive and inconvenient to deploy. Many commercially available devices cannot measure short waves and are not tested in ice. Our purpose was to develop an affordable wave buoy that is lightweight, ice resistant, capable of measuring short waves, and also has a longer operating life than existing research buoys. The buoy is easily deployed with a small boat or even an industrial drone, thus reducing operating costs. The buoy is accurate, and captures waves that are too short for operational wave buoys. This is relevant for coastal planning in, e.g., archipelagos and narrow fjords. We measured waves in ice in the Baltic Sea, and are planning to extend these measurements to Antarctica.

KEYWORDS: Sea ice; Wind waves; Air-sea interaction; Buoy observations


1. Introduction

Wind-generated waves with periods of up to 25 s dominate the spectrum of ocean surface vertical variance (Munk 1950; Holthuijsen 2007). These waves are observed visually, but an objective quantification of wave heights, lengths, and propagation directions requires measurements with in situ or remote sensing technologies. This paper focuses on a newly developed wave measuring buoy.

In situ instruments do not measure wave properties directly. At the sea surface, wave buoys should follow the three-dimensional movement of water particles while measuring the inertial data or the Doppler shift of a GPS signal (Herbers et al. 2012). Below the sea surface, pressure transducers measure wave-induced pressure fluctuations (Cavaleri

1980). Doppler current meters measure the wave-induced orbital motions (Gordon and Lohrmann 2002), and inverted echo sounders measure acoustic travel time between the device and the sea surface (Wadhams 1978). Wave gauges piercing the sea surface measure the up-and-down movement of water through electrical capacitance or resistance (Donelan et al. 1985; Graber et al. 2000). The surface wave spectra is then calculated from the measured physical quantity by mathematical transformations and wave theory.

All the measurements techniques in the above (nonexhaustive) list are feasible, but have their own limitations and peculiarities, for example, gaps in data due to salty water over washing the buoy and blocking the GPS signal (Björkqvist et al. 2016), spurious data in echo soundings generated by breaking waves, and diminishing of short waves in pressure recordings (Bishop and Donelan 1987). More generally, the size of the instrument, the basic measurement principle, and the meteorology–ocean conditions affect the measurement result. Besides inherent limitations, operational and practical considerations, like ease of use and cost of the instrument, might be important.

 Denotes content that is immediately available upon publication as open access.

Corresponding author: Victor Alari, victor.alari@taltech.ee

DOI: 10.1175/JTECH-D-21-0091.1

© 2022 American Meteorological Society. For information regarding reuse of this content and general copyright information, consult the [AMS Copyright Policy](#) ([www.ametsoc.org/PUBSReuseLicenses](#)).

Majority of operational wave measurements are done with surface-following buoys, which may also include sensors for recording atmospheric and upper-ocean state variables (Thomson 2012). These buoys can be tethered to the sea floor or allowed to drift under the influence of wind and currents. An advantage of these buoys is their long operational life (several years). However, the established operational buoys are large and heavy. The National Data Buoy Center of NOAA has tailored meteorology–ocean buoys, equipped with wave measuring sensors, ranging from 1.8 to 12 m in diameter. The widely used Datawell Waverider Mk-III, TRIAXYS Directional Wave Buoy, and Fugro Seawatch Mini II Buoy have diameters of at least 70 cm and weights of over 100 kg. These off-the-shelf operational buoys may not be an affordable choice for simultaneous deployments, and their handling requires expertise as well as vessel for deployment. These issues are somewhat alleviated with buoys as the Datawell DWR-G4, which weighs 17 kg, has a diameter of 40 cm, and has a battery life of 30 days.

Recent advances in accurate and low-cost motion sensors and GPS technology have led to the development of a low-cost easy-to-handle wave measurement platform called Spotter (Raghukumar et al. 2019; Lancaster et al. 2021). It is a sea state detector with unprecedented coverage (Smit et al. 2021; Houghton et al. 2021) and thanks to its small size, it might turn out to be a practical tool for estimating wind speed from wave spectra (Voermans et al. 2020). First field experiments of measuring waves in grease ice with Spotter show promising results in performing these types of observations at a low cost (Kodaira et al. 2020). The simultaneous deployments of several (tens, hundreds) drifting wave buoys is also beneficial for understanding wave–current interaction at coastal and oceanic scales (Pearman et al. 2014; Veras Guimarães et al. 2018) and wave growth in complex archipelagos (Björkqvist et al. 2019) and fjords (Christakos et al. 2021).

In this paper, we describe and validate a new wave buoy called LainePoiss (LP), which uses the microelectromechanical system (MEMS) inertial measurement unit to detect surface motion. LP was originally designed for wave measurements in ice, but has over 3 years of research and development matured into a valid device; it is already used for real-time wave monitoring in the Baltic Sea. When developing the buoy, we have kept the following combination of performance characteristics in focus: ice resistant, lightweight, operational, small, and affordable. These characteristics allow LP to be used for various research and engineering applications. For example, we are currently planning to use LP for wave measurements in the marginal ice zone, extending measurement times of operational wave buoys in the seasonally ice covered Baltic Sea, field measurements of shorter waves in archipelagos and lakes, and using unmanned aerial vehicles (UAV) as a rapid method for deployments. LP is also a core infrastructure for validating operational coastal wave models in Estonia.

The structure of the paper is as follows. In section 2, we describe the wave buoy in detail and introduce algorithms for converting the acceleration data into displacement data. In section 3, the omnidirectional and directional wave parameters are defined. Section 4 describes different laboratory tests

for sensor validation, including standstill measurements of acceleration noise and benchmark tests with monochromatic motions. Thereafter, we will describe the accuracy of the buoy in capturing high-frequency waves in a wave tank. Section 5 deals with the field test results. This includes an extensive validation campaign against a Directional Waverider and an intercomparison of several LP buoys. We also describe drifting experiments results, where a UAV was used as a deployment method. We end section 5 by describing the results of waves-in-ice measurements from the Baltic Sea. In section 6, we discuss the limits and merits of the new technology and conclude our main findings in section 7. Four appendixes end the paper, with the description of the inertial sensor, description of the denoising procedure, calculating validation statistics, and describing our experience of UAV deployments.

2. Materials and methods

a. Technical description of the buoy

LP is a spherical wave buoy with a diameter of 32 cm, a height of 22 cm (Fig. 1), and a weight of 3.5 kg. The enclosure is made of two tough glass fiber halves. Between the halves, there is a seal that makes the hull waterproof after it has been bolted together. After the buoy is sealed, it can be turned on and off by holding a magnet to the outside of the hull. Rechargeable lithium-ion batteries, with a capacity of 335 W h, can power the buoy for roughly 2 months.

The microcontroller of the buoy is connected to the sensors, the memory, and the communication modems through a custom built PCB board (Fig. 2). This controller—using an ARM Cortex-M4 core—was chosen because of its low power consumption, floating point support, and digital signal processing functionality.

The inertial sensors of the buoy are a 3D accelerometer, a 3D gyroscope, and a magnetometer. These sensors are part of the Xsens MTi-3 (see appendix A for more details) attitude and heading reference system (AHRS). The internal processor of the system synchronizes the sensors, applies calibration models, and runs the sensor fusion algorithm (including the extended Kalman filter), in order to convert inertial data from buoy body reference frame to Earth reference frame. Henceforth, raw data will mean the original acceleration data that are transformed to the Earth reference frame by the sensor. After assembling the buoy, we performed a magnetic calibration that corrected for the disturbance inflicted to the magnetic field of Earth by ferromagnetic materials. The device location was logged by a Global Navigation Satellite System (GNSS) receiver.

We configured the output frequency of the inertial data to 50 Hz, and these data are written to an SD card. Depending on the configuration set by the user, the raw 50 Hz data and the processed data (wave spectra and bulk parameters) are also sent to a cloud server in real time (e.g., every 30 min) using cellular LTE or only processed data over satellite Iridium SBD networks. The buoy can be configured to use

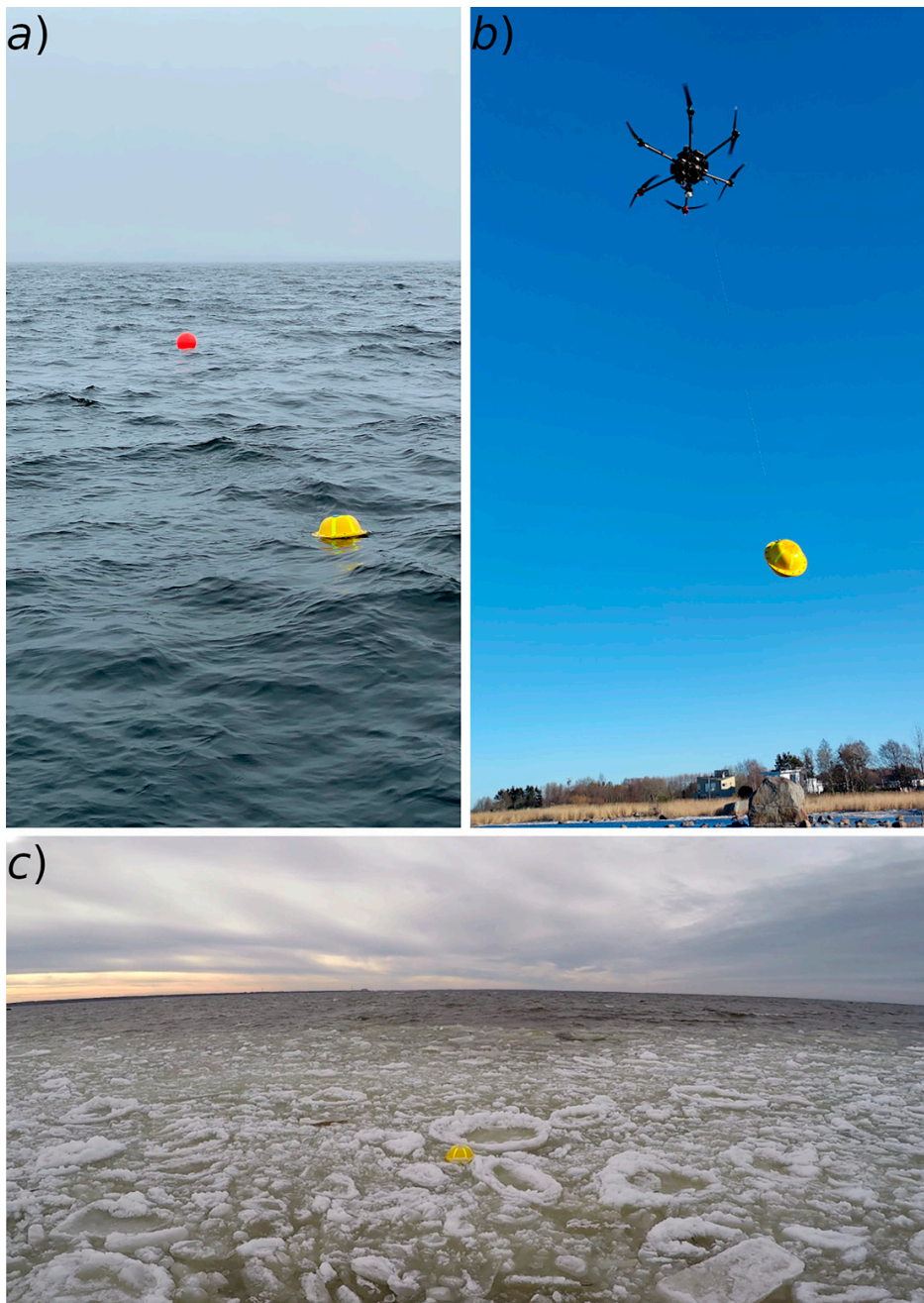


FIG. 1. (a) LainePoiss in a moored configuration, (b) transporting with a UAV, and (c) drifted to pancake ice.

either one or both of these communication options; the buoy always prioritizes the cellular network, but can automatically switch to the satellite network if no cellular coverage exists. We chose the cellular network as the primary communication

channel because of its significantly lower data transmission costs. The buoy can therefore also send the raw data through the cellular network, although this option can be disabled to save power.

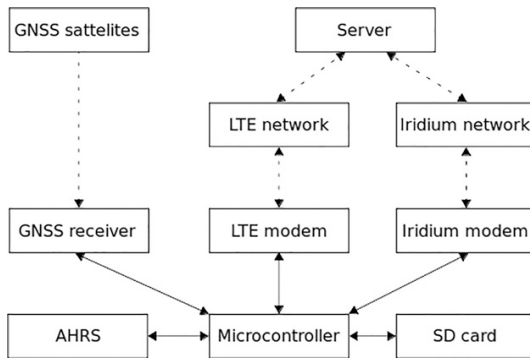


FIG. 2. Scheme of the electronics components of the buoy.

b. Data processing

The buoy sampled the acceleration with a 50 Hz sampling frequency, and (in the field tests) these data were saved in files containing 65 538 measurements (circa 22 min). We have used the raw data which are already transformed into an Earth reference frame by the sensors fusion algorithms. For each deployment, these acceleration data were combined into one long time series from which we constructed 30 min displacement time series with starting times of :00 and :30 using the following procedure:

- 1) We constructed 32 min time series from the continuous acceleration data (:59–:31).
- 2) The x , y , and z accelerations were low-pass filtered (filter “biting” between 1.28 and 5.12 Hz) with a finite impulse response (FIR) filter that had 162 coefficients before being downsampled to a 5.12 Hz resolution using a nearest neighbor interpolation. Because of the original 50 Hz sampling frequency, this resulted in a maximum shift on 100 ms of the measurement.
- 3) The acceleration data were double integrated in Fourier space. Before integration, the white noise was removed for frequencies up to 0.10 Hz, and the amplitudes below 0.05 Hz were set to zero (these cutoffs were appropriate for our specific dataset; see [appendix B](#) for details). We removed 30 s from the start and end of the double integrated time series to cut out transient data caused by the Fourier integration.
- 4) Finally, after accounting for the data lost by FIR filtering and Fourier integration, we cut the time series to start exactly at :00 or :30 to a 9216 point long block. These 30 min block coincided exactly with the displacement time series of the Waverider at Suomenlinna, which we used for validation.

The denoising of the acceleration data was performed by estimating the mean amplitude of the fast Fourier transform (FFT) of the signal between frequencies 1/100 and 1/30 Hz. The integration was performed in Fourier space, where the removing of the low-frequency energy was applied gradually below 0.06 Hz using a half-cosine function, setting the

amplitudes to 0 below 0.05 Hz. This integration procedure is similar to the one used in [Rabault et al. \(2020\)](#). For the field data, a correction to the energy was performed based on the amount of variance that was lost in the denoising. The denoising, compensation and integration procedures are documented in detail in [appendix B](#).

The 30-min displacement time series were then used to calculate wave spectra from 100-s blocks using the Welch method with a 50% overlap (35 segments), resulting in a wave spectrum with a 0.01 Hz resolution. Each segment was tapered with a Hann window. The highest frequency used in the spectrum was 1.28 Hz, which corresponds to a 95 cm deep water wavelength and approximately 3 times the buoy diameter. Higher frequencies were starting to be distorted by the size of the buoy when compared to the wave gauge data (see [section 4c](#) on the wave tank experiment).

Note that the data processing procedures in the laboratory experiments differed slightly from the data collected from field tests, since the time series were shorter. Please see [section 4c](#) for details on the exact procedure for laboratory data. For the waves-in-ice measurements ([section 5d](#)), the data processing procedure differed also a bit from the other field data—namely, the energy after denoising was not added back because the noise was so dominant.

3. Wave parameters

a. Omnidirectional parameters

We used the following definitions of wave parameters. The spectral moments are defined as

$$m_n = \int_{f_0}^{f_1} f^n E(f) df, \quad (1)$$

where a lower integration frequency of $f_0 = 0.10$ Hz and an upper frequency of $f_1 = 0.58$ Hz was used to match the highest frequency that was reliably captured by the Waverider.

Using the spectral moments we defined the significant wave height:

$$H_{m_0} = 4\sqrt{m_0}. \quad (2)$$

The wave periods were defined as

$$T_{m_{-10}} = \frac{m_{-1}}{m_0}, \quad (3)$$

$$T_{m_{01}} = \frac{m_0}{m_1}, \quad (4)$$

$$T_{m_{02}} = \sqrt{\frac{m_0}{m_2}}, \quad (5)$$

$$T_p = [\text{argmax } E(f)]^{-1}, \quad (6)$$

$$T_c = \frac{\int_{f_0}^{f_1} f^{-1} E(f)^4 df}{\int_{f_0}^{f_1} E(f)^4 df}. \quad (7)$$

Here, the peak period T_p was determined using a parabolic fit. The so-called characteristic period T_c is of the same type that was originally developed as an alternative to peak frequency by Young (1995). Björkqvist et al. (2019) proposed it as a more stable alternative characterization of a representative wave frequency in archipelago conditions, where the peak period is often ill defined. Note that we use a slight modification by integrating a weighted average of the inverse of the frequency (f^{-1}) compared to the weighted integration of f by Young (1995) and Björkqvist et al. (2019).

The narrowness of the spectrum was determined by the κ^2 -narrowness parameter (Battjes and van Vledder 1984):

$$\kappa^2 = \frac{1}{m_0^2} \left\{ \left[\int_{f_0}^{f_1} E(f) \cos(2\pi f T_{m_{02}}) df \right]^2 + \left[\int_{f_0}^{f_1} E(f) \sin(2\pi f T_{m_{02}}) df \right]^2 \right\}, \quad (8)$$

where κ^2 takes values between 1 (infinitely narrow spectrum) and 0 (white noise) and has been found to capture the spectral shape better (especially in the archipelago) than width parameters depending on high moments (m_2 or m_4) (Björkqvist et al. 2019).

b. Directional parameters

Directional parameters were calculated using the first pair of Fourier coefficients, $a_1(f)$ and $b_1(f)$. These coefficients were calculated from the cross-spectra following Longuet-Higgins (1961):

$$a_1(f) = \frac{Q_{ve}(f)}{\sqrt{C_{vv}(f)[C_{nn}(f) + C_{ee}(f)]}}, \quad (9)$$

$$b_1(f) = \frac{Q_{vn}(f)}{\sqrt{C_{vv}(f)[C_{nn}(f) + C_{ee}(f)]}}, \quad (10)$$

where $Q(f)$ and $C(f)$ are the quadrature- and cospectra, with subscripts v , e , and n referring to the vertical, east, and north displacements.

The mean direction at each frequency was calculated as

$$\theta_m(f) = \arctan\left[\frac{a_1(f)}{b_1(f)}\right] + 180^\circ, \quad (11)$$

with the mean and peak direction being

$$\theta_m = \arctan\left(\frac{\bar{a}_1}{\bar{b}_1}\right) + 180^\circ, \quad (12)$$

$$\theta_p = \theta(f_p) = \arctan\left[\frac{a_1(f_p)}{b_1(f_p)}\right] + 180^\circ, \quad (13)$$

where f_p is the peak frequency determined without a parabolic fit.

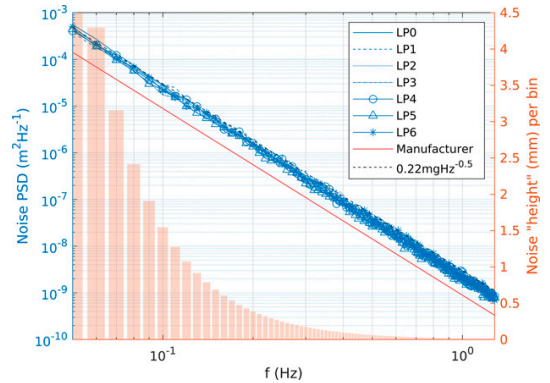


FIG. 3. Noise level of a new (LP0) and used (LP1–LP6) AHRS in comparison with manufacturers value. The noise height is calculated using the fit value to the real sensors.

The directional spread was defined as

$$\sigma(f) = \sqrt{2 - 2m_1^f(f)}, \quad (14)$$

where

$$m_1^f(f) = \sqrt{a_1^2(f) + b_1^2(f)}. \quad (15)$$

The mean and peak spreads were defined as for the directional spread [Eq. (14)] using

$$\bar{m}_1^f = \sqrt{\bar{a}_1^2 + \bar{b}_1^2}, \quad (16)$$

$$m_1^f(f_p) = \sqrt{a_1^2(f_p) + b_1^2(f_p)}. \quad (17)$$

4. Laboratory tests

a. Sensor static noise

The manufacturer of the MEMS sensor reports a static noise density value of $0.12 \text{ mg}(\sqrt{\text{Hz}})^{-1}$ for the acceleration sensor (mg is milli g; it has as value of $9.81/1000$). To test if this represents the actual noise of a single sensor, we conducted a standstill measurement, where, at a room temperature of 21°C , we let the sensor measure for 3 h. We then calculated the power spectrum of the acceleration noise and transformed it to noise displacement spectra by dividing the acceleration spectra with $(2\pi f)^{-4}$. We found that the unused sensor has a higher noise density than the manufacturer's value (Fig. 3). We repeated the same procedure for sensors already used in deployments and found that the noise does not increase with the usage of the sensor (LP1 was used the most, 5100 h). Therefore, for the sensor noise, we will use the value $0.22 \text{ mg}(\sqrt{\text{Hz}})^{-1}$. From a practical point of view, this sensor noise level only becomes important when dealing with very low amplitude waves, e.g., waves in ice. For the field measurements described in this paper, the static noise

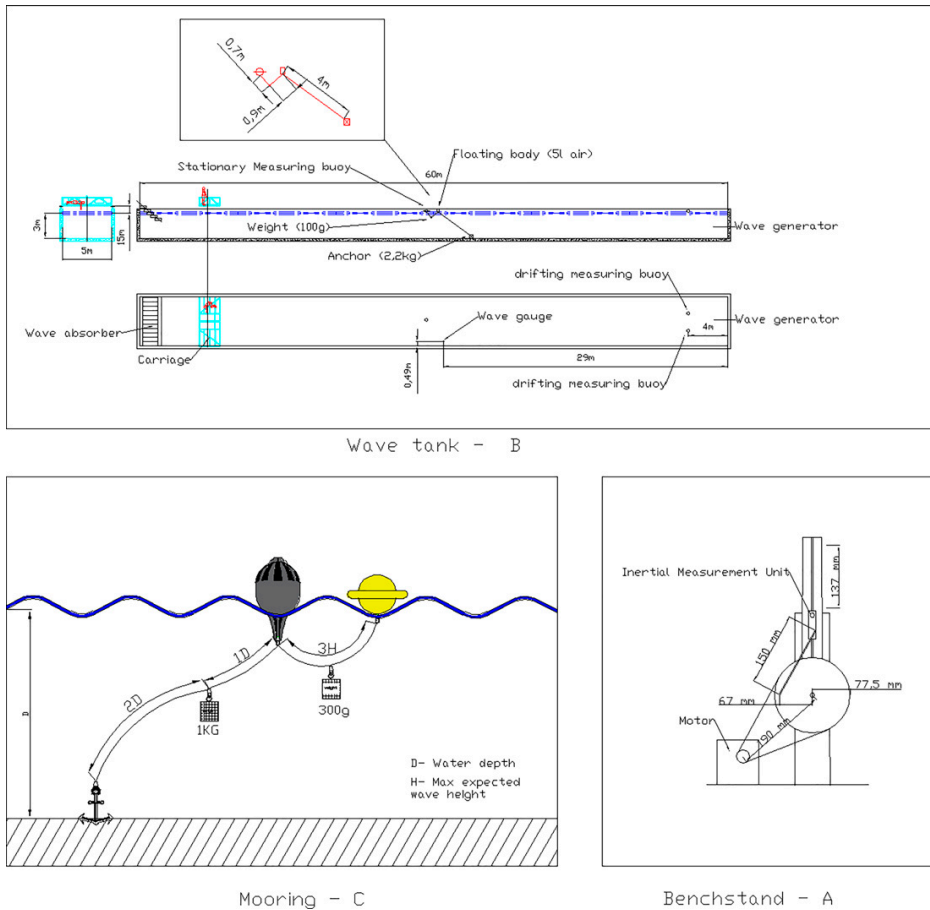


FIG. 4. Technical drawings of (a) benchstand, (b) wave tank, and (c) recommended mooring setup.

of the sensor was subtracted only for the waves-in-ice measurements (section 5d).

b. Benchmark test

The benchmark tests were conducted with a custom-made device (Fig. 4a). The amplitude was kept constant at 68 mm (± 1 mm), while period was varied between 1 and 25 s by adjusting the speed of the device. Since the device did not reproduce a perfect sine wave, all the measured acceleration signals had harmonics at multiples of the dominant signal. The measured acceleration signal was transferred to frequency space, the noise was removed and then double integrated and transferred back to time space. Mean amplitudes of N cycles were calculated. N varied between 8 and 30, depending on the cycle period.

The results of the benchmark test for periods 1, 5, 10, 20, and 25 s are shown in Table 1. The sensor is able to measure movement in the wind-wave and swell period range. The

difference between the prescribed and measured value depends on the acceleration—the measured amplitude starts to deviate with decreasing acceleration, being 6% at 0.04 Hz.

c. Wave tank

We tested the wave buoy’s response to irregular waves in both tethered and free-drift setups. The experiments were conducted in a wave tank (Fig. 4b) owned by the Small Craft

TABLE 1. Test bench results.

Wave period (s)	Prescribed amplitude (mm)	Measured amplitude (mm)
1	68	69
5	68	66
10	68	64
20	68	64
25	68	64

TABLE 2. Wave tank results. H_{m0} was integrated between 0.30 and 1.28 Hz. The peak frequency (f_p) corresponds to the wave gauge.

f_p (Hz)	H_{m0} (m)			
	Wave gauge	LP1	LP3 (moored)	LP4
0.57	0.15	0.16	0.16	0.16
0.63	0.16	0.15	0.17	0.16
0.53	0.17	0.19	0.20	0.20
0.53	0.17	0.19	0.20	0.19
0.77	0.07	0.07	0.07	0.07
0.77	0.06	0.08	0.07	0.07
0.87	0.09	0.11	0.11	0.10
0.73	0.10	0.10	0.11	0.10

Competence Centre of the Tallinn University of Technology. The aim was to validate the high-frequency part of the spectrum and determine the accuracy of LP in conditions which represent wave growth at short fetches.

The 60-m-long, 5-m-wide, and 3-m-deep tank uses 6 paddles to generate waves, which are recorded by a capacitance wave height gauge (developed by Akamina Technologies) in the middle of the tank. The duration of wave generation varied from 210 to 300 s.

For the tests, we moored one buoy 2 m from the wave gauge and let the other two drift. With the JONSWAP spectrum, we made 8 tests (Table 2), in which each combination of peak period and significant wave height was repeated twice. For each test, a 3-min-long time series was analyzed. The time series was converted into a displacement power spectra using the Welch method (block length 30 s, 50% overlap). Neither datasets were decimated; LP data sampled at 50 Hz and wave gauge data sampled at 200 Hz were used.

Significant wave height, integrated between 0.30 and 1.28 Hz, shows a satisfactory match between wave gauge and wave buoys (Table 2). The difference in significant wave height between the buoys and the wave staff was -1 to 3 cm. The wave spectra (Fig. 5) reveals a similar structure between the wave gauge and buoys up to 1.28 Hz and a slight shift of frequencies of the drifting buoys due to Doppler shift.

5. Field tests

The field tests were conducted in the seasonally ice-covered Baltic Sea, which is an enclosed basin with a maximum fetch of 700 km. The deployments were made within 5 km from the coast (Fig. 6).

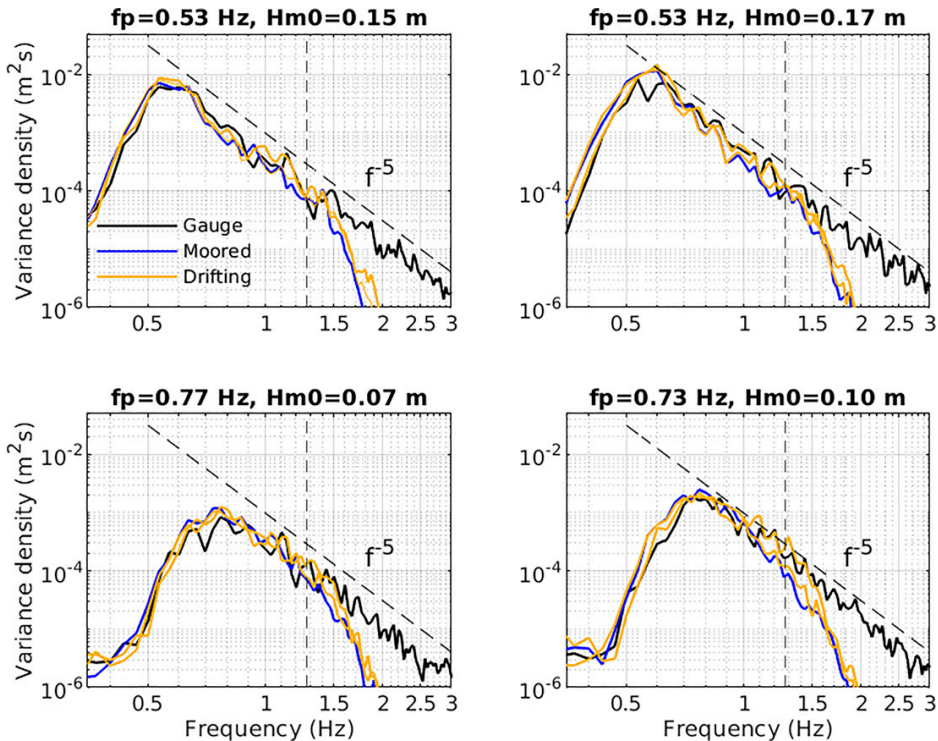


FIG. 5. Comparison of drifting and moored LP's with wave gauge at a wave tank. The wave field corresponds to the JONSWAP spectrum. The 1.28 Hz cutoff frequency is marked by a vertical dashed line.

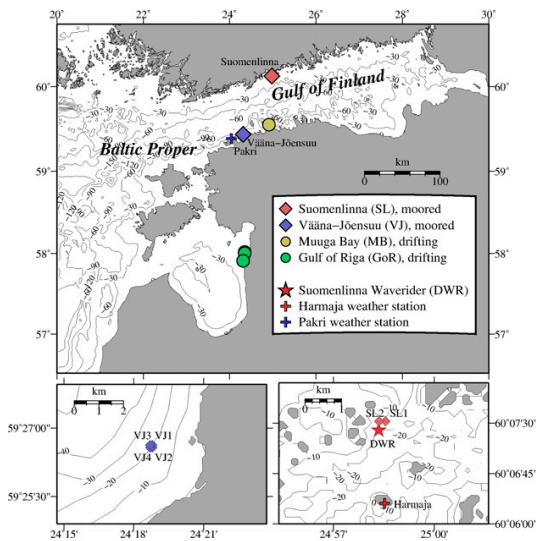


FIG. 6. Field test sites where LainePoiss's were moored (diamond) or deployed as drifters (circle). Existing operational wave and wind measurements are shown with a star and plus signs.

a. Comparison against a Directional Waverider

We deployed buoys at two locations close to the operational Directional Waverider DWR-Mk III,¹ which was moored at a depth of 20 m outside of Suomenlinna in the Finnish Archipelago (Fig. 6). The measurement area is characterized by tens of islands in varying size and busy recreational and commercial vessel traffic, although the commercial traffic during the deployments was reduced because of COVID-19 restrictions to travel.

With some short gaps, the deployments lasted from June to November 2020 (Table 3). Four different buoys were used, because the battery life of one device did not last for the entire campaign. The buoys were moored approximately 300 m north of the DWR (Fig. 6), where the water depth was 17 m. The recommended mooring consisted of an anchor, a surface float, LP, ropes connecting the assembly, and weights (Fig. 4c). The mooring endured strong winds from all major directions. The maximum 10 min averages were 15 m s^{-1} (west), 16 m s^{-1} (north), 14 m s^{-1} (east), and 21 m s^{-1} (south), with the gusts reaching 27 m s^{-1} . The buoy was not dragged from its deployment location, which shows that a 25 kg mooring anchor was sufficient.

Two buoys were deployed in June using a small plastic motorboat. In August, one of these buoys was removed and the second one was replaced (using the same boat). In September, the buoy was replaced again using a motorized sailing vessel, and it was finally retrieved with a pilot boat in the beginning of December.

¹ Then owned by the City of Helsinki, now owned by Finnish Meteorological Institute.

The spectra from both LP and DWR were integrated between 0.10 and 0.58 Hz (note that the actual low-frequency cutoff of the DWR spectra was 0.025 Hz), and both devices generally agreed on the wave statistics for the field experiment (Table 4; see appendix C for the definition of the statistical parameters). The mean significant wave height was 0.42 m, which is 0.10 m higher than the 2016–18 measured average (Björkqvist et al. 2019). Both LP and DWR measured a similar highest significant wave height, with the difference being within the expected sampling variability. The wave periods agreed better the more they were determined by the shorter waves, with T_{m02} showing the best agreement and T_p the worst. The maximum peak period values for LP are probably not realistic but stem from the low-frequency noise dominating the lowest integration frequency when total energy was very low. The dominant wave direction for both instruments was south-southwest. The spreading was, in a mean sense, slightly higher for LP than for DWR.

Overall, the significant wave height measured by LP and DWR matched well (Figs. 7–9), with a 0.01 m bias and 0.99 correlation coefficient (Table 5). During two occasions in the first deployment, LP measured an around 0.2 m higher significant wave height than the DWR (Fig. 7b). Both of these cases took place during around 10 m s^{-1} easterly winds, but LP and DWR matched up well during roughly 13 m s^{-1} easterly winds in the autumn (Fig. 9b). We have not yet determined a definitive reason for the discrepancy during the summer cases. A tangling of the moorings of the LPs is improbable since both LPs measured similar wave heights.

The wave periods determined from spectral moments compared well to those from the DWR (Figs. 10b,d,f). The scatter index was 3%–5%, with the biases being no more than 0.16 s (Table 5). The scatter index is highest (23%) for the peak period (Table 5). The general poor validation for the peak period is explained by the archipelago environments, where the peak of the spectrum is often not well defined (Björkqvist 2020). The wave spectrum was more closely unimodal for the strongest southerly winds, and the peak period therefore matched up well in the case of the highest significant wave heights (Fig. 10j). The characteristic period has been proposed as an alternative to the instances when the peak period is ill defined. The validation of the characteristic period showed that it removed a large part of the scatter between the two devices while keeping the bias at a low 0.03 s value (Fig. 10h, Table 5).

The wave direction measured by LP had a 1° – 2° bias with respect to the DWR (Table 5). While the agreement was good for both the mean and peak directions, the mean parameter expectedly has less scatter (Figs. 10c,e). A large scatter in directional peak parameters are expected (e.g., Pettersson et al. 2003), especially in the archipelago where the peak values are not even necessarily from the same wave component. For the same reason, also the peak directional spreading had a 25% scatter index even though the bias was only 2° (Table 5).

The mean spreading was more robust with a scatter index of only 9% and a correlation of 0.88. Still, LP systematically measured a slightly higher spreading than the DWR

TABLE 3. An overview of the field experiments where LainePoiss was moored.

	Deployment 1	Deployment 2	Deployment 3	Deployment 4
Device	LP1–LP2	LP3	LP4	LP1–LP4
Location	Suomenlinna (S1–S2)	Suomenlinna (S1)	Suomenlinna (S1)	Vääna-Jõesuu (V1–V4)
Depth (m)	17	17	17	19
Period	18 Jun–24 Jul 2020	14 Aug–21 Sep 2020	24 Sep–24 Nov 2020	22 Dec 2020–03 Jan 2021
Mean U_{10} (m s^{-1})	6.3	7.3	8.2	4.1
Mean H_{m0} (m)	0.32	0.39	0.50	0.51
Mean T_c (s)	4.5	4.4	4.3	5.8

(bias = 3°, slope = 1.09; Table 5). A visual comparison (Fig. 10g) reveals that the difference is better explained by a fixed offset than the calculated slope. Le Merle et al. (2021) found an offset of similar magnitude when comparing the (peak) directional spreading between radar and wave buoy measurements. The laboratory data of Lin et al. (2021) also showed that wave buoys can underestimate the directional spread compared to wave gauges with 10%. It is therefore possible that the difference between the spreading measured by LP and the DWR might partially be caused by the size difference between the devices. Lin et al. (2021) found that the impact of the mooring was small in the laboratory, but did not exclude that this factor would be more important in the field. All in all, the agreement in the directional parameters are good, especially considering the possible sources of uncertainty.

An additional validation of the spectral shape was performed by using the spectral narrowness parameter (κ^2). This parameter was proposed by Battjes and van Vledder (1984) and was found to be suitable for archipelago conditions by Björkqvist et al. (2019). The agreement between DWR and LP was reasonable (Fig. 10i), with a correlation of 0.92 and a bias of -0.02 (Table 5). The scatter index was high (23%), although we are not aware of any other cross-instrumental

TABLE 4. LainePoiss and DWR statistics during the deployments ($N = 6357$). N is smaller than the one used in the validation statistics Table 5 because in June–July 2020 two LP’s were simultaneously measuring. In the validation, both buoys were included against the comparison with DWR; here only LP 1 is used (eastern buoy, Fig. 6).

Parameter	LP/WR			
	Mean	Std	Min	Max
H_{m0} (m)	0.42/0.42	0.27/0.29	0.04/0.03	1.84/1.90
T_{m02} (s)	3.05/2.91	0.40/0.43	2.11/1.91	4.87/4.53
T_{m01} (s)	3.26/3.06	0.46/0.49	2.17/1.93	5.48/4.84
T_{m10} (s)	3.84/3.44	0.61/0.59	2.44/2.05	6.73/5.86
T_c (s)	4.40/3.83	1.49/1.12	1.87/1.74	9.53/8.32
T_p (s)	4.72/3.99	2.10/1.41	1.72/1.72	10.00/8.54
κ^2 (–)	0.11/0.13	0.09/0.10	0.00/0.00	0.59/0.68
σ_m (°)	45/41	12/11	27/23	80/80
σ_p (°)	38/32	15/9	11/9	81/80
	Mode	Std	Min	Max
θ_m (°)	202/198	45/44	5/1	359/359
θ_p (°)	202/200	52/49	0/0	359/358

validation for this particular parameter. Several width parameters are defined using higher moments (Cartwright and Longuet-Higgins 1956) and are therefore sensitive to the high-frequency part of the spectrum. The validation was therefore partially limited by the 0.58 Hz upper frequency of the DWR. In the 0.10–0.58 Hz frequency range, LP spectra tend to be slightly wider than those from the DWR, which might be caused by low-frequency artifacts during low sea states.

The spectral comparison shows a qualitatively good match (Fig. 11) between LP and DWR, except for the low-frequency part where LP has artifacts. During the northerly wind case (Fig. 11a), the peak of the spectrum was roughly at 0.5 Hz, just below the cutoff frequency of the DWR. Above the DWR cutoff frequency, LP spectra followed an f^{-4} tail, which is in agreement with theory (Kitaigorodskii 1983; Phillips 1985). For the easterly and westerly wind events, a clear peak

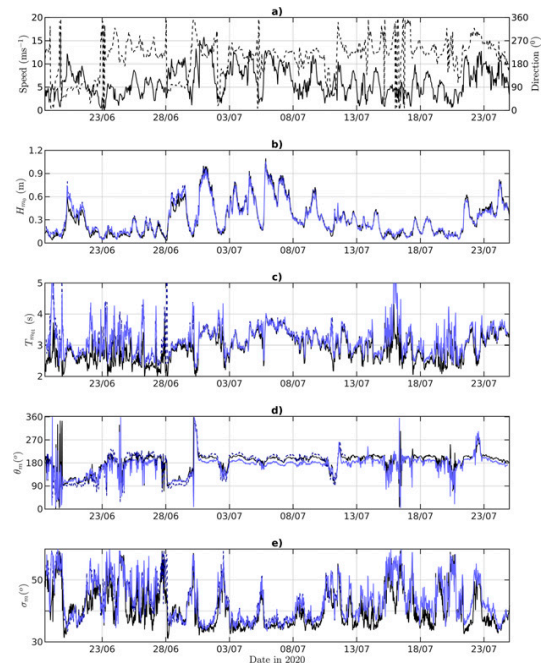


FIG. 7. Suomenlinna validation period 1. (a) Solid black line is wind speed and dashed black line is wind direction. (b)–(e) Black lines are DWR and blue lines are LP.

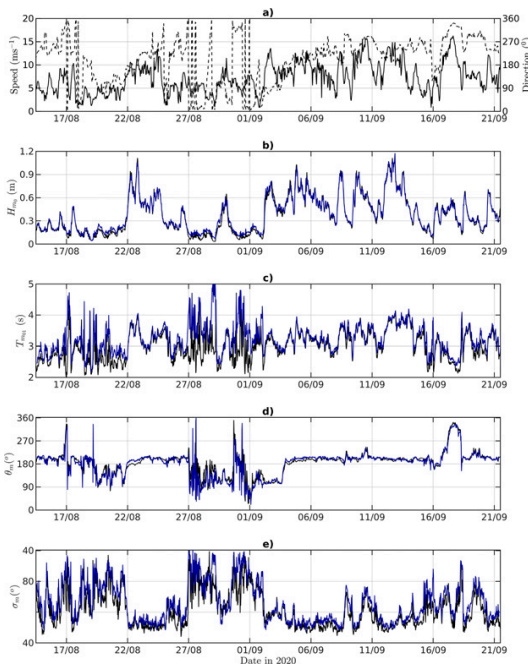


FIG. 8. As in Fig. 7, but for second validation period.

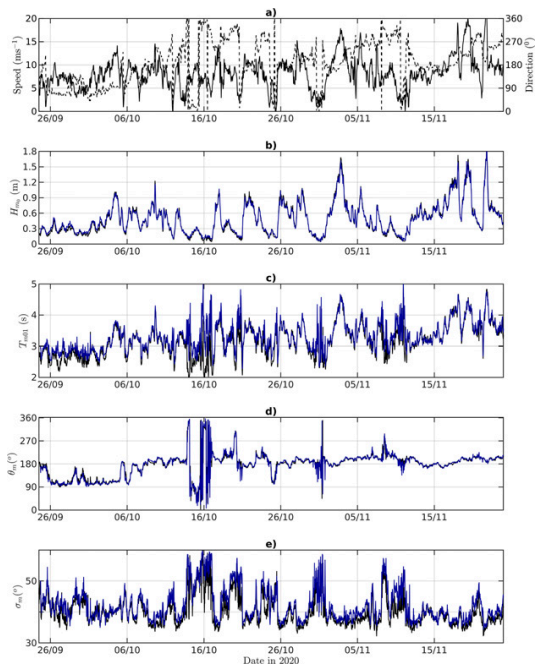


FIG. 9. As in Fig. 7, but for third validation period.

was not defined (Figs. 11b,c), which is a typical situation for the archipelago-type spectrum with many different fetches for a fixed wind direction (Björkqvist 2020). The highest waves measured during the campaign were due to southerly winds, and both the LP and the DWR spectra showed a good match even for the longer waves of a 9 s period (Fig. 11d).

In summary, the validation confirms the accuracy of LP in complex wave conditions. The scatter of the peak parameters is explained more by the ill-defined nature of the parameter than any actual differences between the devices. Otherwise, the validation statistics are similar to those determined for other small buoys when validated against established technologies (Raghukumar et al. 2019; Lancaster et al. 2021).

b. Intercomparison of four moored devices

For an intercomparison of several buoys in the same wave conditions, we moored four buoys in a square layout with a maximum distance of 140 m from each other in places where the water depth was 18–19 m (deduced from nautical charts) (Fig. 6). The buoys were deployed in December and retrieved 10 days later in January with a motorboat. The location was chosen due to its openness to long waves from the northern Baltic proper and its gently sloping bottom, which keeps the spatial wave height gradient small.

The mooring consisted of a 60 m rope from the anchor to the surface float and a 20 m rope from the float to the wave buoy. Unfortunately, LP3 started leaking during the field campaign, causing the MEMS sensor not to register data. We exclude this instrument from further analysis. After

retrieval, the instrument was cleaned and dried, and subsequent tests showed that no permanent harm was done to the electronics.

The mean wind speed during the measurement campaign was 4.1 m s^{-1} , but gusts at the Pakri weather station reached 16.5 m s^{-1} . During moderate wind speeds (over 6 m s^{-1}), the wind was mainly blowing from north or south. The maximum significant wave height was 1.22 m, and the maximum wave period was 5.97 s (Fig. 12). With the exception of the northerly winds, the waves and wind were misaligned. The

TABLE 5. Validation statistics. $N = 7486$ for H_{m0} . For other parameters, only cases where the DWR measured $H_{m0} > 0.25 \text{ m}$ were included ($N = 4827$).

Parameter	Bias	RMSD	SI (%)	Slope	R
H_{m0} (m)	0.01	0.04	8	0.99	0.99
T_{m02} (s)	0.06	0.10	3	1.02	0.98
T_{m01} (s)	0.08	0.12	3	1.02	0.98
T_{m10} (s)	0.16	0.23	5	1.04	0.96
T_c (s)	0.03	0.35	9	1.01	0.91
T_p (s)	0.03	0.89	21	0.99	0.66
κ^c (-)	-0.02	0.04	23	0.85	0.92
σ_m (°)	3	5	9	1.09	0.88
σ_p (°)	2	8	25	1.03	0.49
	Bias	MAD			
θ_m (°)	1	7			
θ_p (°)	2	11			

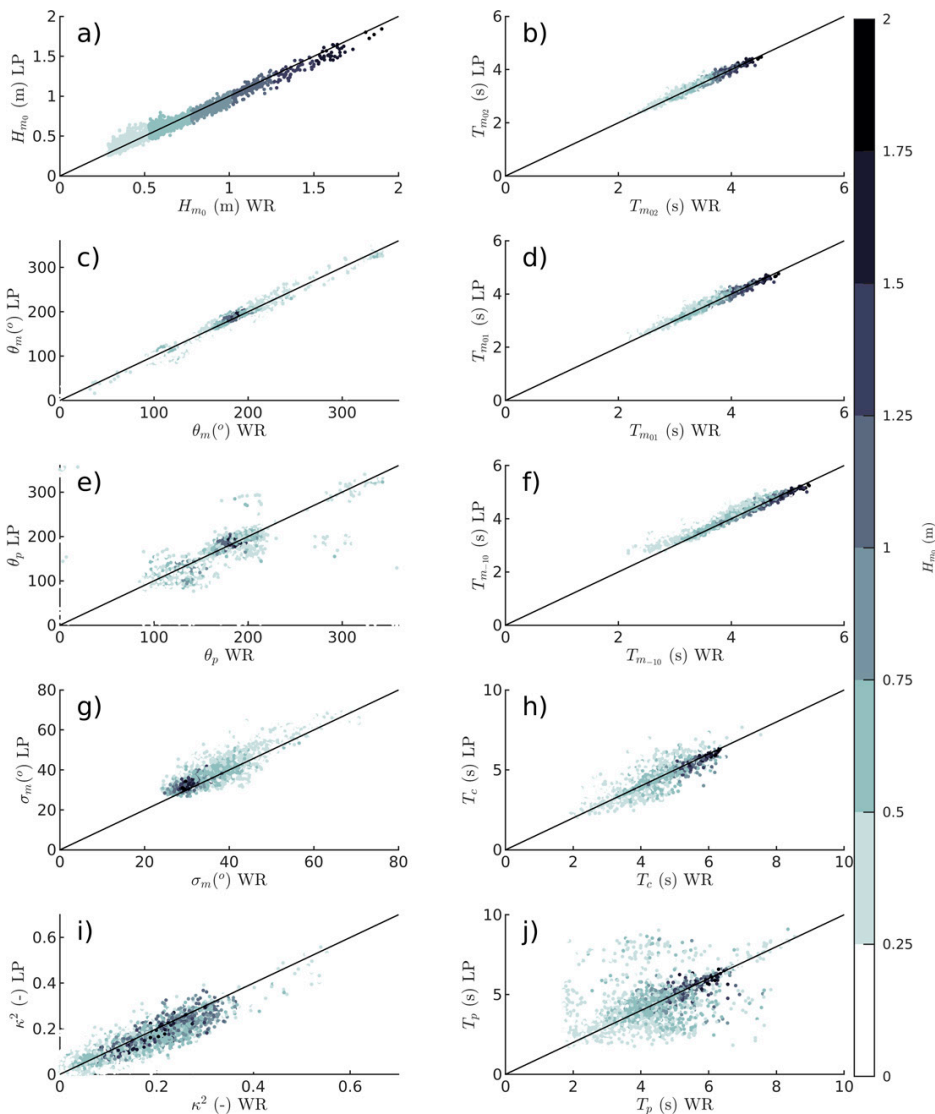


FIG. 10. Scatterplots of wave parameters during Suomenlinna validation deployment grouped by significant wave height. For the definition of variables see section 3.

misalignment was caused by the slanting fetch (Donelan et al. 1985; Petterson et al. 2010) and local topography. The slanting fetch also increased the directional spreading, since longer waves usually came from the west even though the short waves were aligned with the wind. For northerly winds, the wave and wind directions aligned, leading to a lower spreading compared to other wind directions.

The wave parameters between the different buoys agreed well (Fig. 12). The R^2 values (between LP1–LP2, LP1–LP4, and LP2–LP4) for significant wave height are over 0.99 and over 0.98 for mean wave period and for directional spreading.

The scatter index between H_{m0} was 3%–5%, reflecting the variability caused by sampling a random process (Donelan and Pierson 1983; Forristall et al. 1996).

The outlier was the mean wave direction of LP1. During the Suomenlinna UAV deployment (described in the next section) the release system malfunctioned and the buoy fell to rocky ground from approximately 2 m. Although bulk omnidirectional parameters and directional spread (which does not depend on true north reference) were reasonable, the yaw angle probably lost its north referencing capabilities, thus rendering the directional estimates unreliable.

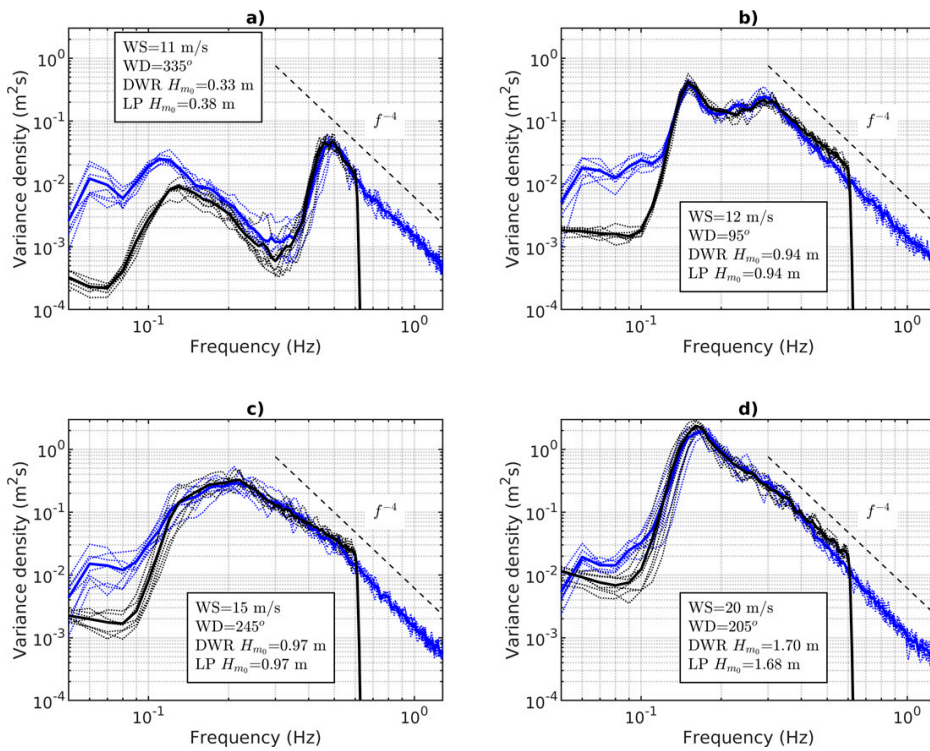


FIG. 11. Comparison of wave spectra at Suomenlinna for four different wind directions. Black lines are DWR; blue lines are LP. The thin dotted lines correspond to 30 min spectra, while the thick lines are averaged spectra of seven individual spectra.

c. Deployment with an unmanned aerial vehicle as a drifter

Vääna-Jõesuu (VJ) was the first ever deployment of LP with a UAV (Fig. 13a; Table 6). The buoy took about 2 h to drift back to the shore. Significant wave height was about 1 m, which also matched the value from a Copernicus CMEMS product (not shown here).

During the Suomenlinna deployment the buoy was dropped near the moored DWR (Fig. 13b). Wind gusts reached 15 m s^{-1} and the significant wave height was around 1 m with a wave direction from SSW. The buoy drifted until the next day and was picked up from a rocky island with a pilot boat.

At Leppneeme (Fig. 13c), the buoy was deployed from the shore. Although the wave direction was toward the shore, alongshore currents transported the buoy eastward for about 12 h before it got stuck in pancake ice close to the coast (Fig. 1c). The significant wave height was roughly 0.5 m.

The UAV ground stations were about 2 km from the deployment sites. During these three experiments, we operationally estimated the drift of the buoys with Seatrack web (<https://stw.smhi.se/>) and found that the wind leeway coefficient is around 2.5%, which is in the same range as similar spherical drifting buoys (Sutherland et al. 2020).

In the Gulf of Riga, we deployed three buoys from ice onto ice (Fig. 13d). UAV ground stations were approximately 2 km from shore at locations where pack ice was still safe to walk on. The buoys drifted with ice (with occasionally entering open water) up to month. One buoy stopped sending data 10 days after the deployment because it was brought directly from another (moored) experiment and the battery level was already low. Luckily, locals found it on shore and notified us using the contact information on the buoy. The results from the measurements in ice are described in section 5d.

The description of the UAV deployment procedures are presented in appendix D.

d. Waves in ice measurements

We deployed three drifting buoys in the eastern part of the Gulf of Riga (see section 5c). On 6 March 2021 a strong southwesterly wind event occurred, with the average measured wind speed and wind gusts being 15 and 21 m s^{-1} , respectively (Fig. 15a). Sentinel-1 overflights in the morning (0400 UTC) and in the evening (1600 UTC) showed that the ice edge retreated more than 10 km in about 12 h (Figs. 14a,b). The Copernicus CMEMS wave field forecast predicted a 2 m significant wave height near the ice edge close to the wave buoys

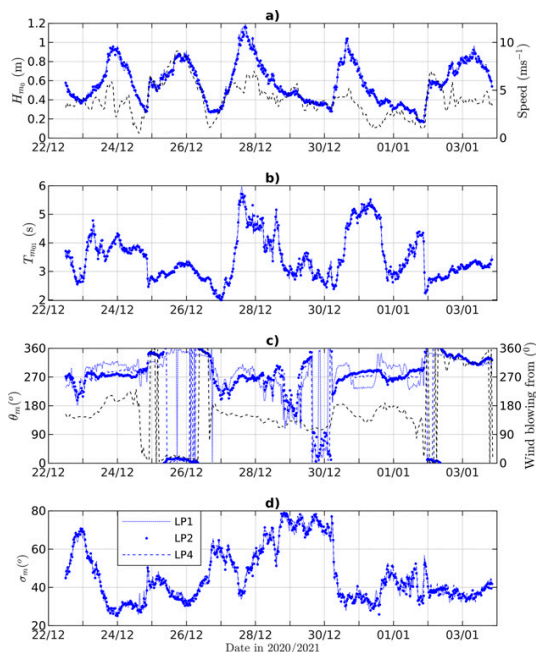


FIG. 12. Intercomparison of three LP's moored simultaneously about 100 m apart. The dashed black line marks (a) the wind speed from Pakri weather station and (c) the wind direction.

(Fig. 14c). The predicted peak period was 7 s, and the wave direction was between SW and W.

All three buoys started picking up the wave signal at around noon, and in the evening the significant wave height reached up to 1.2 cm at the buoy that was closest to the ice edge (Fig. 15b). The measured energy was above the sensor noise threshold for frequencies 0.10–0.14 Hz, and the surface displacement time series showed identifiable wave groups during the time of the maximum significant wave height (Figs. 15c,d). The roll and pitch angles deviated less than 1° , indicating that the buoys were firmly lodged in ice during the wave event.

6. Discussion

Research and development of prototype miniature wave buoys and loggers has increased in the last decade (e.g., Loehr et al. 2013; Kennedy et al. 2014; Hirakawa et al. 2016; Centurioni et al. 2017; Yurovsky and Dulov 2017; Farber et al. 2018; Skinner et al. 2018; Zong et al. 2019; Carandell et al. 2020; Cook et al. 2020). Small and affordable emerging wave buoys, like Spotter (Raghukumar et al. 2019) and LP, open up new possibilities for deploying large numbers of buoys simultaneously. With the Spotter, this has already been implemented on oceanic scales through assimilation of wave data in an operational wave model (Houghton et al. 2021; Smit et al. 2021). The ice resistance allows LP to be deployed in the marginal ice zone in large quantities, thus complementing the

existing waves-in-ice loggers (Kohout et al. 2015; Rabault et al. 2016; Montiel et al. 2018). This is of utmost importance since our knowledge on wave–ice interactions is still limited due to the low number of measurements made in ice (Squire 2020), especially measurements of the directional wave spectrum. Wave heights can be very low in the MIZ, and we have shown that a significant wave height of 1 cm is detectable by LP.

In the seasonally ice-covered water bodies, a cause for concern is the fact that operational devices have to be removed before the arrival of ice to avoid damaging the buoys. Nonetheless, the harshest wind conditions, and therefore wave conditions, can typically distort the wave statistics compiled purely from measurements (Björkqvist et al. 2018). Although LP is not designed to replace operational wave buoys, one possible application would be to complement operational measurements by replacing the operational buoy with LP when it is retrieved, thus capturing the open water time before freezing. LP should survive the ice, but if the buoy is lost, the financial implications are not as severe (buoy costs roughly EUR 5000) as a loss of an expensive operational buoy, nor do they threaten the continuity of the operational measurements as a whole.

Routine measurements also seldom capture waves shorter than 0.5–0.6 Hz, but LP extends the measurement range to 1.28 Hz (roughly 1 m wavelength). These shorter waves have been extensively studied with specialized research setups, e.g., using wave staffs or polarimetric cameras. The reason for the persistent scientific interest for this part of the wave regime is its decisive impact on many sea–atmosphere processes. Waves between 0.58 and 1.28 Hz have been shown to contribute 26% of the so-called Stokes drift (Lenain and Pizzo 2020), and they also carry a significant part of the wave-induced stress (Janssen 1991; Mueller and Veron 2009). These processes then affect the drift of the object, oil, and other surfactants and enhance the upper-layer turbulence and mixing, thus contributing to the sea–atmosphere fluxes of, e.g., CO_2 . One possible niche for LP could be regions like archipelagos, fjords, or small lakes. In these areas, the short waves can carry a major part of the total wave energy, but establishing elaborate research wave measurement stations might not be feasible. From a practical perspective, the measurement of the high-frequency part might require cleaning of the buoy after some time to avoid accumulation of added mass and change of the buoy dimensions due to biofouling (Thomson et al. 2015; Campos et al. 2021).

Peak wave periods can reach 25 s in the world oceans (Hanafin et al. 2012), but low-frequency noise in wave measurements are unfortunately a common feature. Ashton and Johanning (2015) found spurious low-frequency energy caused by high drift forces brought about by currents and mooring. Low-frequency artifacts can also be created by a loss of the GPS signal in buoys that use the Doppler shift to measure the buoy velocity, e.g., the DWR-G4 (Björkqvist et al. 2016). We found that the MEMS sensor of the LP also suffers from low-frequency noise. This noise comes from the gyroscope random noise, which affects the pitch, roll, and yaw angles. These angles are then used to calculate the free acceleration inside the sensor, and the noise is further amplified by

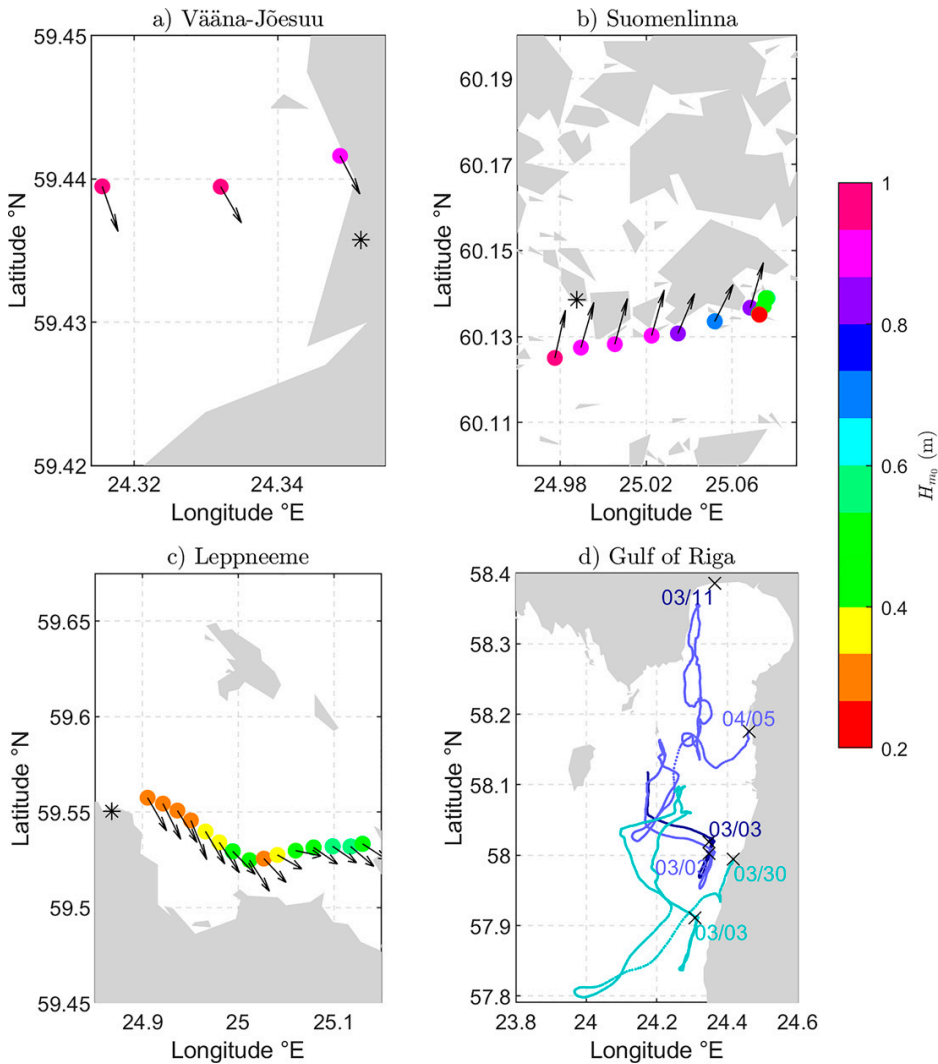


FIG. 13. (a)–(d) Drifting experiments results in four locations. UAV ground stations are marked with asterisks. In (d) only tracks of buoys are displayed, because most of the time no wave motion in ice was present. Also in (d), \times marks the deployment or retrieval locations. For the dates of the experiments, see Table 6.

double integration. Low-frequency noise was also present in drifting buoys.

Yurovsky and Dulov (2020) also identified low-frequency noise, but did not present any correction method. Earle and Bush (1982) and Lang (1987) proposed a method for denoising by subtracting energy present at low frequencies from higher frequency. By comparing several months of LP measurements to coinciding Waverider measurements, we identified biases in the variance density both for the low and high frequencies, and concluded that these biases are possibly related. When the low-frequency part was denoised, we quantified the amount of variance that was lost and reintroduced

this variance back to the higher frequencies in proportion to the already existing variance (see appendix B). This correction was performed in Fourier space, which means that already the time series, determined through the inverse transform after integration in Fourier space was corrected. Although this method is partially ad hoc, it was shown to correct the final spectrum for both dominant waves and the spectral tail. Nonetheless, further development, not excluding changing the MEMS sensor, is currently pursued.

Nontypical deployments, such as aerial deployments by UAVs, have recently been used as an additional tool in observational studies (Zappa et al. 2020). UAVs are gaining

TABLE 6. An overview of drifting experiments where LainePoiss was deployed using a UAV. GoR refers to the Gulf of Riga.

	Deployment 1	Deployment 2	Deployment 3	Deployment 4	Deployment 5	Deployment 6
Device	LP1	LP1	LP5	LP2	LP5	LP6
Location	Vääna-Jõesuu (VJ)	Suomenlinna (SO)	Leppneeme	GoR	GoR	GoR
Type	Drifting	Drifting	Drifting	Drifting	Drifting	Drifting
Period	15 Aug 2019	6–7 Dec 2019	27–28 Feb 2021	3–11 Mar 2021	3 Mar–5 Apr	3–30 Mar
Mean U_{10} (m s^{-1})	8	13	8	In ice	In ice	In ice
Mean H_{m0} (m)	0.94	0.87	0.41	In ice	In ice	In ice
Mean T_{m10} (s)	4.2	4.4	2.7	In ice	In ice	In ice

popularity since they can carry lightweight sensors (Fuertes et al. 2019). These innovative solutions are partially motivated by environmental concerns, but they also allow to bypass the cost of a ship. Because of its low weight, LP can be deployed by an industrial UAV as a drifter. It has already been tested in deployments from shore and from sea ice with the deployment range extending to 2 km. These novel deployment techniques are still being established, but possible applications can include collecting data from surf zones or transporting a buoy onto the MIZ. UAV deployments will continue to be one part of the further development of LP.

It is possible to extend the operation time of LP by replacing rechargeable Li-ion batteries with lithium-thionyl chloride primary batteries. These batteries have an energy density that is about 2.5 times higher than that of rechargeable ones. This would extend the autonomous operating time to 5 months and make measurements in remote locations more feasible. Also, the buoy leaked on two occasions over the course of 18 field deployments. These incidents have been accounted for when designing the new hull (Fig. 16). The new hull is made of molded plastic and has a sealing O-ring on the top. External connectors for charging and accessing data have

been added to remove the need for opening the buoy and to enhance usability. The inertial sensor, electronics, and measurement methodology are kept the same. First laboratory tests of the new design on durability and waterproofness have been carried out successfully, but further testing is ongoing to validate this new design in the field.

7. Conclusions

A wave buoy [LainePoiss (LP)] was developed. LP weighs 3.5 kg, measures waves up to 1.28 Hz, has a rechargeable battery with 2 months of operation, and transmits wave parameters and spectra operationally over cellular or satellite networks. From our study, we can conclude the following:

- Wave parameters measured in the field were in good accordance with those measured by a nearby Directional Waverider: the bias of H_{m0} was 0.01 m, correlation 0.99, and scatter index of 8%. The bias of T_{m-10} was 0.14 s, correlation 0.98, and scatter index 4%. The mean absolute deviation of mean wave direction was 7°.
- The high-frequency part of the spectrum (up to 1.28 Hz) compared well to a wave gauge in the wave tank. The wave

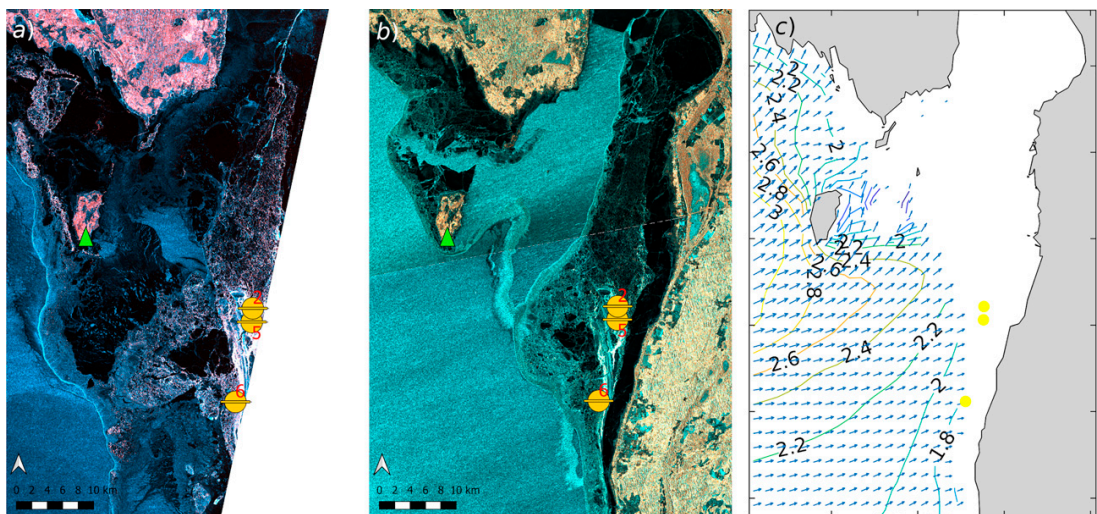


FIG. 14. (a) SAR image at 0400 UTC; (b) SAR image at 1600 UTC; (c) CMEMS model wave field (significant wave height, m; wave directions, arrows) at 1600 UTC. The locations of different LP's at 1600 UTC are shown with yellow marks. Kihnu weather station is marked with a green filled triangle. All panels are on 6 Mar 2021.

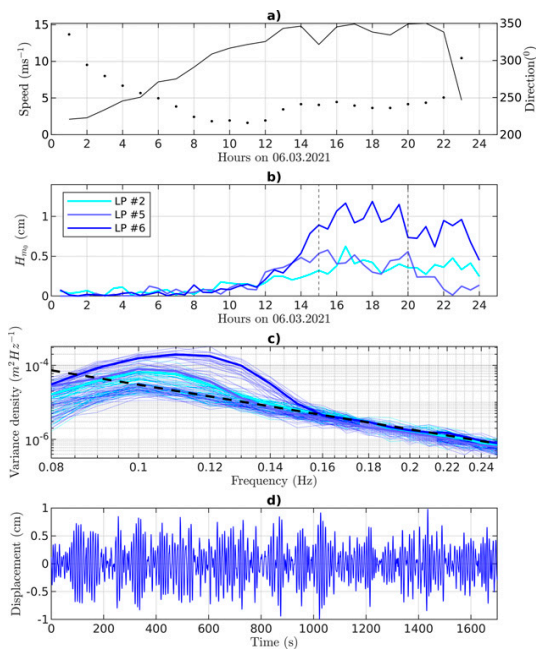


FIG. 15. Waves in ice measurements. (a) Wind speed and direction at Kihnu weather station (for location, see Fig. 14; direction marked with dots); (b) significant wave height from three buoys in ice; (c) spectra of three buoys with thin dotted lines corresponding to 30 min single spectra and thick lines corresponding to averaged spectra; dashed black line shows the sensor noise floor; (d) surface displacement for buoy 6 in ice.

spectrum of LP was validated up to a Waverider cutoff frequency of 0.58 Hz in the field, and the spectral tail of LP had an expected power-law behavior up to 1.28 Hz.

- LP can measure waves in ice with a significant wave height as low as 1 cm. This was confirmed in an over a month-long experiment where several LP's were deployed in ice in the Baltic Sea.
- Because of its low weight, LP can be deployed as a drifter to a distance of at least 2 km using an unmanned aerial vehicle (UAV).

Noise in the gyroscopic sensor resulted in low-frequency artifacts, but the displacement time series can be corrected (see appendix B). However, with the current validation and testing we can only confirm the buoy's capability to measure waves down to 0.1 Hz—this was a suitable range for the data we had available for the validation, although it precludes most of the oceanic applications. We will continue testing the wave buoy and expand our measurement areas outside of the Baltic Sea to capture longer waves. Depending on the MEMS sensor noise levels in these conditions, we can decide whether to replace the wave buoy's sensor for one with several times less noise.

Acknowledgments. This work was supported by the Personal Research Funding of the Estonian Ministry of Education and

Research (Grant PSG22). We thank Lauri Laakso and Roine Tuomo for helping with Suomenlinna field experiments. We appreciate discussions with Kimmo Kahma. We thank Rivo Uiboupin, Jüri Elken, Aarne Männik, and Sigrid Aas for keeping the administrative matters under control. We thank Tarmo Kõuts for helping us with the first versions of real-time display of data on a website. The first author thanks (little) Aran Alari for inspiring the wave buoy name LP. We thank the following institutions and enterprises for their successful participation in the applications of LainePoiss: the Maritime Administration of Estonia, the Estonian Environment Agency, AS Saarte Linid, OÜ LaineMudel, TalTech Small Craft Competence Centre, and the City of Helsinki. We thank the anonymous reviewers for their constructive critique and comments—they helped us improve our article. Valdur Kaldvee and Kristjan Mölder are the founders, and the sole owners and employees of WiseParker OÜ, who produce the LainePoiss wave buoy presented in this manuscript. The development of LainePoiss has been made in cooperation with Tallinn University of Technology

Data availability statement. The data used in this manuscript will be made openly available upon the publication of the final paper. The LainePoiss MATLAB processing scripts are publicly available at <https://github.com/bjorkqvi/LPP/releases/tag/v1.0.0>.

APPENDIX A

The MTi-3 Sensor

This appendix provides the details of the Xsens MTi-3 sensor to the degree the information is publicly available. The sensor measures all 6 degrees of freedom (using a 3D accelerometer and 3D gyroscope) and provides the orientation (using a magnetometer). The technical specifications of the sensor (as provided by the manufacturer) can be found in Tables A1 and A2. The integrated microcontroller unit (MCU) synchronizes the various sensors, which is required for the onboard conversion of the acceleration signals from device to Earth-referenced frame. The role of the MCU is described by the manufacturer (Xsens 2019) as follows:

The MCU applies calibration models (unique to each sensor and including orientation, gain and bias offsets, plus more advanced relationships such as nonlinear temperature effects and other higher order terms) and runs the Xsens optimized strapdown algorithm, which performs highrate dead-reckoning calculations at 800 Hz, allowing accurate capture of high frequency motions and coning and sculling compensation. The Xsens sensor fusion engine combines all sensor inputs and optimally estimates the orientation, position and velocity at an output data rate of up to 100 Hz. The MTi 1-s is easily configurable for the outputs and depending on the application's needs can be set to use one of the filter profiles available within the Xsens sensor fusion engine.

The exact details of the built-in fusion algorithm—which transforms the signal from the sensor references to the Earth referenced frame—are not made public by the manufacturer.

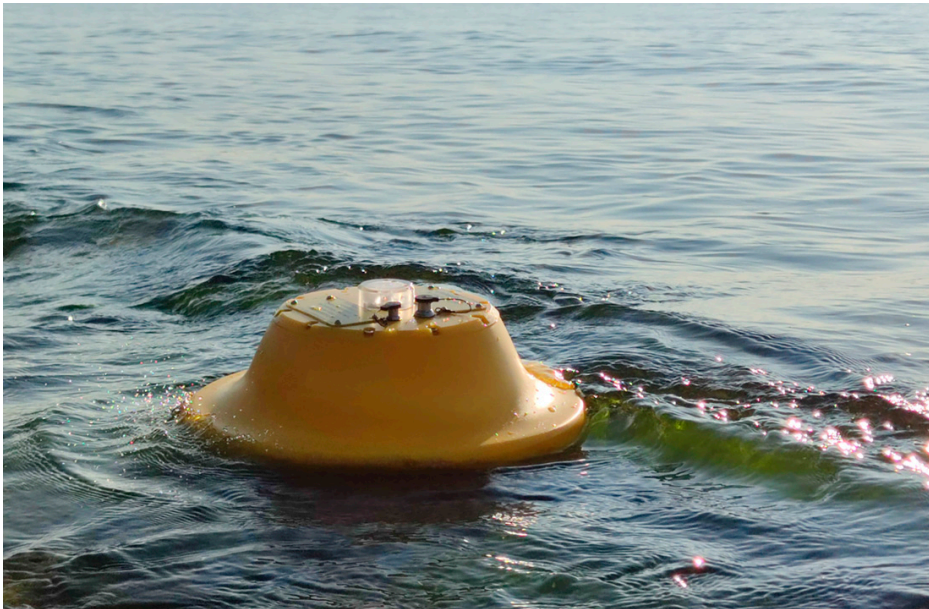


FIG. 16. New version of the buoy, with the charging and data acquisition connectors brought outside the buoy to reduce buoy openings.

However, the process includes an extended Kalman filter (Xsens 2015). The process and the different options for filtering are described by the manufacturer (Xsens 2019):

Xsens sensor fusion algorithm optimally estimates the orientation with respect to an Earth fixed frame utilizing the 3D inertial sensor data (orientation and velocity increments) and 3D magnetometer. The user can set the sensor fusion algorithm with different filter profiles in order to get the best performance based on the application scenario (see Table 16). These filter profiles contain predefined filter parameter settings suitable for different user application scenarios. In addition, all filter profiles can be used with the Active Heading Stabilization (AHS) setting, which significantly reduces heading drift during magnetic disturbances. The Inrun Compass Calibration (ICC) setting can be used to compensate for magnetic distortions that are caused by every object the MTi is attached to.

TABLE A1. Specifications for the gyroscope and accelerometer of MTi-3 as given by the manufacturer (Xsens 2019).

	Gyroscope	Accelerometer
Standard full range	$\pm 2000^\circ \text{ s}^{-1}$	16g
In-run bias stability	10° h^{-1}	0.03 mg
Bandwidth (-3 dB)	255 Hz	324
Noise density	$0.007^\circ (\text{s } \sqrt{\text{Hz}})^{-1}$	$0.12 \text{ mg } (\sqrt{\text{Hz}})^{-1}$
Sensitivity variation	0.05%	0.05%
Nonlinearity	0.1%FS	0.5%FS
g sensitivity (calibrated)	$0.001^\circ (\text{s } g)^{-1}$	—
Max output frequency	800 Hz	800 Hz

Of the available filter profiles, we used the profile “North referenced” (see Table 16 of Xsens 2019). We calibrated the magnetometer for hard iron distortion after assembling the whole device. This was done following the manufacturer’s specification using their Magnetic Field Mapper application. The process consisted of starting the application and rotating the buoy over a large number of orientations. After that, the tool calculated new calibration parameters and those were saved to the sensor memory. This had to be done only once after assembling the device. The calibration of the internal temperature sensor used for thermal compensation was already done by the manufacturer. The manufacturer states that the sensor has been calibrated to operate between -40° and 85°C .

To bring out the difference between the Earth referenced acceleration data and data in the body reference frame of the buoy, consider once more the benchmark tests from

TABLE A2. Specifications and performance statistics for the magnetometer and orientation of MTi-3 as given by the manufacturer (Xsens 2019).

	Value
Standard full range	8 G
Nonlinearity	0.2%
Total RMS noise	0.5 mG
Resolution	0.25 mG
Roll/pitch static RMS	0.5°
Roll/pitch dynamic RMS	0.8°
Yaw dynamic RMS	2°

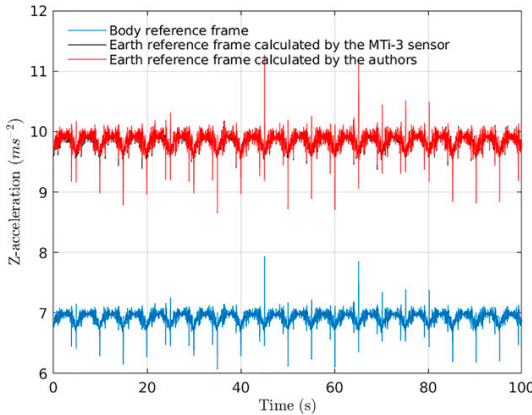


FIG. A1. Raw 50 Hz Z-oriented acceleration data in Earth reference frame and body reference frame.

section 4b. This time the sensor was placed so that the pitch angle was approximately 45° . We repeated the experiment for 5 s motion period (Fig. A1). The acceleration in the body reference frame is a fraction of the acceleration in the Earth reference frame, with a cosine dependence of roll and pitch angles (Bender et al. 2010). We calculated the Earth referenced acceleration by dividing the body referenced acceleration with the cosines of roll and pitch angles and found that it very well matches the values obtained with MTi-3 onboard processing (Fig. A1). The match of course is not one-to-one, since the MTi-3 fusion is much more elaborate and uses the accelerations from all three axes along with pitch and roll. For our benchmark test the implication of using Earth referenced data is straightforward. When the Earth referenced accelerations are used, calculated amplitude is off by 1 mm from the prescribed amplitude, while in the case of using acceleration data in body reference frame the calculated amplitude is 14 mm lower compared to the prescribed amplitude (for the test case of 5 s period motion).

APPENDIX B

Renormalization in Integration

The limitations of the sensor create low-frequency noise, but we have concluded that this noise is actually a misplaced signal from other frequencies. If the low-frequency noise is removed, it should be added back to the frequencies, so that the power spectrum fulfills the following:

$$E(f) = E_0(f) + \frac{\Delta\varepsilon E_0(f)}{\sum_f E_0(f)} \quad (\text{B1})$$

$$= E_0(f) \left[1 + \frac{\Delta\varepsilon}{\sum_f E_0(f)} \right], \quad (\text{B2})$$

where

$$\Delta\varepsilon = \sum_f \hat{E}(f) - \sum_f E_0(f), \quad (\text{B3})$$

and $\hat{E}(f)$ and $E_0(f)$ are the power spectra of the unprocessed and denoised signals. $\Delta\varepsilon$ quantifies how much variance density of the signal has been lost. Especially, if $\Delta\varepsilon = 0$ then no further correction is necessary.

In practice, this denoising and compensation is performed during the integration, which results in a clean displacement signal from which the power spectrum can be calculated in a normal fashion without having to deal with the above compensation after the fact.

Low-frequency acceleration data are first denoised using the following procedure: the average squared Fourier amplitude is calculated for the frequencies 1/100 to 1/30 Hz:

$$\alpha = \left\langle |\hat{A}(f)|^2 \right\rangle_{1/100 \leq f \leq 1/30}, \quad (\text{B4})$$

where $\hat{A}(f) = \mathcal{F}[a(t)]$ is the Fourier transform of the acceleration signal and $|\hat{A}(f)|$ is its modulus.

This mean value (the noise) is then removed from the Fourier transform by

$$A_0(f) = \max \left\{ 0, \hat{A}(f) \frac{\hat{A}(f) - \alpha [1 - R_f(f)]}{\hat{A}(f)} \right\}, \quad (\text{B5})$$

where $R(f)$ is a response function:

$$R_f(f) = \begin{cases} 0, & 0 < f < f_1 \\ \frac{1}{2} \left[1 - \cos \left(\pi \frac{f - f_1}{f_2 - f_1} \right) \right], & f_1 \leq f \leq f_2 \\ 1 & f_2 < f \leq f_N \end{cases} \quad (\text{B6})$$

Here $f_1 = 0.08$ Hz and $f_2 = 0.10$ Hz. In other words, the Fourier transform for $f > 0.10$ Hz is not touched. The 0.1 Hz cutoff was appropriate for our datasets in the Baltic Sea. For oceanic conditions this cutoff needs to be set to a lower value, but validating these lower frequencies would require additional field measurements that include longer waves.

Following, e.g., Rabault et al. (2020), the acceleration values are then integrated in Fourier space:

$$X_0(f) = -A_0(f) R_f(f) \cdot (2\pi f)^{-2}, \quad (\text{B7})$$

$$\hat{X}(f) = -\hat{A}(f) R_f(f) \cdot (2\pi f)^{-2}, \quad (\text{B8})$$

where $f_1 = 0.05$ Hz and $f_2 = 0.06$ Hz in the response function $R_f(f)$.

That is, $\hat{X}(f)$ and $X_0(f)$ are now the uncorrected and denoised Fourier transform of the displacement signal. We quantify how much of the squared amplitudes of the signal were lost by the low-frequency correction:

$$\Delta\chi^2 = \sum_f |\hat{X}(f)|^2 - \sum_f |X_0(f)|^2. \quad (\text{B9})$$

This lost signal information will be added back in a way that will compensate the power spectrum as outlined in Eq. (B2):

$$X(f) = X_0(f) \sqrt{1 + \frac{\Delta X^2}{\sum_f |X_0(f)|^2}} \quad (\text{B10})$$

$$= X_0(f) \sqrt{1 + \frac{\sum_f |\hat{X}(f)|^2 - \sum_f |X_0(f)|^2}{\sum_f |X_0(f)|^2}} \quad (\text{B11})$$

$$= X_0(f) \sqrt{1 + \frac{\sum_f |\hat{X}(f)|^2}{\sum_f |X_0(f)|^2} - 1} \quad (\text{B12})$$

$$= X_0(f) \sqrt{\frac{\sum_f |\hat{X}(f)|^2}{\sum_f |X_0(f)|^2}}. \quad (\text{B13})$$

The displacement time series is then given by the inverse Fourier transform:

$$x(t) = \mathcal{F}^{-1}[X(f)]. \quad (\text{B14})$$

This time series is now corrected for the low-frequency artifacts, which has been redistributed to the other frequencies. The power spectrum or any other statistics can now be calculated from this displacement time series without further corrections.

APPENDIX C

Statistical Parameters

With N is the number of data points we used the following statistical parameters:

$$\text{Mean} = \bar{x}_i = \frac{1}{N} \sum_i x_i. \quad (\text{C1})$$

For angular quantities, θ , the mean is defined as

$$\bar{\theta}_i = \arctan \left[\frac{\overline{\sin(\theta_i)}}{\overline{\cos(\theta_i)}} \right] \quad (\text{C2})$$

and the difference

$$|\theta_1 - \theta_2| = \min\{|\theta_1 - \theta_2|, 360^\circ - |\theta_1 - \theta_2|\}. \quad (\text{C3})$$

The covariance is

$$\text{Cov}(x_i, r_i) = \sqrt{\frac{1}{N-1} \sum_i (x_i - \bar{x}_i)(r_i - \bar{r}_i)}. \quad (\text{C4})$$

where x_i are observations and r_i are the reference values (typically from the Waverider).

The variance and standard deviation are

$$\text{Var}(x_i) = \text{Cov}(x_i, x_i), \quad (\text{C5})$$

$$\text{Std}(x_i) = \sqrt{\text{Var}(x_i)}. \quad (\text{C6})$$

For cross comparison of datasets, we defined the following parameters:

$$\text{Bias} = \bar{x}_i - \bar{r}_i. \quad (\text{C7})$$

The root-mean-square deviation, mean absolute deviation and scatter index (in percent) are defined:

$$\text{RMSD} = \sqrt{\frac{1}{N} \sum_i (x_i - r_i)^2}, \quad (\text{C8})$$

$$\text{MAD} = \frac{\sum_i |x_i - r_i|}{N}, \quad (\text{C9})$$

$$\text{SI} = 100 \sqrt{\frac{\sum_i [(x_i - \bar{x}_i) - (r_i - \bar{r}_i)]^2}{\sum_i r_i^2}}. \quad (\text{C10})$$

The slope is defined as a least squares fit $x = Kr$

$$K = \frac{\sum_i x_i r_i}{\sum_i r_i^2}, \quad (\text{C11})$$

and the Pearson correlation coefficient is

$$R = \frac{\text{Cov}(x_i, r_i)}{\text{Std}(x_i) \text{Std}(r_i)}. \quad (\text{C12})$$

APPENDIX D

Experiences from UAV Deployments

In this appendix, we document our experiences from six events where an industrial UAV was used to deploy LP as a floating device. Our deployments were made in Estonia and Finland during 2019–21. The guidelines and regulations governing the use of UAV's change and differ from country to country, especially outside of the European Union. Make sure to get correct information and follow any local laws and ordinances when considering deploying LP with a UAV. Also note that the steps below do not guarantee a safe or successful deployment.

The UAV should be regularly maintained to be sure of the condition of the equipment; motors, blades, batteries, and the remote controller have to be working properly. Firmware and software should also be up to date. Notifications through, e.g., the remote controller or pilot

application should be taken seriously, and they need to be resolved before flight. Before deploying the actual device, we recommend practicing with, e.g., sandbags that have the same weight as LP.

A successful UAV deployment starts with a comprehensive preparation and plan for the flight and requires at least two persons. The first person flies the drone while the second person assists at lift-off and landing. We used a DJI Matrice 600 Pro industrial drone with a release mechanism (Fig. 1b). A 5-m-long fishing thread (we used Dyneema 0.3 mm with a breaking strength of 25 kg) was found suitable for connecting the UAV and the wave buoy. A longer thread could make releasing the LP more convenient as the UAV can be higher, thus having a stronger signal strength. Nonetheless, a shorter thread minimizes the motion of the buoy during flight. The lift-off is the riskiest part: the second person has to hold the thread downwind and low to the ground to minimize the risk of the thread being caught by the UAV motors. This has to be done while keeping a distance of at least a few meters from the UAV. For the safety of the assisting person, the pilot should guide the UAV upward for the first couple of meters as quickly as possible. The rest of the lift-off can happen at a slower pace until the wave buoy is up in the air. We used a flight height of 20–30 m when transporting the wave buoy to the drop-off location.

With fully charged batteries at lift-off, we deployed the buoy at a distance of up to 2 km. We started guiding the UAV back toward the ground station before the battery dropped below 50%. In our deployments we flew upwind with the heavy weight, thus returning to the ground station downwind. We found that the battery charge at landing was still at about 20%.

Below is a step-by-step checklist that we have used in our deployments:

- The pilot does a UAV precheck a day before flight as well as on the field. If applicable, follow the messages from the pilot application.
- The second person, crouching at least 2 m from the UAV, holds the thread under tension between the UAV and the person's hand, ready to give slack as the UAV is ascending.
- The pilot loudly notifies the other persons before activating motors and makes sure everybody is ready for lift-off.
- The pilot ascends the first 2 m as quickly as possible, and the second person gives slack to the thread as the UAV takes off.
- A second person must hold the thread under tension between the UAV and their hand until the LP is up in the air.
- Thread should be downwind, even though the UAV might deviate also downwind where the second person is holding the thread.

Recommendations for the pilot:

- Flight height between 20 and 30 m.
- Do not fly farther than 50% of the battery capacity; ideally fly upwind with payload and return with tailwind.

REFERENCES

- Ashton, I., and L. Johannang, 2015: On errors in low frequency wave measurements from wave buoys. *Ocean Eng.*, **95**, 11–22, <https://doi.org/10.1016/j.oceaneng.2014.11.033>.
- Battjes, J. A., and G. P. van Vledder, 1984: Verification of Kimura's theory for wave group statistics. *Proc. 19th Int. Conf. on Coastal Engineering*, New York, NY, ASCE, 642–648, <https://doi.org/10.1061/9780872624382.044>.
- Bender, L. C., N. L. Guinasso, J. N. Walpert, and S. D. Howden, 2010: A comparison of methods for determining significant wave heights—Applied to a 3-m discus buoy during Hurricane Katrina. *J. Atmos. Oceanic Technol.*, **27**, 1012–1028, <https://doi.org/10.1175/2010JTECH0724.1>.
- Bishop, C. T., and M. A. Donelan, 1987: Measuring waves with pressure transducers. *Coastal Eng.*, **11**, 309–328, [https://doi.org/10.1016/0378-3839\(87\)90031-7](https://doi.org/10.1016/0378-3839(87)90031-7).
- Björkqvist, J.-V., 2020: Waves in archipelagos. Ph.D. thesis, University of Helsinki, 58 pp.
- , H. Pettersson, L. Laakso, K. K. Kahma, H. Jokinen, and P. Kosloff, 2016: Removing low-frequency artefacts from Datawell DWR-G4 wave buoy measurements. *Geosci. Instrum. Methods Data Syst.*, **5**, 17–25, <https://doi.org/10.5194/gi-5-17-2016>.
- , I. Lukas, V. Alari, G. P. van Vledder, S. Hulst, H. Pettersson, A. Behrens, and A. Männik, 2018: Comparing a 41-year model hindcast with decades of wave measurements from the Baltic Sea. *Ocean Eng.*, **152**, 57–71, <https://doi.org/10.1016/j.oceaneng.2018.01.048>.
- , H. Pettersson, and K. K. Kahma, 2019: The wave spectrum in archipelagos. *Ocean Sci.*, **15**, 1469–1487, <https://doi.org/10.5194/os-15-1469-2019>.
- Campos, R. M., H. Islam, T. R. Ferreira, and C. Guedes Soares, 2021: Impact of heavy biofouling on a nearshore heave-pitch-roll wave buoy performance. *Appl. Ocean Res.*, **107**, 102500, <https://doi.org/10.1016/j.apor.2020.102500>.
- Carandell, M., D. M. Toma, J. P. Pinto, M. Gasulla, and J. del Río, 2020: Impact on the wave parameters estimation of a kinetic energy harvester embedded into a drifter. *Global Oceans 2020: Singapore–U.S. Gulf Coast*, Biloxi, MS, IEEE, <https://doi.org/10.1109/IEEECONF38699.2020.9389127>.
- Cartwright, D. E., and M. S. Longuet-Higgins, 1956: The statistical distribution of the maxima of a random function. *Proc. Roy. Soc. London*, **237A**, 212–232, <https://doi.org/10.1098/rspa.1956.0173>.
- Cavaleri, L., 1980: Wave measurement using pressure transducer. *Oceanol. Acta*, **3**, 339–346.
- Centurioni, L., L. Braasch, E. Di Lauro, P. Contestabile, F. De Leo, R. Casotti, L. Franco, and D. Vicinanza, 2017: A new strategic wave measurement station off Naples port main breakwater. *Coastal Eng. Proc.*, **1**, 36, <https://doi.org/10.9753/icce.v35.waves.36>.
- Christakos, K., J.-V. Björkqvist, L. Tuomi, B. R. Furevik, and Ø. Breivik, 2021: Modelling wave growth in narrow fetch geometries: The white-capping and wind input formulations. *Ocean Modell.*, **157**, 101730, <https://doi.org/10.1016/j.ocemod.2020.101730>.
- Cook, A., A. Babanin, D. Sgaroto, P. Graham, J. Mathew, A. Skvortsov, R. Manasseh, and D. Tothova, 2020: A UAV 'mobile buoy' for measuring surface waves. *22nd Australasian Fluid Mechanics Conf.*, Brisbane, Australia, University of Queensland, <https://doi.org/10.14264/8e7141e>.

- Donelan, M. A., and W. J. Pierson, 1983: The sampling variability of estimates of spectra of wind-generated gravity waves. *J. Geophys. Res.*, **88**, 4381–4392, <https://doi.org/10.1029/JC088iC07p04381>.
- , J. Hamilton, and W. H. Hui, 1985: Directional spectra of wind-generated waves. *Philos. Trans. Roy. Soc. London*, **315A**, 509–562, <https://doi.org/10.1098/rsta.1985.0054>.
- Earle, M., and K. Bush, 1982: Strapped-down accelerometer effects on NDBO wave measurements. *OCEANS 82*, Washington, DC, IEEE, 838–848, <https://doi.org/10.1109/OCEANS.1982.1151908>.
- Farber, S., H. Allaka, I. Klein, and M. Groper, 2018: Estimating sea state using a low cost buoy. *2018 IEEE Int. Conf. on the Science of Electrical Engineering in Israel*, Eilat, Israel, IEEE, <https://doi.org/10.1109/ICSEE.2018.8646100>.
- Forristall, G. Z., J. C. Heideman, I. M. Leggett, B. Roskam, and L. Vanderschuren, 1996: Effect of sampling variability on hindcast and measured wave heights. *J. Waterw. Port Coastal Ocean Eng.*, **122**, 216–225, [https://doi.org/10.1061/\(ASCE\)0733-950X\(1996\)122:5\(216\)](https://doi.org/10.1061/(ASCE)0733-950X(1996)122:5(216)).
- Fuertes, F. C., L. Wilhelm, and F. Porté-Agel, 2019: Multirotor UAV-based platform for the measurement of atmospheric turbulence: Validation and signature detection of tip vortices of wind turbine blades. *J. Atmos. Oceanic Technol.*, **36**, 941–955, <https://doi.org/10.1175/JTECH-D-17-0220.1>.
- Gordon, L., and A. Lohrmann, 2002: Near-shore Doppler current meter wave spectra. *Proc. Int. Symp. on Ocean Wave Measurement and Analysis*, San Francisco, CA, American Society of Civil Engineers, 33–43, [https://doi.org/10.1061/40604\(273\)4](https://doi.org/10.1061/40604(273)4).
- Graber, H. C., E. A. Terray, M. A. Donelan, W. M. Drennan, J. C. Van Leer, D. B. Peters, and J. C. V. Leer, 2000: ASIS—A new air–sea interaction spar buoy: Design and performance at sea. *J. Atmos. Oceanic Technol.*, **17**, 708–720, [https://doi.org/10.1175/1520-0426\(2000\)017<0708:AAANSI>2.0.CO;2](https://doi.org/10.1175/1520-0426(2000)017<0708:AAANSI>2.0.CO;2).
- Hanafin, J. A., and Coauthors, 2012: Phenomenal sea states and swell from a North Atlantic storm in February 2011: A comprehensive analysis. *Bull. Amer. Meteor. Soc.*, **93**, 1825–1832, <https://doi.org/10.1175/BAMS-D-11-00128.1>.
- Herbers, T. H. C., P. F. Jessen, T. T. Janssen, D. B. Colbert, and J. H. MacMahan, 2012: Observing ocean surface waves with GPS-tracked buoys. *J. Atmos. Oceanic Technol.*, **29**, 944–959, <https://doi.org/10.1175/JTECH-D-11-00128.1>.
- Hirakawa, Y., T. Takayama, T. Hirayama, and H. Susaki, 2016: Development of mini-buoy for short term measurement of ocean wave. *OCEANS 2016 MTS/IEEE Monterey*, Monterey, CA, IEEE, <https://doi.org/10.1109/OCEANS.2016.7761337>.
- Holthuijsen, L., 2007: *Waves in Oceanic and Coastal Waters*. Cambridge University Press, 387 pp.
- Houghton, I., P. Smit, D. Clark, C. Dunning, A. Fisher, N. Nidzicko, P. Chamberlain, and T. Janssen, 2021: Performance statistics of a real-time Pacific Ocean weather sensor network. *J. Atmos. Oceanic Technol.*, **38**, 1047–1058, <https://doi.org/10.1175/JTECH-D-20-0187.1>.
- Janssen, P. A., 1991: Quasi-linear theory of wind-wave generation applied to wave forecasting. *J. Phys. Oceanogr.*, **21**, 1631–1642, [https://doi.org/10.1175/1520-0485\(1991\)021<1631:QLTOWW>2.0.CO;2](https://doi.org/10.1175/1520-0485(1991)021<1631:QLTOWW>2.0.CO;2).
- Kennedy, D., M. Walsh, and B. O'Flynn, 2014: Development of a miniature, low-cost wave measurement solution. *2014 Oceans—St. John's*, St. John's, NL, Canada, IEEE, <https://doi.org/10.1109/OCEANS.2014.7003217>.
- Kitaigorodskii, S. A., 1983: On the theory of the equilibrium range in the spectrum of wind-generated gravity waves. *J. Phys. Oceanogr.*, **13**, 816–827, [https://doi.org/10.1175/1520-0485\(1983\)013<0816:OTTOTE>2.0.CO;2](https://doi.org/10.1175/1520-0485(1983)013<0816:OTTOTE>2.0.CO;2).
- Kodaira, T., T. Waseda, T. Nose, K. Sato, J. Inoue, J. Voermans, and A. Babanin, 2020: Observation of on-ice wind waves under grease ice in the western Arctic Ocean. *Polar Sci.*, **27**, 100567, <https://doi.org/10.1016/j.polar.2020.100567>.
- Kohout, A. L., B. Penrose, S. Penrose, and M. J. Williams, 2015: A device for measuring wave-induced motion of ice floes in the Antarctic marginal ice zone. *Ann. Glaciol.*, **56**, 415–424, <https://doi.org/10.3189/2015AoG69A600>.
- Lancaster, O., R. Cossu, S. Boulay, S. Hunter, and T. E. Baldock, 2021: Comparative wave measurements at a wave energy site with a recently developed low-cost wave buoy (Spotter), ADCP, and pressure loggers. *J. Atmos. Oceanic Technol.*, **38**, 1019–1033, <https://doi.org/10.1175/JTECH-D-20-0168.1>.
- Lang, N., 1987: The empirical determination of a noise function for NDBC buoys with strapped-down accelerometers. *OCEANS'87*, Halifax, NS, Canada, IEEE, 225–228, <https://doi.org/10.1109/OCEANS.1987.1160904>.
- Le Merle, E., D. Hauser, C. Peureux, L. Aouf, P. Schippers, C. Dufour, and A. Dalphiné, 2021: Directional and frequency spread of surface ocean waves from SWIM measurements. *J. Geophys. Res. Oceans*, **126**, e2021JC017220, <https://doi.org/10.1029/2021JC017220>.
- Lenain, L., and N. Pizzo, 2020: The contribution of high-frequency wind-generated surface waves to the Stokes drift. *J. Phys. Oceanogr.*, **50**, 3455–3465, <https://doi.org/10.1175/JPO-D-20-0116.1>.
- Lin, Z., T. A. A. Adcock, and M. L. McAllister, 2021: Estimating ocean wave directional spreading using wave following buoys: A comparison of experimental buoy and gauge data. *J. Ocean Eng. Mar. Energy*, **8**, 83–97, <https://doi.org/10.1007/s40722-021-00218-7>.
- Loehr, H., and Coauthors, 2013: Development of a low cost wave buoy by utilising smartphone technology. *21st Australasian Coastal and Ocean Engineering Conf.—14th Australasian Port and Harbour Conf.*, Barton, Australia, Engineers Australia.
- Longuet-Higgins, M. S., 1961: Observations of the directional spectrum of sea waves using the motions of a floating buoy. *Ocean Wave Spectra*, Prentice-Hall, 111–136.
- Montiel, F., V. Squire, M. Doble, J. Thomson, and P. Wadhams, 2018: Attenuation and directional spreading of ocean waves during a storm event in the autumn Beaufort Sea marginal ice zone. *J. Geophys. Res. Oceans*, **123**, 5912–5932, <https://doi.org/10.1029/2018JC013763>.
- Mueller, J. A., and F. Veron, 2009: Nonlinear formulation of the bulk surface stress over breaking waves: Feedback mechanisms from air-flow separation. *Bound.-Layer Meteor.*, **130**, 117–134, <https://doi.org/10.1007/s10546-008-9334-6>.
- Munk, W. H., 1950: Origin and generation of waves. *Proc. First Conf. Coastal Engineering*, Long Beach, CA, ASCE, 1–4, <https://doi.org/10.9753/icce.v1.1>.
- Pearman, D., T. Herbers, T. Janssen, H. van Ettinger, S. McIntyre, and P. Jessen, 2014: Drifter observations of the effects of shoals and tidal-currents on wave evolution in San Francisco Bight. *Cont. Shelf Res.*, **91**, 109–119, <https://doi.org/10.1016/j.csr.2014.08.011>.
- Pettersson, H., H. C. Graber, D. Hauser, C. Quentin, K. K. Kahma, W. M. Drennan, and M. A. Donelan, 2003: Directional wave measurements from three wave sensors

- during the FETCH experiment. *J. Geophys. Res.*, **108**, 8061, <https://doi.org/10.1029/2001JC001164>.
- , K. K. Kahma, and L. Tuomi, 2010: Wave directions in a narrow bay. *J. Phys. Oceanogr.*, **40**, 155–169, <https://doi.org/10.1175/2009JPO4220.1>.
- Phillips, O. M., 1985: Spectral and statistical properties of the equilibrium range in wind-generated gravity waves. *J. Fluid Mech.*, **156**, 505–531, <https://doi.org/10.1017/S0022112085002221>.
- Rabault, J., G. Sutherland, B. Ward, K. H. Christensen, T. Halsne, and A. Jensen, 2016: Measurements of waves in landfast ice using inertial motion units. *IEEE Trans. Geosci. Remote Sens.*, **54**, 6399–6408, <https://doi.org/10.1109/TGRS.2016.2584182>.
- , —, O. Gundersen, A. Jensen, A. Marchenko, and Ø. Breivik, 2020: An open source, versatile, affordable waves in ice instrument for scientific measurements in the polar regions. *Cold Reg. Sci. Technol.*, **170**, 102955, <https://doi.org/10.1016/j.coldregions.2019.102955>.
- Raghukumar, K., G. Chang, F. Spada, C. Jones, T. Janssen, and A. Gans, 2019: Performance characteristics of “Spotter,” a newly developed real-time wave measurement buoy. *J. Atmos. Oceanic Technol.*, **36**, 1127–1141, <https://doi.org/10.1175/JTECH-D-18-0151.1>.
- Skinner, E., M. Rooney, and M. Hinders, 2018: Low-cost wave characterization modules for oil spill response. *J. Ocean Eng. Sci.*, **3**, 96–108, <https://doi.org/10.1016/j.joes.2018.05.003>.
- Smit, P. B., I. A. Houghton, K. Jordanova, T. Portwood, E. Shapiro, D. Clark, M. Sosa, and T. T. Janssen, 2021: Assimilation of significant wave height from distributed ocean wave sensors. *Ocean Modell.*, **159**, 101738, <https://doi.org/10.1016/j.oceanmod.2020.101738>.
- Squire, V. A., 2020: Ocean wave interactions with sea ice: A reappraisal. *Annu. Rev. Fluid Mech.*, **52**, 37–60, <https://doi.org/10.1146/annurev-fluid-010719-060301>.
- Sutherland, G., and Coauthors, 2020: Evaluating the leeway coefficient of ocean drifters using operational marine environmental prediction systems. *J. Atmos. Oceanic Technol.*, **37**, 1943–1954, <https://doi.org/10.1175/JTECH-D-20-0013.1>.
- Thomson, J., 2012: Wave breaking dissipation observed with “swift” drifters. *J. Atmos. Oceanic Technol.*, **29**, 1866–1882, <https://doi.org/10.1175/JTECH-D-12-00018.1>.
- , and Coauthors, 2015: Biofouling effects on the response of a wave measurement buoy in deep water. *J. Atmos. Oceanic Technol.*, **32**, 1281–1286, <https://doi.org/10.1175/JTECH-D-15-0029.1>.
- Veras Guimarães, P., and Coauthors, 2018: A surface kinematics buoy (SKIB) for wave–current interaction studies. *Ocean Sci.*, **14**, 1449–1460, <https://doi.org/10.5194/os-14-1449-2018>.
- Voermans, J., P. Smit, T. Janssen, and A. Babanin, 2020: Estimating wind speed and direction using wave spectra. *J. Geophys. Res. Oceans*, **125**, e2019JC015717, <https://doi.org/10.1029/2019JC015717>.
- Wadhams, P., 1978: Wave decay in the marginal ice zone measured from a submarine. *Deep-Sea Res.*, **25**, 23–40, [https://doi.org/10.1016/S0146-6291\(21\)00004-7](https://doi.org/10.1016/S0146-6291(21)00004-7).
- Xsens, 2015: Data sheet MTi 1-series: 3D AHRS/VRU/IMU module. Xsens Doc. MT0512P, Revision B, 35 pp., http://www.sensores-de-medida.es/uploads/xsens_mti-1-series_datasheet.pdf.
- , 2019: MTi 1-series datasheet: IMU, VRU, AHRS and GNSS/INS module. Xsens Doc. MT0512P, Revision 2019.A, 40 pp., <https://www.xsens.com/hubfs/Downloads/Manuals/MTi-1-series-datasheet.pdf>.
- Young, I. R., 1995: The determination of confidence limits associated with estimates of the spectral peak frequency. *Ocean Eng.*, **22**, 669–686, [https://doi.org/10.1016/0029-8018\(95\)00002-3](https://doi.org/10.1016/0029-8018(95)00002-3).
- Yurovsky, Y. Y., and V. Dulov, 2017: Compact low-cost Arduino-based buoy for sea surface wave measurements. *2017 Progress in Electromagnetics Research Symp.—Fall*, Singapore, IEEE, 2315–2322, <https://doi.org/10.1109/PIERS-FALL.2017.8293523>.
- , and —, 2020: MEMS-based wave buoy: Towards short wind-wave sensing. *Ocean Eng.*, **217**, 108043, <https://doi.org/10.1016/j.oceaneng.2020.108043>.
- Zappa, C. J., S. M. Brown, N. J. M. Laxague, T. Dhakal, R. A. Harris, A. M. Farber, and A. Subramaniam, 2020: Using ship-deployed high-endurance unmanned aerial vehicles for the study of ocean surface and atmospheric boundary layer processes. *Front. Mar. Sci.*, **6**, 777, <https://doi.org/10.3389/fmars.2019.00777>.
- Zong, Y., H.-Y. Cheng, H. Chien, and B. Koppe, 2019: Miniature wave buoy—Laboratory and field tests for development of a robust low-cost measuring technique. *Coastal Structures 2019*, Hannover, Germany, Bundesanstalt für Wasserbau, 453–462, https://doi.org/10.18451/978-3-939230-64-9_046.

Paper III

Pärt, S., Björkqvist, J. V., Alari, V., Maljutenko, I., & Uiboupin, R. (2023). **An ocean-wave-trajectory forecasting system for the eastern Baltic Sea: Validation against drifting buoys and implementation for oil spill modeling.** *Marine Pollution Bulletin*, 195(August). <https://doi.org/10.1016/j.marpolbul.2023.115497>



Contents lists available at ScienceDirect

Marine Pollution Bulletin

journal homepage: www.elsevier.com/locate/marpolbul

An ocean–wave–trajectory forecasting system for the eastern Baltic Sea: Validation against drifting buoys and implementation for oil spill modeling

Siim Pärt^{a,*}, Jan-Victor Björkqvist^{b,c}, Victor Alari^a, Ilja Maljutenko^a, Rivo Uiboupin^a

^a Tallinn University of Technology, Department of Marine Systems, Akadeemia tee 15a, Tallinn 12618, Estonia

^b Norwegian Meteorological Institute, Allégaten 70, Bergen 5007, Norway

^c Finnish Meteorological Institute, Erik Palménin aukio 1, Helsinki 00560, Finland

ARTICLE INFO

Keywords:

Trajectory modeling
Oil spill modeling
Baltic Sea
OpenDrift
Drifting buoys
Hypothetical oil spills

ABSTRACT

We present the implementation and validation of OpenDrift, an open-source Lagrangian particle trajectory modeling framework for oil spill modeling in the coastal waters of Estonia in the Baltic Sea. The framework was coupled with ECMWF winds, NEMO-EST05 hydrodynamical model, and SWAN-EST wave model, and validated using six drift experiments from 2022. The sensitivity analysis revealed the importance of incorporating additional forcing factors, such as Stokes drift and currents, which generally improved the accuracy of the trajectory model compared to using wind alone. Nevertheless, the benefits of providing OpenDrift with, for example, the Stokes drift seemed to depend on whether currents are also included or not. The wind drift factors of the utilized drifters align closely with those commonly employed in oil spill modeling. Furthermore, the modeling results for hypothetical oil spills in severe weather conditions and high-risk regions emphasize the critical need for preparedness and rapid response strategies.

1. Introduction

Liquid fossil hydrocarbons, commonly referred to as oils, are a critical resource for energy and chemical synthesis. The impact of the production, transportation, and consumption of various hydrocarbon products on the marine environment has long been recognized and studied (e.g. Teal and Howarth, 1984; HELCOM, 2013; Zhang et al., 2018; Chilvers et al., 2021).

Oil pollution may originate from land or directly from sea and can come from a variety of sources: natural oil and gas seeps, oil extraction, oil transportation, and oil consumption (NAS, 2022). Although almost 30 % of global seaborne trade can be accounted for as oil and its products (Riazi, 2021) and the volume of global oil trade increases (Chen et al., 2019), the number of large oil spills has decreased over the years (Chen et al., 2019; NAS, 2022; ITOPE, 2022). Most of the smaller sea-based oil pollution originates from shipping activities or offshore platforms, the so-called operational discharges, which can be accidental or deliberate.

Potentially polluting shipwrecks are another substantial source of oil pollution (Michel et al., 2005; Landquist et al., 2013; Amir-Heidari et al., 2019; NAS, 2022). Most of these wrecks date back to World War II and have an ever-growing risk of structural damage and leakage due to more

than 75 years of corrosion (Landquist et al., 2014; Carter et al., 2021).

Detection and monitoring of oil spills is a crucial part of the contingency planning for such incidents. Currently, oil spill detection and monitoring is carried out mainly by satellite and aerial surveillance (Fingas and Brown, 2018; HELCOM, 2018a; Al-Ruzouq et al., 2020). To complement these remote sensing methods, different in situ platforms are also being developed (Moroni et al., 2016; Xu et al., 2020; Pärt et al., 2021).

After the detection of a significant oil spill, one of the main concerns in spill response activities is the trajectory of the pollution and its spatial distribution. Various operational models are used around the world to simulate and forecast the movement and evolution of oil spills (Spaulding, 2017; Hole, 2018; Keramea et al., 2021). MEDSLIK-II (De Dominicis et al., 2013a,b), GNOME (Beegle-Krause, 2005; Elizaryev et al., 2018), OSCAR (Aamo et al., 2005; Barreto et al., 2021), OpenDrift (Dagestad et al., 2018) to name just a few of the most used.

The Baltic Sea is a brackish inland sea with limited water exchange (e.g. Gustafsson, 1997; Winsor et al., 2001), complex coastlines and seasonal ice cover. According to HELCOM (2003) the relatively small Baltic Sea accounts for up to 15 % of world's maritime transport and, at the same time due to its special geographical, climatological and oceanographic characteristics, is highly sensitive to the environmental

* Corresponding author.

E-mail address: siim.part@taltech.ee (S. Pärt).

<https://doi.org/10.1016/j.marpolbul.2023.115497>

Received 30 June 2023; Received in revised form 20 August 2023; Accepted 2 September 2023

Available online 21 September 2023

0025-326X/© 2023 Published by Elsevier Ltd.

impacts of human activities. Regarding oil pollution, the main source in the Baltic Sea is operational oil discharges from ships (HELCOM, 2018a, 2018b), and as is in the other parts of the world's ocean and seas, potentially polluting wrecks are an emerging problem (Landquist et al., 2016; Lindgren et al., 2020).

In the Baltic Sea area, the most developed and widely used operational oil, chemical, and object drift modeling system is Seatrack Web (STW) (Ambjörn, 2006; Ambjörn et al., 2014). STW has been in operation since the early 1990s and has been continuously used, developed, and updated since then. The advantage of STW is that it provides a user interface that relieves the end user of setting up and running the actual underlying numerical model. This automatization, however, also means that the user does not have full insight and control into the modeling process, which might be a drawback in areas for which STW has not been fully optimized, such as Estonian coastal waters in the eastern Baltic Sea (Fig. 1).

Recently, Estonia has implemented two local high-resolution operational models, namely NEMO-EST05 for hydrodynamics and SWAN-EST for waves. This development has motivated the integration of these forecasts into a drift modeling system. However, the existing STW system does not support this integration. As an alternative, we have chosen to utilize OpenDrift, an open-source, Python-based Lagrangian particle trajectory modeling framework (Dagestad et al., 2018). OpenDrift is developed and currently used operationally at the Norwegian Meteorological Institute (MET Norway). While the framework has been employed in studies related to the Baltic Sea (Miettunen et al., 2020), Mediterranean Sea (Keramea et al., 2021; Clavel-Henry et al., 2021), and the Black Sea (Stanev and Ricker, 2019), most evaluations against drifter and oil slick observations have primarily focused on oceanic conditions in the Nordic Seas (Jones et al., 2016b; Röhrs et al., 2018; Brekke et al., 2021).

The aim of this work is to present the setup and validation of the OpenDrift framework coupled with the local hydrodynamical and wave models for modeling oil spills in the sea area of Estonia. In addition, we present modeling results for hypothetical oil spills in area with heavy marine traffic, future wind park location, and from a potentially polluting wreck.

The structure of this paper is as follows: In Section 2, we provide an overview of the implemented atmospheric and hydrodynamical and wave models, the setup of OpenDrift and its module OpenOil, the field experiments involving drifting buoys, the validation procedures, and the metric employed for simulation assessment. Section 3 presents the results obtained from the numerical modeling experiments and the outcomes of hypothetical oil spill cases. These results are discussed in Section 4. Finally, Section 5 provides a summary of the key findings.

2. Materials and methods

2.1. Met-ocean forcing system

2.1.1. Wind

For meteorological input, we use the ECMWF IFS deterministic forecast, which provides 10-m wind speed and direction at hourly intervals (Owens and Hewson, 2018). Both the NEMO-EST05 and SWAN-EST configurations are forced with the same meteorological data, ensuring consistency in the simulation.

2.1.2. Ocean

NEMO (Nucleus for European Modeling of the Ocean) is a modeling framework developed by an international collaboration, containing many submodels, allowing them to be used in a multitude of oceanological and climatological research and forecasting applications (Madec and the NEMO Team, 2022). Originally developed as an ocean model, the model has also been successfully applied to research in the Baltic Sea (Hordoir et al., 2019) and its subbasins in the Gulf of Finland (Vankevich et al., 2016; Westerlund et al., 2018, 2019) and the Bothnian Sea (Westerlund and Tuomi, 2016). Furthermore, the Baltic Sea Monitoring and Forecasting Center (BALMFC) has developed an operational NEMO set-up for the Copernicus European Marine Monitoring Service (CMEMS), called NEMO-Nordic, which covers the entire Baltic Sea (Hordoir et al., 2019; Kärnä et al., 2021).

The operational system NEMO-EST05 (Maljutenko et al., 2022) is developed for the Estonian sea area and is based on the NEMO-Nordic 2.0 configuration (Kärnä et al., 2021). The regional configuration

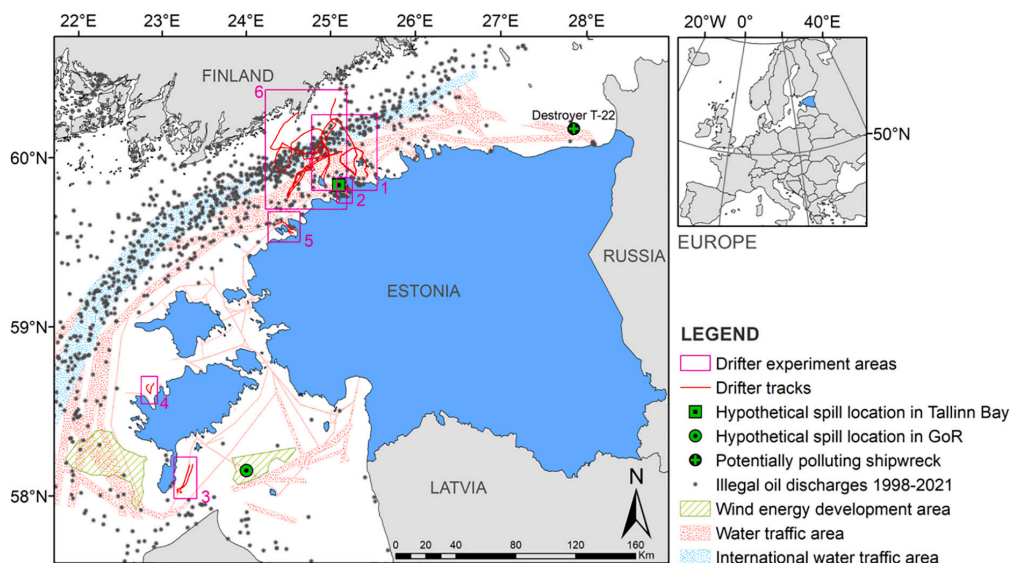


Fig. 1. Study area. Illegal oil discharges were observed during aerial surveillance flights by HELCOM Contracting Parties during 1998–2021 (HELCOM, 2022). The marine traffic and wind energy development areas are from the Estonian maritime spatial plan (Estonian Ministry of Finance and Hendrikson and Ko, 2021) and the corresponding map layers are accessible from web-map (Hendrikson and Ko, 2022).

covers the region from 21.55°E to 30.35°E longitudes and 56.94°N to 60.725°N latitudes with a gridstep of approximately 1 km. The vertical computational grid is divided into 110 layers with a vertical step of 1 m between 0 and 80 m and a step of 2 m between 90 and 130 m.

From the NEMO-EST05 ocean model, the three components of sea water velocity, sea water temperature and salinity, sea ice fraction, water depth, and vertical diffusivity were provided to OpenDrift.

2.1.3. Waves

The SWAN model (Booij et al., 1999; Ris et al., 1999) is a third-generation spectral wave model developed at Delft University of Technology, used to simulate wind-generated waves and swells in open oceans, shallow coastal areas, and inland waters with given wind and bathymetry conditions. The model has been widely used to simulate and describe the wave condition and the overall wave climate in the Baltic Sea (Kriezi and Broman, 2008; Suursaar et al., 2014; Viitak et al., 2016; Björkqvist et al., 2018; Soomere, 2022).

A wave forecast based on the SWAN model, SWAN-EST, with 0.5 nmi resolution has been operational since November 2021. The model output containing essential bulk wave parameters is on the same horizontal grid as NEMO-EST05. Since the Stokes drift vector is not calculated by default in SWAN, we implemented it in the operational model code for the prognostic part of the wave spectrum. The model was run with a 20 min integration time step, and the wave spectrum in SWAN was discretized with 24 equally spaced directions and 32 frequencies distributed logarithmically in the frequency range of 0.05–1 Hz. Following Rogers et al. (2003) and Pallares et al. (2014), the white-capping coefficient δ was set at 1 and as suggested by Zijlema et al. (2012), the bottom friction coefficient was set at $0.038 \text{ m}^2\text{s}^{-3}$. Wind drag parameterization proposed by Wu (2012) was used, since Björkqvist et al. (2018) reported that the default drag in SWAN, proposed by Zijlema et al. (2012), resulted in a negative bias for the highest wave heights.

From the SWAN-EST wave model, the significant wave height, the Stokes drift, and the mean and peak wave periods were provided to OpenDrift.

2.2. OpenDrift and OpenOil

OpenDrift, a software package developed by Dagestad et al. (2018), is a versatile open-source tool used to model the trajectories and fate of drifting objects or substances in the ocean. This framework consists of specialized modules tailored for different applications, such as oil drift (OpenOil), search and rescue (Leeway), plastic drift (PlastDrift), pelagic egg drift (PelagicEgg), chemical drift (ChemicalDrift), recently introduced by Aghito et al. (2022), and more.

In our validation process, we utilize the OceanDrift module. However, since the modules share common functionality, the validation applies to each of them, including OpenOil, which we use for hypothetical spill modeling. OpenDrift's OpenOil module is specifically designed for oil spill drift and fate modeling, encompassing the simulation of oil spill transformation and tracking oil changes over time and space. The oil properties used in OpenOil are sourced from the ADIOS Oil Database (adios.orr.noaa.gov), which contains information on the physical and chemical characteristics of numerous oils and petroleum products, accounting for simulated weathering. The simulations conducted by OpenOil encompass various oil weathering processes, such as evaporation, emulsification, vertical mixing, and biodegradation.

To operate effectively, OpenDrift and its modules require input data from oceanographic and atmospheric sources. In our setup, to simulate drifter trajectories we provided the OceanDrift module with wind speed and direction from the ECMWF model, current speed and direction from the NEMO-EST05 model, and wave-induced Stokes drift data from the SWAN-EST model. These variables are also provided to the OpenOil module, which could be run without any additional forcing fields.

Nonetheless, to enhance its capabilities we incorporate additional variables from NEMO-EST05 and SWAN-EST models. Sea water temperature and salinity influences the physical properties of both water and oil, affecting oil weathering and transport. Furthermore, temperature affects the evaporation rate of oil and the sea ice fraction affects the calculation of various drift factors. Water depth, upward seawater velocity, and vertical diffusivity affect the vertical distribution of oil particles in the water column. As waves play an important role in the entrainment and dispersion processes, mean and peak wave periods were provided in addition to Stokes drift. While these variables are not essential for basic trajectory modeling, they improve the parameterizations of weathering and transport processes associated with oil. The details of the fate and transport physics specific to oil in this module are described in more detail by Röhrs et al. (2018).

For the hypothetical oil spill scenarios, a total volume of 10 m^3 of the oil type "GENERIC HEAVY FUEL OIL" is utilized, characterized by a density of 971.1 kg/m^3 and a dynamic viscosity of $5.02 \cdot 10^{-4} \text{ kg/(m}\cdot\text{s)}$. This oil is represented in the simulations using 1000 particles, which are released simultaneously. In oil spill modeling, wind and Stokes drift are often amalgamated and represented by a wind drift factor (WDF) of 3 % or 3.5 % (e.g. Schwartzberg, 1971; Stolzenbach et al., 1977; Reed et al., 1994; ASCE, 1996). In OpenOil Stokes drift is treated independently and we apply a WDF of 0.02 (equivalent to 2 % of the 10 m wind), as outlined in previous studies (e.g. Jones et al., 2016a; Brekke et al., 2021). In this paper the movement component of objects or substances influenced by the wind is referred to as the "wind drift factor", but alternative terms such as "windage" or "leeway" are also used in other works.

2.3. Field experiments

2.3.1. Drifter buoys

The drifters used in this study are wave buoys named LainePoiss® (LP, Alari et al., 2022), which are manufactured by WiseParker OÜ. LP is an accelerometre-based floating spherical buoy with a diameter of ca 40 cm. It can be deployed as a moored or drifting device, and the GPS position is sent every 22 min. A photograph of these buoys deployed as drifters during one of the experiments is found in Fig. 2 (A).

Two versions of LPs were used in the drift experiments. The older versions (V0.1) and the newer versions (V1.0) differ slightly in shape and in the addition of a chain to the base LP V1.0 (Fig. 2 (B)).

2.3.2. Drift experiments

In 2022, we conducted six drift experiments specifically aimed at obtaining data to validate the drift model. These experiments were carried out in locations characterized by heavy marine traffic or sheltered areas for ships, which are known to have a higher likelihood of oil spills. Table 1 and Fig. 1 provide general information on the experiments.

The first drift experiment took place in Muuga Bay in the Gulf of Finland (Fig. 1, Area 1), and was divided into two parts. Three LP V0.1 buoys and one LP V1.0 buoy were used. In Part A, all four drifters were deployed from the same starting point and retrieved after approximately five hours. In Part B, two LP V0.1 were redeployed from the same starting point and drifted for five days before beaching.

The second experiment was conducted in Tallinn Bay in the Gulf of Finland (Fig. 1, Area 2), where five LPs (one V0.1 and four V1.0) were deployed at the same point. The experiment lasted between 5 and 9 h, depending on the buoy, due to prevailing westerly winds and the relatively short distance to the shore.

The third experiment took place in Tagalaht Bay, located on the northern coast of Saaremaa Island (Fig. 1, Area 3). Only one LP V1.0 was used and the experiment lasted for approximately 46 h.

The fourth experiment, conducted near the southern coast of Saaremaa Island in the Gulf of Riga (Fig. 1, Area 4), ran simultaneously with the third experiment. Two LP V1.0 buoys were deployed approximately

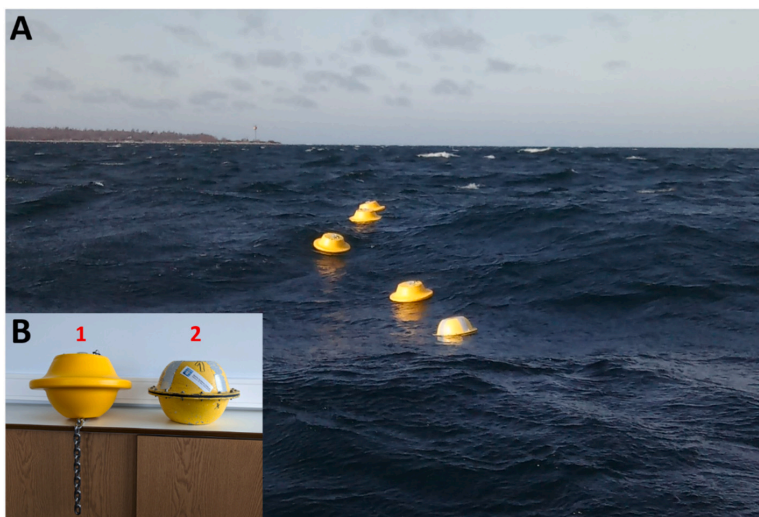


Fig. 2. (A) LainePoiss wave buoys in Tallinn Bay. The closest buoy is the LP V0.1 and the other are the LP V1.0. (B) LP V1.0 (1) and LP V0.1 (2). (Photographs: Kaimo Vahter and WiseParker OÜ).

Table 1

Overview of the drift experiments conducted in 2022. The presented wave data is from the LainePoiss buoys and wind and current data along the buoys' tracks are from the models. An overview of the locations and tracks is given in Fig. 1.

Nr.	Location	Time	Nr of buoys	Wave height (m)	Wind (m/s)	Wind direction	Current (m/s)
1.	Muuga Bay	26.01–31.01	4(6)	0–2.61	2.6–13.7	Northerly/Easterly	0–0.24
2.	Tallinn Bay	11.03	5	0.33–0.89	6.2–8.0	Westerly	0–0.03
3.	Gulf of Riga	21.09–23.09	2	0.05–0.65	0.9–6.2	Northerly/Southerly	0.02–0.12
4.	Tagalaht Bay	21.09–23.09	1	0.08–0.54	0.7–5.0	Northerly/Southerly	0.01–0.11
5.	Pakri Bay	26.09–27.09	3	0.09–0.42	4.2–5.9	Northerly/Easterly	0.01–0.23
6.	Gulf of Finland	11.12–21.12	2	0.26–3.83	0.1–18.8	Variable	0–0.20

4.5 km apart and drifted for 45 h.

The fifth experiment was conducted in Pakri Bay in the Gulf of Finland (Fig. 1, Area 5), with three buoys (LP V1.0) deployed to cover the largest possible area of the bay. Two buoys beached, the first after about six hours and the second after nine hours. The third buoy was retrieved after 22 h.

The sixth experiment aimed to collect data during the Birgit storm (internationally known as Gaia). Two buoys (LP V1.0) were deployed approximately 2.5 km apart and approximately 30 km from the mainland in the Gulf of Finland (Fig. 1, Area 6). Both drifters beached on Finnish coastal islands, with the first one after approximately seven days and the second after about nine days of drifting.

2.4. Validation procedures

2.4.1. Track comparison and wind drift factors

In the event of an oil spill, response operations, including modeling the spill's trajectory, are most critical within the first few days. The response time can even be shorter when dealing with short distances and complex coastal lines. For the reason mentioned above and to maximize available data, the buoy data were divided into six-hour segments. Subsequently, we released a numerical drifter at the start of each segment and calculated its drift at intervals of 6, 12 and 24 h. To match the LP measurement interval, the trajectory of the simulated buoy was also calculated in 22 min time steps.

A floating object on the surface of the sea is influenced by a combination of currents, waves, and wind. We determined the optimal direct wind drag for two versions of the LP buoys following Dagestad and

Röhrs (2019). To this end, we simulated 11 trajectories for each segment, with WDFs ranging from 0 % to 5 %. From these trajectories, we identified the best-fit trajectory and the corresponding WDF.

Fig. 3 provides an example of simulations that have been started every 6 h using the 11 different WDFs. All the simulations shown in Fig. 3 were also forced with the currents and the Stokes drift. However, to explore the sensitivity of the model to different forcing parameters, additional simulation runs were conducted with different forcing combinations, namely wind only, wind and Stokes drift, and wind and currents.

2.4.2. Skill score

To evaluate the model's ability to simulate trajectories, the Normalized Cumulative Lagrangian Separation (NCLS) was used, which is also known as the Liu-Weisberg skill score (Liu and Weisberg, 2011). This skill score (SS) evaluates the separation of drifter and model trajectories along their entire path, normalized by the total length of the path:

$$SS = \begin{cases} 1 - \frac{s}{n} & \text{if } s \leq n \\ 0 & \text{if } s > n, \end{cases} \quad (1)$$

where s is the cumulative Lagrangian separation distance normalized by the associated cumulative observed trajectory length, and n is the tolerance threshold, which we set to 1, following Liu and Weisberg (2011) and Liu et al. (2014).

The cumulative Lagrangian separation distance, s , is calculated as

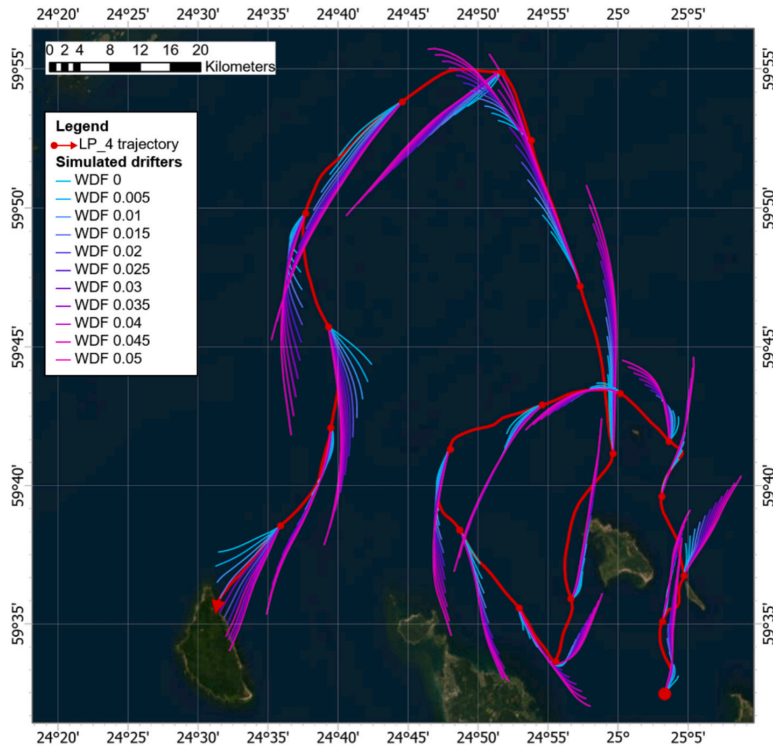


Fig. 3. Trajectory of the LP 4 starting in Muuga Bay (Fig. 1, Area 1) and simulated 6 h trajectories with WDFs between 0 % and 5 %, with forcing of wind, currents and Stokes drift. The simulations are reinitialized every 6 h.

Table 2
Skill scores (SS) and WDFs determined from drift experiments.

	LP V0.1			LP V1.0		
	6 h	12 h	24 h	6 h	12 h	24 h
Wind						
Number of runs	40	28	16	90	81	63
SS (mean)	0.198–0.951 (0.692)	0.448–0.914 (0.729)	0.624–0.917 (0.798)	0.001–0.932 (0.491)	0.002–0.926 (0.489)	0.042–0.870 (0.512)
WDF (mean)	0.020–0.050 (0.034)	0.025–0.050 (0.034)	0.025–0.045 (0.035)	0–0.050 (0.025)	0–0.050 (0.025)	0–0.045 (0.020)
Wind + Stokes drift						
Number of runs	38	27	8	90	80	59
SS (mean)	0.208–0.949 (0.705)	0.449–0.922 (0.733)	0.713–0.931 (0.836)	0–0.940 (0.494)	0–0.921 (0.481)	0.010–0.864 (0.478)
WDF (mean)	0.010–0.050(0.025)	0.015–0.040 (0.025)	0.025–0.035 (0.030)	0–0.050 (0.018)	0–0.050 (0.018)	0–0.040 (0.013)
Wind + Currents						
Number of runs	38	31	16	89	75	60
SS (mean)	0.326–0.948 (0.717)	0.555–0.908 (0.774)	0.573–0.930 (0.819)	0–0.951 (0.541)	0–0.954 (0.555)	0–0.916 (0.602)
WDF (mean)	0.015–0.050(0.030)	0.020–0.400 (0.042)	0.020–0.040 (0.028)	0–0.050 (0.020)	0–0.050 (0.021)	0–0.050 (0.020)
Wind + Currents + Stokes drift						
Number of runs	38	29	12	89	77	56
SS (mean)	0.392–0.934 (0.723)	0.562–0.905 (0.770)	0.576–0.919 (0.791)	0–0.969 (0.535)	0–0.940 (0.541)	0–0.932 (0.569)
WDF (mean)	0.005–0.045 (0.022)	0.010–0.040 (0.021)	0.010–0.030 (0.018)	0–0.050 (0.015)	0–0.050 (0.016)	0–0.050 (0.014)

Mean WDF for LPs		
	LP V0.1	LP V1.0
Wind	0.034	0.023
Wind + Stokes drift	0.027	0.017
Wind + Currents	0.033	0.021
Wind + Currents + Stokes drift	0.020	0.015

Table 3
Average skill scores (SS) for 6-h forecast interval with different combinations of forcing, using the best estimates of the WDFs.

Forcing combination	Wind	Wind + Stokes drift	Wind + Currents	Wind + Currents + Stokes drift
LP V0.1				
Muuga Bay LP_3	0.639	0.631	0.649	0.669
Muuga Bay LP_4	0.642	0.631	0.634	0.654
Number of runs	42	42	41	41
Mean of SSs	0.641	0.631	0.642	0.662
Weighted average SS	0.641	0.631	0.642	0.662
LP V1.0				
Gulf of Riga LP_13	0.393	0.467	0.625	0.662
Gulf of Riga LP_14	0.391	0.441	0.583	0.583
Tagalaht Bay LP_17	0.439	0.441	0.362	0.349
Pakri Bay LP_13	0.609	0.588	0.530	0.546
Pakri Bay LP_14	0.515	0.497	0.565	0.526
Gulf of Finland LP_16	0.352	0.354	0.377	0.368
Gulf of Finland LP_17	0.337	0.342	0.371	0.365
Tallinn Bay LP_7	0.715	0.774	0.730	0.782
Tallinn Bay LP_9	0.735	0.800	0.753	0.807
Tallinn Bay LP_10	0.709	0.773	0.725	0.779
Tallinn Bay LP_11	0.716	0.839	0.736	0.845
Number of runs	96	97	97	96
Mean of SSs	0.537	0.574	0.578	0.601
Weighted average SS	0.385	0.404	0.434	0.428

the sum of the Lagrangian separation distances at each time step along the simulated trajectories, normalized by the total length of the observed trajectories:

$$s = \frac{\sum_{t=1}^N d(t)}{L}, \quad (2)$$

where N is the total number of time steps, $d(t)$ is the Lagrangian separation distance at time step t , and L is the total length of the observed trajectories.

This skill score is especially useful when there is only a limited number of observed trajectories to use and has been widely used for different types of trajectory model evaluation (e.g. Ivichev et al., 2012; De Dominicis et al., 2014; French-McCay et al., 2017; Pereiro et al., 2018; de Aguiar et al., 2022).

3. Results

3.1. Model validation against drifting buoys

3.1.1. Wind drift factor for LainePois drifters

To simulate drifter trajectories, OpenDrift requires the user to specify a WDF, which represents the proportion of the wind speed that affects the drifter's movement. As the LP buoys have not been previously employed for this specific purpose, determining the optimal WDF for these buoys is crucial to improve the accuracy of trajectory forecasts and ensure the reliability of the validation procedures conducted in this study.

Table 2 shows skill scores and the corresponding WDFs for the two types of LP, calculated for different track lengths (6, 12, and 24 h) of different forcing combinations. Trajectories that resulted in buoys reaching shore were excluded from the analysis, as their trajectories were truncated, and their Lagrangian separation distance was not fully captured. Additionally, six drifter buoy tracks lasting less than 6 h were excluded from the analysis. The optimal WDF was determined by averaging over all model runs and time intervals.

The optimal WDFs calculated for each combination of forcing for these buoys can be seen in Table 2. The WDFs found for the LP V0.1 were 2 % when considering the forcing of the wind, currents and Stokes drift, and 3 % without including Stokes drift (Table 2). These values are close to the corresponding values of 1.6 % and 2.8 % obtained for drifters with a similar design and size (iSphere) by Sutherland et al. (2020) but lower than 3 % and 4 % attained by Dagestad and Röhrs (2019). Jones et al.

(2016a) and Brekke et al. (2021) have reported a comparable WDF of 2 % for the iSphere, when incorporating wind, currents, and Stokes drift.

The bottom chain and small design differences of LP V1.0 resulted in a WDF of 1.5 % with Stokes drift included and 2.1 % without (Table 2).

3.1.2. Validation of the OpenDrift setup

To evaluate the accuracy of our setup of the drift model, we utilized the previously calculated best estimates of WDF values for the LPs. Using these values, we reran the simulations with the same track lengths and forcing combinations as before. The skill scores for the 6-h simulations are provided in Table 3. In Fig. 4, we present an example of these simulations, specifically the LP_14 track in the Gulf of Riga, along with the corresponding 6-h, 12-h, and 24-h trajectory simulations.

The weighted average skill score provides an overall assessment of the performance of the different forcing combinations. For the LP V0.1 the weighted average skill scores range from 0.631 to 0.662, with the highest value achieved when wind, currents, and Stokes drift are combined. For the LP V1.0 the weighted average skill scores range from 0.385 to 0.434, indicating moderate forecast accuracy overall.

Across all the simulations, skill scores for the LP V0.1 show relatively high values, ranging from 0.631 to 0.669. In general, when considering wind forcing alone, the skill score is 0.641. The addition of currents slightly increases the score to 0.642. Adding only the Stokes drift actually reduces the skill score to 0.631. Interestingly, adding both the currents and the Stokes drift increases the skill score to 0.662, showing that the effects of the different forcings are not merely additive, but the effect of a single forcing, such as the Stokes drift, might be dependent on the presence of another forcing, such as the currents.

The LP V1.0 forcing combination exhibits varying skill scores across different simulations, varying from 0.337 to 0.845. Among the simulations considered, Tallinn Bay consistently showed the highest scores, ranging from 0.709 to 0.845. Moreover, there is minimal variability in skill scores based on different buoy tracks in Tallinn Bay, likely due to the same starting point and the very similar and close tracks of the buoys.

Gulf of Finland and Tagalaht Bay simulations generally display the lowest skill scores. Notably, Tagalaht Bay stands out as the only simulation with the lowest skill score when forced by wind, currents and Stokes drift. On the contrary, simulations based on the LP_13 track in Pakri Bay demonstrate the highest skill score values with only wind forcing.

For LP V1.0, the mean skill scores over all the simulations were higher when using the combination of wind, currents, and Stokes drift

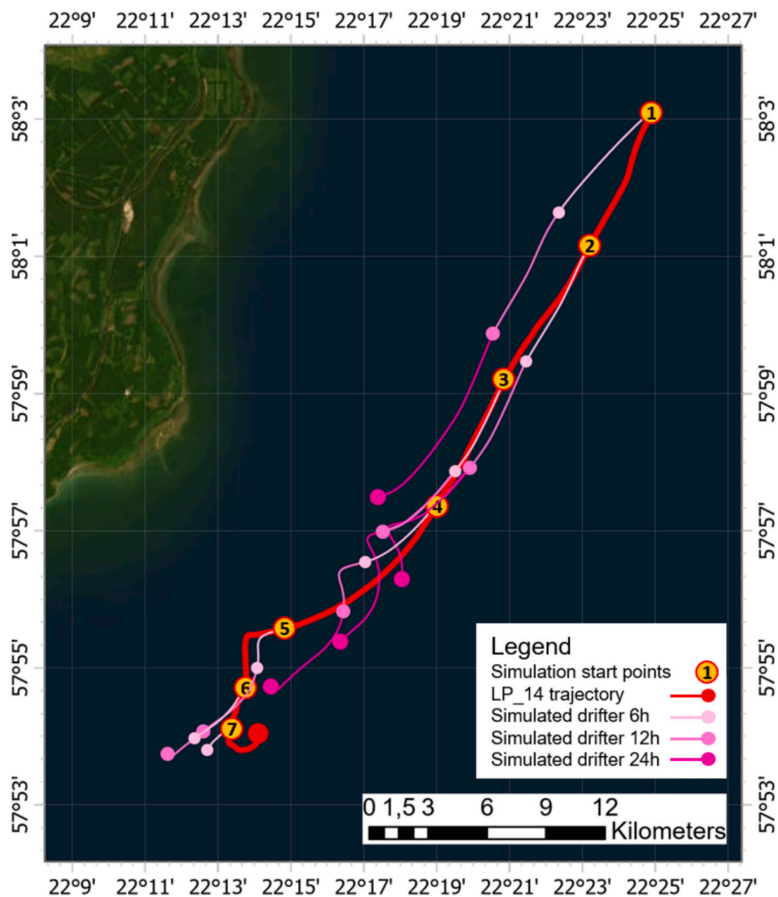


Fig. 4. Trajectory of LP₁₄ in the Gulf of Riga (Fig. 1, Area 3) and the trajectory simulations, that are reinitialized every 6 h and simulated 6, 12 and 24 h forward. Simulations are forced with wind, currents and Stokes drift.

compared to other combination of forcing. However, when considering the weighted average skill scores, which account for the number of runs for each simulation, placing more weight on simulations with a larger number of runs, the combination of wind and currents yields the highest values, overall.

The skill scores of 12-h and 24-h simulations are presented in the Appendix, in Tables A1 and A2.

3.2. Hypothetical spill cases

Three locations with a high probability of oil spills were chosen for hypothetical spill case studies (Fig. 1). Two of these locations involve surface spills, while the third involves a bottom spill resulting from a shipwreck. All cases were initialized during the Birgit storm, which reached the study area on approximately December 11, 2022. The hypothetical spills take place at the same time as the sixth drifter experiment, during which, in the open sea of the Gulf of Finland, LP recorded maximum wave heights exceeding 6 m. The simulations were initialized on December 12, 2022, at 00:00 UTC and lasted 96 h.

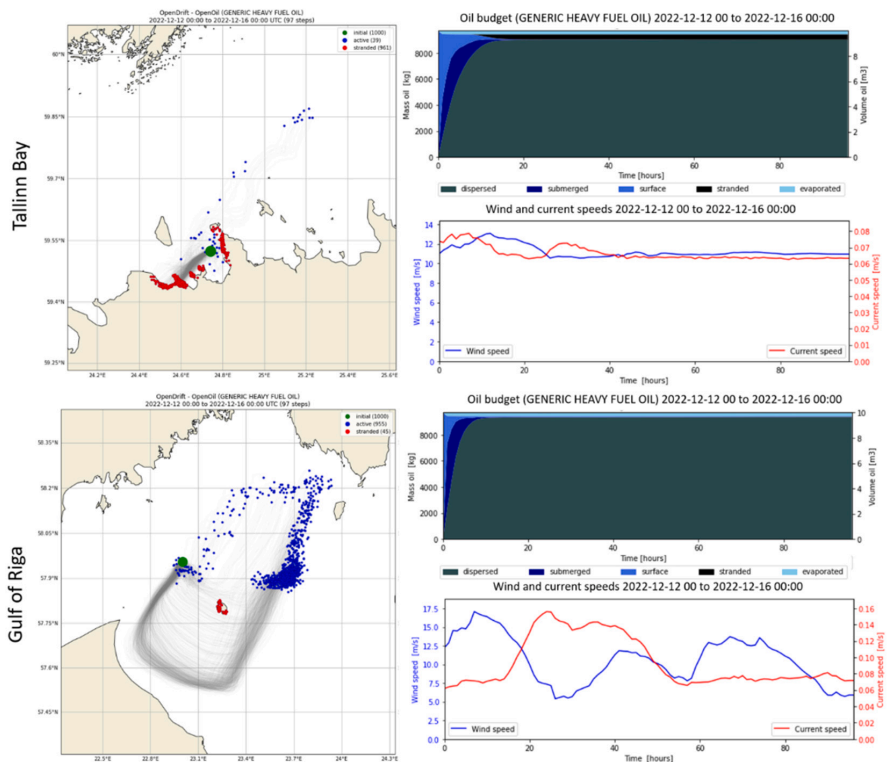
The results of the hypothetical spills are presented in Fig. 5. The distribution and tracks of the particles are shown on the map, and an oil mass budget plot is used to illustrate the distribution and fate of the oil over time during the simulated spill. The oil mass budget is partitioned among different components, including dispersed, submerged, surface,

stranded, and evaporated. The dispersed component represents oil that has been broken down into smaller droplets or particles and is dispersed throughout the water column. The submerged component refers to oil that is not dispersed but has physically sunk or settled below the water surface. The surface component denotes the portion of the oil that remains on the surface of the water. The stranded component accounts for oil that has come into contact with shorelines. The evaporated component quantifies the amount of oil that has been lost from the spill due to evaporation.

The first hypothetical surface spill site was chosen to be Tallinn Bay, an area characterized by significant shipping traffic. The maritime connection between Tallinn and Helsinki is recognized as one of the busiest in the world (Tapaninen and Palu, 2022). From the oil budget plot in Fig. 5, it can be observed that within an hour, half of the oil was either submerged or dispersed throughout the water column. The particles began to reach the shoreline after 8 h and after 12 h 90 % of the oil had dispersed. Although most of the particles were stranded, it only represented approximately 4 % of the mass of the oil. Due to the characteristics of the oil and its rapid disappearance from the surface, about 3 % of the oil evaporated.

The second hypothetical site of surface spill was selected to be within a future wind energy park in the Gulf of Riga (Estonian Ministry of Finance and Hendrikson and Ko, 2021). Oil spills in these areas can occur due to ship collisions with offshore wind turbines (Biehl and

SURFACE SPILLS



SPILL FROM THE SEABED

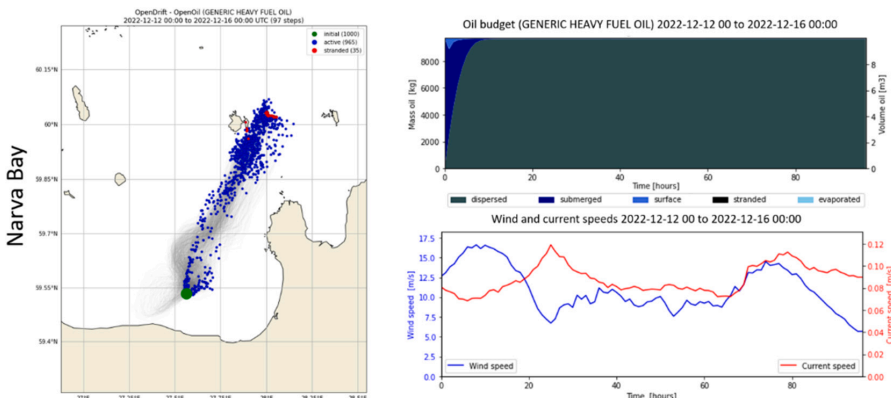


Fig. 5. Results of hypothetical spill cases. The green circle marks the seeding location, the blue particles indicate the oil distribution, and the red particles have stranded. Trajectories are indicated with gray lines. Only the last step of the simulations is shown. The adjacent column shows the oil mass budget and the wind and current speed during the simulation run. (For interpretation of the references to colour in this figure legend, the reader is referred to the web version of this article.)

Lehmann, 2006; Etkin, 2008; Presencia and Shafiee, 2018; Yu et al., 2020) or events such as accidents, natural disasters, fires, etc., that can lead to turbine-related spills (e.g., electrical insulation oil) (Etkin, 2008). Due to more severe weather conditions, an hour after the initialization of the simulation 75 % of the oil was either submerged or dispersed. After 9 h 95 % of the oil had dispersed. Similarly to the previous case, around 3 % of the total oil amount evaporated. The distribution map shows that

approximately 45 particles get stranded on an island, accounting for approximately 0.03 % of the total volume of the spill.

For the hypothetical seabed scenario, a sunken ship from World War II was chosen. The German Destroyer T-22, which sank in 1944, lies at a depth of 32 m in Narva Bay and is estimated to carry a maximum of 374 tons of heavy fuel oil (Kose, 2021). In the initial hour of the simulation, approximately 9 % of the oil reached the surface, after which the amount

quickly decreased. As the spill originated from the sea floor, most of the oil was initially submerged, but within 9 h over 99 % of the original amount had dispersed. From 85 h into the simulation, some particles ended up on the shores of small islands north of the seeding location, but the amount of oil they represented was minimal.

Wind and current speeds – calculated as a mean over all particles – are shown in Fig. 5. Wind and current speeds in the Gulf of Riga and Narva Bay were higher and more variable compared to the relatively sheltered location of Tallinn Bay (Fig. 5). Since all spills were initiated simultaneously, the direction of the wind and the resulting spill movements were similar across all locations. However, the temporal and spatial characteristics of each area differed.

4. Discussion

Our objective is to validate how accurately our setup of the Open-Drift model can predict the trajectories of oil spills. For that purpose we used drifter buoys to serve as proxies, as obtaining adequate data for accidental spills is often limited and orchestrating a spill for scientific research purposes a difficult undertaking in every way. The use of such technology has been successfully applied to oil spill studies since the 1970s (Novelli et al., 2018).

Accurately estimating the WDF of the drifter buoys and incorporating it into the model allows for better interpretation and comparison of the model's performance. If the simulated trajectories align better with the observed drift patterns of the drifter buoy, it provides confidence in the model's predictive capabilities. The WDFs found for LPs in Section 3.1.1, generally agree with previous findings for similar buoys (Röhrs and Christensen, 2015; Pisano et al., 2016; Brekke et al., 2021), especially when taking into account the differences in buoy design and the fact that WDFs can vary depending on aspects, such as region (Rio and Hernandez, 2003; Poulain et al., 2009), season (Rio and Hernandez, 2003), and the rate at which wind forcing changes over time (Röhrs and Christensen, 2015; De Dominicis et al., 2016).

The small differences in the design of the two versions of the LP also resulted in different WDFs. The LP V1.0 features a more streamlined shape and its bottom chain acts somewhat like a drogue, reducing its susceptibility to wind and Stokes drift and increasing its reliance on currents, thus resulting in lower WDF values. These lower WDF values align more closely with those reported for near-surface drifters (e.g. Sutherland et al., 2020; Delpêche-Ellmann et al., 2021; Pärn et al., 2023). The WDFs obtained for the LPs also show a strong similarity to those reported for oil spill modeling (e.g. Schwartzberg, 1971; Stolzenbach et al., 1977; Reed et al., 1994; ASCE, 1996; Drivdal et al., 2014; Jones et al., 2016a), particularly for LP V0.1. This similarity demonstrates that the knowledge and insights acquired from the LP tests can be applied to oil spill modeling with greater confidence. Additionally, it suggests that LPs are well-suited for use as tracking buoys in oil spill response operations.

The overall skill scores for the LP V0.1, which experience more wind drag, are significantly higher than those for the LP V1.0, indicating better predictability of wind. The low skill scores for the Gulf of Finland simulations could be because they took place during and after a stormy event, involving complex and dynamic hydrometeorological conditions. These complex conditions, especially strong and rapid variations in the current field, might be difficult to fully capture even with the high-resolution models used in this study. Therefore, this could introduce uncertainties in the input data provided to the drift model and reduce accuracy and the skill score.

Discrepancies or inconsistencies in the wind data used by each model could introduce errors and inconsistencies in the simulation results, leading to unrealistic or unreliable predictions. In our modeling setup, the currents simulated by NEMO-EST05 and the waves simulated by SWAN-EST are driven by the same ECMWF wind fields used in Open-Drift. This use of a single source for wind data in all three systems enables a coherent and synchronized representation of the environmental

conditions, and their impact on drift trajectories.

When interpreting the results of simulated oil spills, it is essential to acknowledge that the outcomes are shaped by the specific location and environmental conditions during the simulation and the inherent properties of the oil being modeled.

The relatively fast dispersion of the simulated spill scenarios emphasizes the importance of immediate response actions to mitigate environmental damage. Swift response times enable more effective containment and cleanup efforts, reducing harm to marine ecosystems, wildlife, plants, and sensitive habitats. Additionally, addressing oil spills in open sea locations is easier and less costly compared to dealing with shoreline contamination (Etkin, 2000; Ventikos et al., 2004). In particular, Tallinn Bay exhibited the highest proportion of oil stranding, highlighting the significance of the proximity of the spill to the shore. Given the Baltic Sea's short distances from potential spill sites to the coastline, there is an elevated risk of oil reaching sensitive coastal areas. Therefore, the implementation of rapid response measures is crucial to prevent or minimize oil contamination on the shore.

The spill scenario in Narva Bay, originating from a sunken ship on the seabed, exhibited a bit different behavior. Only a small amount of oil surfaced for a few hours before dispersing. It is important to note that spills from wrecks are often continuous rather than one-time event like in this simulation. This continuous leakage of oil over an extended period poses unique challenges for spill response and mitigation efforts (Gilbert et al., 2003; Daniel et al., 2020). It means that the potential for environmental contamination persists for a longer duration, increasing the cumulative impact on marine ecosystems, wildlife, and coastal areas (Hampton et al., 2003). The continuous nature of these spills requires sustained monitoring and response measures to minimize the spread of oil, mitigate environmental damage, and protect sensitive habitats. Furthermore, it can affect the effectiveness of containment and cleanup operations. The oil may disperse, spread, and undergo weathering processes over time, which can alter its behavior and make it more challenging to contain and recover. The persistence of the spill also increases the potential for oil to reach shorelines, further exacerbating the ecological and economic consequences (Asif et al., 2022).

It should be noted that the response to oil spills can be significantly influenced by weather conditions (Nordvik, 1995; Robertson et al., 2017). Severe weather conditions, such as those used for our simulations, can hinder response efforts, making containment and cleanup operations more challenging or even impossible. Therefore, oil spill response should take into account the potential impact of adverse weather conditions and ensure the availability of appropriate response measures even under challenging circumstances. Additionally, the simulations show that under such conditions, only a relatively small amount of oil remains on the water surface, with a significant portion dispersing into the water column. This also poses a significant challenge in terms of oil removal and mitigation. The dispersed oil in the water column is more difficult to address and may have long-term ecological consequences.

Parts of the Baltic Sea, including the Estonian sea area, are subject to seasonal ice cover. The NEMO-EST05 model provides information about sea ice, and de Aguiar et al. (2022) have incorporated the capability for oil-ice interaction in OpenOil, where the drift of oil can be influenced by the drift of ice when ice concentrations exceed 30 %. Although the ice concentration in our hypothetical spill sites did not exceed this threshold, the ability to model oil fate and transport in the presence of sea ice enhances the utility of the system and opens up avenues for further research and potential operational applications of the validated model setup.

5. Conclusions

This study implements and validates OpenDrift, an open-source Lagrangian particle trajectory modeling framework, within the coastal waters of Estonia in the Baltic Sea. OpenDrift was forced with ECMWF

winds and local high-resolution hydrodynamical and wave models, which used the same wind forcing. We validated the setup using data from six drift experiments from 2022. Furthermore, we used the OpenOil module of OpenDrift to examine hypothetical oil spills during severe weather in regions that might be exposed to such incidents.

Two versions of LainePoiss (LP) buoys, with slightly different designs, were used in the drift experiments. We determined that the wind drift factors (WDFs) for the LP buoys resembled those commonly used in oil spill modeling. This similarity reinforces the applicability of the LP buoys for oil spill studies.

We found that incorporating other forcing factors in addition to the wind, such as Stokes drift and currents, generally improved the skill scores of the OpenDrift simulations. Interestingly, our results indicate that the effect of a single forcing, such as the Stokes drift, may depend on the presence of another forcing, such as the currents. This suggests a more complex interplay between different forcings rather than a simple additive effect.

Simulations performed for harsh weather conditions showed that over 90 % of the 10 m³ of generic heavy fuel oil can disperse within the first 12 h. Although the oil spill in the simulations were hypothetical, they were performed in a regions that might be prone to such accidents. Thus, the results emphasize a critical need to be prepared with prompt and efficient response strategies to effectively address oil spill incidents.

CRedit authorship contribution statement

Siim Pärt: Conceptualization, Methodology, Validation, Formal analysis, Investigation, Writing – original draft, Writing – review & editing, Visualization. **Jan-Victor Björkqvist:** Conceptualization,

Formal analysis, Writing – review & editing, Supervision. **Victor Alari:** Investigation, Software, Resources, Writing – review & editing, Supervision, Project administration, Funding acquisition. **Ilja Maljutenko:** Software, Writing – review & editing. **Rivo Uiboupin:** Writing – review & editing, Supervision, Funding acquisition.

Declaration of competing interest

The authors declare that they have no known competing financial interests or personal relationships that could have appeared to influence the work reported in this paper.

Data availability

Data will be made available on request.

Acknowledgements

This study was undertaken within the scope of the project "Operational and user-friendly oil drift and Search and Rescue (SAR) forecast system for Estonian marine waters" (KIK21067), which received funding from the Environmental Investment Center. We would like to sincerely acknowledge the valuable assistance of Kaimo Vahter in conducting the drifter experiments. We also express our gratitude to Knut-Frode Dag-estad from the Norwegian Meteorological Institute for his insights and discussions into the workings of the OpenDrift framework. Additionally, we extend our appreciation to WiseParker OÜ for their assistance in the data management of the LainePoiss buoys.

Appendix A. Tables presenting the skill scores of 12-h and 24-h simulations for the validation of the OpenDrift setup

Table A1

Average skill scores (SS) for 12-h forecast interval with different combinations of forcing, using the best estimates of the WDFs.

Forcing combination	Wind	Wind + Stokes drift	Wind + Currents	Wind + Currents + Stokes drift
LP V0.1				
Muuga Bay LP_3	0.675	0.668	0.690	0.710
Muuga Bay LP_4	0.683	0.670	0.691	0.713
Number of runs	40	38	37	40
Mean of SSs	0.679	0.669	0.690	0.712
Weighted average SS	0.679	0.669	0.690	0.712
LP V1.0				
Gulf of Riga LP_13	0.395	0.453	0.663	0.723
Gulf of Riga LP_14	0.408	0.451	0.651	0.659
Tagalaht Bay LP_17	0.484	0.466	0.413	0.389
Pakri Bay LP_13	0.658	0.632	0.516	0.557
Pakri Bay LP_14	–	–	–	–
Gulf of Finland LP_16	0.401	0.388	0.410	0.390
Gulf of Finland LP_17	0.370	0.368	0.377	0.380
Tallinn Bay LP_7	–	–	–	–
Tallinn Bay LP_9	–	–	–	–
Tallinn Bay LP_10	–	–	–	–
Tallinn Bay LP_11	–	–	–	–
Number of runs	85	85	83	85
Mean of SSs	0.452	0.460	0.505	0.516
Weighted average SS	0.403	0.402	0.437	0.433

Table A2

Average skill scores (SS) for 24-h forecast interval with different combinations of forcing, using the best estimates of the WDFs.

Forcing combination	Wind	Wind + Stokes drift	Wind + Currents	Wind + Currents + Stokes drift
LP V0.1				
Muuga Bay LP_3	0.717	0.717	0.734	0.759
Muuga Bay LP_4	0.722	0.723	0.720	0.742
Number of runs	29	31	24	28
Mean of SSs	0.720	0.720	0.727	0.750

(continued on next page)

Table A2 (continued)

Forcing combination	Wind	Wind + Stokes drift	Wind + Currents	Wind + Currents + Stokes drift
Weighted average SS	0.720	0.720	0.727	0.750
LP V1.0				
Gulf of Riga LP_13	0.414	450	0.711	0.835
Gulf of Riga LP_14	0.426	0.460	0.692	0.718
Tagalaht Bay LP_17	0.544	0.530	0.470	0.458
Pakri Bay LP_13	–	–	–	–
Pakri Bay LP_14	–	–	–	–
Gulf of Finland LP_16	0.478	0.444	0.466	0.441
Gulf of Finland LP_17	0.417	0.407	0.420	0.404
Tallinn Bay LP_7	–	–	–	–
Tallinn Bay LP_9	–	–	–	–
Tallinn Bay LP_10	–	–	–	–
Tallinn Bay LP_11	–	–	–	–
Number of runs	73	72	72	68
Mean of SSs	0.456	0.458	0.552	0.571
Weighted average SS	0.453	0.436	0.477	0.469

References

- Aamo, O.M., Reed, M., Downing, K., 2005. Oil spill contingency and response (OSCAR) model system: sensitivity studies. 2005 international oil spill conference. IOSC 2005, 5486–5495. <https://doi.org/10.7901/2169-3358-1997-1-429>.
- Aghito, M., Calgalo, L., Dagestad, K.F., Ferrarin, C., Marcomini, A., Breivik, Ø., Hole, L. R., 2022. ChemicalDrift 1.0: an open-source Lagrangian chemical fate and transport model for organic aquatic pollutants. In: Geoscientific Model Development Discussions, pp. 1–28. <https://doi.org/10.5194/gmd-2022-212>.
- de Aguiar, V., Dagestad, K.F., Hole, L.R., Barthel, K., 2022. Quantitative assessment of two oil-in-ice surface drift algorithms. Mar. Pollut. Bull. 175, 113393. <https://doi.org/10.1016/j.marpolbul.2022.113393>.
- Alari, V., Björkqvist, J.V., Kaldvee, V., Mölder, K., Rikka, S., Kask-Korb, A., Vahter, K., Pärt, S., Vidjajev, N., Tõnisson, H., 2022. LainePoiss V — a lightweight and ice-resistant wave buoy. J. Atmos. Ocean. Technol. 39, 573–594. <https://doi.org/10.1175/JTECH-D-21-0091.1>.
- Al-Ruzouq, R., Gibril, M.B.A., Shanableh, A., Kais, A., Hamed, O., Al-Mansoori, S., Khalil, M.A., 2020. Sensors, features, and machine learning for oil spill detection and monitoring: a review. Remote Sens. 12, 1–42. <https://doi.org/10.3390/rs12203338>.
- Ambjörn, C., 2006. Seatrack web, forecast of oil spills, the new version. In: 2006 IEEE US/EU Baltic International Symposium, pp. 1–7. <https://doi.org/10.1109/BALTIC.2006.7266187>.
- Ambjörn, C., Liungman, O., Mattsson, J., Håkansson, B., 2014. Seatrack web: the HELCOM tool for oil spill prediction and identification of illegal polluters. Handbook of Environmental Chemistry 27, 155–183. <https://doi.org/10.1007/978-2011-120>.
- Amir-Heidari, P., Arneborg, L., Lindgren, J.F., Lindhe, A., Rosén, L., Raie, M., Axell, L., Hassellöv, I.M., 2019. A state-of-the-art model for spatial and stochastic oil spill risk assessment: a case study of oil spill from a shipwreck. Environ. Int. 126, 309–320. <https://doi.org/10.1016/j.envint.2019.02.037>.
- ASCE, 1996. State-of-the-art review of modeling transport and fate of oil spills. J. Hydraul. Eng. 122, 594–609. [https://doi.org/10.1061/\(asce\)0733-9429\(1996\)122:11\(594\)](https://doi.org/10.1061/(asce)0733-9429(1996)122:11(594)).
- Asif, Z., Chen, Z., An, C., 2022. Environmental impacts and challenges associated with oil spills on shorelines. Journal of Marine Science and Engineering. <https://doi.org/10.3390/jmse10060762>.
- Barreto, F.T., Dammann, D.O., Tessarolo, L.F., Skancke, J., Khegouche, I., Innocentini, V., Winther-Kaland, N., Marton, L., 2021. Comparison of the coupled model for oil spill prediction (CMOP) and the oil spill contingency and response model (OSCAR) during the DeepSpill field experiment. Ocean Coast. Manag. 204. <https://doi.org/10.1016/j.ocecoaman.2021.105552>.
- Beegle-Krause, C.J., 2005. General NOAA oil modeling environment (GNOME): a new spill trajectory model. 2005 international oil spill conference. IOSC 2005, 3277–3283. <https://doi.org/10.7901/2169-3358-2001-2-865>.
- Biehl, F., Lehmann, E., 2006. Collisions of ships with offshore wind turbines: calculation and risk evaluation. In: Offshore Wind Energy: Research on Environmental Impacts, pp. 281–304. https://doi.org/10.1007/978-3-540-34677-7_17.
- Björkqvist, J.V., Lukas, I., Alari, V., van Vledder, G.P., Hulst, S., Petterson, H., Behrens, A., Männik, A., 2018. Comparing a 41-year model hindcast with decades of wave measurements from the Baltic Sea. Ocean Eng. 152, 57–71. <https://doi.org/10.1016/j.oceaneng.2018.01.048>. arXiv:1705.00559.
- Booij, N., Ris, R.C., Holthuijsen, L.H., 1999. A third-generation wave model for coastal regions I. Model description and validation. J. Geophys. Res. Oceans 104, 7649–7666. <https://doi.org/10.1029/98JC02622>.
- Brekke, C., Espeseth, M.M., Dagestad, K.F., Röhrs, J., Hole, L.R., Reigber, A., 2021. Integrated analysis of multisensor datasets and oil drift simulations—a free-floating oil experiment in the open ocean. J. Geophys. Res. Oceans 126, 1–26. <https://doi.org/10.1029/2020JC016499>.
- Carter, M., Goodsir, F., Cundall, P., Devlin, M., Fuller, S., Jeffery, B., Hil, G., Talouli, A., 2021. Ticking ecological time bombs: risk characterisation and management of oil polluting world war II shipwrecks in the Pacific Ocean. Mar. Pollut. Bull. 164, 112087. <https://doi.org/10.1016/j.marpolbul.2021.112087>.
- Chen, J., Zhang, W., Wan, Z., Li, S., Huang, T., Fei, Y., 2019. Oil spills from global tankers: status review and future governance. J. Clean. Prod. 227, 20–32. <https://doi.org/10.1016/j.jclepro.2019.04.020>.
- Chilvers, B.L., Morgan, K.J., White, B.J., 2021. Sources and reporting of oil spills and impacts on wildlife 1970–2018. Environ. Sci. Pollut. Res. 28, 754–762. <https://doi.org/10.1007/s11356-020-10538-0>.
- Clavel-Henry, M., North, E.W., Solé, J., Bahamon, N., Carretón, M., Company, J.B., 2021. Estimating the spawning locations of the deep-sea red and blue shrimp *Aristeus antennatus* (Crustacea: Decapoda) in the northwestern Mediterranean Sea with a backtracking larval transport model. Deep-Sea research part I. In: Oceanographic Research Papers, 174. <https://doi.org/10.1016/j.dsr.2021.103558>.
- Dagestad, K.F., Röhrs, J., 2019. Prediction of ocean surface trajectories using satellite derived vs. modeled ocean currents. Remote Sens. Environ. 223, 130–142. <https://doi.org/10.1016/j.rse.2019.01.001>.
- Dagestad, K.F., Röhrs, J., Breivik, O., Ådlandsvik, B., 2018. OpenDrift v1.0: a generic framework for trajectory modelling. Geosci. Model Dev. 11, 1405–1420. <https://doi.org/10.5194/gmd-11-1405-2018>.
- Daniel, P., Paradis, D., Gouriou, V., Roux, A.L., Garreau, P., Le Roux, J.F., Loazel, S., 2020. Forecast of oil slick drift from Ulysse/CSL Virginia and Grande America accidents Pierre. In: 2020 International Oil Spill Conference, pp. 1–19.
- De Dominicis, M., Pinardi, N., Zodiatis, G., Archetti, R., 2013a. MEDSLIK-II, a Lagrangian marine surface oil spill model for short-term forecasting-part 2: numerical simulations and validations. Geosci. Model Dev. 6, 1871–1888. <https://doi.org/10.5194/gmd-6-1871-2013>.
- De Dominicis, M., Pinardi, N., Zodiatis, G., Lardner, R., 2013b. MEDSLIK-II, a Lagrangian marine surface oil spill model for short-term forecasting-part 1: theory. Geosci. Model Dev. 6, 1851–1869. <https://doi.org/10.5194/gmd-6-1851-2013>.
- De Dominicis, M., Falchetti, S., Trotta, F., Pinardi, N., Giacomelli, L., Napolitano, E., Fazioli, L., Sorgente, R., Haley, P.J., Lermusiaux, P.F., Martins, F., Cocco, M., 2014. A relocatable ocean model in support of environmental emergencies. Ocean Dyn. 64, 667–688. <https://doi.org/10.1007/s10236-014-0705-x>.
- De Dominicis, M., Bruciaferri, D., Gerin, R., Pinardi, N., Poulain, P.M., Garreau, P., Zodiatis, G., Perivoliotis, I., Fazioli, L., Sorgente, R., Manganiello, C., 2016. A multi-model assessment of the impact of currents, waves and wind in modelling surface drifters and oil spill. Deep-Sea Research Part II: Topical Studies in Oceanography 133, 21–38. <https://doi.org/10.1016/j.dsr2.2016.04.002>.
- Delpêche-Ellmann, N., Giudici, A., Råstep, M., Soomere, T., 2021. Observations of surface drift and effects induced by wind and surface waves in the Baltic Sea for the period 2011–2018. Estuar. Coast. Shelf Sci. 249. <https://doi.org/10.1016/j.ecss.2020.107071>.
- Drivdal, M., Broström, G., Christensen, K.H., 2014. Wave-induced mixing and transport of buoyant particles: application to the Staffjord a oil spill. Ocean Sci. 10, 977–991. <https://doi.org/10.5194/os-10-977-2014>.
- Elizaryev, A., Maniakova, G., Longobardi, A., Elizareva, E., Gabdulkhakov, R., Nurudinov, A., Khakinov, R., 2018. Numerical simulation of oil spills based on the GNOME and ADIOS. International Journal of Engineering and Technology (UAJ) 7, 24–27. <https://doi.org/10.14419/ijet.v7i2.23.11876>.
- Estonian Ministry of Finance, Hendrikson & Ko, 2021. Estonian Maritime Spatial Plan Explanatory Memorandum.
- Etkin, D.S., 2000. Worldwide Analysis of Marine Oil Spill Cleanup Cost Factors, in: Arctic and Marine Oilspill Program Technical Seminar.
- Etkin, D.S., 2008. Oil spill risk analysis for cape wind energy project. In: International Oil Spill Conference - IOSC 2008, Proceedings, pp. 571–580. <https://doi.org/10.7901/2169-3358-2008-1-571>.
- Fingas, M., Brown, C.E., 2018. A review of oil spill remote sensing. Sensors (Switzerland) 18, 1–18. <https://doi.org/10.3390/s18010091>.
- French-McCay, D.P., Tajalli-Bakhsh, T., Jayko, K., Spaulding, M.L., Li, Z., 2017. Validation of oil spill transport and fate modeling in Arctic ice. Arctic Science 97, 71–97. <https://doi.org/10.1139/as-2017-0027>.

- Gilbert, T., Nawadra, S., Taflelchig, A., Yinug, L., 2003. Response to an oil spill from a sunken WWII oil tanker in Yap State, Micronesia. In: 2003 International Oil Spill Conference, pp. 175–182.
- Gustafsson, B., 1997. Interaction between Baltic Sea and North Sea. *Deutsche Hydrografische Zeitschrift* 49, 165–183. <https://doi.org/10.1007/BF02764031>.
- Hampton, S., Ford, R.G., Carter, H.R., Abraham, C., Humple, D., 2003. Chronic oiling and seabird mortality from the sunken vessel S.S. Jacob Luckenbach in Central California. *Mar. Ornithol.* 31, 35–41.
- HELCOM, 2003. The Baltic Marine Environment 1999–2002 (Technical Report).
- HELCOM, 2013. Risks of Oil and Chemical Pollution. Technical Report. HELCOM.
- HELCOM, 2018a. Maritime Activities in the Baltic Sea (Technical Report).
- HELCOM, 2018b. Operational Oil Spills from Ships - HELCOM Core indicator Report (Technical Report).
- HELCOM, 2022. Helcom Metadata Catalogue - Detected Spills of Mineral Oil and Other Substances. URL <https://metadata.helcom.fi/geonetwork/srv/eng/catalog.search?search#metadata/345c9b95-6e9c-44a4-b02a-ee4304cccffc>. (Accessed 29 June 2023).
- Hendrikson & Ko, 2022. Estonian Maritime Spatial Plan. URL <http://mereala.hendrikson.ee/kaardirakendus-en.html>. (Accessed 29 June 2023).
- Hole, L.R., 2018. APP4SEA - Report on Existing Oil Spill Response Models (Technical Report).
- Horðoír, R., Axell, L., Höglund, A., Dieterich, C., Fransser, F., Gröger, M., Liu, Y., Pemberton, P., Schinamke, S., Andersson, H., Ljungemyr, P., Nygren, P., Falahat, S., Nord, A., Jönsson, A., Lake, I., Döös, K., Hieronymy, M., Dietze, H., Löptien, U., Kuznetsov, I., Westerlund, A., Tuomi, L., Haapala, J., 2019. Nemo-Nordic 1.0: A NEMO-based ocean model for the Baltic and North seas - Research and operational applications. In: *Geoscientific Model Development*, 12, pp. 363–386. <https://doi.org/10.5194/gmd-12-363-2019>.
- ITOPF, 2022. Oil Tanker Spill Statistics 2021.
- Ivichev, I., Hole, L.R., Karlin, L., Wettre, C., Röhrs, J., 2012. Comparison of operational oil spill trajectory forecasts with surface drifter trajectories in the Barents Sea. *Journal of Geology & Geosciences* 01. <https://doi.org/10.4172/2329-6755.1000105>.
- Jones, C.E., Dagestad, K.F., Breivik, Ø., Holt, B., Röhrs, J., Christensen, K.H., Espeseth, M., Brekke, C., Skrunes, S., 2016a. Measurement and modeling of oil slick transport. *J. Geophys. Res. Oceans* 1–14. <https://doi.org/10.1002/2016JC012113>.
- Jones, H.F., Poot, M.T., Mullarney, J.C., de Lange, W.P., Bryan, K.R., 2016b. Oil dispersal modelling: reanalysis of the Rena oil spill using open-source modelling tools. *N. Z. J. Mar. Freshw. Res.* 50, 10–27. <https://doi.org/10.1080/00288330.2015.1112819>.
- Kärnä, T., Ljungemyr, P., Falahat, S., Ringgaard, I., Axell, L., Korabel, V., Murawski, J., Maljutenko, I., Lindenthal, A., Jandt-Scheelke, S., Verjovkina, S., Lorkowski, I., Lagemaa, P., She, J., Tuomi, L., Nord, A., Huess, V., 2021. Nemo-Nordic 2.0: operational marine forecast model for the Baltic Sea. *Geosci. Model Dev.* 14, 5731–5749. <https://doi.org/10.5194/gmd-14-5731-2021>.
- Keramea, P., Spanoudaki, K., Zodiatis, G., Gikas, G., Sylaiois, S., 2021. Oil spill modeling: a critical review on current trends, perspectives, and challenges. *Journal of Marine Science and Engineering* 9, 1–41. <https://doi.org/10.3390/jmse9020181>.
- Kose, M., 2021. Hazardous Wrecks in Estonian Sea Area. URL: [https://portal.helcom.fi/meetings/RESPONSE29-2021877/Documents/06 Project "Environmental risk assessment of potentially hazardous wrecks in Estonian marine area".pdf](https://portal.helcom.fi/meetings/RESPONSE29-2021877/Documents/06%20Project%20Environmental%20risk%20assessmentofpotentiallyhazardouswrecksinEstonianmarinerearea.pdf). presentationgivenonlineatthe29thMeetingoftheResponseWorkingGroup.
- Kriez, E.E., Broman, B., 2008. Past and future wave climate in the Baltic sea produced by the SWAN model with forcing from the regional climate model RCA of the rossby centre. US/EU-Baltic International Symposium. In: *Ocean Observations, Ecosystem-Based Management and Forecasting - Provisional Symposium Proceedings. BAL TIC*. <https://doi.org/10.1109/BAL TIC.2008.4625539>.
- Landquist, H., Hassellöv, I.M., Rosén, L., Lindgren, J.F., Dahllöf, I., 2013. Evaluating the needs of risk assessment methods of potentially polluting shipwrecks. *J. Environ. Manag.* 119, 85–92. <https://doi.org/10.1016/j.jenvman.2012.12.036>.
- Landquist, H., Rosén, L., Lindhe, A., Norberg, T., Hassellöv, I.M., Lindgren, J.F., Dahllöf, I., 2014. A fault tree model to assess probability of contaminant discharge from shipwrecks. *Mar. Pollut. Bull.* 88, 239–248. <https://doi.org/10.1016/j.marpolbul.2014.08.037>.
- Landquist, H., Rosén, L., Lindhe, A., Hassellöv, I.M., 2016. VRAKA-A probabilistic risk assessment method for potentially polluting shipwrecks. *Front. Environ. Sci.* 4, 1–14. <https://doi.org/10.3389/fenvs.2016.00049>.
- Lindgren, J.F., Åberg, F., Johansson, J.R., 2020. Polluting shipwrecks in Swedish waters: investigations, risk assessment methodology and oil removal operations. In: 2020 International Oil Spill Conference, pp. 1–20.
- Liu, Y., Weisberg, R.H., 2011. Evaluation of trajectory modeling in different dynamic regions using normalized cumulative Lagrangian separation. *J. Geophys. Res. Oceans* 116, 1–13. <https://doi.org/10.1029/2010JC006837>.
- Liu, Y., Weisberg, R.H., Vignudelli, S., Mitchum, G.T., 2014. Evaluation of Altimetry-Derived Surface Current Products Using Lagrangian Drifter Trajectories in the Eastern Gulf of Mexico. *Oceans, Journal of Geophysical Research*, pp. 3868–3882. <https://doi.org/10.1002/2013JC009710>.
- Madec, G., the NEMO Team, 2022. NEMO Ocean engine. Scientific Notes of Climate Modelling Center 1–386. <https://doi.org/10.5281/zenodo.1464816>.
- Maljutenko, I., Lagemaa, P., Verjovkina, S., 2022. Mere operatiivmudelüstesteei NEMO kasutuselevõtt ja tööloarandamine mereala operatiivprognooside parandamiseks. Technical Report. (In Estonian).
- Michel, J., Gilbert, T., Etkin, D.S., Urban, R., Waldron, J., Blockidge, C.T., 2005. An issue paper prepared for the 2005 international oil spill conference: potentially polluting wrecks in marine waters. *International oil spill conference 2005*, 1–40.
- Miettunen, E., Tuomi, L., Myrberg, K., 2020. Water exchange between the inner and outer archipelago areas of the Finnish Archipelago Sea in the Baltic Sea. *Ocean Dyn.* 70, 1421–1437. <https://doi.org/10.1007/s10236-020-01407-y>.
- Moroni, D., Pieri, G., Salvetti, O., Tampucci, M., Domenici, C., Tonacci, A., 2016. Sensorized buoy for oil spill early detection. *Methods in Oceanography* 17, 221–231. <https://doi.org/10.1016/j.mio.2016.10.002>.
- NAS, 2022. Oil in the Sea: Inputs, Fates, and Effects, 1. The National Academies Press, Washington, DC. <https://doi.org/10.17226/26410>.
- Nordvik, A.B., 1995. The technology windows-of-opportunity for marine oil spill response as related to oil weathering and operations. *Spill Sci. Technol. Bull.* 2, 17–46. [https://doi.org/10.1016/1353-2561\(95\)00013-1](https://doi.org/10.1016/1353-2561(95)00013-1).
- Novelli, G., Guigand, C.M., Özgökmen, T.M., 2018. Technological advances in drifters for oil transport studies. *Mar. Technol. Soc. J.* 52, 53–61. <https://doi.org/10.4031/MTSJ.52.6.9>.
- Owens, R.G., Hewson, T., 2018. ECMWF forecast user guide. ECMWF. <https://doi.org/10.21957/mlcs7h>.
- Pallares, E., Sánchez-Arcilla, A., Espino, M., 2014. Wave energy balance in wave models (SWAN) for semi-enclosed domains—application to the Catalan coast. *Cont. Shelf Res.* 87, 41–53. <https://doi.org/10.1016/j.csr.2014.03.008>.
- Pärn, O., Davulien, L., Macias, D., Vahter, K., Stips, A., Torsvik, T., 2023. Effects of Eulerian current, Stokes drift and wind while simulating surface drifter trajectories in the Baltic Sea. *Oceanologia* 1–13. <https://doi.org/10.1016/j.oceano.2023.02.001>.
- Pärt, S., Kankaanpää, H., Björkqvist, J.V., Uiboupin, R., 2021. Oil spill detection using fluorometric sensors: laboratory validation and implementation to a FerryBox and a moored SmartBuoy. *Front. Mar. Sci.* 8, 1–17. <https://doi.org/10.3389/fmars.2021.778136>.
- Pereiro, D., Souto, C., Gago, J., 2018. Calibration of a marine floating litter transport model. *Journal of Operational Oceanography* 11, 125–133. <https://doi.org/10.1080/1755876X.2018.1470892>.
- Pisano, A., De Dominicis, M., Biamino, W., Bignami, F., Gherardi, S., Colao, F., Coppini, G., Marullo, S., Sprovieri, M., Trivero, P., Zambianchi, E., Santoleri, R., 2016. An oceanographic survey for oil spill monitoring and model forecasting validation using remote sensing and in situ data in the Mediterranean Sea. *Deep-Sea Research Part II: Topical Studies in Oceanography* 133, 132–145. <https://doi.org/10.1016/j.dsr2.2016.02.013>.
- Poulain, P.M., Gerin, R., Mauri, E., Pennel, R., 2009. Wind effects on drogued and undrogued drifters in the eastern Mediterranean. *J. Atmos. Ocean. Technol.* 26, 1144–1156. <https://doi.org/10.1175/2008JTECH0618.1>.
- Presencia, C.E., Shafiee, M., 2018. Risk analysis of maintenance ship collisions with offshore wind turbines. *International Journal of Sustainable Energy* 37, 576–596. <https://doi.org/10.1080/14786451.2017.1327437>.
- Reed, M., Turner, C., Odulo, A., 1994. The role of wind and emulsification in modelling oil spill and surface drifter trajectories. *Spill Sci. Technol. Bull.* 1, 143–157. [https://doi.org/10.1016/1353-2561\(94\)90022-1](https://doi.org/10.1016/1353-2561(94)90022-1).
- Riaz, M.R., 2021. Oil Spill Occurrence, Simulation, and Behavior. CRC Press/Taylor & Francis Group, LLC, Boca Raton, FL.
- Rio, M.H., Hernandez, F., 2003. High-frequency response of wind-driven currents measured by drifting buoys and altimetry over the world ocean. *J. Geophys. Res. Oceans* 108. <https://doi.org/10.1029/2002JC001655>.
- Ris, R.C., Holthuisen, L.H., Booij, N., 1999. A third-generation wave model for coastal regions 2. Verification. *J. Geophys. Res.* 104, 7667–7681. <https://doi.org/10.1029/1998JC900123>.
- Robertson, T., Hignam, B., Dahlslett, H.P., 2017. Analyzing the impact of Meteocean conditions on marine oil spill response. In: *OCEANS 2017, ANCHORAGE*, pp. 9–14.
- Rogers, W.E., Hwang, P.A., Wang, D.W., 2003. Investigation of wave growth and decay in the SWAN model: three regional-scale applications. *J. Phys. Oceanogr.* 33 (2), 366–389. [https://doi.org/10.1175/1520-0485\(2003\)033<0366:IOGWAD>2.0.CO;2](https://doi.org/10.1175/1520-0485(2003)033<0366:IOGWAD>2.0.CO;2).
- Röhrs, J., Christensen, K.H., 2015. Drift in the uppermost part of the ocean. *Geophys. Res. Lett.* 42, 10349–10356. <https://doi.org/10.1002/2015GL066733>.
- Röhrs, J., Dagestad, K.F., Asbjørnsen, H., Nordam, T., Skancke, J., Jones, C.E., Brekke, C., 2018. The effect of vertical mixing on the horizontal drift of oil spills. *Ocean Sci.* 14, 1581–1601. <https://doi.org/10.5194/os-14-1581-2018>.
- Schwartzberg, H.G., 1971. The movement of oil spills. In: *International Oil Spill Conference Proceedings*, 1971, pp. 489–494. <https://doi.org/10.7901/2169-3358-1971-1-489>.
- Soomere, T., 2022. Numerical simulations of wave climate in the Baltic Sea: a review. *Oceanologia*. <https://doi.org/10.1016/j.oceano.2022.01.004>.
- Spaulding, M.L., 2017. State of the art review and future directions in oil spill modeling. *Mar. Pollut. Bull.* 115, 7–19. <https://doi.org/10.1016/j.marpolbul.2017.01.001>.
- Stanev, E.V., Ricker, M., 2019. The fate of marine litter in semi-enclosed seas: a case study of the Black Sea. *Front. Mar. Sci.* 6, 1–16. <https://doi.org/10.3389/fmars.2019.00660>.
- Stolzenbach, K., Madsen, O., Adams, E., Pollack, A., Cooper, C., 1977. A Review and Evaluation of Basic Techniques for Predicting the Behaviour of Surface Oil Slicks. Technical Report. Massachusetts Institute of Technology.
- Sutherland, G., Soontinen, N., Davidson, F., Smith, G.C., Bernier, N., Blanken, H., Schillinger, D., Marcotte, G., Röhrs, J., Dagestad, K.F., Christensen, K.H., Breivik, Ø., 2020. Evaluating the leeway coefficient of ocean drifters using operational marine environmental prediction systems. *J. Atmos. Ocean. Technol.* 37, 1943–1954. <https://doi.org/10.1175/JTECH-D-20-0013.1>.
- Suursaar, Ü., Alari, V., Tõnisson, H., 2014. Multi-scale analysis of wave conditions and coastal changes in the North-Eastern Baltic Sea. *J. Coast. Res.* 70, 223–228. <https://doi.org/10.2112/SI70-038.1>.

- Tapaninen, U., Palu, R., 2022. Recovery of ro-pax ferry traffic from covid-19 under tightening environmental regulations: case Helsinki-Tallinn. *Journal of Shipping and Trade* 7. <https://doi.org/10.1186/s41072-022-00112-x>.
- Teal, J.M., Howarth, R.W., 1984. Oil spill studies: a review of ecological effects. *Environ. Manag.* 8, 27–43. <https://doi.org/10.1007/BF01867871>.
- Vankevich, R.E., Sofina, E.V., Eremina, T.E., Ryabchenko, V.A., Molchanov, M.S., Isaev, A.V., 2016. Effects of lateral processes on the seasonal water stratification of the Gulf of Finland: 3-D NEMO-based model study. *Ocean Sci.* 12, 987–1001. <https://doi.org/10.5194/os-12-987-2016>.
- Ventikos, N.P., Vergetis, E., Psarafitis, H.N., Triantafyllou, G., 2004. A high-level synthesis of oil spill response equipment and countermeasures. *J. Hazard. Mater.* 107, 51–58. <https://doi.org/10.1016/j.jhazmat.2003.11.009>.
- Viitak, M., Maljutenko, I., Alari, V., Suursaar, Ü., Rikka, S., Lagemaa, P., 2016. The impact of surface currents and sea level on the wave field evolution during St. Jude storm in the eastern Baltic Sea. *Oceanologia* 58, 176–186. <https://doi.org/10.1016/j.oceano.2016.01.004>.
- Westerlund, A., Tuomi, L., 2016. Vertical temperature dynamics in the northern Baltic Sea based on 3D modelling and data from shallow-water Argo floats. *J. Mar. Syst.* 158, 34–44. <https://doi.org/10.1016/j.jmarsys.2016.01.006>.
- Westerlund, A., Tuomi, L., Alenius, P., Miettunen, E., Vankevich, R.E., 2018. Attributing mean circulation patterns to physical phenomena in the Gulf of Finland. *Oceanologia* 60, 16–31. <https://doi.org/10.1016/j.oceano.2017.05.003>.
- Westerlund, A., Tuomi, L., Alenius, P., Myrberg, K., Miettunen, E., Vankevich, R.E., Hordoir, R., 2019. Circulation patterns in the Gulf of Finland from daily to seasonal timescales. *Tellus Ser. A Dyn. Meteorol. Oceanogr.* 71, 1–24. <https://doi.org/10.1080/16000870.2019.1627149>.
- Winsor, P., Rodhe, J., Omstedt, A., 2001. Baltic Sea ocean climate: an analysis of 100 yr of hydrographical data with focus on the freshwater budget. *Clim. Res.* 18, 1–11. <https://doi.org/10.3354/cr018005>.
- Wu, J., 2012. Wind-stress coefficients over sea surface from breeze to hurricane. *J. Geophys. Res.* 87 (C12), 9704–9706. <https://doi.org/10.1029/JC087iC12p09704>.
- Xu, J., Wang, H., Cui, C., Zhao, B., Li, B., 2020. Oil spill monitoring of shipborne radar image features using SVM and local adaptive threshold. *Algorithms* 13. <https://doi.org/10.3390/a13030069>.
- Yu, Q., Liu, K., Chang, C.H., Yang, Z., 2020. Realising advanced risk assessment of vessel traffic flows near offshore wind farms. *Reliab. Eng. Syst. Saf.* 203, 107086. <https://doi.org/10.1016/j.ress.2020.107086>.
- Zhang, B., Matchinski, E.J., Chen, B., Ye, X., Jing, L., Lee, K., 2018. *Marine Oil Spills-Oil Pollution, Sources and Effects*, Second edition. Elsevier Ltd. <https://doi.org/10.1016/B978-0-12-805052-1.00024-3>.
- Zijlema, M., van Vledder, G.P., Holthuijsen, L.H., 2012. Bottom friction and wind drag for wave models. *Coast. Eng.* 65, 19–26. <https://doi.org/10.1016/j.coastaleng.2012.03.002>.

Curriculum Vitae

Personal data

Name	Siim Pärt
Date of birth	21.12.1986
Place of birth	Estonia
Nationality	Estonian

Contact information

E-mail	siim.part@taltech.ee
--------	----------------------

Education

2019–2024	Tallinn University of Technology, School of Science, Physical Sciences, Oceanography and Meteorology, PhD
2009–2014	University of Tartu, Faculty of Science and Technology, Ecology of Waterbodies, MSc
2006–2009	University of Tartu, Faculty of Science and Technology, Ecology and Biodiversity Conservation, BSc
2003–2006	Tallinn ARTE Gymnasium, High School

Language competence

Estonian	Native
English	Fluent
Finnish	Intermediate
Russian	Basic

Professional employment

2019–present	Tallinn University of Technology, School of Science, Department of Marine Systems, Junior Researcher
2017–2019	Tallinn University of Technology, School of Science, Department of Marine Systems, Engineer
2014–2016	Tallinn University of Technology, Institute of Marine Systems at TUT, Engineer

Academic degrees

- Siim Pärt, Master's Degree, 2013, (sup) Priit Kersen; Tiina Paalme, Kassari lahe lah-tise punavetikakoosuse ruumiline muutlikkus (Spatial variability of the loose lying red algal community in the Kassari bay), University of Tartu, Faculty of Science and Technology (old), Institute of Ecology and Earth Sciences, Tartu University, Department of Zoology.
- Siim Pärt, PhD student, (sup) Rivo Uiboupin; Jan-Victor Ingevall Björkqvist, Enhancing Oil Spill Detection, Response and Modeling in the Baltic Sea, Tallinn University of Technology School of Science, Department of Marine Systems

Scientific work

Publications according to ETIS

- 1.1 Pärt, S.; Björkqvist, J.-V.; Alari, V.; Maljutenko, I.; Uiboupin, R. (2023). An ocean-wave-trajectory forecasting system for the eastern Baltic Sea: Validation against drifting buoys and implementation for oil spill modeling. *Marine Pollution Bulletin*, 195, 115497. DOI: 10.1016/j.marpolbul.2023.115497.
- 1.1 Alari, V.; Björkqvist, J.-V.; Kaldvee, V.; Mölder, K.; Rikka, S.; Kask-Korb, A.; Vahter, K.; Pärt, S.; Vidjajev, N.; Tõnisson, H. (2022). LainePoiss[®] - a lightweight and ice-resistant wave buoy. *Journal of Atmospheric and Oceanic Technology*, 39 (5), 573-594. DOI: 10.1175/JTECH-D-21-0091.1.
- 1.1 Pärt, S.; Kankaanpää, H.; Björkqvist, J.-V.; Uiboupin, R. (2021). Oil Spill Detection Using Fluorometric Sensors: Laboratory Validation and Implementation to a FerryBox and a Moored SmartBuoy. *Frontiers in Marine Science*, 8. DOI: 10.3389/fmars.2021.778136.
- 1.1 Björkqvist, J.-V.; Pärt, S.; Alari, V.; Rikka, S.; Lindgren, E.; Tuomi, L. (2021). Swell hind-cast statistics for the Baltic Sea. *Ocean Science*, 17 (6), 1815-1829. DOI: 10.5194/os-17-1815-2021.
- 1.1 Rikka, S.; Uiboupin, R.; Kõuts, T.; Vahter, K.; Pärt, S. (2019). A Method for Significant Wave Height Estimation From Circularly Polarized X-Band Coastal Marine Radar Images. *IEEE Geoscience and Remote Sensing Letters*, 16 (6), 844-848. DOI: 10.1109/LGRS.2018.2886631.

Elulookirjeldus

Isikuandmed

Nimi	Siim Pärt
Sünniaeg	21.12.1986
Sünnikoht	Eesti
Kodakondsus	Eesti

Kontaktandmed

E-post	siim.part@taltech.ee
--------	----------------------

Haridus

2019–2024	Tallinna Tehnikaülikool, Loodusteaduskond, Füüsikalised loodusteadused, Okeanograafia ja meteoroloogia, PhD
2009–2014	Tartu Ülikool, Loodus- ja Tehnoloogiateaduskond, Veekogude ökoloogia, MSc
2006–2009	Tartu Ülikool, Loodus- ja Tehnoloogiateaduskond, Ökoloogia ja elustiku kaitse, BSc
2003–2006	Tallinna ARTE Gümnaasium, Keskkool

Keelteoskus

eesti keel	emakeel
inglise keel	kõrgtase
soome keel	kesktase
vene keel	algtase

Teenistuskäik

2019–present	Tallinna Tehnikaülikool, Loodusteaduskond, TTÜ Meresüsteemide instituut doktorant-nooremteadur
2017–2019	Tallinna Tehnikaülikool, Loodusteaduskond, TTÜ Meresüsteemide instituut, insener
2014–2016	Tallinna Tehnikaülikool, TTÜ Meresüsteemide instituut, insener

Kaitstud lõputööd

- Siim Pärt, magistr kraad, 2013, (juh) Priit Kersen; Tiina Paalme, Kassari lahe lahtise punavetikakoosluse ruumiline muutlikkus, Tartu Ülikool, Loodus- ja tehnoloogia-teaduskond, Tartu Ülikooli Ökoloogia- ja Maateaduste Instituut, Zooloogia osakond.
- Siim Pärt, doktorant, (juh) Rivo Uiboupin; Jan-Victor Ingevall Björkqvist, Enhancing Oil Spill Detection, Response and Modeling in the Baltic Sea (Õlireostuse tuvas-tamise, modelleerimise ja sellele reageerimise tõhustamine Läänemeres), Tallinna Tehnikaülikool, Loodusteaduskond, Meresüsteemide instituut

Teadustegevus

Publikatsioonid Eesti Teadusinfosüsteemi klassifikaatori järgi

- 1.1 Pärt, S.; Björkqvist, J.-V.; Alari, V.; Maljutenko, I.; Uiboupin, R. (2023). An ocean–wave–trajectory forecasting system for the eastern Baltic Sea: Validation against drifting buoys and implementation for oil spill modeling. *Marine Pollution Bulletin*, 195, 115497. DOI: 10.1016/j.marpolbul.2023.115497.
- 1.1 Alari, V.; Björkqvist, J.-V.; Kaldvee, V.; Mölder, K.; Rikka, S.; Kask-Korb, A.; Vahter, K.; Pärt, S.; Vidjajev, N.; Tõnisson, H. (2022). LainePoiss® - a lightweight and ice-resistant wave buoy. *Journal of Atmospheric and Oceanic Technology*, 39 (5), 573-594. DOI: 10.1175/JTECH-D-21-0091.1.
- 1.1 Pärt, S.; Kankaanpää, H.; Björkqvist, J.-V.; Uiboupin, R. (2021). Oil Spill Detection Using Fluorometric Sensors: Laboratory Validation and Implementation to a FerryBox and a Moored SmartBuoy. *Frontiers in Marine Science*, 8. DOI: 10.3389/fmars.2021.778136.
- 1.1 Björkqvist, J.-V.; Pärt, S.; Alari, V.; Rikka, S.; Lindgren, E.; Tuomi, L. (2021). Swell hind-cast statistics for the Baltic Sea. *Ocean Science*, 17 (6), 1815-1829. DOI: 10.5194/os-17-1815-2021.
- 1.1 Rikka, S.; Uiboupin, R.; Kõuts, T.; Vahter, K.; Pärt, S. (2019). A Method for Significant Wave Height Estimation From Circularly Polarized X-Band Coastal Marine Radar Images. *IEEE Geoscience and Remote Sensing Letters*, 16 (6), 844-848. DOI: 10.1109/LGRS.2018.2886631.

ISSN 2585-6901 (PDF)
ISBN 978-9916-80-215-1 (PDF)